PB83-114769

PREPARATION AND CHARACTERIZATION OF ANALYTICAL REFERENCE MINERALS

Jean L. Graf
Paul K. Ase
Ronald G. Draftz
IIT Research Institute
Chicago, Illinois 60616

NIOSH Contract No. 210-75-0043

U.S. DEPARTMENT OF HEALTH, EDUCATION, AND WELFARE
Public Health Service
Center for Disease Control
National Institute for Occupational Safety and Health
Division of Physical Science and Engineering
Cincinnati, Ohio 45226

October 1978

50272-101			
REPORT DOCUMENTATION PAGE	1. REPORT NO. 210-75-0043	2. NA	3. Recipient's Accession No. PB83 114769

4. Title and Subtitle
Preparation and Characteristics of Analytical Reference Minerals

5. Report Date
October 1978

6. NA

7. Author(s)
Graf, J. L., P. K. Ase, and R. G. Draftz

8. Performing Organization Rept. No. NA

9. Performing Organization Name and Address
IIT Research Institute
Chicago, Illinois

10. Project/Task/Work Unit No. NA

11. Contract(C) or Grant(G) No.
(C) 210-75-0043
(G)

12. Sponsoring Organization Name and Address
NIOSH
Cincinnati, Ohio

13. Type of Report & Period Covered
Contract

14. NA

15. Supplementary Notes
NA

16. Abstract (Limit: 200 words)

The preparation and characterization of analytical reference minerals for monitoring of workplace contaminants are discussed. The purity, particle size, and characterization of 18 reference minerals are summarized. The abundance, sites of occurrence, and purity of material deposits of the 18 reference minerals are described, and mineral specimen sources obtained from mineral and industrial suppliers, museums, the National Stockpile synthesis, and field sampling are listed. Cristobalite and tridymite synthesis and phase confirmation analyses are described. Selection procedures of the best mineral samples as standards by macroscopic evaluation, polarized light microscopy (PLM), x-ray diffraction, and differential thermal analysis are summarized. Beneficiation procedures to remove residual impurities and size reduction to desired particle size are described. Two sizing methods, optical microscopy and MICROTRAC analysis, which were used to monitor particle size distribution, are described and results are summarized. PLM, which identified and quantitated mineral phase impurities, is described and results are summarized along with x-ray diffraction results.

17. Document Analysis a. Descriptors

Physical-properties, Analytical-methods, Air-monitoring, Inorganic-compounds, Sampling, equipment, Sample-collection

b. Identifiers/Open-Ended Terms

c. COSATI Field/Group

18. Availability Statement	19. Security Class (This Report)	21. No. of Pages
Available to Public	NA	221
	20. Security Class (This Page)	22. Price

DISCLAIMER

The contents of this report are reproduced herein as received from the contractor.

The opinions, findings, and conclusions expressed herein are not necessarily those of the National Institute for Occupational Safety and Health, nor does mention of company names or products constitute endorsement by the National Institute for Occupational Safety and Health.

NIOSH Project Officer: Janet Haartz
Principal Investigator: Ronald Draftz

ACKNOWLEDGMENTS

The completion of this study was possible only through the efforts of a number of key people. We would like to thank them and recognize their contributions.

For supplying and suggesting sources of mineral samples:

Sarkis G. Ampian and Robert Clifton, U.S. Bureau of Mines; John S. White, Jr., Smithsonian Institution; George Jameson, Director of Stockpile Disposal; John Carter, Rapid City, South Dakota; W. L. Griffin, Mineralogisk-Geologisk Museum of Norway; John Moore, National Institute of Environmental Health Sciences; Willis M. Johns, Montana Bureau of Mines; R.E.G. Rendall, National Research Institute for Occupational Disease, South Africa; Anttic Tossavainen, Institute of Occupational Health of Finland; Fred G. Hewett, Cassiar Asbestos Company; Dr. Jack Schelz, Johnson and Johnson Company; A. W. Samuel, Reserve Mining; Richard P. Fink, Iron Ore Company of Canada; Blair L. Ingalls and Harrison B. Rhodes, Union Carbide Corporation; D. W. Jaquays, Jaquays Mining; Wiley Cochran, Tamora Mining Company; C. B. Rash, Ozark Mahoning Company; R. J. Anuskiewicz, Brush Wellman Company; Harry G. Colgan and John Frankenberry, Pennsylvania Glass Sand Corporation; Jane S. Martin, Sobin Chemical Company; Hinz Windisch, Worldwide Minerals; Hing Lum, Winnie's Treasure Shop; Leonard I. Cowan, L. I. Cowan Mineral Company.

For carefully synthesizing the much needed silica polymorphs, cristobalite, and tridymite:

Rustum Roy, Della Roy, and their staff, Materials Research Laboratory, the Pennsylvania State University.

For performing thermal analyses of the final comminuted standards:

Leslie E. Cross and Gerald Zimmerman, Materials Research Laboratory, the Pennsylvania State University.

For the difficult and tedious task of grinding, separating, sizing, and analyzing the standards with diligent care:

Mark Cokeing, Ewart Grove, Carla Plemich, Joseph Puretz, Richard Scholl, Kathryn Severin, Alan Snelson, Daman Walia, of the IIT Research Institute.

For being our professional rockhound, mineral authority, and advisor:

Bertram G. Woodland, the Field Museum.

For being a continual source of enthusiasm, encouragement and excellence:

Janet Haartz, the National Institute for Occupational Safety and Health.

CONTENTS

FIGURES

TABLES

SECTION 1

INTRODUCTION

The National Institute for Occupational Safety and Health (NIOSH) has the responsibility for developing and recommending analytical methods for monitoring workplace contaminants. These workplace contaminants include various mineral dusts in a broad variety of industrial environments.

Reference standards are the key to developing instrumental or chemical methods of analyses for these contaminants. Standards are needed not only to provide reliable reference spectra but also to test and evaluate candidate methods of analysis. Therefore, the optimum mineral standards are those that are free of impurities and have a particle size distribution similar to those found in the workplace.

Currently, standards are needed for asbestos and silica--minerals that are widely used and processed in industry or that occur as byproduct contaminants. The asbestos minerals include chrysotile, crocidolite, fibrous grunerite (amosite), and the fibrous varieties of anthophyllite and tremolite. They also occur as the nonfibrous species--antigorite, riebeckite, cummingtonite/grunerite, anthophyllite, and tremolite. Nonfibrous minerals are needed as standards to develop analytical methods that can distinguish between both forms, which can and do occur in the same raw materials. Tremolite-free talc is also needed to establish analytical methods for determining the concentration of tremolite in talc.

The standards needed for silica include polymorphs of silicon dioxide--quartz, cristobalite, and tridymite--chemically similar minerals that often occur in the same working environment. The last important group of standards includes fluorite, beryl, and nickel oxide (bunsenite), which are used as internal standards in current analytical methods for the analysis of the silica polymorphs.

No high purity standards are available for these 18 minerals, especially in the size ranges encountered as industrial dusts. Without these standards, there is little hope of developing reliable and sensitive analytical methods to monitor the safety of workplace environments.

In an effort to obtain these standards, NIOSH awarded a contract to the IIT Research Institute (IITRI) to obtain, prepare, and characterize each of the 18 minerals as phase-pure powders. More than 100 mineral specimens--obtained from mineral and industrial suppliers, museums, the National Stockpile, synthesis, and through field sampling--were screened to identify analytically the best specimen of each of the 18 mineral types. These samples were then ground to the desired particle size, treated to remove residual impurities, and analyzed for conformity to mineral species in order to produce an adequate supply of standards for analytical methods development.

SECTION 2

REFERENCE MINERALS CRITERIA

The 18 minerals required as standards are shown in Table 1. These minerals were organized in four groups, which differ slightly in their standards criteria. The contract specified that the criteria include purity, particle size, and methods of characterization, which are discussed below by group. Specimens of each mineral type from four different physical locations were to be evaluated in order to choose the best candidates for producing the standards.

GROUP 1: QUARTZ, CRISTOBALITE, TRIDYMITE, NICKEL OXIDE (BUNSENITE), FLUORITE, AND BERYL

Purity

The purity shall be greater than 99 percent as inferred from infrared and x-ray diffraction analyses. The silica polymorphs shall be free of each other and from noncrystalline silica.

Particle Size

The materials shall be ground to a mass median aerodynamic diameter between 0.5 and 5.0 μm, with a geometric standard deviation greater than 1.4 but less than 4.0. All particles shall be less than 10 μm in diameter. Sizing shall be performed for at least 200 particles.

Characterization

(1) Each mineral shall be analyzed by x-ray diffraction (XRD) with copper K-alpha (Cu K_α) radiation at a scan rate of $\leq 0.5°$ per minute for the range 7° to 90° 2θ on a logarithmic scale at high resolution.

(2) Thermogravimetry (TG) and differential thermal analysis (DTA) runs shall be made from 25° to 1600°C with assignment of transitions.

(3) Infrared (IR) spectroscopy scans from 300 cm^{-1} to 1500 cm^{-1} shall be performed noting any unexpected bands and their possible cause.

Table 1. List of reference minerals.

Mineral	Chemical Formula
GROUP 1	
Quartz	SiO_2
Cristobalite	SiO_2
Tridymite	SiO_2
Nickel Oxide (Bunsenite)	NiO
Fluorite	CaF_2
Beryl	$Be_3Al_2(SiO_3)_6$
GROUP 2	
Chrysotile	$Mg_3Si_2O_5(OH)_4$
Crocidolite	$Na_2Fe_5Si_8O_{22}(OH)_2$
Fibrous Grunerite (Amosite)	$(Fe,Mg,Mn)_7Si_8O_{22}(OH)_2$
Fibrous Anthophyllite	$(Mg,Fe)_7Si_8O_{22}(OH)_2$
Fibrous Tremolite	$Ca_2Mg_5Si_8O_{22}(OH)_2$
GROUP 3	
Antigorite	$Mg_3Si_2O_5(OH)_4$
Riebeckite	$Na_2Fe_5Si_8O_{22}(OH)_2$
Grunerite	$(Fe,Mg,Mn)_7Si_8O_{22}(OH)_2$
Cummingtonite	$(Mg,Fe)_7Si_8O_{22}(OH)_2$
Anthophyllite	$(Mg,Fe)_7Si_8O_{22}(OH)_2$
Tremolite	$Ca_2Mg_5Si_8O_{22}(OH)_2$
GROUP 4	
Talc	$Mg_3(Si_2O_5)_2(OH)_2$

GROUP 2: CHRYSOTILE, CROCIDOLITE, FIBROUS GRUNERITE (AMOSITE), FIBROUS ANTHOPHYLLITE, AND FIBROUS TREMOLITE

Purity

The minerals shall be free of their corresponding nonfibrous varieties and from other asbestos minerals, as shown by polarized light microscopy and XRD.

Particle Size

The minerals shall have a median fiber length in the range of 2 to 10 μm with no fibers longer than 200 μm. A minimum of 200 fibers shall be sized.

Characterization

(1) Each mineral shall be analyzed by XRD with Cu K_α radiation at a scan rate of $\leq$0.5° per minute for the range 7° to 90° 2θ on a logarithmic scale at high resolution.

(2) TG and DTA runs shall be made from 25° to 1600°C with assignment of transitions.

(3) Photomicrographs shall be provided for each mineral showing the typical particle morphology.

GROUP 3: ANTIGORITE, RIEBECKITE, GRUNERITE, CUMMINGTONITE, ANTHOPHYLLITE, AND TREMOLITE

Purity

The minerals shall be free of asbestos fibers and other asbestos minerals as shown by polarized light microscopy and XRD.

Particle Size

The materials shall be ground to a mass median aerodynamic diameter between 0.5 and 5.0 μm, with a geometric standard deviation greater than 1.4 but less than 4.0. All particles shall be less than 10 μm in diameter. Sizing shall be performed for at least 200 particles.

Characterization

(1) Each mineral shall be analyzed by XRD with Cu K_α radiation at a scan rate of $\leq$0.5° per minute for the range 7° to 90° 2θ on a logarithmic scale at high resolutions.

(2) TG and DTA runs shall be made from 25° to 1600°C with assignment of transitions.

(3) Photomicrographs shall be provided for each mineral showing the typical particle morphology.

GROUP 4: TALC

Purity

The standard shall be free of asbestos, tremolite, and free silica.

Particle Size

The mineral shall be ground to a mass median aerodynamic diameter between 0.5 and 5.0 μm, with a geometric standard deviation greater than 1.4 but less than 4.0 All particles shall be less than 10 μm in diameter. Sizing shall be performed for at least 200 particles.

Characterization

(1) The mineral shall be analyzed by XRD with Cu K_α radiation at a scan rate of <0.5° per minute for the range 7° to 90° 2θ on a logarithmic scale at high resolution.

(2) TG and DTA runs shall be made from 25° to 1600°C with assignment of transitions.

(3) An IR spectroscopy scan from 300 cm^{-1} to 1500 cm^{-1} shall be performed noting any unexpected bands and their possible cause.

STANDARDS QUANTITIES

Each ground and characterized mineral shall be supplied to NIOSH in ten 100-g lots.

CRITERIA FOR SELECTING FIBROUS SPECIMENS

The term "fibrous" is variously applied to asbestos minerals in literature, depending primarily on the field of research (e.g., mineralogy, health effects, mining, environmental pollution, occupational exposure). The controversy surrounding the definition of "fibrous" habit and thus the correct identification of mineral particles as asbestos has been fully discussed at the workshop on asbestos sponsored by the National Bureau of Standards (NBS) in July 1977.[1]

It was thus necessary for us to define the concept of "fibrous" at the start of the program in order to clarify which mineral specimens were to be acquired and processed as standard reference asbestos minerals. For the purposes of the program we agreed to apply the mineralogical criteria for distinguishing the fibrous from the prismatic nonfibrous habit of each mineral type. In the mineralogical criteria, macroscopic specimens are classified as fibrous if:

- elongated crystal types grouped in bundles with all individual crystals being parallel predominate;

- individual crystals becoming progressively smaller in diameter (short dimension) may be readily teased (i.e., with a needle) from the elongated crystal bundles;

- small (diameter) crystal bundles and the individual crystals teased from them are easily flexed along the elongated dimension without breaking.

Although the prismatic form of a mineral may occur in groups of elongated crystals, the individual crystals comprising the group are not parallel (e.g., they radiate outward from one common point), and they cannot be easily teased to produce smaller diameter crystals. More rigorous techniques are required to separate individual particles from the bundles, and the individual particles separated cannot be flexed.

A fuller explanation of selection of fibrous and nonfibrous specimens of one mineral type is given in the paper written during the course of the program[2] that was presented at the NBS symposium.[1]

SECTION 3

SAMPLE SOURCES

GEOLOGICAL OCCURRENCE

The natural geological occurrence of most of the mineral types sought for this study is widespread throughout North America as well as in the rest of the world.[3-9] Some of these minerals, however, occur as recoverable deposits in relatively small locales of specific continents. For the purpose of this program, three mineral types (cristobalite, tridymite, and bunsenite) do not occur naturally in sufficiently pure form, or large enough quantities, or both.

The abundance, locale of occurrence, and purity of natural deposits dictated in part the approach taken to obtain specimens of the desired minerals. The decision not to hand-collect specimens of each mineral type was primarily determined by the financial limitations of the study. In addition, specimens collected in one area of a mineral field can differ completely from those collected only a few meters away, and mineral fields are not permanent (e.g., covered over by a housing development). Hand collection thus offers no advantage over commercial suppliers in being able to provide specimens from the same sources years later.

The natural occurrences of each of the mineral types required are described in the following sections.

Group 1 Minerals

Quartz--

Quartz, one of the most abundant minerals, occurs as an essential constituent of many igneous, sedimentary, and metamorphic rocks. It also occurs as a secondary mineral, often forming a cementing medium in sediments. Because of its chemical and physical resistance to corrosion, quartz becomes concentrated during sedimentary processes and gives rise to sands and sandstone of various types. The large, well-formed crystals of quartz usually form in igneous rocks and less frequently in metamorphic rocks.

Occurrence of relatively pure, highly crystalline quartz is widespread throughout the United States, as well as in the rest of the world. Deposits of large, well-formed, individual crystals are rare, however. Minor deposits have been reported in the United States in Arkansas, California, Idaho, New York, Virginia, and Oklahoma, and in the Malagasy

Republic, the United Kingdom, Argentina, West Germany, Uganda, and Australia. The world's principal quartz-producing districts are situated on the Brazilian great plateau underlain by Precambrian and lower Paleozoic rocks. The quartz deposits lie in the states of Minas Gerais, Goiaz, and Bahia.

Cristobalite--

Cristobalite, a high-temperature form of silica (stable above 1470°C), occurs in siliceous volcanic rocks (obsidian, rhyolite) as inclusions and in cavities within these rocks, and in basalt, metamorphosed sandstone, and opal. It is often a late product of crystallization, sometimes replacing tridymite. The mineral name is derived from an early noted locality, Cerro San Cristobal in Mexico.

Although the occurrence of cristobalite has been frequently reported, the reports typically describe microcrystals, inclusions, or well-dispersed grains. Reports of larger crystals are quite old (circa 1935) and thus the current availability of these larger crystals is unlikely. Since the mineral is of no commercial value, reports of large crystal occurrence are understandably quite old and sparse.

Tridymite--

Although tridymite is stable between 870° and 1470°C, it persists metastably in cavities in siliceous volcanic rocks (rhyolite, obsidian, and rhyolite tuft), as well as in slag, silica brick, and glass. It may be produced by the late-stage action of hot gases. Tridymite--from the Greek tridumos meaning threefold--is often found in threefold groups of twins.

Tridymite has been reported as an "abundant" mineral in some of the rhyolitic tufts of the Tertiary volcanic rocks of the San Juan region, Colorado. It is the chief silica mineral in the rhyolites and quartz latites of this region, amounting to as much as 25%, which is far below the phase purity requirements of the program. Again, lack of economic value of tridymite has minimized efforts to locate and define extensive or recoverable deposits.

Beryl--

Beryl occurs chiefly in pegmatite dikes and as a gangue mineral of tungsten and tin ores. It is an accessory mineral: the larger and richer pegmatites contain only 0.5 to 1.0% beryl. Beryl is especially abundant in scrap-mica zones where albite is the dominant mineral and, in fact, the best beryl deposits are found in those pegmatites that contain much albite.

Beryl commonly occurs as simple prismatic hexagonal crystals. The mineral is also found as equant crystals and in anhedral masses.

Beryl is produced from thousands of pegmatites, widely distributed through many countries. The Custer and Keystone districts in the Black Hills of South Dakota, Tass County in New Mexico, three districts in Colorado, and New Hampshire are the major producers of beryl in the United States. Minor deposits also occur in Connecticut, Idaho, Nevada, and

North Carolina. Major foreign producers of beryl include Brazil, Argentina, Mozambique, Uganda, Rhodesia, South Africa, and the Malagasy Republic.

Fluorite--

Fluorite is found in a wide variety of geological occurrences, evidence that it was deposited under an extended range of physical and chemical conditions. At one extreme, it is present as an accessory mineral in granites and related igneous rocks; at the other extreme, it is found as crystals in geodes and as botryoidal linings in caves. Its occurrence in igneous rocks, as well as in limestone, indicates that limestone is not essential to its deposition.

Fluorite occurs as aggregates of cubic crystals, as granular masses, and in banded or crusted veins. Economically, the most important modes of occurrence are fissure veins in igneous, metamorphic, and sedimentary rocks; stratiform replacements in carbonate rocks; replacements in carbonate rocks along contacts with acid igneous intrusives; stockworks and fillings in shattered zones; deposits in the marginal portions of carbonate and alkalic rock complexes; residual concentrations resulting from the weathering of primary deposits; and as recoverable gangue mineral in base metal deposits.

The United States is the largest producer of fluorite. The major vein deposit in the United States is the Rosiclare-Goodhope vein system along the Ohio River in southern Illinois and western Kentucky. Widely scattered, lower quality, nonvein deposits occur in Montana, New Mexico, Alaska, Utah, Colorado, Nevada, and Idaho. Outside of the United States, vein deposits of high-quality fluorite occur in the Massif Central, Maures, Esterel, eastern Pyrenees and Vosges districts of France; the Osor deposit in northeastern Spain; the Torgola deposit in northern Italy; the Muscadroxiu-Genna Tres Montis vein system in Sardinia; and the Longstone Edge-Sallet Hale deposit in England. Major nonvein deposits occur in the Coahuila, Rio Verde, San Luis Potasi, and Aguachile districts of Mexico; the Transvaal province of South Africa; Ambadongar, India; the Asturias district of northwestern Spain; and the Castel Guiliano area of Italy.

Nickel Oxide--

The nickel oxide mineral bunsenite rarely occurs naturally in large deposits. It may be found as small, isolated, hexagonal green crystals near and within nickel ore deposits.

There are only two types of commercial nickel ore deposits--residual concentrations of nickel silicates from the weathering of ultrabasic igneous rock, and nickel-copper sulfide deposits formed either by replacement or magmatic injection. A third type of nickel occurrence, as iron-nickel ore, has found little commercial development because of the low nickel content and refractory nature of the ore.

The most important nickel deposits of the world are in Canada--the Sudbury, Ontario, Lynn Lake, Manitoba, and Thompson-Moak Lake, Manitoba districts. Less important deposits occur in the ultrabasic rocks of the Ural Mountains and the sulfide deposits at Petsamo, in the Soviet Union;

residual deposits in New Caledonia; residual iron-nickel-cobalt-chromium deposits in Cuba; and low-grade ore deposits in Oregon.

Groups 2 and 3 Minerals

Although minerals in the serpentine and amphibole groups occur in metamorphic and igneous rock terrains, and in weathered sediments in close proximity to these rock types, they form only under specific geologic conditions. These conditions are fairly well defined for the serpentine and amphibole minerals of interest to the program. The specific conditions under which the rare fibrous (asbestiform) serpentine and amphibole minerals form are not well defined. Sedimentary rock deposits, invaded by molten igneous rocks or compressed by large-scale crustal movements, metamorphose from their original mineralogy to a secondary mineralogy. The secondary mineralogy depends on original and invading rock compositions, temperatures, and pressures and may contain fibrous phases. The igneous rock itself may directly crystallize into fibrous forms or may later alter to asbestiform phases.

Chrysotile and Antigorite--

Chrysotile and antigorite, as well as the other members of the metamorphic mineral group termed serpentine, are secondary minerals resulting from the alteration of magnesium-bearing minerals such as olivine, hornblende, tremolite, and augite. Serpentinite, the basic rock type primarily composed of serpentine minerals, is predominantly ascribed to late- or post-magmatic hydrothermal alteration of minerals in the ultramafic (magnesium and iron-rich) igneous rocks pyroxenite, peridotite, and dunite.

Chrysotile occurs primarily in serpentine altered from ultrabasic igneous rocks such as peridotite and dunite; a very minor portion of chrysotile occurs in serpentine altered from magnesian limestones or dolomite. The fibrous chrysotile is formed in unstressed rock; the nonfibrous antigorite tends to form when the serpentine rock is subjected to stress. Unlike most of the amphiboles, both the fibrous and nonfibrous serpentine forms are frequently found quite intermixed in serpentine rocks.

Serpentine formations are widespread throughout the world. Close examination of geological data reveals that the occurrence of the fibrous form generally coincides with the earth's major chains of mountains. The world's largest chrysotile deposits occur in the eastern townships of Quebec, Canada, and the Bazhenov, Dzhefygara, and Akfovrak districts in the Soviet Union. Smaller Canadian deposits occur in the Yukon Territory, British Columbia, Newfoundland, and Ontario. The third largest producer of chrysotile is Africa, with deposits in Rhodesia, South Africa, and Swaziland. China is suspected of having vast chrysotile deposits, but little is known of the geology of these deposits. Other areas of chrysotile production include Brazil and Columbia; Balanzero, Italy; northern Greece; Troodos, Cyprus; Yugoslavia; and New South Wales, Australia. The United States ranks sixth in chrysotile production with recoverable deposits in Eden, Vermont; Globe, Arizona; and in the Pacific (between Copperopolis and Sonora in the foothils of the Sierras) and Idria-Coalinga (Fresno County) deposits in California.

Since more than 90% of chrysotile is found in serpentine altered from ultrabasic igneous rocks, the serpentine areas containing antigorite free from fibrous forms would be those where serpentinized magnesian limestones occur, such as the New England region of the United States.

Crocidolite and Riebeckite--

Riebeckite, a member of the glaucophane-riebeckite (alkali) amphibole series, has primarily an igneous paragenesis. It occurs in granites, quartz-syenites, syenites, and nepheline-syenites. Riebeckite is also characteristically found in acid volcanic rock and in sodium-rich rhyolites. Riebeckite is reported in a few low-grade, regionally metamorphosed schists, since other members of this series are typically metamorphic in origin.

The occurrence of riebeckite is not very common. Major deposits are known in northern Nigeria and in nonmetamorphosed rocks of the Transvaal and Cape Provinces of South Africa. In the United States, riebeckite occurs in the Green River Formation of Nevada, Colorado, and Utah.

Crocidolite occurs in metamorphosed siliceous-ferruginous sediments such as the banded ironstones of South Africa. Although it is not known with certainty, this fibrous form of riebeckite is believed to be a later metamorphosism of the already formed massive mineral caused by stress (elevated temperatures and pressures). Under conditions of stress, the fibrous mineral appears to have been the more stable form.

The major deposits of crocidolite are in the Transvaal system of South Africa. Recent discoveries, which have not yet been exploited, have been made in Mysore, India. Crocidolite deposits in the Hammersley range of western Australia and at Lusaka, northern Rhodesia, have been commercially developed. Crocidolite has also been reported in Bolivia and China.

Cummingtonite-Grunerite--

The members of the cummingtonite-grunerite amphibole series are typically found in both regionally and contact-metamorphosed rocks. This mineral series generally occurs in metamorphosed iron formations but may also occur in middle grades of metamorphosed mafic igneous rocks.

Cummingtonite of regionally metamorphosed terrains is generally intimately associated with hornblende and plagioclase. Cummingtonite tends to occur only in the highly metamorphosed rocks and may result from the decomposition of hornblende into cummingtonite and plagioclase.

Cummingtonite is found in the Homestake District of the Black Hills of South Dakota and in several localities in California. Because of its unimportant commercial status, no great listing of occurrences exists in the literature. Major occurrences of geological interest have been reported in the Central Abukuma Plateau, Japan and at Teisko, Finland.

Grunerite is a characteristic mineral of metamorphosed iron-rich siliceous sediments. Where metamorphism has been dominantly regional, magnetite-grunerite-quartz schists are common. In rocks that have undergone

both thermal and regional metamorphism, grunerite may be associated with fayalite, hedenbergite, and almandine.

Grunerite, a mineral commercially important as an iron ore, occurs extensively in the metamorphosed iron formations of northern (upper) Michigan and in the Wabush Iron Formation of Newfoundland, Canada. Grunerite is also reported, though not exploited to any great extent commercially, in western Australia and Finland.

The formation and occurrence of the fibrous form of grunerite are similar to those of the fibrous form of riebeckite (crocidolite). It typically occurs in banded ironstone formations that originally contained the massive grunerite form; the fibrous form again appears to have been the more stable form under conditions of stress.

Fibrous grunerite occurs almost exclusively in the Transvaal System of South Africa. Recent reports indicate it may also be present in the newly discovered fibrous mineral deposit of Mysore, India.

Anthophyllite--

The orthorhombic amphibole anthophyllite is restricted to metamorphic and metasomatic formation; igneous parageneses are unknown. It may be found, however, within igneous rock formations.

Anthophyllite is commonly developed during the regional metamorphism of ultrabasic rocks. In this paragenesis, it occurs as a series of lenses in amphibolitized and serpentinized ultrabasic rocks. The anthophyllite is thus frequently associated with talc, olivine, phlogopite, and serpentine. In deposits resulting from magnesium metasomatism, anthophyllite occurs in schists and gneisses associated with other members of the anthophyllite-gedrite series, as well as other amphiboles, plagioclase, sillimanite, and quartz.

The best known deposit of nonfibrous anthophyllite is the Bamble formation (metasomatic origins) of Bamble, Norway. Geologic descriptions of other anthophyllite deposits in Ontario, Canada, Egypt, India, Greenland, and Japan make no distinction between fibrous and nonfibrous forms.

Although the occurrence of fibrous anthophyllite is significant, its economic importance is not nearly as great as that of chrysotile, crocidolite and fibrous grunerite, and thus the method of formation of the fibrous form versus the nonfibrous form has been given little attention. Shear stress, particularly in the ultrabasic rock occurrences, appears to be an important factor in the fiber formation. The nonfibrous anthophyllite form tends to occur mostly via the metasomatic mechanism.

Finland is the world's most important producer of fibrous anthophyllite (from metamorphosed ultrabasic rocks). Deposits are mined at Paakkila and Maljusmi. In the United States, fibrous anthophyllite is mined in Yancey County, North Carolina. Fibrous deposits have also been reported in Montana, Kamiah, Idaho, and Carville, California.

Tremolite--

Tremolite is essentially a metamorphic mineral that is particularly characteristic of regional metamorphosed rocks but also occurs in contact-metamorphosed rocks. In one type of occurrence, tremolite is an early product of the thermal metamorphism of dolomite containing silica impurities; calcite is a typical byproduct of the reactions producing the tremolite. Continued metamorphosis converts tremolite to diopside, among other minerals, depending upon the availability of silica. Tremolite also occurs in regionally metamorphosed carbonate rocks and in low-grade, regionally metamorphosed ultrabasic igneous rocks. In this latter rock type, residual amounts of olivine and pyroxene, from which the tremolite was derived, as well as talc, carbonates, serpentine, and chlorite, which are later alteration products of tremolite, commonly occur with the tremolite.

Although in mineralogical descriptions tremolite is indicated to be "commonly fibrous" in habit, the truly gross (macroscopic) fibrous morphology is rarely seen. Thus, extensive investigations into the mechanism of formation of the truly fibrous versus nonfibrous forms have not been made. Perhaps the characterization of "fibrous habit" lies in the high degree of cleavage along the vertical axis of the prisms of this mineral.

Because the descriptions of the habit of occurrence of tremolite are ambiguous, and because of termolite's minimal commercial value, few detailed descriptions of locales of occurrence of the fibrous versus nonfibrous variety exist. The only locales of occurrence of economically important fibrous tremolite are reported to be in Italy, in the Sondria (near Milan) and Aosta (near Turin) districts, and in India, in the states of Rajasthani and Saraikela. Deposits of apparent massive tremolite (so labeled because macroscopic bundles of flexible fibers are not evident) are reported in the New England states in association with talc deposits, and in the Black Hills of South Dakota.

Group 4 - Talc

Talc commonly forms during hydrothermal alteration of ultrabasic igneous rocks and low-grade thermal metamorphism of siliceous dolomites. It thus occurs in regionally metamorphosed limestones, altered ultrabasic igneous rocks, and in contact metamorphic zones adjacent to basic igneous rocks; it is typically late in the mineral formation sequence.

The formation of talc-rich schists by hydrothermal alteration of ultrabasic rocks is described as steatization, a process commonly but not always associated with serpentinization (one can occur without the other). In ultrabasic rocks, talc commonly occurs as lenticular veins and along faults and shear planes.

Talc is the first new mineral to form as the result of thermal metamorphism of siliceous dolomites. Mineral sets are typically talc-calcite-dolomite and talc-calcite-quartz. At a higher grade of metamorphism, talc is replaced by tremolite.

In addition to the extensive deposits in the United States, talc deposits are found in many countries. Good-quality talc ores are found in Africa, Canada, Australia, China, Finland, France, Greece, Italy, North and South Korea, Manchuria, Norway, Romania, Sardinia, and the Soviet Union. France, Italy, Norway, and India are the most important sources except for the United States and the Communist countries.

In the United States, there are 11 states with major talc deposits: California, Georgia, Maryland, Montana, Nevada, New Mexico, New York, North Carolina, Texas, Vermont, and Virginia. Talc varies in origin throughout the United States. The basis of classifying talc as likely of being serpentine and amphibole-free cannot be eastern-versus-western-United States-derived, since talc deposits containing, or free of, potential asbestiform minerals occur in all areas of the United States. The specific geographical (and thus geological) origin of a talc sample must be known if its likelihood of containing asbestos-related minerals is to be determined.

SPECIMEN SOURCES

The task of obtaining specimens of each mineral from at least four different geographic locations proved to be formidable. The data on geological occurrence indicated in some instances that it would not be possible to obtain multiple samples from distinctly different geographical areas simply because the minerals occurred as recoverable or accessable deposits in only one or two locales. For example, crocidolite and fibrous grunerite are almost strictly confined to the Transvaal area of South Africa. In these cases, specimens were obtained from several commercial suppliers out of separate mines. Geographical occurrence data also dictated the acquisition of synthetic samples of nickel oxide, cristobalite, and tridymite since no known reasonably pure and recoverable natural deposits of these minerals exist. For most of the required minerals, however, the data indicated the existence of multiple natural deposits sufficiently pure and large for commercial exploitation (for mineral types of commercial value) or field sampling (for mineral types of no commercial value).

Most of the mineral specimens were obtained through letter and telephone contacts with mineral dealers, commercial mining companies, museums, and governmental agencies. A few specimens were also obtained by field sampling.

Source contacts were obtained through text references[10-20] and personal contacts. Discussions with Dr. Bertram Woodland of the Chicago Field Museum of Natural History (consultant to the program); Sarkis G. Ampian and Robert S. Clifton of the U.S. Bureau of Mines; Mr. George Jameson, Director of Stockpile Disposal, General Services Administration; and Dr. John S. White, Jr. of the Smithsonian Institution provided additional valuable information on sources for mineral specimens.

The suppliers of the mineral specimens for the study are listed in Table 2; the specimens received for study are summarized in Table 3. Appendix 1 lists sources that were contacted but could not supply specimens.

Table 2. Mineral specimens and their sources.

Supplier	Mineral	Locale	IITRI No.*
Mineral Dealers:			
Wards Natural Science Establishment	Quartz	Brazil	Q-2
		Arkansas	Q-3
Rochester, N.Y. 14603	Beryl	Afghanistan	B-12
	Fluorite	Illinois	F-16
	Cristobalite	California	CB-24
	Tridymite	Sicily	TY-26
	Crocidolite	South Africa	CR-34
	Fibrous Grunerite	South Africa	GF-38
	Fibrous Anthophyllite	North Carolina	AF-43
		Montana	AF-45
	Fibrous Tremolite	Indiana	TF-48
	Antigorite	Maryland	AG-53
	Riebeckite	Colorado	R-60
		South Africa	R-62
	Tremolite	New York	T-78
	Talc	Ontario	TA-91
		New York	TA-92
Mackinaw Geological Supply	Fibrous Anthophyllite	Canada	AF-42
	Antigorite	Michigan	AG-51
P.O. Box 375	Riebeckite	Michigan	R-59
Ishpeming, Mich. 49849	Grunerite	Michigan	G-64
	Tremolite	Michigan	T-75
Mr. John Carter	Beryl	South Dakota	B-11
608 St. Cloud Ave.	Grunerite	South Dakota	G-63
Rapid City, S. Dak.	Cummingtonite	South Dakota	C-71
57701	Tremolite	South Dakota	T-77
Minerals Unlimited	Fibrous Anthophyllite	Maryland	AF-47
P.O. Box 877	Grunerite	South Dakota	G-67
Ridgecrest, Cal. 9355	Cummingtonite	South Dakota	C-72
Winnies Treasure Shop	Tremolite	Canada	T-80
22 Bridge St.			
Bancroft, Ont.			
Canada			
Heinz Windisch	Tremolite	Canada	T-81
Worldwide Minerals			
Philipsburg, Que.			
Canada			

*Specimen number assigned by IIT Research Institute for this study.

Table 2. (continued)

Supplier	Mineral	Locale	IITRI No.
L.I. Cowan Mineral Co. 72 Morrow Road Barrie, Ont. Canada	Tremolite	Canada	T-82
Commercial Mining Companies:			
Brush-Wellman Co. 17876 St. Clair Ave. Cleveland, O. 44110	Beryl	Africa Brazil	B-9 B-10
Ozark Mahoning Co. Box 57 Rosiclare, Ill. 62982	Fluorite	Illinois	F-14
Tamora Mining Co. Wiley Cochran Rosiclare, Ill. 62982	Fluorite	Illinois	F-15
Jaquays Mining 1219 S. 19th Ave. Phoenix, Ariz. 85009	Chrysotile	Arizona	CH-28
Union Carbide Corp. Calidria Asbestos P.O. Box 579 Niagara Falls, N.Y. 14302	Chrysotile Antigorite	California California	CH-29 AG-52
Cassiar Asbestos Co. Cassiar, B.C. Canada	Chrysotile	British Columbia	CH-33
Iron Ore Co. of Canada Labrador City, Nfld. Canada	Grunerite Grunerite Grunerite	Newfoundland Newfoundland Newfoundland	G-68 G-69 G-70
Reserve Mining Silver Bay, Minn. 55614	Cummingtonite	Minnesota	C-73
Johnson & Johnson Co. Route 1 New Brunswick, N.J. 08903	Talc	Vermont	TA-97

Table 2. (continued)

Supplier	Mineral	Locale	IITRI No.
Commercial Chemical Companies:			
Sobin Chemical Co. Sobin Park Boston, Mass. 02210	Quartz	North Carolina	Q-1
Sawyer Research 35400 Lakeland Blvd. Eastlake, O. 44094	Quartz	Synthetic	Q-5
Pennsylvania Glass Sand Corp. 3 Penn Center Pittsburgh, Pa. 15235	Quartz	Commercially Processed	Q-106 Q-107
Baker Chemical Co. Phillipsburg, N.J. 08865	Fluorite Nickel Oxide	Synthetic Synthetic	F-17 N-108
Johnson Matthey Co. London, England	Nickel Oxide	Synthetic	N-20 N-22
Fisher Scientific Co. Fair Lawn, N.J. 07410	Nickel Oxide	Synthetic	N-21 N-23
Governmental Agencies:			
Stockpile Inspect. Division General Services Administration (GSA) Washington, D.C. 20406	Quartz Beryl Fluorite Chrysotile Crocidolite Fibrous Grunerite Talc	Unknown India Illinois Rhodesia South Africa South Africa India	Q-6 B-13 F-19 CH-30 CR-35 GF-40 TA-98
Montana Bureau of Mines Butte, Mt. 59701	Quartz Fluorite Talc	Montana Montana Montana	Q-7 F-18 TA-99
National Research Institute for Occupational Disease (NRIOD) P.O. Box 4788 Johannesburg 200, South Africa	Quartz Chrysotile Crocidolite Fibrous Grunerite	South Africa Rhodesia South Africa South Africa South Africa South Africa South Africa	Q-8 CH-31 CH-32 CR-36 CR-37 GF-39 GF-41

Table 2. (continued)

Supplier	Mineral	Locale	IITRI No.
(NRIOD) (cont.)	Fibrous Anthophyllite	Finland	AF-46
	Antigorite	South Africa	AG-58
	Riebeckite	South Africa	R-61
	Grunerite	South Africa	G-65
Institute of Occupational Health of Finland Haartmaninkatu 1, 00290 Helsinki 29, Finland	Fibrous Anthophyllite	Finland	AF-105
Dr. Janet Haartz National Institute for Occupational Safety and Health (NIOSH) Cincinnati, O. 45226	Talc	Sierra	TA-101
Dr. John Moore National Institute of Environmental Health Sciences Research Triangle Park, N.C. 27711	Tremolite	New York	T-79
Museums:			
Field Museum of Natural History Chicago, Ill.	Fibrous Tremolite	Alaska	TF-49
	Fibrous Tremolite	Italy	TF-50
Mineralogisk-Geologisk Museum of Norway Sars Gate 1 Oslo 5, Norway	Anthophyllite	Norway	A-102
		Norway	A-103
Field Collections:			
Dr. Bertram Woodland Field Museum of Natural History Chicago, Ill.	Quartz	Pennsylvania	Q-4
	Fibrous Anthophyllite	Pennsylvania	AF-44
	Antigorite	Pennsylvania	AG-54
		Pennsylvania	AG-55
		Pennsylvania	AG-56
		Pennsylvania	AG-57
	Grunerite	Minnesota	G-66
	Anthophyllite	England	A-104
	Tremolite	Pennsylvania	T-76

Table 2. (concluded)

Supplier	Mineral	Locale	IITRI No.
Dr. Woodland (cont.)	Talc	Pennsylvania	TA-93
		New Jersey	TA-94
		New York	TA-95
		Pennsylvania	TA-96
Special Synthesis:			
Dr. Rustum Roy Materials Research Laboratory Pennsylvania State University University Park, Pa.	Cristobalite		CB-25
	Tridymite		TY-27

Table 3. Mineral specimens obtained for evaluation.

	IITRI Code Prefix	No. of Specimens Obtained	No. of Geographical Locations Represented	No. of Synthetic Samples
Group 1				
Quartz	Q	10	6*	3
Beryl	B	5	5	-
Fluorite	F	6	2*	1
Nickel Oxide (Bunsenite)	N	5	0	5
Cristobalite	CB	2	1	1
Tridymite	TY	2	1	1
Group 2				
Chrysotile	CH	6	5	-
Crocidolite	CR	4	1	-
Fibrous Grunerite (Amosite)	GF	4	1	-
Fibrous Anthophyllite	AF	7	6	-
Fibrous Tremolite	TF	3	3	-
Group 3				
Antigorite	AG	8	8	-
Riebeckite	R	4	3	-
Grunerite	G	8	6	-
Cummingtonite	C	4	2	-
Anthophyllite	A	3	3	-
Tremolite	T	8	5	-
Group 4				
Talc	TA	10	9	-

* Unknown geographical source for one sample.

CRISTOBALITE AND TRIDYMITE SYNTHESIS

Since the natural cristobalite and tridymite samples were of low purity and could not be beneficiated, it was necessary to synthesize them. The syntheses were performed at the Materials Research Laboratory, the Pennsylvania State University, University Park, Pennsylvania, under the direction of Professor Rustum Roy.

Cristobalite was prepared by sintering reagent grade silicic acid in platinum crucibles at a temperature of approximately 1475°C. Sintering periods of 24 hours were sufficient for formation of the well-crystallized stable form.

Tridymite was prepared by fusing sodium carbonate and reagent grade silicic acid. The stable tridymite-sodium silicate (Na_2O-SiO_2) that formed was washed extensively with water to dissolve the glassy sodium silicate.

The phase diagram for the Na_2O-SiO_2 system is shown in Figure 1. The specific procedures for formation of the silica polymorphs follow.

Cristobalite and Tridymite Synthesis

The reagent for preparing cristobalite was Baker reagent grade silicic acid n-hydrate; the manufacturer's assay for the specific lot used appears in Table 4.

Table 4. Assay of Baker's reagent grade silicic acid n-hydrate.

Lot #512968	Assay, %
SiO	85.5
non-volatile HF	0.1
chloride (Cl)	<0.01
sulfate (SO_4)	<0.005
heavy metals (as Pb)	<0.002
iron (Fe)	<0.001
loss on ignition (as H_2O)	14.5

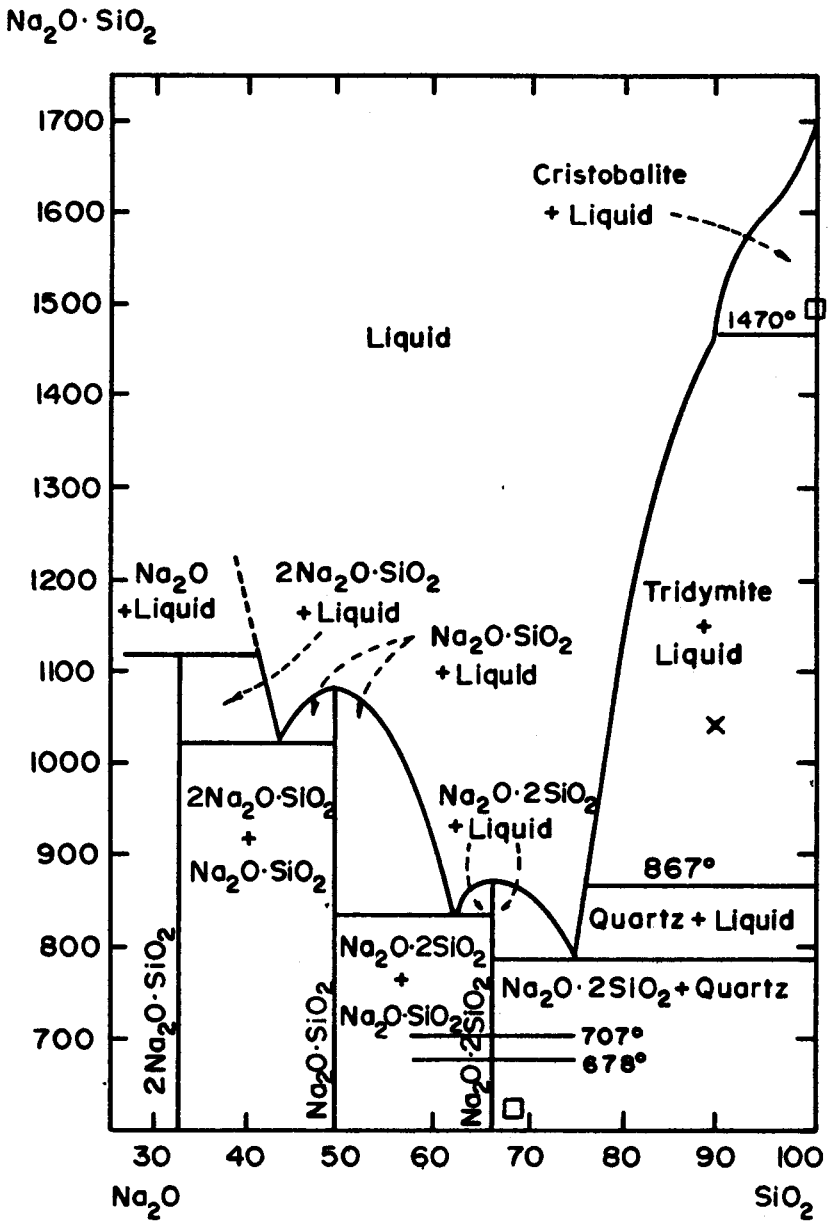

□ Cristobalite: temperature and composition used

× Tridymite: temperature and composition used

Figure 1. System SiO_2-$2Na_2O{\cdot}SiO_2$.

The synthesis proceeded by steps:

1. Silicic acid was dehydrated for approximately 6 hours at 380°C in a pot furnace.

2. The dehydrated silicic acid was prereacted in platinum crucibles at 1200°C in a Globar furnace; this resulted in the formation of disordered cristobalite.

3. The disordered cristobalite from step 2 was heat-treated for 24 hours at 1500°C to form ordered 3-C cristobalite.

4. No further treatment of cristobalite was found necessary.

The synthesis of tridymite employed the same lot of Baker reagent grade silicic acid n-hydrate that was used for cristobalite along with anhydrous sodium carbonate.

The manufacturer's assay of the specific lot of sodium carbonate used appears in Table 5.

Table 5. Assay of anhydrous sodium carbonate.

Lot #752763	Assay, ppm
iron (Fe)	2
silica (SiO_2)	20
chloride (Cl)	5
arsenic (As)	0.2
insoluble matter	80
loss on heating (285°C)	2000
nitrogen compounds (as N)	10
phosphate (PO_4)	3
sulfur compounds (as SO_4)	10
ammonium hydroxide	7
calcium and magnesium	7
potassium (K)	20
heavy metals (as Pb)	2

The synthesis proceeded in steps:

1. Silicic acid was dehydrated for approximately 6 hours at 380°C in a pot furnace.

2. Sodium carbonate (Na_2CO_3), in the weight ratio of 1:10, was added to the dehydrated silicic acid, and the mix was homogenized by gentle stirring in a porcelain mortar.

3. The silicic acid-Na_2CO_3 mix was reacted in platinum crucibles at 1050°C for 6 hours.

4. The product was gently crushed and rehomogenized in an agate mortar.

5. The product was heated at 1050°C for an additional 16 hours to complete the reaction.

6. To remove the sodium silicate glass phase ($Na_2O \cdot nSiO_2$), the final product was washed in boiling distilled water for 3 days. The water was stirred with Teflon-covered magnetic stirrers and decanted periodically. Sodium silicate glasses are water soluble when the weight ratio of Na:Si is approximately 2.

7. Throughout the wash process, the tridymite was monitored optically. Washing continued until the isotropic glass phase was visibly less than 1% of all the particles.

Phase Confirmation Analysis

The final product of each of the 10 reaction lots of cristobalite and 24 lots of tridymite was analyzed by the techniques below to assure the chemical and phase purity of each lot.

Individual lots were kept separate throughout their preparation. This was necessary since the character of each lot varied slightly because of the characteristic polytypism of the silica polymorphs. The cristobalite is, for the most part, 3-C ordered cristobalite. The tridymite is somewhat more variable, consisting predominantly of tridymite-S (stable) but undoubtedly containing some tridymite-M (metastable).

A petrographic microscope, with the use of immersion oils and a monochromatic sodium light source, was employed to determine general optical characteristics and to check the phase purity of each lot visually.

A General Electric wide-range x-ray diffractometer (Cu K_{α_2} radiation, Ni filter) was used for phase identification and to check for phase purity of each lot.

A DuPont 900 Thermal Analyzer provided differential thermal analysis (DTA) curves in order to verify the phase purity and the identity of each lot of cristobalite and tridymite. A tin reference (M.P. 231.85°C) was used with cristobalite and an indium reference (M.P. 156°C) with tridymite.

A semi-quantitative emission spectrographic analysis determined the chemical purity of each lot, especially the lots of tridymite, which required sodium flux in their synthesis. The absence of sodium in the chemical analysis, therefore, indicated phase as well as chemical purity. In addition, a Perkin-Elmer 612 Ratio Comparator Grating Spectrophotometer was used to check the phase purity and identity of each lot.

Heavy liquid density separation of the glass phase from the tridymite was attempted but was found impractical on a large scale because the density of the two phases (approximately 2.26 g/cm^3) is almost identical. It did, however, serve as a general indicator of phase purity and established that quartz (density = 2.65 g/cm^3) was not an impurity phase.

Discussion of Analyses

Because of the variability in particles which resulted from the crystallographic complications accompanying phase inversions, a detailed optical microscope characterization of individual lots was considered impractical and unnecessary. The following general characteristics noted for each lot are sufficient for identification and a check of phase purity.

Euhedral cristobalite particles were unstressed, sometimes twinned, lath-shaped particles of low first-order gray birefringence. They possessed an average index of refraction of approximately 1.485, were uniaxial, negative in sign, and displayed parallel extinction. Quartz was not found as an impurity. It would have been very conspicuous due to its higher index of refraction (approximately 1.54), slightly higher first-order gray birefringence, and positive sign.

Euhedral tridymite particles were, for the most part, unstressed and consisted of laths and twinned, wedge-shaped sectors that varied in proportion among lots. They possessed a first-order gray birefringence and an average refractive index of approximately 1.47. Extinction was parallel to subparallel. Gas bubbles as inclusions were present in varying degree for each lot. Glass, present as an impurity in amounts less than 1%, was conspicuous by its considerably different index of refraction, isotropic character, and irregular, anhedral shapes. The optical microscope method thus provides a very sensitive means of detection of this glass phase.

Each lot was scanned by x-ray diffraction (XRD) from 60° to 10° 2θ (Cu K_α radiation) for identification and as a check for unwanted phases. None was found. The critical range of 25° to 18° was rescanned for positive identification of the critical peaks. Additional XRD patterns of artificial mixes were run to determine the detectability of quartz in cristobalite and quartz, glass, and cristobalite as impurities in tridymite. It was found that the prominent (101 plane) quartz peak at 26.66° 2θ would be conspicuous in the patterns of either cristobalite or tridymite when quartz was present even in amounts less than 5%. As this peak was not detectable in any of the lots, quartz was not considered an impurity, confirming optical results. Figure 2 illustrates the peak for 10%, 5%, and 2% quartz in tridymite.

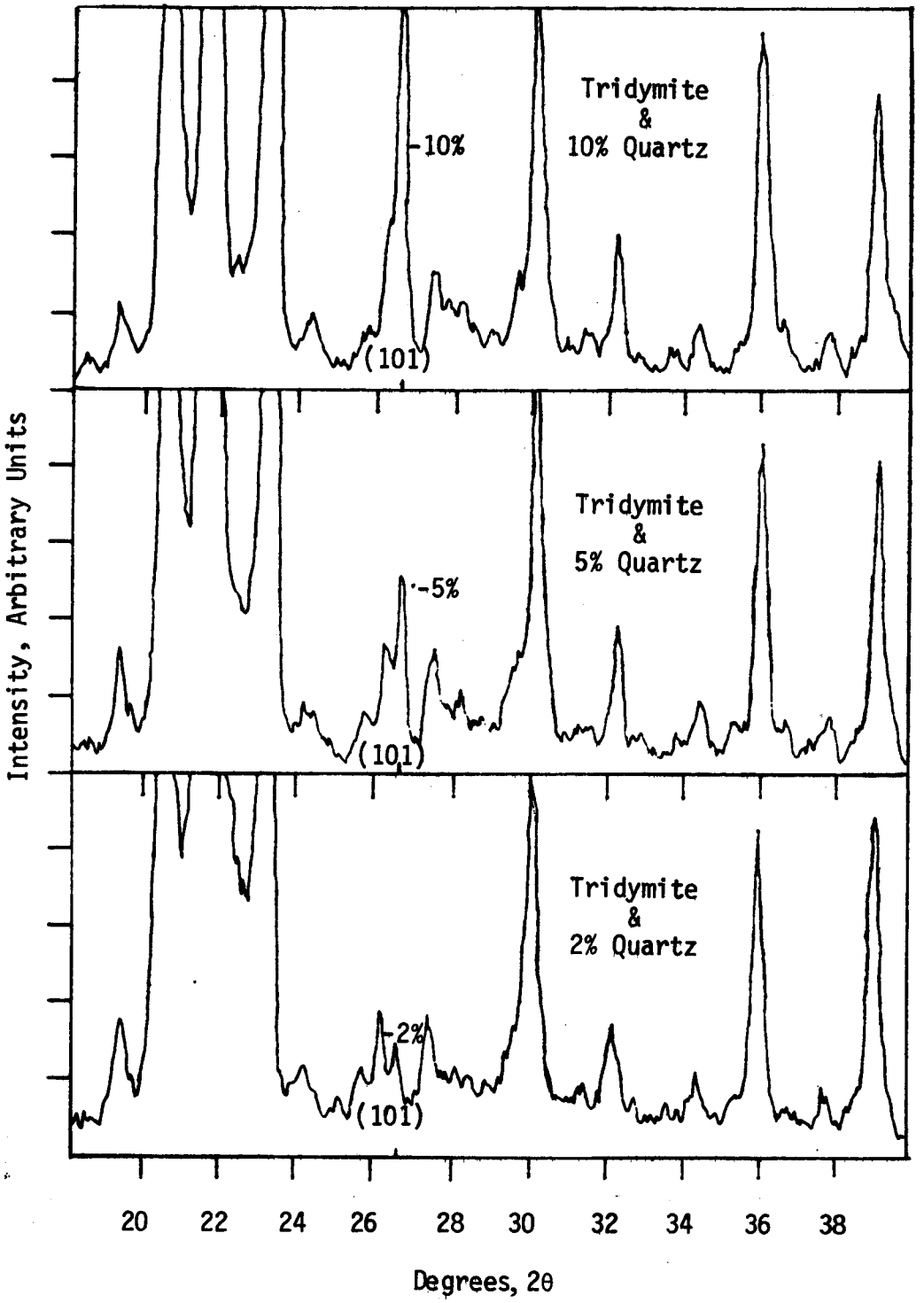

Figure 2. Detectability of quartz in tridymite on basis of (101) peak of quartz. Mixtures are of 10%, 5%, and 2% quartz in tridymite, batch #19, Cu K_α, 2° θ/min.

Removal of the glass phase by washing was evident from the reduction in the diffuse background of the tridymite XRD patterns when patterns from washed and unwashed samples of each lot were compared.

The detectability of cristobalite in tridymite is illustrated in Figure 3. The (102 plane) peak of cristobalite at 31.49° 2θ may be detected for amounts somewhat less than the 10% illustrated. If a lot was suspicious, it was possible to resolve the prominent (100 plane) cristobalite peak at 21.45° 2θ and the (100 plane) tridymite peak at 21.64° 2θ by slow scans at 0.4°/min 2θ. The cristobalite XRD pattern closely matches the JCPDS pattern, File No. 11-695, for 3-C cristobalite.

The minor peaks of tridymite are known to vary considerably. In the present case, because of the mixed polytype nature of each lot of tridymite, an invariable XRD pattern was neither expected nor found. The identification of tridymite is, however, unmistakable, and the peaks match closely those of JCPDS File No. 18-1170.

DTA patterns were examined for most lots. The method of tangents has been used to calculate inversion temperatures and are, therefore, a little less than the commonly reported peak temperatures, which are based on peak apices.

Cristobalite can be identified when, on heating, an endothermic peak appears in the range 255° to 260°C, representing the α to β inversion of cristobalite and, on cooling, the reverse inversion occurs in the range 230° to 237°C. The slight temperature variation is a function of the degree of ordering within the crystal lattices of the particles of the various lots. The lack of any other peaks in the DTA patterns, especially those for quartz or tridymite, verifies the phase purity of the cristobalite.

Tridymite is characterized by the occurrence of two endothermic peaks in the ranges 104.6° to 112.6°C (representing the α to β inversion of tridymite) and 153.6° to 159.6°C (representing the β_1 to β_2 inversion) and their separation by approximately 46°. These temperatures correspond to the commonly reported 117°C and 163°C peak temperatures for these two displacive phase changes. When tridymite exists completely in the stable form, the designation for the two phase changes is more properly: $S_{II} \rightarrow S_{III}$ at 113°, and $S_{III} \rightarrow S_{IV}$ at 138°C.

Artificial mixtures of tridymite and cristobalite were analyzed by DTA to check the detectability of cristobalite in tridymite (Figure 4). It was determined that 10% cristobalite in tridymite is very easily detected; considerably smaller amounts would also be detected. All tridymite lots were heated beyond the α to β cristobalite inversion temperature of 260°C as a check for this possible impurity in tridymite. No peak was encountered; the tridymite is, therefore, phase pure with respect to cristobalite for all lots. No other impurity phases were encountered in the range of temperature up to 300°C.

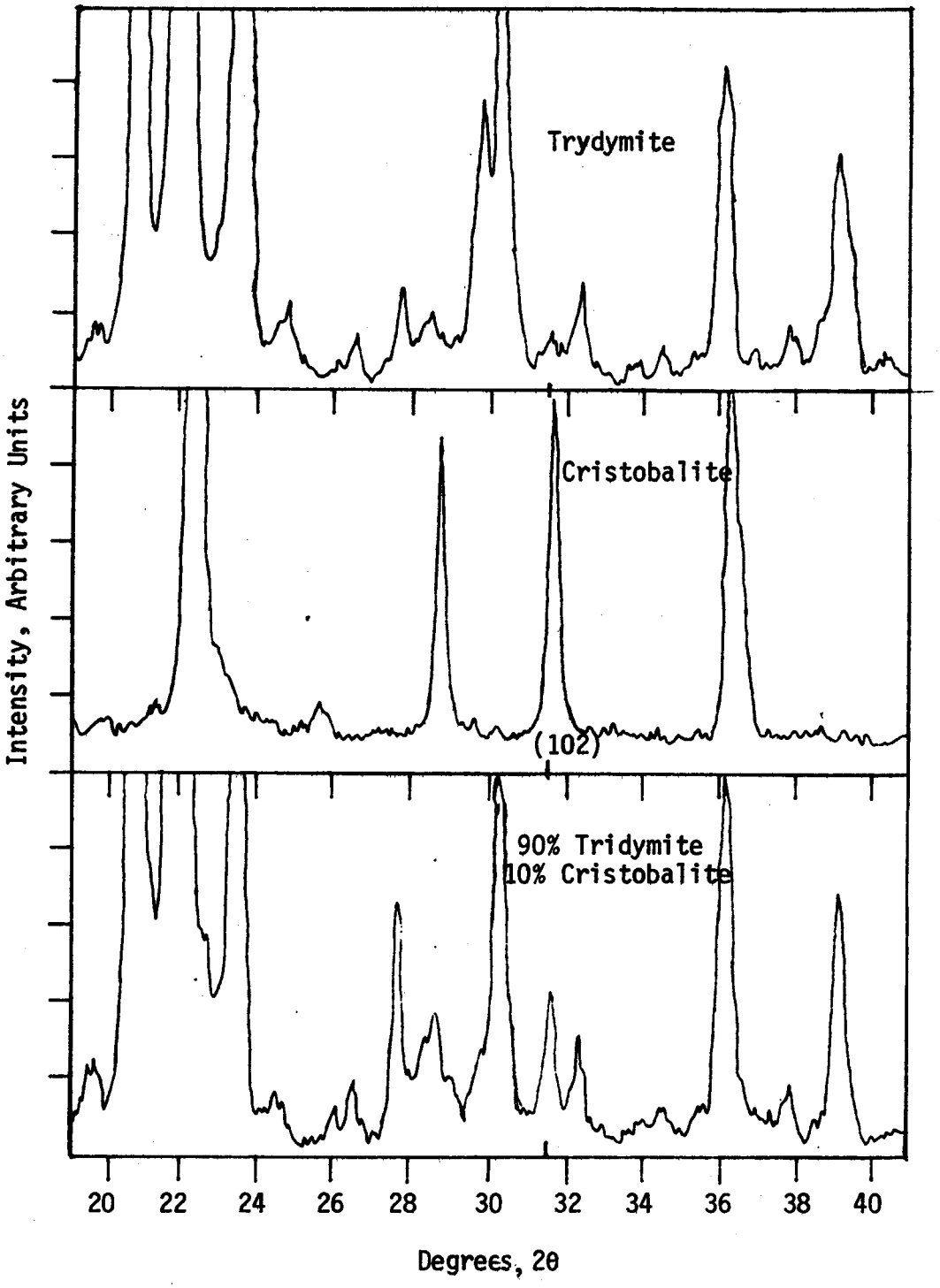

Figure 3. Detectability of cristobalite in tridymite based on the use (102) peak of cristobalite at 31.49° 2θ.

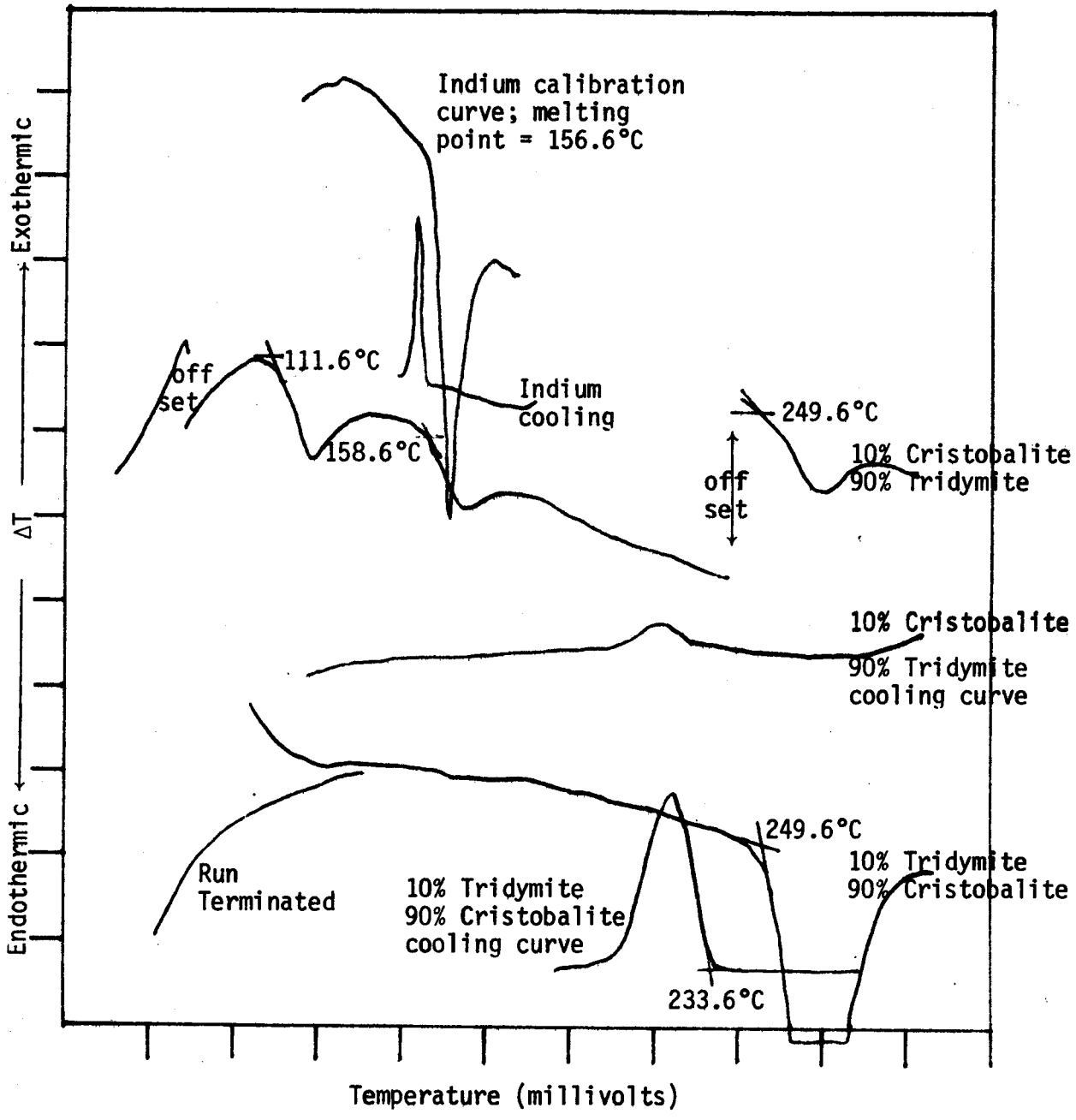

Figure 4. Thermal detectability of 10% cristobalite in tridymite.

SECTION 4

SCREENING FOR SELECTION OF BEST MINERAL SAMPLES

A minimum of four specimens of each mineral were originally to be characterized by polarized light microscopy (PLM), x-ray diffraction (XRD) and differential thermal analysis (DTA) in order to select the best specimens for processing as the final mineral standards. The number of mineral specimens obtained, in some cases fewer than four, as well as the first stages in specimen evaluation determined the actual number of specimens of each mineral type submitted for instrumental analysis.

The screening scheme was multi-level--i.e., the first evaluation stages dictated whether or not further characterizations need be conducted. Each specimen, upon receipt, was assigned a number, then submitted to macroscopic evaluation. Specimens which passed this first, gross scrutiny, underwent a PLM examination. Though some specimens were rejected at this stage, most were submitted to further instrumental characterization--more detailed PLM, and XRD and DTA--in order to establish sufficient data to choose the best specimen for processing as the final standard.

MACROSCOPIC EVALUATION

The macroscopic evaluation was a visual inspection of the specimen with a handheld magnifier. This inspection determined the gross purity of the specimen, the mode of occurrence of the desired mineral phase within the specimen (i.e., as fine grains dispersed within a complex rock matrix or as large crystals or masses surrounded by discrete contaminant mineral phases), morphological quality, and estimated quantity of the desired mineral phase.

For a number of reasons, several specimens were rejected from further consideration after preliminary macroscopic inspection. When the desired mineral phase occurred as fine crystals dispersed throughout the bulk rock and it was deemed either impossible or too costly to recover, the specimen was rejected. When a specimen supplied as a fibrous variety did not meet our criteria for the fibrous form (macroscopic fiber flexibility, ability to tease away finer fibers from a macroscopic bundle of apparent fibers), it too was rejected. Most frequently, however, the rejection was determined by time--several specimens that had already been instrumentally characterized proved to be of equal or better quality than the specimen just arrived, and the new specimen was then rejected.

Table 6 lists the specimens rejected after macroscopic evaluation and the reasons for rejection.

PREPARATION OF SPECIMENS FOR INSTRUMENTAL CHARACTERIZATION

Mineral specimens judged to be possible candidates for processing as final standards after macroscopic evaluation were ground for preliminary instrumental characterization. Representative portions (~100 g) of the mineral specimen, containing both the desired mineral phase and all contaminants, were submitted for grinding. Any surface encrustations of other minerals, which contaminated the specimen, were chipped away before grinding.

Particle size reduction for instrumental characterization was accomplished primarily by grinding in an agate mortar, followed by sieving through a 325-mesh (44 μm) screen. Five to 10 grams of the minus 325-mesh material were individually bottled and distributed to analysts for detailed PLM, XRD, and DTA characterizations. Several of the fibrous minerals that were supplied in a disaggregated form were prepared for instrumental characterization by ball milling.

POLARIZED LIGHT MICROSCOPY (PLM)

The specimens examined by PLM were prepared in two forms--as ground powders and as thin sections. All samples which passed macroscopic examination were prepared as ground powders. To conserve time and money, thin section analysis was performed only on those specimens that seemed to be the most likely candidates for final processing as standards, based on powder sample PLM examination, XRD, and DTA. The thin section analysis ensured that the ground powders were indeed representative of their bulk mineral specimens. Wards Natural Science Establishment prepared the thin sections, which were then examined by PLM by Dr. Bertram Woodland.

The components of each mineral specimen were then identified by PLM. Crystalline substances possess precise, definable optical properties such as color, refractive index, birefringence, interference colors, and optic sign, which can be determined by PLM. These optical properties are unique for each crystalline substance. Much of the optical data for the minerals of interest to this program (and the contaminants with which these minerals are commonly associated) has been determined and reported in the literature. Specimen components were identified by comparing observed optical properties with reported optical properties, or with optical properties observed in reference samples.

The PLM examinations also provided estimates of the quantities of each component present, and especially in the case of the fibrous and nonfibrous mineral groups, determined particle morphologies. Mass concentrations were estimated from particle sizes measured microscopically and the number concentrations of particles of each component present. Fibrous mineral specimens were evaluated for their freedom from nonfibrous asbestos mineral phases; nonfibrous specimens were evaluated for their freedom from fibrous forms.

Table 6. Mineral specimens rejected by macroscopic evaluation.

Mineral	IITRI Number	Supplier	Locale	Reasons for Rejection
Quartz	Q-6	National Stockpiles	Unknown	Late arrival
Quartz	Q-7	Montana Bureau of Mines	Montana	Contaminants occurred as dispersed phases
Beryl	B-3	National Stockpiles	India	Late arrival; contaminants occurred as dispersed phases
Fluorite	F-15	Tamora Mining	Rosiclare, Illinois	Contaminants occurred as dispersed phases; purchase price was prohibitive
Fluorite	F-18	Montana Bureau of Mines	Montana	Contaminants occurred as dispersed phases
Cristobalite	CB-24	Wards National Science Establishment	California	Cristobalite occurred as dispersed phase
Tridymite	TY-26	Wards National Science Establishment	Sicily	Tridymite occured as dispersed phase
Chrysotile	CH-32	National Research Institute for Occupational Diseases (NRIOD)	South Africa	Fibrous phase was intermixed with a nonfibrous serpentine phase
Chrysotile	CH-33	Cassiar Asbestos Company	British Columbia, Canada	Late arrival

Table 6. (continued)

Mineral	IITRI Number	Supplier	Locale	Reasons for Rejection
Fibrous Anthophyllite	AF-44	Dr. Bertram Woodland	Valley Green, Pennsylvania	Quantity of fibrous anthophyllite present was too small to warrant processing
Fibrous Anthophyllite	AF-47	Minerals Unlimited	Maryland	Specimen was too small; cost of purchasing more was prohibitive.
Antigorite	AG-52	Union Carbide Corporation	Idria Range, California	Antigorite was present as an encrustration on a mixed serpentine rock
Antigorite	AG-53	Wards National Science Establishment	Cardriff, Maryland	Antigorite occurred as a finely dispersed phase
Antigorite	AG-56	Dr. Bertram Woodland	Barren Road, Pennsylvania	Contaminants occurred as finely dispersed phases
Grunerite	G-67	Minerals Unlimited	South Dakota	Contaminants occurred as finely dispersed phases; specimen was too small
Grunerite	G-70	Iron Ore Company of Canada	Sherwood, Newfoundland	Grunerite occurred as a finely dispersed phase
Cummingtonite	C-73	Reserve Mining	Silver Bay, Minnesota	Chemical analysis was required to establish this specimen as cummingtonite
Anthophyllite	A-104	Dr. Bertram Woodland	England	Anthophyllite occurred as a finely dispersed phase

Table 6. (continued)

Minerals	IITRI Number	Supplier	Locale	Reasons for Rejection
Tremolite	T-80	Worldwide Minerals	Canada	Late arrival
Tremolite	T-81	Winnies Treasure Shop	Canada	Late arrival
Tremolite	T-82	L. I. Cowan Mineral Company	Canada	Late arrival
Talc	TA-93	Dr. Bertram Woodland	Easton, Pennsylvania	Contaminants occurred as finely dispersed phases
Talc	TA-94	Dr. Bertram Woodland	Phillipsburg, New Jersey	Contaminants occurred as finely dispersed phases
Talc	TA-96	Dr. Bertram Woodland	Philadelphia, Pennsylvania	Contaminants occurred as finely dispersed phases

The results of the PLM analysis are described below. Specimen identification numbers, suppliers, and geographical origins are provided for ease of comparison of analysis results.

Quartz

Q-1, Sobin Chemical Company, North Carolina Sand--
The sample contained few contaminants; iron oxide was present at a concentration much lower than 1%. The individual particles exhibited typical quartz conchoidal fracture.

Q-2, Wards Natural Science Establishment, Minas Gerais, Brazil--
No contaminant mineral phases were detected. The individual particles exhibited typical quartz conchoidal fracture.

Q-3, Wards Natural Science Establishment, Hot Springs, Arkansas--
The sample was comparable to Q-2 in phase purity and particle morphology.

Q-4, Dr. Bertram Woodland, Northampton, Pennsylvania--
The sample was not as pure as samples Q-1, Q-2 and Q-3: feldspars and iron oxides at concentrations of 5% and 1%, respectively, were present.

Q-5, Sawyer Research, Synthetic--
No contaminants were detected in this sample. Particle morphology was typical of quartz.

Q-8, NRIOD, South Africa--
The sample was received as a ground powder. Four contaminant mineral phases, which together constituted less than 1% of the sample mass, were detected. These contaminants included iron oxides, feldspars, and carbonates. The quartz particle size was small: the maximum dimension noted was 16 μm.

Q-106, Pennsylvania Glass Sand Corporation Commercial Processed (Min-U-Sil-5 μm)--
No contaminants were detected in this sample, which was received as a ground powder. The particles were extremely irregular in shape and did not exhibit the conchoidal fracture typical of quartz. Particle size was larger than that indicated by the manufacturer.

Q-107, Pennsylvania Glass Sand Corporation, Commercial Processed (Min-U-Sil-10 μm)--
Except for the larger overall particle size, the sample was identical in appearance to the Q-106 samples.

Beryl

B-9, Brush-Wellman, Africa--
The sample contained at least three contaminant phases. Quartz (less than 2% by mass), iron oxides (less than 1% by mass), and an unidentified phase consisting of amorphous, isotropic tan particles (less than 1% by mass) were present.

B-10, Brush-Wellman, Brazil--

This sample contained more contaminant phases than were noted in the B-9 sample. Quartz (less than 2% by mass) and talc (less than 1% by mass) were identified as contaminants. An unidentified isotropic mineral (less than 1% by mass) and amorphous, low birefringence tan particles (less than 1% by mass) and high birefringence particles (less than 3% by mass) were also present.

B-11, John Carter, Pennington County, South Dakota--

The sample contained four contaminant phases, all of which were present at low concentrations. Quartz (less than 1%), carbonates (much less than 1%), iron oxides (much less than 1%), and mica (much less than 1%) were present. In thin section, a trace of muscovite (mica), iron oxide stains, and some clay smears were present.

B-12, Wards Natural Science Establishment, Afghanistan--

Of the beryl samples examined, this sample was determined to be the least desirable because it contained the highest concentration (less than 5%) of quartz. Other contaminants included tourmaline (less than 2%), iron oxide (less than 1%), unidentified high birefringence particles (less than 1%), and unidentified blue, birefringent particles (less than 1%).

Fluorite

F-14, Ozark-Mahoning Company, Rosiclare, Illinois--

Two contaminant phases were detected in this sample. Calcite and calcium sulfate, each at concentrations below 1% were present.

F-16, Wards Natural Science Establishment, Rosiclare, Illinois.

The specimen was supplied as a large lump of intergrown fluorite cubes with a heavy surface encrustration of calcite and apatite. After removal of the surface encrustration, one ground cube was determined to contain five contaminant phases, each of which represented less than 1% of the sample mass. These contaminants were calcite, apatite, gypsum, iron oxide, and another unidentified birefringent mineral.

F-17, Baker Chemical Company, Synthetic--

This sample was as pure as the natural specimens examined and because it was supplied as a fine powder (modal size of 8 μm) would not be further contaminated by grinding procedures. Contaminants detected at less than 1% level were calcite and calcium sulfate. Iron oxides were present at a level below 1%.

F-19, National Stockpiles, Unknown (domestic) Origin--

This sample was also supplied in a reduced particle size form. Contaminants were present as discrete particles as well as intergrowths in, or coatings on the fluorite particles. The contaminants were carbonates (less than 5%), hematite (less than 2%), and quartz (less than 2%).

Nickel Oxide (Bunsenite)

N-20, Johnson-Matthey Company, Synthetic (lot 50133)--
The sample consisted of less-than-100-μm aggregates of particles. Approximately 2% of the sample was dark green crystals that were identified as metallic nickel. Iron oxide (less than 1%) was also present.

N-21, Fisher Scientific, Synthetic (lot 795205)--
No contaminants were detected in this sample. The sample consisted of loose agglomerates of discrete, 0.4 to 6 μm particles.

N-22, Johnson Matthey, Synthetic (lot 10936)--
This sample was nearly identical in composition and morphology to the N-20 sample. Metallic nickel concentration was slightly lower and particle size was slightly smaller in this sample compared to the N-20 sample.

N-23, Fisher Scientific, Synthetic (lot 75463)--
The sample was identical to the N-21 sample. Modal particle size was determined to be 1 μm.

N-108, Baker Chemical Company, Synthetic (mixed lots)--
No contaminant phases were detected in this sample. Morphologically, it was quite similar to the N-21 and N-23 samples.

Cristobalite

CB-24, Dr. Rustum Roy, Synthetic--
Very rough surfaced, globular, irregular particles with low birefringence comprised the sample. The particle size range was wide (1 to 150 μm) due to the friability of the large crystals.

Tridymite

TY-27, Dr. Rustum Roy, Synthetic--
The sample consisted of irregularly shaped, but smooth-edged particles with low birefringence. The particle size ranged from 4 to 100 μm; the modal size was approximately 30 μm.

Chrysotile

CH-28, Jaquays Mining Company, Gila County, Arizona--
The grinding procedure used to prepare the specimen for PLM resulted in tangled mattes of fibers. Discrete fine particles of several mineral types (none of which were antigorite or other asbestos minerals) were seen dispersed through the fiber mattes. Contaminants were identified as iron oxides (less than 5%), feldspars (less than 3%), carbonates (less than 1%), and coal (less than 1%). Flotation would easily remove these contaminants.

CH-29, Union Carbide Corporation, Idria Range, California--
This sample was provided as a commercially processed powder. Contaminants included mica (less than 2%), quartz (less than 2%), carbonates (less than 3%), other unidentified mineral (less than 1%), and hematite.

Approximately 1% of the sample was metallic fragments, probably introduced during mining and processing of the crude asbestos ore. The sample displayed good fibrous structure; no nonfibrous serpentine minerals were detected. The fibers existed in bundles with rounded ends. Bundles ranged from 0.5 to 68 μm in width, and 1 to 300 μm in length. Thin section analysis revealed the presence of white to green waxy aggregates of fine fibers, some fine-grained biotite, and particles of iron ore (possibly magnetite).

CH-30, National Stockpiles, Southern Rhodesia--

This specimen contained more contaminants than either the CH-28 or CH-29 specimens. Because the sample was supplied as disaggregated bundles of fibers, ball milling was employed to produce samples for instrumental characterization. The ball milling reduced the size of the contaminant particles to a point where identification was difficult. Three different probable feldspars constituted approximately 6% of the sample. Carbonates (less than 5%), magnetite (less than 3%), other iron oxides (less than 1%), and carbonaceous material (less than 1%) were also present. No nonfibrous serpentine minerals were detected.

CH-31, NRIOD, Rhodesia--

This specimen was supplied as a ground powder and was one of the UICC (Union Internationale Contre Le Cancer) asbestos standards. Like CH-30, specimen CH-31, also contained a higher level of contamination than either the CH-28 or CH-29 specimens. Carbonates (less than 5%) olivine (less than 3%) quartz (less than 2%), and several unidentified minerals totalling another 2% of the sample were present. Grinding contaminants represented 1% of the sample. Although fibrous morphology was excellent, this sample was considered unsuitable for processing as a final standard mineral because of the presence of antigorite (less than 1%).

Crocidolite

CR-34, Wards Natural Science Establishment, South Africa--

The sample was supplied as rocks containing fiber bundles perpendicular to plates of nonfibrous mineral. Through wind and handling abrasion, most of the fiber bundle surfaces had been sufficiently teased to subdivide, producing clumps of ultrafine fluffy light blue fibers. The large fiber bundles were relatively uncontaminated, whereas the clumps of fluffy fibers contained most of the specimen contaminants. Mineral contaminants included unidentified, high birefringence types (less than 10%), low birefringence types (less than 2%), calcite (less than 2%), quartz (less than 2%), and two types of iron oxides (less than 2%). Nonmineral contaminants included carbonaceous particles (less than 2%), paper fibers (less than 1%), and metal fragments (less than 1%). No riebeckite was detected. The thin section analysis showed thin laminae of quartz and magnetite; streaks of opaques (possibly magnetite) and some unresolvable material were found parallel to fiber bundles.

CR-35, National Stockpiles, South Africa--

This specimen was supplied as disaggreated bundles of fibers. Ball milling was employed to produce samples for instrumental characterization; this again reduced the particle sizes of the contaminant phases, making identification difficult. Quartz, carbonates, hematite, magetite, and four unidentified minerals (none of which were riebeckite) represented approximately 10% of the sample mass.

CR-36, NRIOD, South Africa--

The specimen was another of the UICC asbestos standards and was thus supplied as a ground powder. Carbonate, quartz, feldspar (two types), iron oxide (two types), and other mineral contaminants represented 25% of the sample mass. Grinding contaminants were also present. Riebeckite (less than 1%) was also noted.

CR-37, NRIOD, South Africa--

This was a bulk rock sample from the stockpile out of which CR-36 had been prepared. Fiber bundles were intact and unabraded. At least six different mineral phases were found within the fiber bundles. Together, however, they constituted less than 2% of the sample mass. The thin section exhibited layers of dark, fine-grained material composed of quartz, magnetite, plus unidentified minerals. The fibers were elastic and easily separated into fluffy masses.

Fibrous Grunerite (Amosite)

GF-38, Wards Natural Science Establishment, Lyndenburg, South Africa--

This specimen, supplied as large rocks containing rows of fiber bundles perpendicular to plates of massive, nonfibrous mineral, exhibited true fibrous structure. Contaminants present included micaceous minerals (less than 4%), carbonates (less than 5%), magnetite (less than 2%) and isotropic minerals (less than 1%). Thin section analysis demonstrated the presence of dense masses of fiber, with sparse biotite, iron oxide (magnetite), small masses of silicate minerals (possibly hornblende), and a trace of calcite.

GF-39, NRIOD, South Africa--

This specimen, one of the UICC asbestos standards, was supplied as a round powder. Contaminants, difficult to identify because of fine particle size, constituted approximately 15% of the sample mass: quartz, carbonates, feldspars (two types), iron oxides (three types), mica (two types), talc, a tan birefringent mineral (probably an amphibole), carbonaceous particles, and grinding contaminants.

GF-40, National Stockpiles, South Africa--

As with other asbestos specimens obtained from the National Stockpiles, the GF-40 specimen was supplied as disaggregated fiber bundles. Ball milling was employed to produce samples for instrumental characterization. At least ten different mineral phases (too small in particle size for absolute identification) were present and together represented at least 10% of the sample mass. One of the contaminants appeared to be the nonfibrous grunerite.

GF-41, NRIOD, South Africa--
This was a sample of the bulk rock from which the GF-39 specimen had been prepared. Fiber bundle lengths were consideralby shorter than those in the GF-38 sample. Contaminants included probable clay aggregates (less than 7%), quartz (less than 2%), magnetite (less than 2%), carbonates (less than 1%), and feldspars (less than 1%).

Fibrous Anthophyllite

AF-42, Mackinaw Geological Supply, Ontario, Canada--
The specimen contained 5 to 10% unidentified opaque minerals, as well as quartz (less than 5%) and magnetite (less than 5%). The anthophyllite particles were mostly prismatic rather than fibrous--i.e., the larger (less than 10 μm diameter) particles did not appear to be composed of finer structures which could be further separated parallel to the prism's longest dimension. The fibrous type particles comprised only 20 to 30% of the sample.

AF-43, Wards Natural Science Establishment, North Carolina--
This specimen also contained some (approximately 10%) prismatic as opposed to fibrous particles. Other mineral phases constituted a significant portion of the sample mass: feldspars (less than 10%), talc (less than 5%), quartz (less than 5%), magnetite (less than 5%), calcite (less than 3%), and other birefringent minerals (less than 2%).

AF-45, Wards Natural Science Establishment, Montana--
This specimen exhibited a fibrous morphology rather than the prismatic morphology noted in the AF-42 and AF-43 specimens. Contaminants were also fewer in number and lower in total concentration in the AF-45 specimen. Magnetite, mica, quartz, talc, and calcite together comprised less than 11% of the sample. Thin section analysis indicated the presence of parallel fiber bundles that readily disaggreated into finer fiber masses. The fiber bundles in the thin section appeared pure, except for iron staining and superificial calcite coatings.

AF-46, NRIOD, Finland--
This was the last of the UICC asbestos standards submitted for evaluation. The specimen was similar to the AF-45 specimen in that a truly fibrous morphology predominated. Contaminants present included mica (less than 5%), talc (less than 3%), quartz (less than 2%), feldspars (less than 2%), carbonates (less than 1%), iron oxides (less than 1%), and grinding contaminants.

AF-105, Institute of Occupational Health of Finland, Paakkila, Finland--
The specimen was submitted as a ground powder; a chunk of rock from which the ground material had been produced was also supplied. Although the particle morphology was fibrous, the high level of contamination rendered this sample unsuitable for further consideration. Contaminants included micaceous minerals (20 to 30%), talc (less than 10%), magnetite (less than 1%), and several unidentified minerals (less than 2%).

Fibrous Tremolite

TF-48, Wards Natural Science Establishment, Rajasthani, India--
The specimen was provided as disaggregated bundles of fibers 0.5 to 1.5 cm in length. Contaminants trapped within the fiber bundles included carbonates (less than 1%), micaceous minerals (less than 1%), iron-rich silicate minerals (less than 1%), and carbonaceous material (less than 1%). In thin section, the fiber bundles and individual fibers separated from the bundles were pure, with only rare contaminants (undetermined) and some fine dust.

TF-49, Dr. Bertram Woodland, Kobuk River, Alaska--
The specimen consisted of one small bundle of fibrous mineral. Contaminants included micaceaous minerals (less than 1%), carbonates (less than 1%), and three other mineral phases (less than 1% in total). In addition aggregates of fine spheres (possibly glassy flyash) were noted on the surfaces of many of the fibers.

TF-50, Dr. Bertram Woodland, Tuscany, Italy--
This specimen was also only a very small specimen, submitted for reference purposes. Because of its unique macroscopic structure--it resembles spun glass wool--the sample was not ground prior to microscopic examination; a few of the 1 to 4 cm fine, hair-like fibers were carefully mounted for PLM. The fibers were seen to be lightly coated with less than 1 μm carbonaceous particles. Otherwise, the sample was pure tremolite. The macroscopic "fibers" were actually determined to be bundles of fibers of smaller diameter.

Antigorite

AG-51, Mackinaw Geological Supply, Ishpeming, Michigan--
The specimen contained several contaminant phases, one of which was a fibrous serpentine mineral. The other mineral contaminants were talc (less than 5%), quartz (less than 5%), and magnetite (less than 5%). The fibrous phase was estimated to be 5% of the sample.

AG-54, Dr. Bertram Woodland, Lenni Mills, Pennsylvania--
A fibrous serpentine mineral represented approximately 2% of this specimen. Other mineral contaminants present included talc (less than 10%), magnetite (less than 10%), quartz (less than 5%), calcite (less than 5%), and iron oxide (less than 1%). Several unidentified mineral phases were also present, constituting another 10% of the sample.

AG-55, Dr. Bertram Woodland, West Chester, Pennsylvania--
Compared to the AG-51, AG-54, and AG-57 specimens, (described below) the AG-55 was far superior because of its low fibrous serpentine phase concentration (less than 1%). The specimen was, however, considerably impure. Contaminants included magnetite (less than 10%), quartz (less than 5%), carbonates (less than 2%), hematite (less than 2%), talc (less than 1%), and anthophyllite (less than 1%). The thin section showed a mass of antigorite (or perhaps lizardite) with a network of iron ore

grains and thin blebs. Thin (20 μm wide), rare veins of fibrous mineral, probably chrysotile were present; in some places there was a suggestion of small areas of poorly developed fiber structure but this may have been antigorite. Rare grains of talc and chlorite were noted.

AG-57, Dr. Bertram Woodland, Easton, Pennsylvania--

Fibrous serpentine and amphibole minerals constituted approximately 5% of the specimen. Other identifiable minerals included talc (less than 10%), quartz (less than 10%), magnetite (less than 5%), iron oxide (less than 2%), and calcite (less than 1%). Several unidentified minerals were also present; these represented less than 10% of the specimen.

AG-58, NRIOD, South Africa--

The host rock for the CH-32 specimen was suspected to be antigorite. A piece of rock visually free from fibrous chrysotile was chipped off the bulk specimen and ground for PLM examination. Approximately 75% of the specimen mass turned out to be (micro) fibrous chrysotile. Carbonates, magnetite, quartz, and feldspars together represented another 5% of the sample.

Riebeckite

R-59, Mackinaw Geological Supply, Palmer, Michigan--

Approximately 5% of the particles produced by grinding this specimen exhibited a fibrous morphology. Other mineral contaminants included quartz (less than 5%), calcite (less than 5%), magnetite (less than 5%), iron oxide (less than 3%), and talc (less than 3%).

R-60, Wards Natural Science Establishment, El Paso County, Colorado--

The riebeckite occurred as isolated, narrow (0.5 to 1.0 cm) veins imbedded in a chert rock matrix. The riebeckite particles, produced by grinding a vein removed from the rock matrix, were prismatic in shape and distinctly different from crocidolite fibers examined in the CR-34 through CR-37 specimens. Mineral contaminants included quartz (less than 5%), iron oxides (less than 2%), tourmaline (less than 2%), mica (less than 1%), and several unidentifiable minerals present at very low concentrations (total less than 2%). The thin section showed large pure riebeckite prisms with traces of plagioclase, muscovite, and possibly sphene.

R-61, NRIOD, South Africa--

This specimen was obtained from the CR-37 specimen: the massive plates between which the fiber bundles occurred in the CR-37 specimen were sawed off and became the R-61 specimen. Few other mineral contaminants were present in the ground powder submitted: micas and feldspars each constituted less than 1% of the specimen. The riebeckite particle morphologies were quite unusual. The minus 325-mesh particles were not prismatic; rather, they appeared to be highly compacted masses of extremely fine fibers. Further grinding produced finer fiber-like particles.

R-62, Wards Natural Science Establishment, South Africa--

The specimen was also obtained by removing the nonfibrous plates from the corresponding fibrous specimen (CR-34). The ground specimen was determined to contain less than 15% riebeckite which occurred as prismatic particles, as opposed to the fiber-like particles seen in the R-61 specimen. The other mineral phases included quartz (less than 55%), magnetite (less than 15%), carbonates (less than 5%), and unidentified types (less than 10%).

Grunerite

G-63, John Carter, South Dakota--

This specimen consisted primarily of grunerite, but contained several other intermixed mineral phases. The mineral contaminants included quartz (less than 8%), magnetite (less than 3%), carbonates (less than 2%), and unidentified types (less than 5% in total). The grunerite particles were prismatic; they contained no finer structure that might lead to separation of fiber-like particles. No fibrous phases were noted.

G-64, Mackinaw Geological Supply, Michigamme, Michigan--

This specimen also contained many mineral contaminants. Magnetite, quartz, and chlorite each represented approximately 5% of the specimen. Spinel constituted less than 3%. Particle morphologies were somewhat unusual; while gross morphologies (minus-325-sized particles) would be characterized as prismatic, each prism exhibited finer structures which could (and did) easily break away from the main particle, forming fiber-like particles. High magnification examination of some of these small-diameter (less than 10 μm) fiber-like particles revealed splintered ends which again suggested the less-than-10-μm fiber-like particles could be further subdivided.

G-66, Dr. Bertram Woodland, Silver Bay, Minnesota--

This specimen contained a large number of contaminants, many of which exhibited unusual morphologies in the ground state. Quartz, magnetite, and talc each represented at least 5% of the specimen. Other iron oxides (less than 2%) and unidentified minerals (10%) were also present. The grunerite particles exhibited morphologies ranging from hard, solid prisms, as in G-63, to the splintering prismatic particle type noted in G-66. The talc mineral present also exhibited an unusual morphology: it was in the form of sheets composed of individual needles which readily separated to produce fiber-like particles.

G-68, Iron Ore Company of Canada, Luce Lake, Newfoundland--

Grunerite constituted only 50 to 60% of this specimen. Quartz was present in nearly as high a concentration as the grunerite. Magnetite and several unidentified mineral phases together comprised less than 5% of the sample. The grunerite particles were prismatic, as they were in the G-63 specimen.

G-69, Iron Ore Company of Canada, Carol West, Newfoundland--
This specimen contained less quartz than G-68, though at 30% it was still a major constituent. Magnetite (less than 1%) and other unidentified minerals (less than 2%) were noted. Grunerite particle morphologies were similar to those noted in G-68. The prisms of G-69 tended to be more elongated than those in G-68 and also tended to cleave more readily along the prism lengths.

Cummingtonite

C-71, John Carter, Lead (Homestake Mine), Lawrence County, South Dakota--
The specimen was contaminated by several mineral phases. Micas (less than 10%), quartz (less than 5%), chlorite (less than 3%), iron oxides (less than 3%), carbonates (less than 2%), and several other mineral phases (totalling less than 1%) were detected. The cummingtonite particles were prismatic; no fibrous phases were detected. Thin section analysis showed the cummingtonite to be present as radial aggregates; biotite, chlorite, carbonate, opaques (including graphite), and garnet (rare) were detected.

C-72, Minerals Unlimited, South Dakota--
This specimen was quite similar in composition and morphology to the C-71 specimen. Carbonates (less than 5%), micas (less than 5%), quartz (less than 1%), feldspars (less than 1%), iron oxides (less than 1%), and carbonaceous particles (less than 1%) were detected as contaminants.

Anthophyllite

A-102, Mineralogisk-Geologisk Museum, Bamble, Norway--
This specimen was primarily anthophyllite but did contain large amounts of contaminants. Quartz (less than 25%), rutile (less than 5%), talc (less than 3%), and iron oxides (less than 1%) were identified as the main contaminants. Several unidentified minerals together comprised less than 2% of the sample. The particles were prismatic; they contained no visible fiber structures. The thin section showed neutral-to-light-brownish anthophyllite prisms with some quartz, sparse plagioclase, biotite (phlogopite), and some rutile; some anthophyllite was slightly altered to talc.

A-103, Mineralogisk-Geologisk Museum, Modum, Norway--
The sample consisted of one large black slab. Very little, if any, of the sample was anthophyllite. The major portion of the sample was another amphibole mineral, probably of the anthophyllite-gedrite series. Other contaminants included mica (less than 10%), quartz (less than 7%), rutile (less than 3%), and magnetite (less than 1%).

Tremolite

T-75, Mackinaw Geological Supply, Felch, Michigan--
Only approximately 50% of the specimen was prismatic tremolite. Carbonates--both calcite and dolomite--were the other components.

T-76, Dr. Bertram Woodland, Easton, Pennsylvania--
Tremolite occurred as prismatic crystals in this specimen. Contaminants included talc (less than 5%), carbonates (less than 5%), quartz (less than 2%), plus three other high birefringence minerals which together contributed another 5% of the sample.

T-77, John Carter, Pennington County, South Dakota--
The specimen was composed of radiating needles of tremolite, which yielded prismatic particles when ground. Carbonates were major components of the sample and represented more than 10% of the mass. The contaminants present were few in number and relatively low in concentration: iron oxides (less than 1%), micas (less than 2%), and unidentified minerals (less than 1%). Thin section analysis revealed the presence of radiating masses of white prismatic tremolite with appreciable carbonates and sparse phlogopite.

T-78, Wards Natural Science Establishment, Gouverneur, New York--
Although this specimen was massive in appearance, the ground powder contained both tremolite prisms and elongated fiber-like (splintered ends) particles of tremolite. Contaminants present included talc (less than 10%), quartz (less than 3%), carbonates (less than 4%), and several unidentified mineral types (totaling less than 2%).

T-79, NIEHS, Gouverneur, New York--
This specimen was received in a ground powder form. Particles of tremolite were prismatic for the most part, although a small proportion (less than 2%) of the tremolite prisms exhibited finer structures that could result in the formation of fiber-like particles. This specimen was much less contaminated by other mineral phases than specimens T-75 through T-78. Other phases present included talc (less than 1%), carbonates (less than 1%), hematite (less than 1%), and metallic fragments (less than 1%). Although this specimen was considerably more phase pure than the other prismatic tremolite specimens, the presence of serpentine minerals in both fibrous and nonfibrous forms made this specimen less desirable as a final standard for tremolite.

Talc

TA-91, Wards Natural Science Establishment, Madoc, Ontario, Canada--
Contaminants in this specimen included calcite (less than 5%), prismatic tremolite (less than 5%), fluorite (less than 2%), and several other high birefringence minerals (totalling less than 5%). Although the talc particles were platey, they showed no tendency to cleave into (elongated) prisms.

TA-92, Wards Natural Science Establishment, Fowler, New York--
This specimen contained fewer contaminants than TA-92: prismatic tremolite represented less than 5% of the sample, and quartz was present at a 1% concentration. Unlike TA-91, however, the talc plates in this specimen readily cleaved to yield elongated prisms.

TA-95, Dr. Bertram Woodland, Gouverneur, New York--

This specimen was obtained from the same general mineral deposit as TA-92 and therefore was quite similar in compostion. Quartz (less than 2%), and prismatic tremolite (less than 2%) were the contaminants detected. The platey talc particles readily cleaved into elongated prisms, as in TA-92.

TA-97, Johnson and Johnson Company, Vermont--

This specimen was received in a powdered form. Mineral contaminants present were few in number, low in concentration and very difficult to identify due to their small particle size. Together, the detected contaminants represented approximately 2% of the sample. Although the talc particles were quite platey, they did not tend to cleave into elongated prisms.

TA-98, National Stockpiles, India--

This was one of the purest bulk rock specimens examined. Hematite (less than 1%) and several other minerals (totalling less than 1%) were present. The particle morphology of this specimen was quite different from that noted in the northeastern American talc specimens (TA-91,TA-92, TA-95, TA-97). Particles were ragged and irregular, with no perfect platelike structures evident.

TA-99, Montana Bureau of Mines, Montana--

This specimen was quite similar in purity and particle morphologies to TA-98. Contaminants included carbonates (less than 1%), quartz (less than 1%), mica (less than 1%), and hematite (less than 1%). In thin section, the specimen was seen to be fine-grained, with a felted texture of irregular plates and shreds; rare phlogopite (ranging in size from 8 to 12 μm, rarely reaching 80 μm), partly altered to chlorite, was present.

TA-101, NIOSH, "Sierra"--

This specimen was submitted by Dr. Janet Haartz as a ground powder. Contaminants included carbonates (less than 4%), feldspars (less than 2%), mica (less than 1%), spinel (less than 1%), iron oxides (less than 1%), and metallic fragments (less than 1%). Maximum particle size noted was 48 μm; modal particle size was approximately 2 μm. The particle morphology was quite similar to that seen in TA-98 and TA-99, i.e., irregular, rough-surfaced, ragged-edged particles, as opposed to the thin, smooth, flat talc plates of the northeastern American samples. Elongated, needle-shaped (but with irregular, rough edges) particles were present, as they were in the TA-98 and TA-99 specimens. These needles were not the sharp-edged cleavage fragments which were seen in the talc samples from northeastern America.

X-RAY DIFFRACTION (XRD) ANALYSIS

Each mineral sample that passed the macroscopic and PLM screening stages was examined by XRD in order to corroborate that the desired mineral phase conformed to standard XRD patterns published by the Joint Committee for Powder Diffraction Standards (JCPDS).[21] The XRD scans were also used to confirm the identity or absence of undesired impurity minerals, for example,

tremolite in talc. No attempt was made to quantify the impurity phases because the samples prepared for screening did not, in most cases, have the same concentration of impurities in each rock fragment.

Each sample was crushed and ground with a mortar and pestle to pass a 325-mesh sieve. The powder was then packed into a shallow plastic holder for XRD analysis. The minus 325-mesh powder was poured into a shallow plastic sample holder and compacted by placing a clean glass microscope slide over the powder and applying hand pressure. This sample packing technique can produce XRD patterns that exhibit preferred crystal orientations. The primary goal of these XRD analyses, however, was to determine whether the interplanar crystal spacings of the samples matched published patterns which would not be affected by preferred particle orientation.

X-ray diffraction scans were performed with a General Electric XRD-5DF diffractometer. The usual instrument operating parameters were:

copper K-alpha x-ray source (40 kvp, 18 ma)
3° beam slit
medium resolution soller slit (MR)
0.2° detector slit
2° per minute scan note
0.5 second time constant, linear range

Full-scale peak intensity was varied to keep the main XRD peak on-scale for each sample. With these instrument operating conditions, the detectability of contaminant mineral species was limited to an estimated 5 weight percent. A total of 60 samples was screened by XRD.

The microscopical screening described in the previous section provided greater sensitivity than the XRD analyses, often less than an estimated 0.1%. The microscopical screening was essential for the detection of fibrous and nonfibrous varieties of the same minerals in the amphibole and serpentine minerals (groups 2 and 3), which could not be distinguished by XRD.

Figures 5 and 6 are representative examples of the XRD patterns for two samples of the nickel oxide from different sources (N-20, Johnson-Matthey Company, and N-21, Fisher Scientific).

The N-20 sample shows an XRD peak at 2.04 Å (Figure 5), which is due to a nickel metal impurity. This nickel metal peak is absent in the N-21 sample (Figure 6). The presence of nickel metal was confirmed microscopically by simply observing the motion of the dark, opaque nickel particles as a magnet was moved near the sample.

Many of the XRD scans of samples of the same mineral showed no detectable contaminants. For example, talc samples TA-95 (Gouveneur, New York; Dr. Woodland), Figure 7, and TA-97 (Vermont; Johnson and Johnson Company), Figure 8, appeared free of contaminants. The least contaminated sample was then selected on the basis of the PLM results, anticipated ease of particle size reduction, and sample quantity and availability.

Cu K_α X-ray source; 45 kvp, 18 ma	2° per minute scan rate
Nickel Filter	1 second time constant
3° beam slit	10,000 counts per second,
0.2° detector slit	full scale

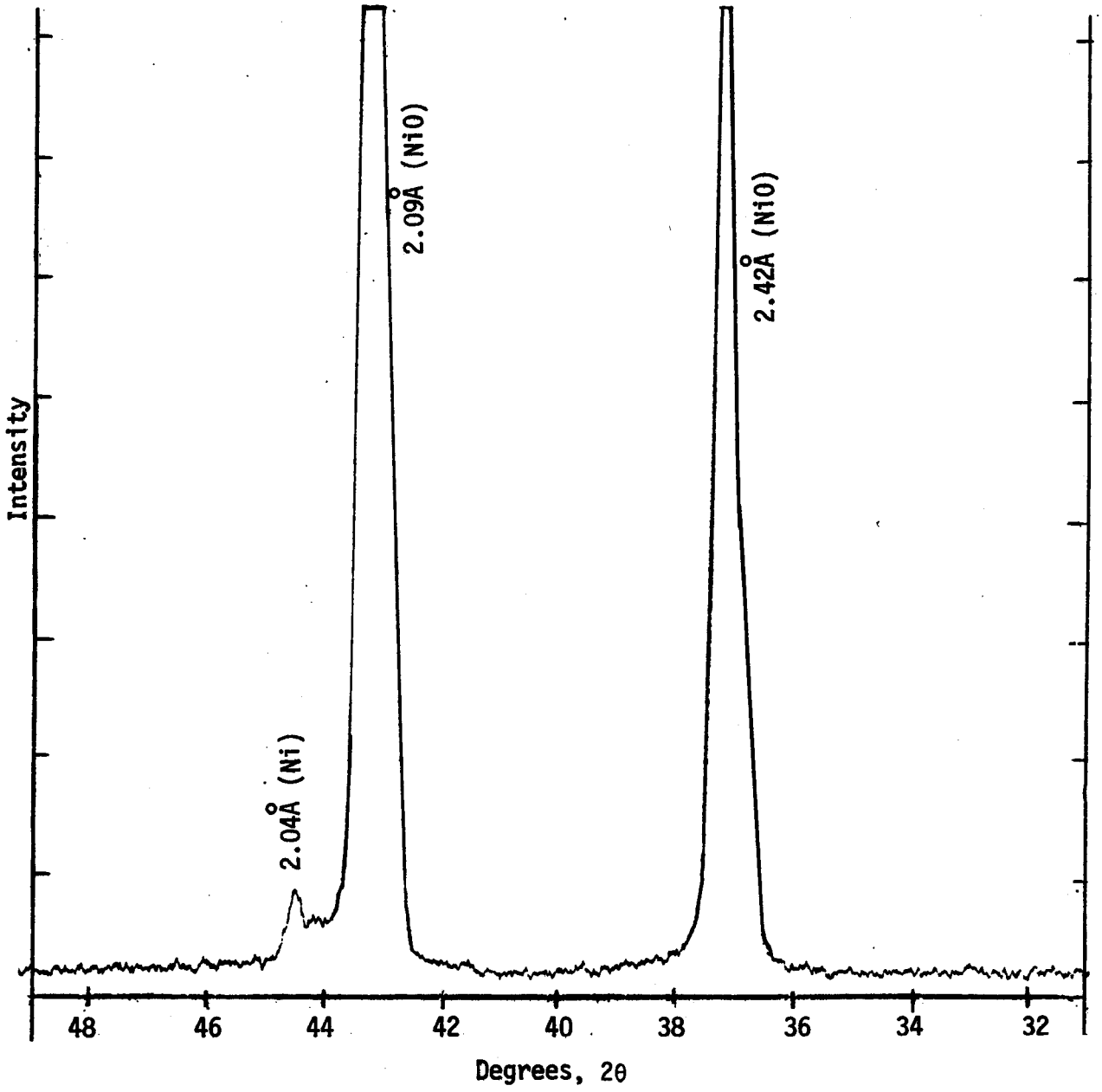

Figure 5. Segment of the XRD pattern for N-20 (nickel oxide), showing a 2.0359 Å peak for nickel metal.

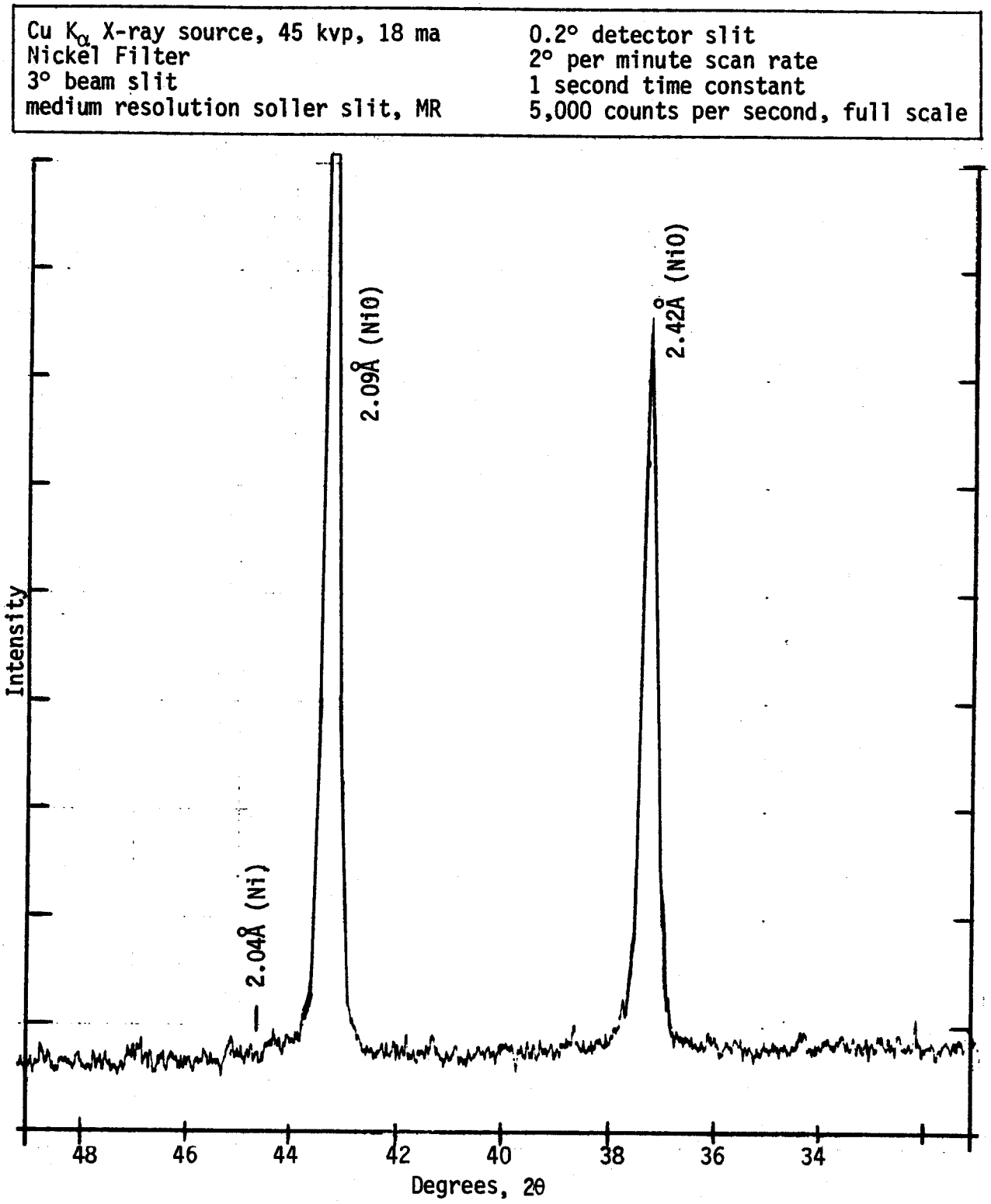

Figure 6. Segment of the XRD pattern of N-21 (nickel oxide) showing no Ni metal peak.

Cu K_α X-ray source, 45 kvp, 18 ma	0.2 detector slit
Nickel Filter	2 per minute scan rate
3° beam slit	0.5 second time constant
medium resolution soller slit, MR	5,000 counts per second, full scale

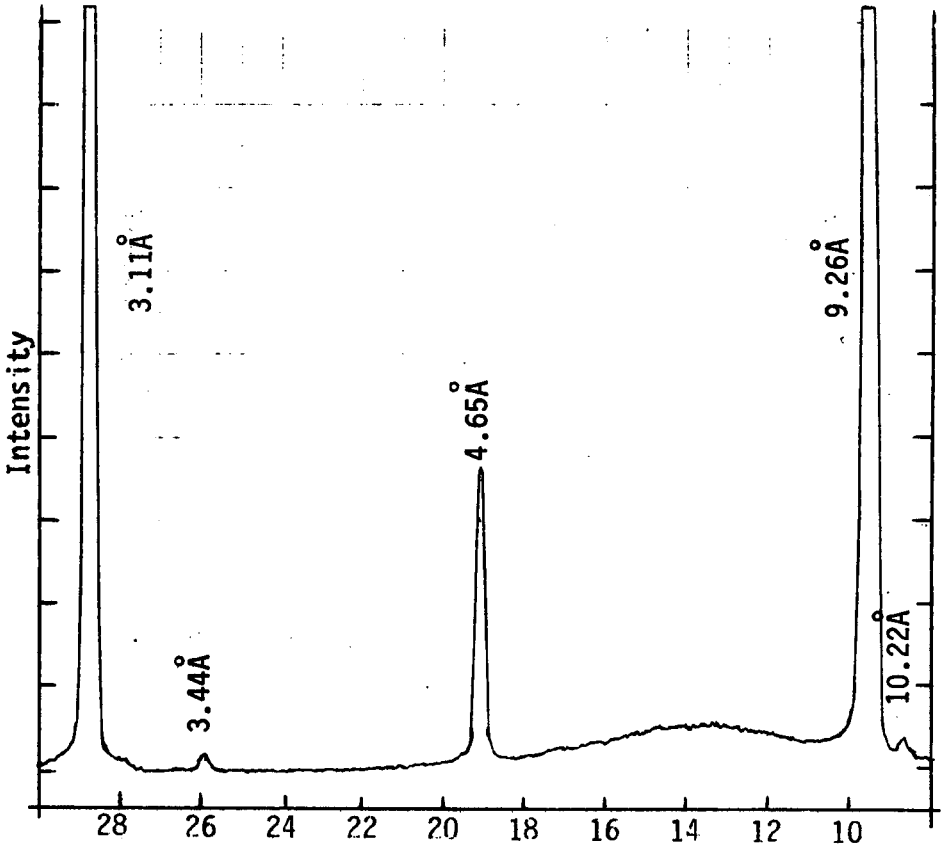

Figure 7. Segment of the XRD pattern of TA-95 (talc, Gouverneur, New York).

Cu K_α X-ray source, 45 kvp, 18 ma	0.2° detector slit
Nickel Filter	2° per minute scan rate
3° beam slit	0.5 second time constant
medium resolution soller slit, MR	10,000 counts per second, full scale

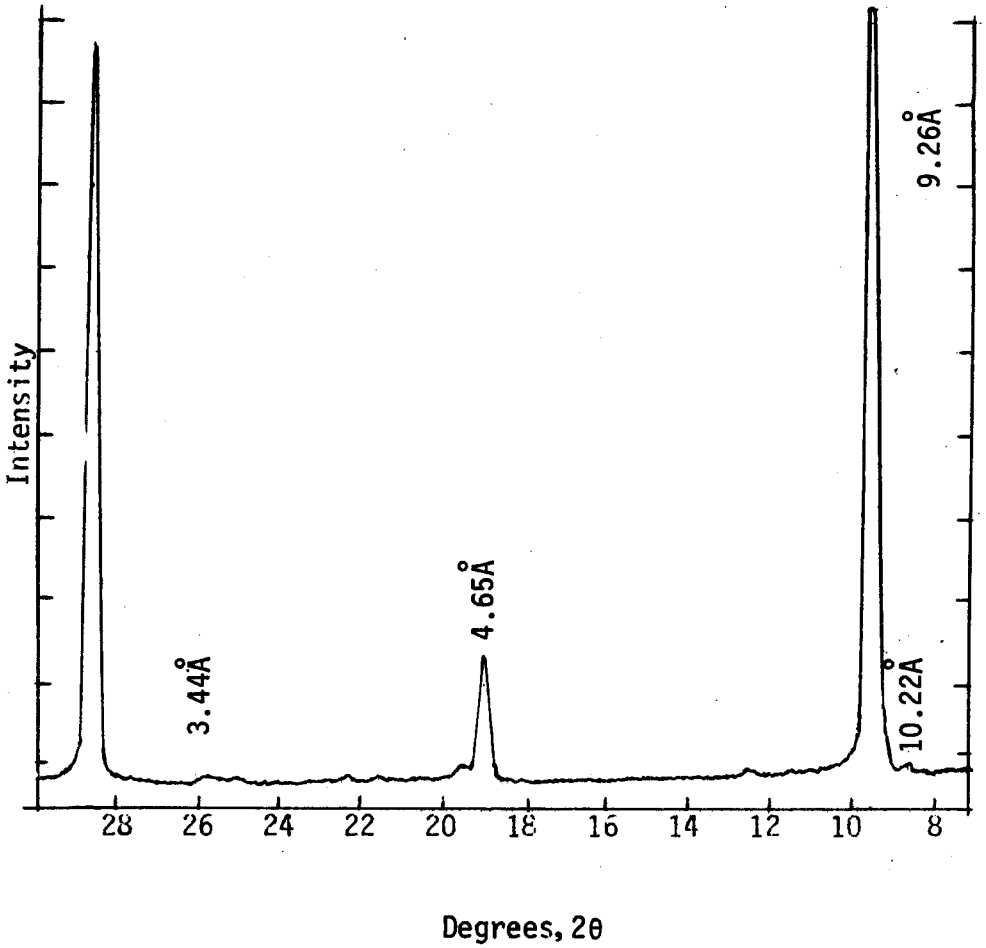

Figure 8. Segment of the XRD pattern for TA-97 (talc, Vermont).

The fibrous amphibole and serpentine mineral specimens were expected to exhibit preferred orientation peak intensities in their XRD patterns. It was surprising, however, to see strong preferred orientation patterns for fluorite. Fluorite is commonly used as an internal standard for the quantitative XRD analysis of quartz. If the fluorite XRD peaks are affected by preferred orientation of fluorite crystal grains, then the XRD results for quartz will be incorrect.

The published patterns[21] for fluorite list the 1.93 Å peak as the strongest line (relative intensity assigned as 100), whereas the 3.15 Å peak has a relative intensity of 70. The XRD scan for F-16 (fluorite, Rosiclare, Illinois; Wards), Figure 9, shows that the peak intensities for the 3.15 Å and 1.93 Å lines are 45 and 100, respectively. These reversed peak intensities are explained by the perfect cleavage of fluorite along its 111 plane (3.15 Å peak) which occurs during grinding.[22] Unless extraordinary care is used when employing fluorite as an internal standard in XRD, quantatitive results for the analysis of quartz may be erroneous.

THERMAL ANALYSES

The thermal analyses conducted on the mineral samples consisted of differential thermal analysis (DTA) and thermogravimetry (TG). Cristobalite and tridymite were also analyzed by differential scanning calorimetry (DSC).

The following section gives a brief description of the equipment and analytical procedures. The thermal analyses on the final mineral samples were performed at Pennsylvania State University under the direction of Professor Leslie E. Cross. The thermal analysis curves found for these minerals in the literature and the actual thermal analysis data for the comminuted minerals are discussed in Section 6.

Differential Thermal Analysis (DTA)

In DTA, the difference in temperature between a sample and an inert reference material is recorded as the two are heated side by side in a suitable holder. When there is no reaction in the sample, there is no temperature difference between the two, but when a reaction occurs, the sample becomes hotter (in response to an exothermic reaction) or cooler (in response to an endothermic reaction) than the inert reference material. When the reaction terminates, the difference in temperature between the two returns to zero and the curve returns to its baseline.

The DTA unit used in these analyses is manufactured by the Robert L. Stone Company, Austin, Texas. The unit is equipped with several sample holder arrangements, two of which are useful for the present application: a module with platinum cups and one with an Inconel cell block. The maximum amount of sample that can be placed in either type of holder is the same, but the Inconel block uses bare thermocouples, which are more sensitive and therefore require much less sample than the cup design. The cup holder is useful when the sample is corrosive or otherwise detrimental to the thermocouple.

Cu K_α X-ray source, 45 kvp, 18 ma	0.2° detector slit
Nickel Filter	2° per minute scan rate
3° beam slit	1 second time constant
medium resolution soller slit, MR	5,000 counts per second, full scale

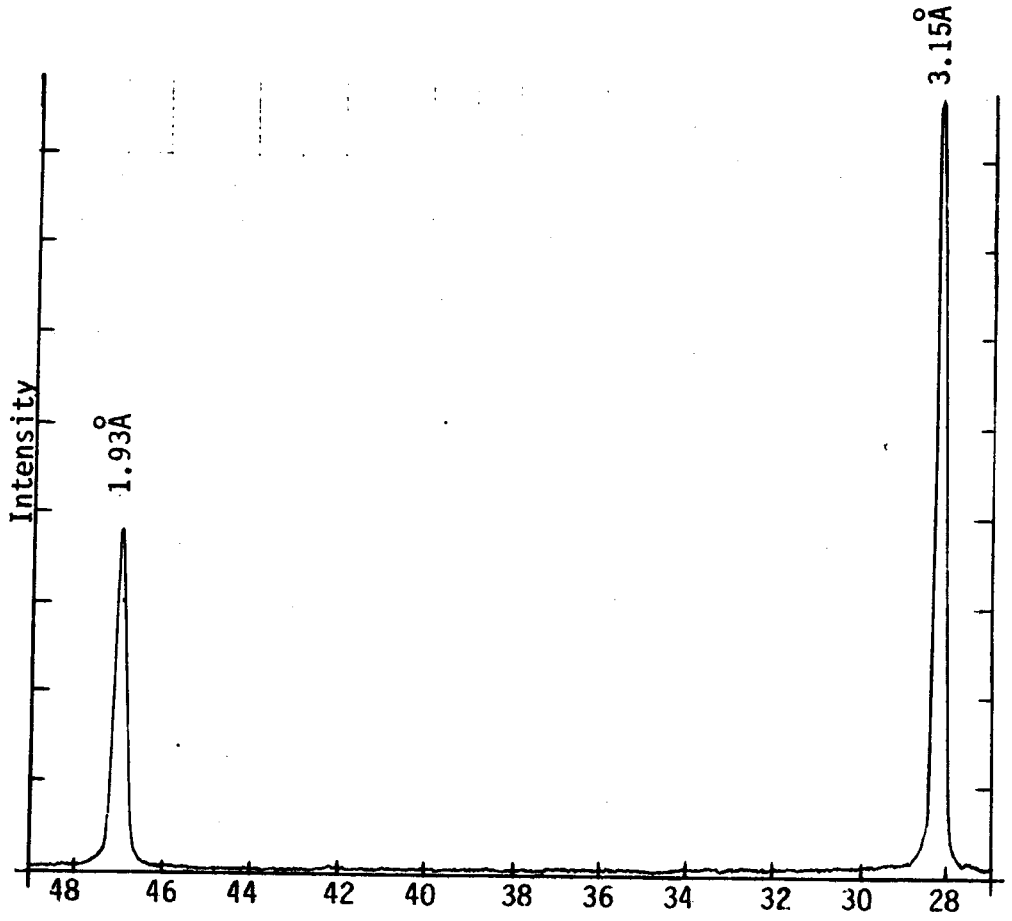

Figure 9. Segment of the XRD pattern for F-16 (fluorite).

The Inconel block holder is 38.1 mm in diameter and 15.9 mm high. Each cavity for the sample and reference material is 6.4 mm in diameter by 19.1 mm deep.

The furnace is heated with platinum wire, which is noninductively wound. The sample was heated at approximately 10°C/min from room temperature to cover 1200°C in an atmosphere of air flowing at a rate of 10 ml/min. Platinum versus platinum-10% rhodium thermocouples are used to measure both the differential temperature and the furnace temperature. A block diagram of the DTA unit is given in Figure 10. Two recorders are used: one gives the furnace temperature as a function of time and the other, the differential temperature as a function of time with temperature tick marks at 100°C intervals. The furnace temperature calibration was checked periodically with quartz (quartz silica, National Bureau of Standards-International Committee on Thermal Analysis Standard Reference Material).

Alpha alumina powder (RR alundum 120 grit, Norton Company) was used as the reference material. It was used both in the reference cell and in the sample cell. In the sample cell, a small cavity was formed in the reference powder around the thermocouple bead; the sample was placed in this cavity and covered with more reference powder. Light tamping was used to consolidate the powder in both cells. This helps to reduce baseline drift and achieve reproducible traces.

The sample size, heating rate, and amplifier signal level are coordinated to optimize the DTA pattern. The differential temperature, ΔT, during a reaction is almost proportional to sample size so that the amount of sample used can be adjusted to increase the thermal response of a small peak. Peak overlap, however, can result from samples that are too large. Small peaks can be increased by using higher heating rates but again, at the expense of some peak overlap. The best DTA conditions for a given sample thus depend on the thermal operating parameters of the specimen, the holder, the furnace heating rate, and the sensitivity of the amplifier system.

Thermogravimetry (TG) and Derivative Thermogravimetry (DTG)

In TG, a sample is heated in a furnace while its weight is continuously monitored. The weight loss can result from dehydration, evaporation, or decomposition. Weight gains can occur when the atmospheric gases combine with the sample, as in the case of oxidation of the sample by oxygen in the air. When combined with DTA, the results of TG can be used to better characterize the process involved in the DTA curve.

In derivative thermogravimetry (DTG), the slope of the TG curve is used to generate a curve that takes on a form much like the DTA curve. It offers a convenience in analyzing the TG curve.

The TG and DTG are conducted with complimentary units that are part of the Robert L. Stone thermal analysis instruments. The TG uses a Cahn RG recording microbalance integrated into the Stone equipment. A noninductively wound platinum furnace provides the heat, which is monitored with a platinum versus platinum-10% rhodium thermocouple.

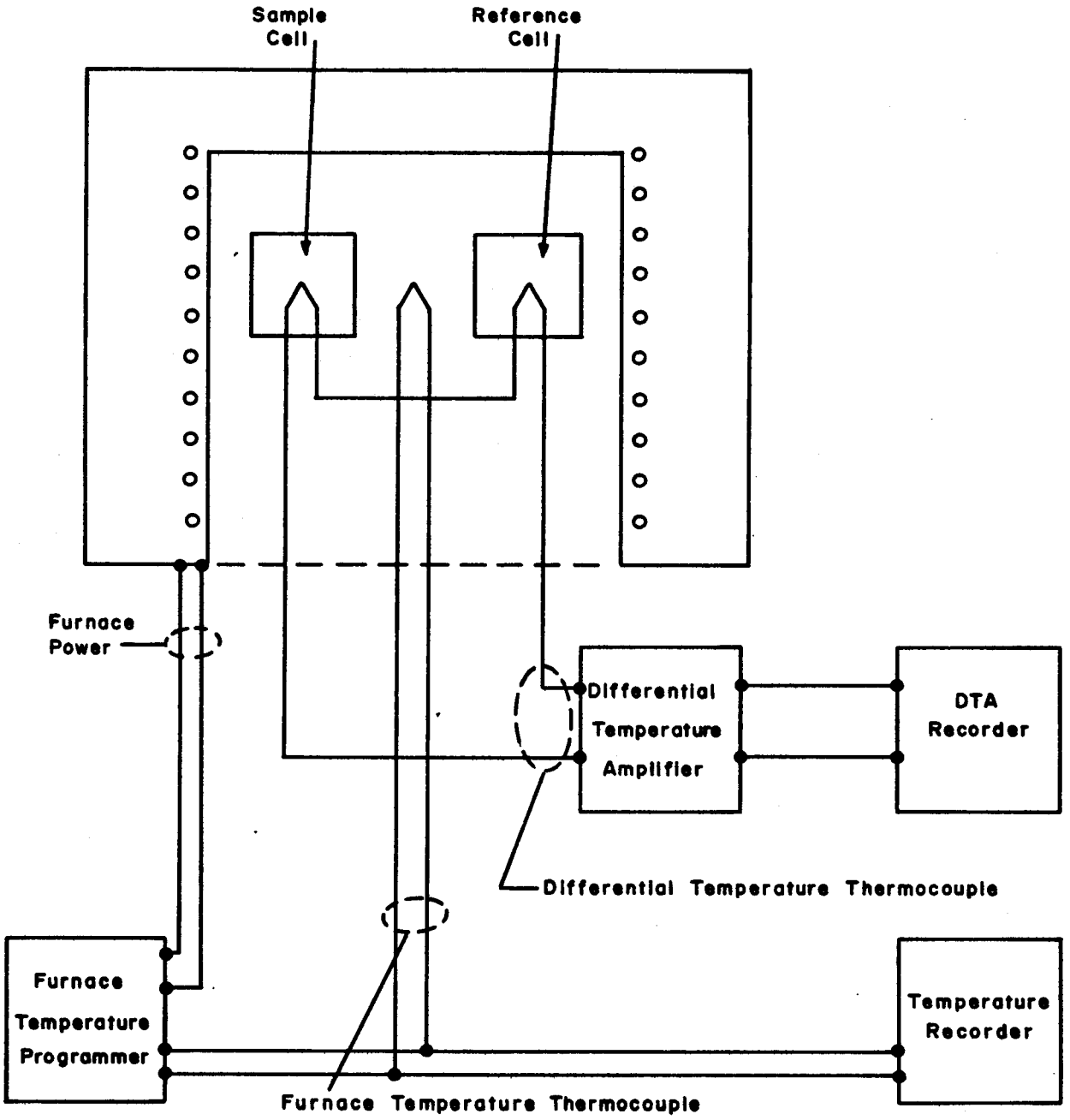

Figure 10. Block diagram of the DTA apparatus.

Figure 11 shows a block diagram of the TG apparatus. Three recorders are used. The first gives the furnace temperature as a function of time, the same as for DTA; the second gives the sample weight as a function of time (TG); and the third gives the weight change as a function of time (DTG). Temperature tick marks at 100°C intervals are synchronized with the record of the monitored furnace temperature.

The sample in the furnace was heated at a rate of approximately 5°C/min in an air stream flowing at 20 ml/min. Since the thermal lag of the TG sample is greater than that for the DTA sample at lower temperatures, the slower heating rate was used.

Thermal convection noises are especially bothersome. These were minimized by using a 16-mm I.D. furnace tube. A 9-mm-diameter platinum sample stirrup pan was used in the tube to heat up to 50 mg of sample.

Differential Scanning Calorimeter (DSC)

The DSC is an evolutionary development from the DTA. Like the DTA, a sample and inert reference material are heated together. Unlike the DTA, however, the DSC monitors the energy required to maintain the two at the same temperature. Endothermic reactions, exothermic reactions, and heat capacities can all be measured on the DSC.

The Perkin-Elmer DSC-1B was used. It is very sensitive to low energy levels and usually requires only 1 to 20 mg of sample. The design of the DSC-1B has placed an upper temperature limit of 500°C on the instrument. This prevented its more active use on the program. For cristobalite and tridymite, however, which each have characteristic solid state transformations between room temperature and 300°C, the DSC was invaluable in determining comminution methods which would not destroy these specimens. The transition energies of the comminuted materials were measured and compared with values obtained for the initial materials. Changes in the transition energies are interpreted in terms of the changes in structure brought about by the comminution processes.

Thermal Analysis, Preliminary DTA

Preliminary DTA were run on 40 mineral powders, which were prepared in order to screen for candidates for the final mineral standards. All of these samples were run, except for several quartz, beryl, and fluorite specimens that were redundant with other samples of higher quality.

Group 1 Minerals--

Quartz

The DTA patterns for the Q-1, Q-2, and Q-3 quartz specimens each showed the characteristic α to β transition. The peak was of very similar size and shape for each of the samples, and no other distinguishing features were present. They all appeared qualitatively equivalent (Figure 12).

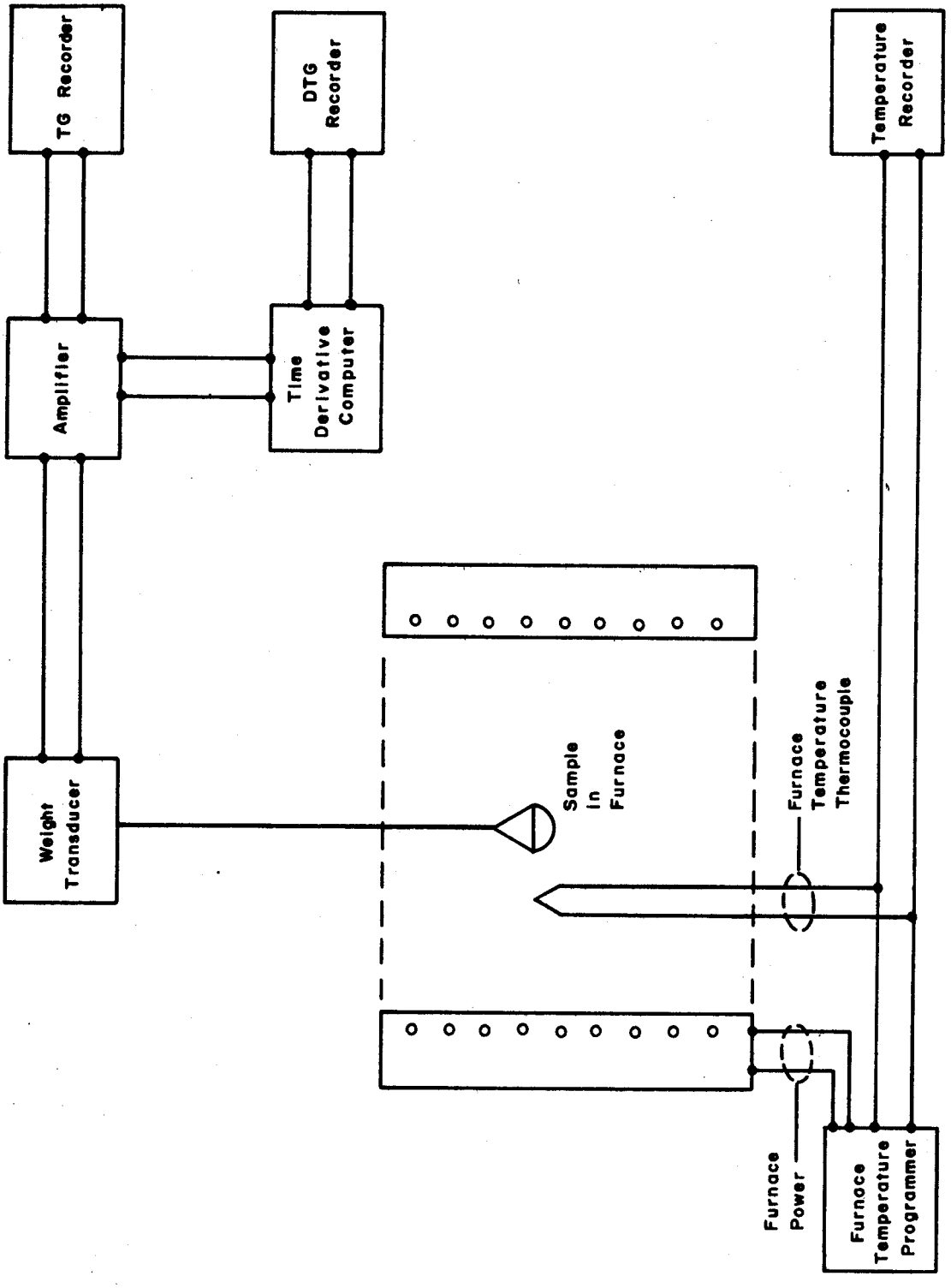

Figure 11. Block diagram of the TGA apparatus.

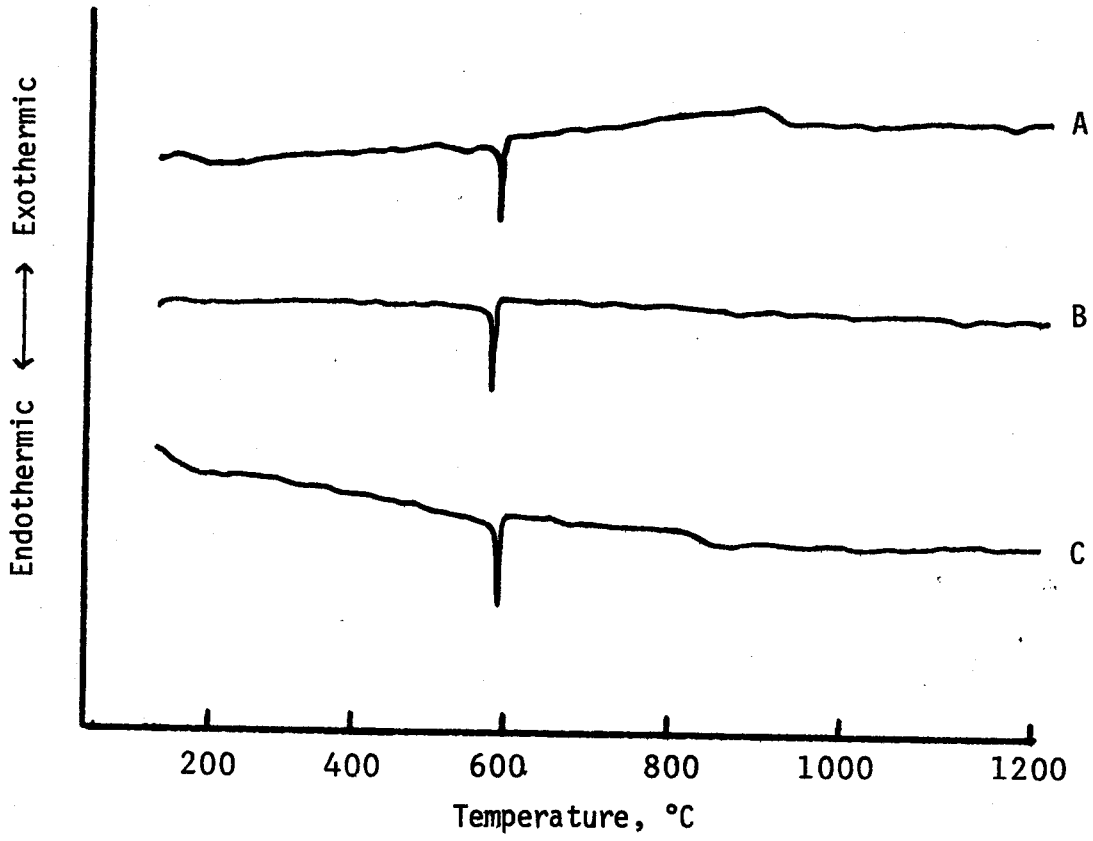

Figure 12. DTA patterns of quartz samples:

A. Q-2, Wards, Brazil
B. Q-1, Sobin Chemical, North Carolina
C. Q-3, Wards, Hot Springs, Arkansas

Beryl, Fluorite, Nickel Oxide

Specimens B-11, F-16, and N-20 had flat, featureless DTA curves with no distinquishing thermal transitions (Figure 13). They formed hard, fused masses on the DTA thermocouple which were difficult to remove.

Groups 2 and 3 Minerals

Because fibrous and nonfibrous varieties of these minerals do not show distinguishing thermal characteristics that can be used to tell them apart, they are considered together here. Examples of DTA patterns selected from the literature are shown in Section 6 of this document.

Chrysotile and Antigorite

The DTA traces for the serpentine survey are shown in Figures 13 and 14. The AG-51 specimen showed the greatest similarity to that of reported curves for antigorite. The AG-54 specimen displayed the largest endotherm and exotherm peaks. The AG-55 specimen was again slightly different. Although the AG-57 specimen showed peaks similar to the AG-51 specimen, the peaks were only half as large. The impurities in AG-57 could not be readily removed so it was eliminated from further consideration.

The DTA pattern for the chrysotile sample (CH-28) was distinguished from the other serpentine samples shown only by the broad, flat space between the endotherm at 620°C and the exotherm at 820°C. The interval was much smaller for the other serpentine samples which all happened to be nonfibrous.

Crocidolite and Riebeckite

In Figure 15, the two crocidolite samples each show an endotherm in the region of 900 to 1000°C. The uncertain wavy pattern in the curves preceeding this endotherm was not repeatable as such. It may have been due to the material, which was very fluffy and difficult to pack into the DTA cell. The riebeckite (R-62) removed from the crocidolite specimen (CR-34) also showed the endotherm at 950°C.

Other riebeckite DTA patterns are shown in Figure 16. A steep well-defined peak at 950°C appeared much more characteristic of crocidolite than of riebeckite. The reported riebeckite peak appeared close to 1100°C, whereas the crocidolite peak was around 910°C. The R-60 mineral had a second, smaller endotherm at 850°C. The R-50 sample endotherm at 950°C was about half the size of that of the R-60 sample and lacked the second endotherm at 850°C; otherwise, the DTA pattern was undistinguished in spite of the high level of contamination it suffered.

The R-62 specimen was also known to have a high contamination level--55% quartz estimated by microscopical examination. The quartz, however, appeared only faintly as a small blip on the thermogram. The only reasonable explanation is that the quartz was so intimately mixed with the rest of the mineral matrix that it could not show its characteristic α to β transition (573°C). Thus, the lack of a characteristic DTA pattern cannot by itself indicate that a contaminant is absent; each case must be determined individually until a better generalization can be made.

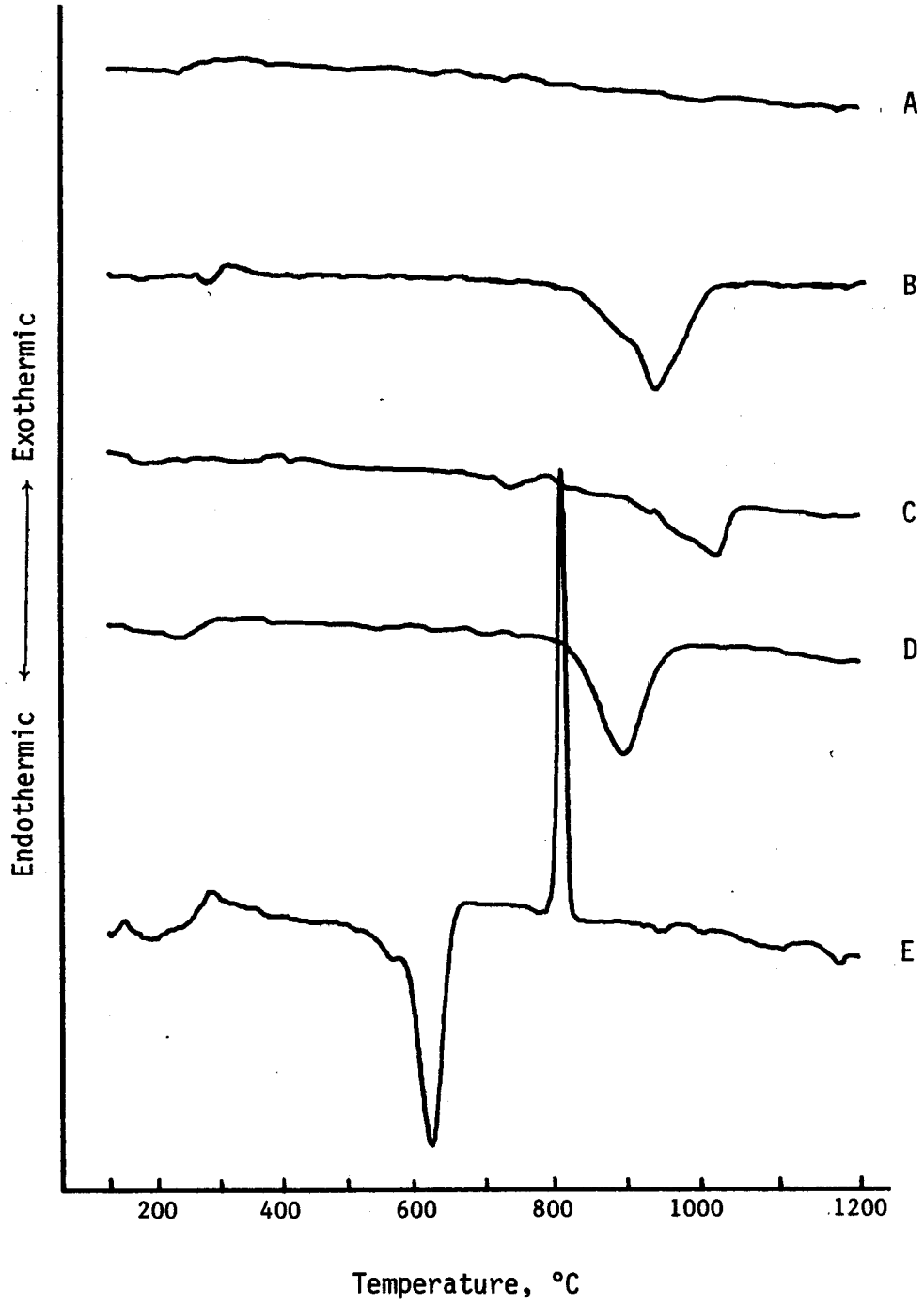

Figure 13. DTA patterns of:

A. Nickel oxide, N-20, Johnson-Matthey Company, Synthetic
B. Talc, TA-99, Montana Bureau of Mines, Montana
C. Talc, TA-95, Dr. Woodland, Gouverneur, New York
D. Talc, TA-98, National Stockpiles, India
E. Chrysotile, CH-28, Union Carbide Corporation, Idria Range, California

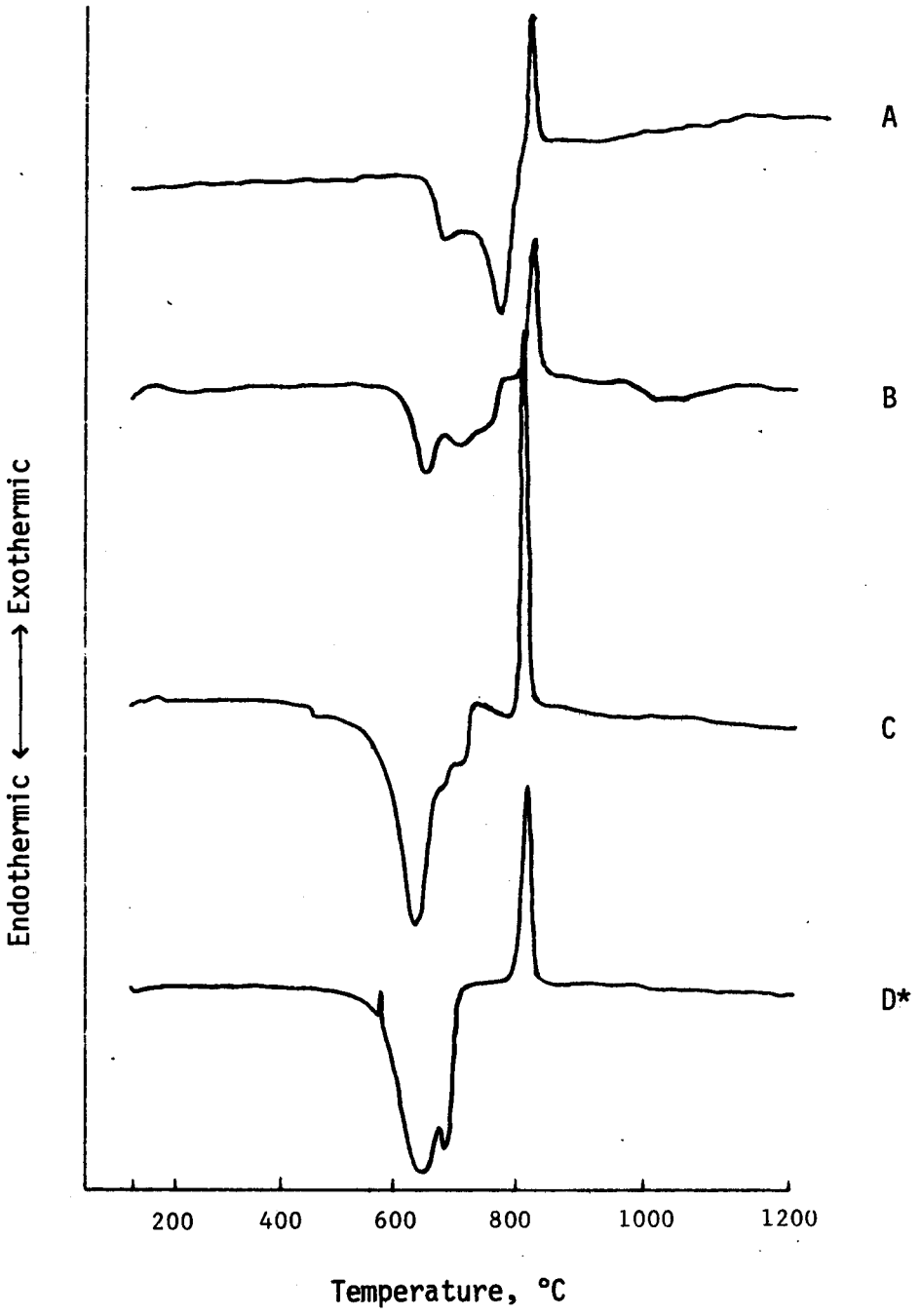

Figure 14. DTA patterns of antigorite samples:

A. AG-51, Mackinaw Geological Supply, Ishpeming, Michigan
B. AG-57, Dr. Woodland, Easton, Pennsylvania
C. AG-54, Dr. Woodland, Lenni Mills, Pennsylvania
D. AG-55, Dr. Woodland, West Chester, Pennsylvania

*Small exotherm at 570°C is due to quartz powder placed in reference cell.

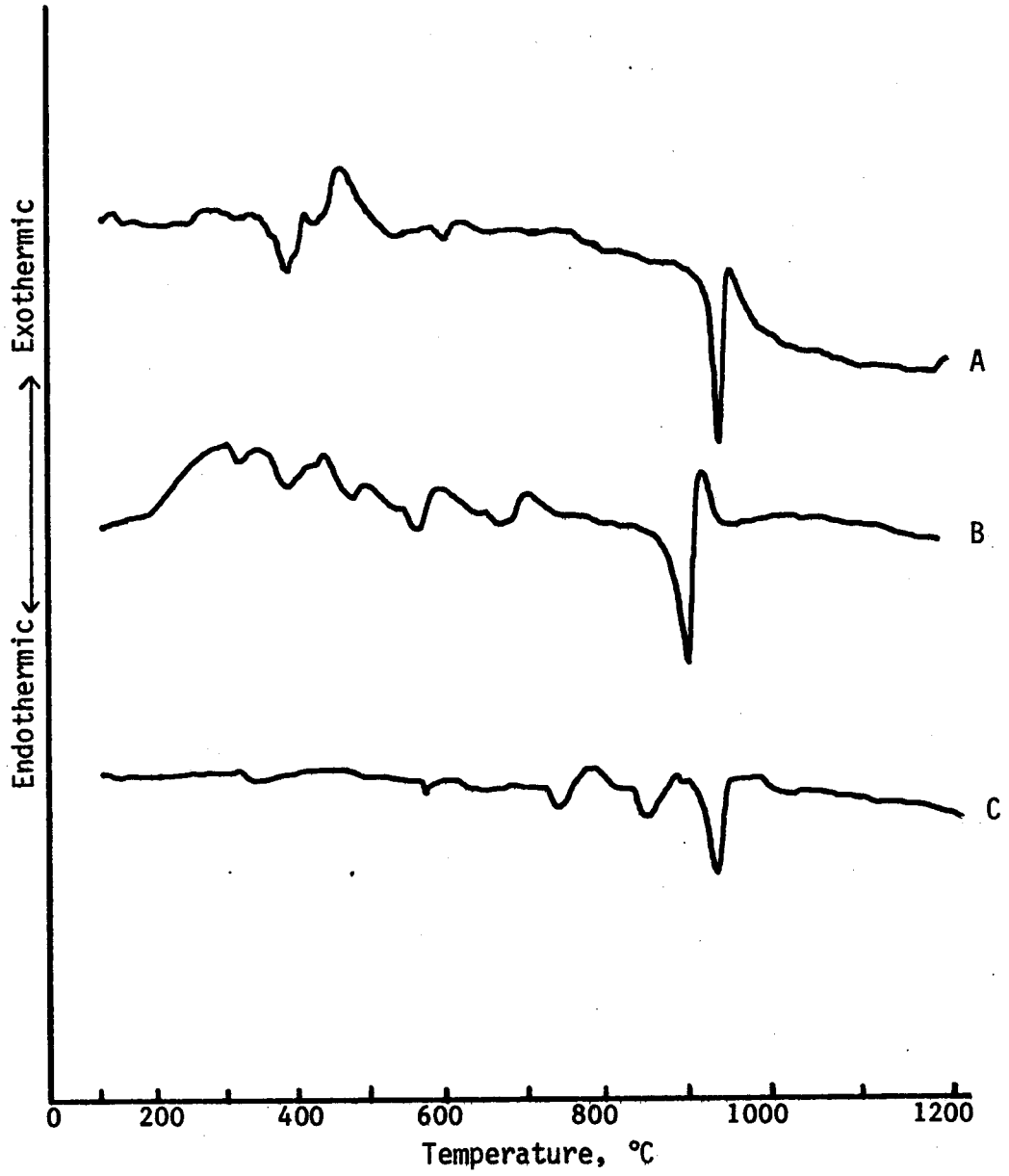

Figure 15. DTA patterns of:

A. Crocidolite, CR-35, National Stockpiles, South Africa
B. Crocidolite, CR-34, Wards, South Africa
C. Riebeckite, R-62, Wards, South Africa

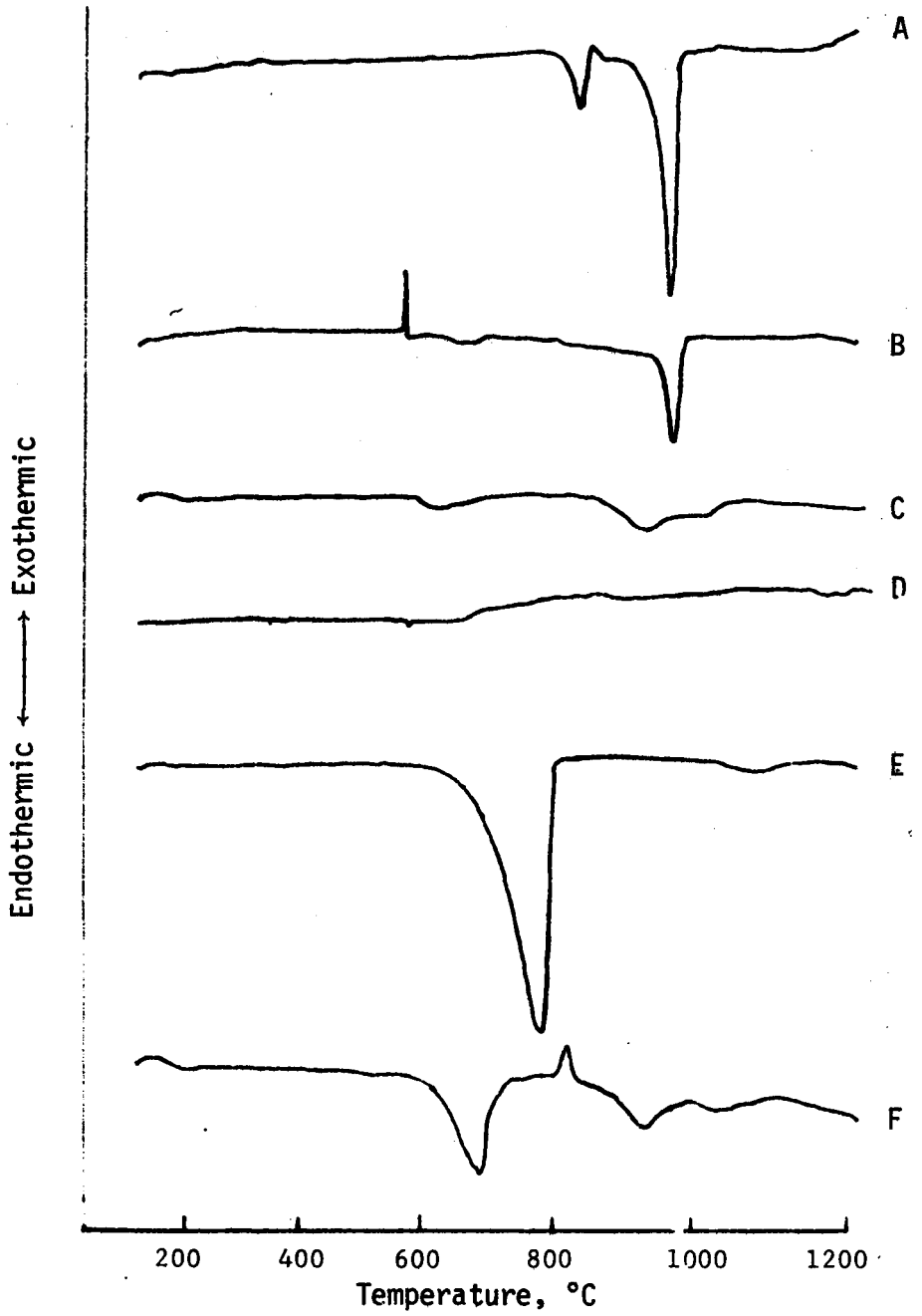

Figure 16. DTA patterns of amphiboles:

A. Riebeckite, R-60, Wards, El Paso County, Colorado
B. Riebeckite, R-59, Mackinaw Geological Supply, Palmer, Michigan
C. Fibrous Anthophyllite, AF-43, Wards, North Carolina
D. Fibrous Anthophyllite, AF-42, Mackinaw Geological Supply, Ontario, Canada
E. Tremolite, T-75, Mackinaw Geological Supply, Felch, Michigan
F. Tremolite, T-76, Dr. Woodland, Easton, Pennsylvania

Tremolite

Tremolite DTA patterns are shown in Figures 16 and 17. The one fibrous tremolite sample, TR-48, available in sufficient quantity for DTA, had a well-defined endotherm at approximately 950°C, with an apparent second endotherm on its upscale shoulder. The five nonfibrous tremolites analyzed by DTA showed the former endotherm anywhere from 920° to 1050°C. For the fibrous sample, this peak was the only distinguishing feature of the thermogram.

The T-79 (Figure 17) and T-76 (Figure 16) specimens displayed similar patterns. They showed two endotherms of about equal size at 600° and 1050°C separated by a sharp exotherm at 800°C. A faint repetition of this pattern seemed evident in the DTA for the fibrous anthophyllite, AF-45 (Figure 17).

The third tremolite sample, T-77 (Figure 17) showed a very large endotherm at 750°C. The shape and position of this endotherm was similar to that of the T-75 sample (Figure 16). The T-77 sample showed a second endotherm at approximately 1050°C, about one-third as large as the first peak. The second peak was only faintly evident in the T-75 sample.

Grunerite

The G-63 grunerite sample (Figure 17) had a large endotherm at 1200°C, which was cut off before completion in the present run. A much attenuated version of this peak was noted in the G-66 sample (Figure 18). A moderate endotherm at 1050°C and a hint of one at 800°C were also features of this DTA pattern.

Cummingtonite

The C-71 cummingtonite sample (Figure 18) had an essentially flat pattern, with no distinguishing features.

Fibrous Grunerite (Amosite)

The fibrous grunerite (amosite), GF-38, (Figure 17) had no distinquishing features except a broad exotherm that peaked at 300°C. A second broad exotherm peaked at 300°C.

Anthophyllite

The fibrous anthophyllite, AF-45, peak (Figure 17) was small but similar to those of the T-79 and T-76 tremolites.

Group 4 Minerals--
Talc

The talc DTA trace was distinguished by a single moderate-sized endotherm at 840 to 1050°C. The talc curves are shown in Figures 13 and 18. Except for TA-91 (Figure 18e), the talc traces all showed single, similar peaks. Even for samples shown to be relatively pure by microscopical analysis, the peak temperature, size, and even shape were distinctively different for each of the specimens run.

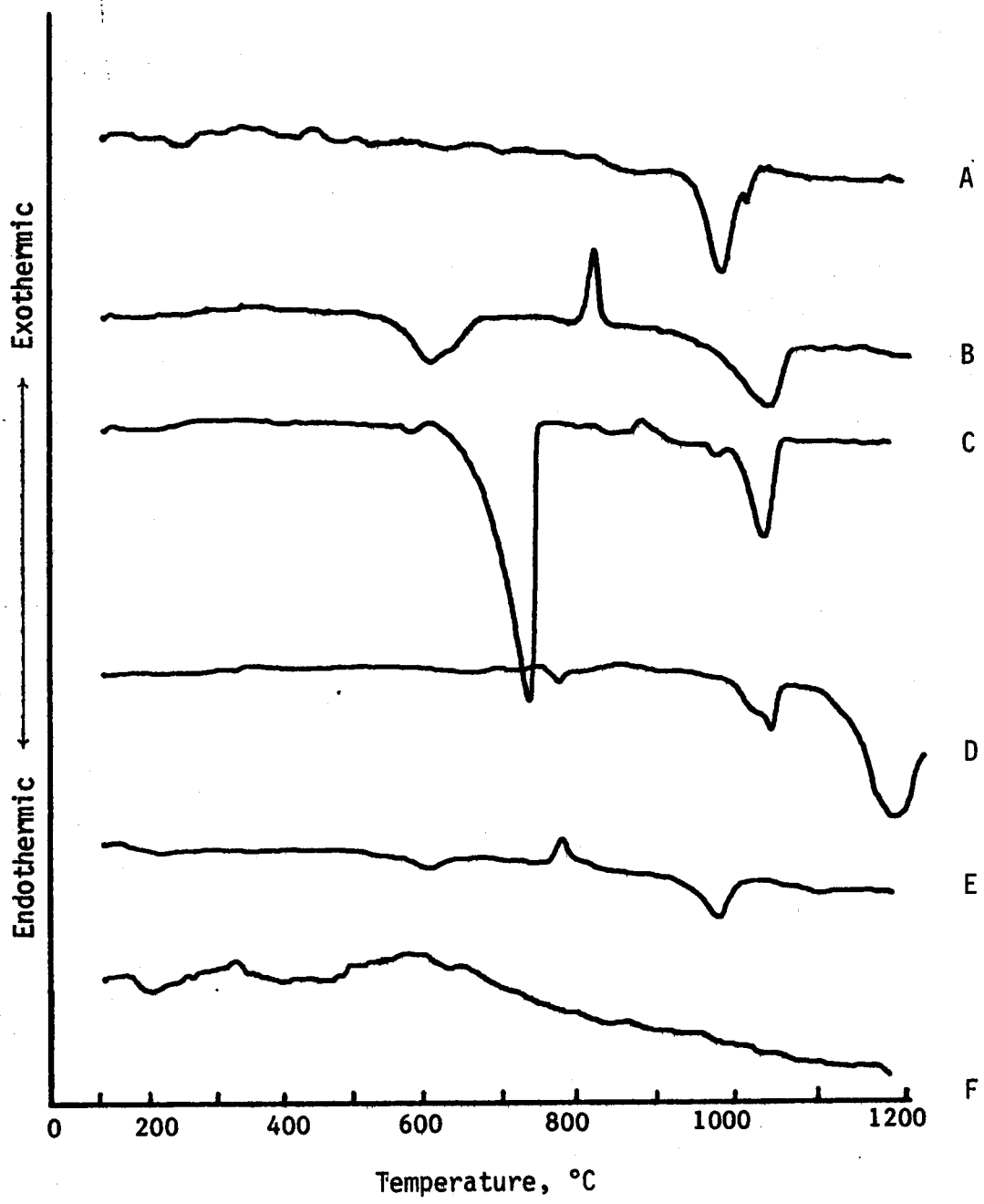

Figure 17. DTA pattern of several amphiboles:

A. Fibrous Tremolite, TF-48, Wards, Rajasthani, India
B. Tremolite, T-79, NIEHS, Gouverneur, New York
C. Tremolite, T-77, John Carter, Pennington Coutny, South Dakota
D. Grunertie, G-63, John Carter, South Dakota
E. Fibrous Anthophyllite, AF-45, Montana Bureau of Mines, Montana
F. Fibrous Grunerite, GF-38, Wards, Lyndenburg, South Africa

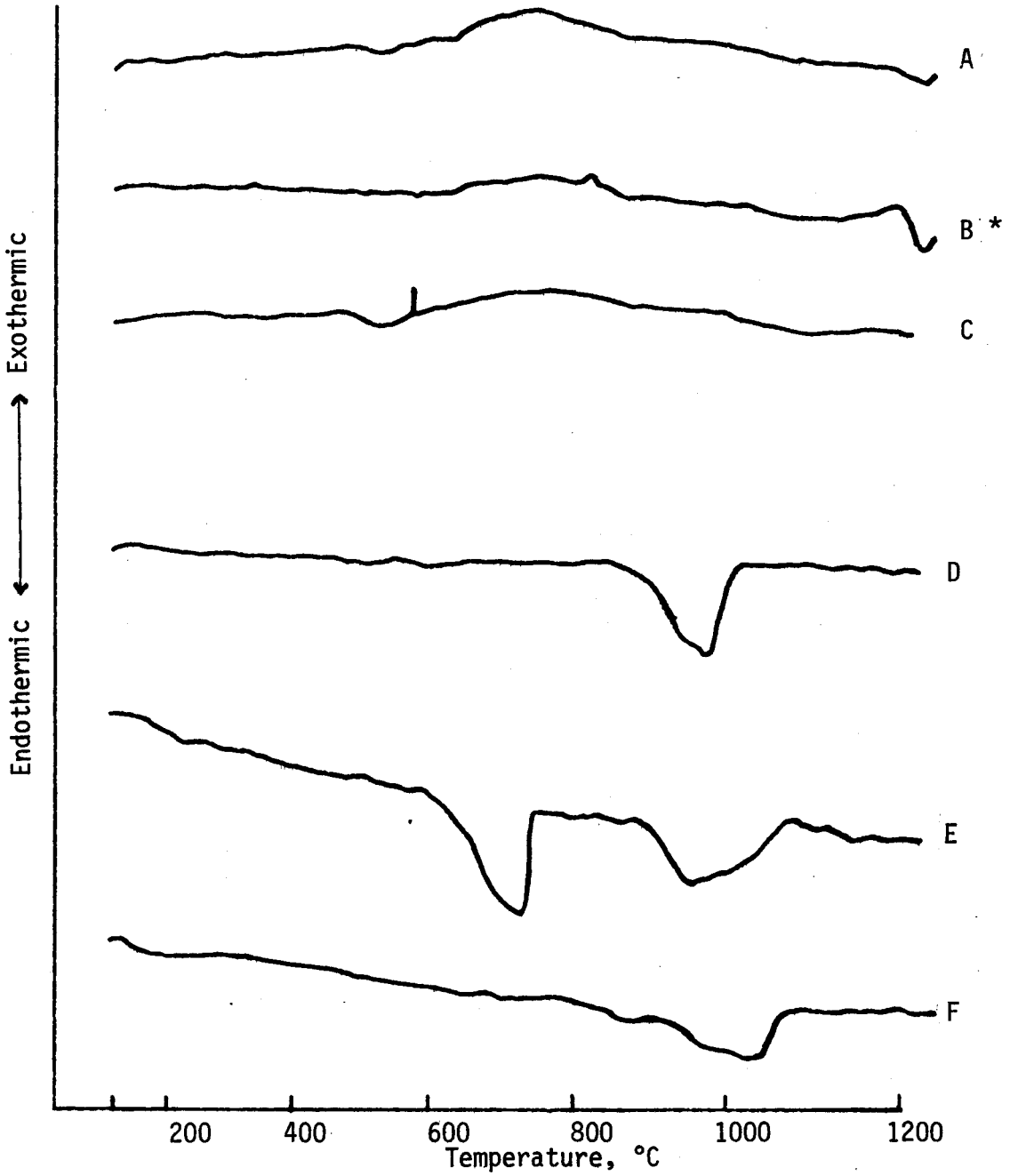

Figure 18. DTA patterns of amphiboles and talc:

A. Cummingtonite, C-71, John Carter Lead (Homestead Mine), Lawrence County, South Dakota
B. Grunerite, G-66, Dr. Woodland, Silver Bay, Minnesota
C. Grunerite, G-64, Mackinaw Geological Supply, Michigamme, Michigan
D. Talc, TA-97, Johnson and Johnson, Vermont
E. Talc, TA-91, Wards, Madoc, Ontario, Canada
F. Talc, TA-92, Wards, Fowler, New York

*Small exotherm at 570°C is due to quartz powder placed in reference cell.

MINERALS SELECTED AS STANDARDS

The results of combined polarized light microscopical, x-ray diffraction, and thermal analyses of each sample made it possible to select the best specimen of each mineral in each category readily. Minerals selected for processing as the final standards, as well as specific sample source and general locale of origin, are listed in Table 7.

It should be noted that two samples each of quartz and nonfibrous tremolite were selected for processing. Because the commercially processed quartz (Q-107) had been used by NIOSH for testing, a second, natural quartz sample (Q-1) was selected by IITRI as the primary reference material so that comparisons of crystallinity could be studied. Both of these quartz samples were supplied to NIOSH but only the Q-1 sample was fully characterized, as specified under the contract. Two tremolite samples, T-77 and T-79, were also processed and delivered to NIOSH. The T-7 sample, a western states tremolite, was fully characterized by IITRI so it could be compared to the T-7 sample, an eastern tremolite, that had been previously studied by NIOSH.

The following paragraphs detail the origins (geographical or synthetic) of the selected mineral samples.

Q-1, Quartz, Sobin Chemical Company, Spruce Pine, Mitchell County, North Carolina

The material is commercially supplied as a high purity quartz sand termed IOTA quartz. The mineral is not mined as a quartz sand, but rather is a byproduct of feldspar production. The feldspar is mined from a large deposit in Mitchell County, North Carolina. The quartz, separated from the feldspar by froth flotation, is then purified by further density separations and acid washing.

Q-107, Quartz, Pennsylvania Glass Sand Corporation

This commercial quartz, Min-U-Sil, is produced from high purity, raw silica sands. A nonacid wash before and after grinding cleans the samples from surface impurities associated with the raw sand and those introduced by grinding. Mechanical grinding methods are employed to produce the desired size ranges.

B-11, Beryl, John Carter, Pennington County, South Dakota

Beryl is characteristic of certain pegmatite occurrences in the Black Hills of South Dakota, as is this sample.

Table 7. Minerals selected as standards.

IITRI No.	Material	Source	Locale
Q-1	Quartz	Sobin Chemical Company	North Carolina
Q-107*	Quartz	Pennsylvania Glass Sand Corporation	Commercial
B-11	Beryl	Mr. John Carter	South Dakota
F-17	Fluorite	Baker Chemical Company	Synthetic
N-108	Nickel Oxide	Baker Chemical Company	Synthetic
CB-25	Cristobalite	Pennsylvania State University	Synthetic
TY-27	Tridymite	Pennsylvania State University	Synthetic
CH-29	Chrysotile	Union Carbide Corporation	California
CR-37	Crocidolite	National Research Institute for Occupational Disease (NRIOD)	South Africa
GF-38	Fibrous Grunerite (Amosite)	Wards Natural Science Establishment	South Africa
AF-45	Fibrous Anthophyllite	Wards Natural Science Establishment	Montana
TF-48	Fibrous Tremolite	Wards Natural Science Establishment	India
AG-55	Antigorite	Dr. Bertram Woodland	Pennsylvania
R-60	Riebeckite	Wards Natural Science Establishment	Colorado
G-68	Grunerite	Iron Ore Company of Canada	Newfoundland
C-71	Cummingtonite	Mr. John Carter	South Dakota
A-102	Anthophyllite	Mineralogisk-Geologisk Museum of Norway	Norway
T-77	Tremolite	Mr. John Carter	South Dakota
T-79*	Tremolite	National Institute of Environmental Health Sciences	New York
TA-99	Talc	Montana Bureau of Mines	Montana

* One-kg samples were supplied as beneficiated, comminuted minerals, but without the required data on size and phase purity.

F-17, Fluorite, J.T. Baker Chemical Company, Phillipsburg, New Jersey

According to Baker Chemical Company, "calcium fluoride is manufactured by reacting hydrofluoric acid and calcium carbonate to precipitate calcium fluoride with the liberation of water and carbon dioxide."

N-108, Nickel Oxide, J.T. Baker Chemical Company, Phillipsburg, New Jersey

According to J.T. Baker Chemical Company, nickel metal is reacted with nitric acid to yield nickel nitrate. This product is then heated at 700°C for a time sufficient to remove all nitrates and meet a minimum assay specification. The green nickel oxide is then graded and blended to give a uniform product.

CB-25, Cristobalite, Dr. Rustum Roy, Pennsylvania State University

Details of the synthesis procedure are given in Section 3, pp. 22-24.

TY-27, Tridymite, Dr. Rustum Roy, Pennsylvania State University

Details of the synthesis procedure are given in Section 3, pp. 24-25.

CH-29, Chrysotile, Union Carbide Corporation, Idria Range, San Benito County California

Chrysotile occurs as fibrous veins in serpentine rock, which is derived from the alteration of ultrabasic igneous rock. Likely contaminants are antigorite (or lizardite), iron ores, and possibly talc. This occurrence is unusual in that it is in a sheared mass, and appears nonfibrous to the naked eye. The serpentine deposit mined by Union Carbide is located in the Idria Range (Santa Rita Mine) in San Benito County.

CR-37, Crocidolite, National Research Institute for Occupational Diseases, Transvaal and Northwest Cape Provinces, South Africa

The geological occurrence of crocidolite is in banded ironstones of Precambrian age. Associated minerals (and thus possible contaminants) are quartz, magnetite, some hematite and pyrite, rare pyroxene, and some nontronite as an alteration product. Precise geographic location from which this sample was obtained is not known since the NRIOD composited representative samples from operating mines in the Northwest Cape and Transvaal asbestos districts of South Africa.

GF-38, Fibrous Grunerite, (Amosite), Wards Natural Science Establishment, Lyndenburg, Transvaal Province, South Africa

The geological occurrence of fibrous grunerite is in banded ironstone formations of Precambrian age. Accompanying minerals are magnetite, quartz, and grunerite and cummingtonite prisms, as well as carbonate and alteration

products, such as nontronite. The precise geographic location from which this sample was obtained is not know. Its general source was the Lyndenburg-Petersburg belt in the Transvaal, South Africa.

AF-45, Fibrous Anthophyllite, Wards Natural Science Establishments, Gallatin County, Montana

The geological occurrence and precise geographical origin of this sample were not given. The sample, however, probably originated in the Karst Resort area of Gallatin County, Montana. Anthophyllite occurs in altered peridotite dikes in Precambrian schist and gneiss. Probable associated minerals include iron ore, serpentine, talc, and other amphiboles.

TF-48, Fibrous Tremolite, Wards Natural Science Establishment, Rajasthani, India

The geological occurrence of this specimen is not known. Fibrous tremolite commonly occurs in shear zones of altered dolomitic limestones or marble. Contaminants may be carbonate, prismatic tremolite, and possibly talc.

AG-55, Antigorite, Dr. Bertram Woodland, West Chester, Chester County, Pennsylvania

The geological occurrence is as a lens of serpentinized ultrabasic rock in a metasedimentary sequence. Magnetite (or chromite) is ubiquitous, and amphibole (anthophyllite) and talc may occur.

R-60, Riebeckite, Wards Natural Science Establishment, El Paso County, Colorado

The riebeckite occurs in coarse pegmatitic granite, one of the characteristic occurrences. The central portion of Colorado, in which El Paso County is located, is characterized by instrusive rocks of both Precambrian and Genogoic age and associated metamorphic rocks.

G-68, Grunerite, Iron Ore Company of Canada, Luce Lake, Newfoundland

The geological occurrence is in the Wabush Iron Formation of Precambrian age. Associated minerals are likely to be quartz, magnetite, actinolite, diopside, and carbonate, also possibly hypersthene, garnet, and chlorite.

C-71, Cummingtonite, John Carter, Lead (Homestake Mine), Lawrence County, South Dakota

The geological occurrence is in the metamorphosed Homestake Formation. Associated minerals include quartz, chlorite, biotite, garnet, with sulfides, (particularly pyrrhotite and pyrite), iron oxides, plagioclase, and more rarely, graphite. Not all of these occur in every hand sample.

A-102, Anthophyllite, Mineralogisk-Geologisk Museum of Norway, Bamble, Norway

The geological occurrence is in a complex series of metamorphis rocks. The accompanying minerals may be cordierite, rutile, biotite, and apatite. In other occurrences they may be plagioclase, quartz, biotite, rutile, and tourmaline; or hornblende, muscovite, and quartz.

T-77, Tremolite, John Carter, Pennington County (Black Hills Meridian), South Dakota

The tremolite occurs in metamorphosed dolomitic limestones; carbonate is thus a normal matrix mineral.

T-79, Tremolite, National Institute of Environmental Health Sciences, Gouverneur, Lawrence County, New York

Tremolite from this locality occurs in metamorphosed magnesian limestone of Precambrian age. Carbonate is a probable contaminant, and a little talc may possibly also occur.

TA-99, Talc, Montana Bureau of Mines (Beaverhead Mine) Madison County, Montana

The sample was obtained from ore piles at the Beaverhead Mine. The geological occurrence is as lenses in hydrothermally altered dolomitic marble. It may contain unaltered carbonate rare chlorite, graphite, iron and manganese oxides, and perhaps, rarely, tremolite and quartz. It is most unlikely that all these would be present in a sample; normally the talc is very pure.

SECTION 5

BENEFICIATION AND SIZE REDUCTION PROCEDURES

METHODS FOR REMOVING BULK IMPURITIES

Nearly all of the specimens of the groups 2, 3, and 4 minerals required some type of beneficiation to produce a high quality final product. Beneficiation could be achieved at any one, or all three, stages of sample processing: disaggregation, pre-grinding (after crushing to an appropriate feed size for the mill to be employed), or post-grinding. Beneficiation techniques employed included hand cobbing, chemical dissolution, density separation, and magnetic separation. Table 8 summarizes the beneficiation techniques used on each sample. The following subsections describe procedures involved in each of the beneficiation techniques.

Sample Preparation

The starting materials, received as natural rock fragments, were first washed with a brush under flowing laboratory tap water to remove, as much as practicable, soil, iron oxide stains, dust, packing material, weathered rock, and organic debris such as lichens. The specimens were then air-dried and stored in clean containers that could be sealed. Quartz (Q-1) and fibrous tremolite (TF-48) were received clean and in sealed containers. Washing was unnecessary or impractical for the commercially processed, powdered minerals and synthetic minerals.

Three small (15 to 50 cm^3 each) representative samples were taken from each selected starting material for retention in historical records. Each sample was sealed in a small plastic bag and labelled with the name of the material, IITRI code number, geographic source, and supplier.

The selected materials were weighed after the washing procedure had been completed, but before sampling or any preparative work was performed. Very limited quantities of some of these materials were available and weighing was necessary to determine whether an adequate supply was on hand to enable the preparation of at least 1 kg of the desired product.

The data from the macroscopic characterization and instrumental analyses were then reviewed. A consensus was developed from these evaluations, regarding what contaminant minerals were present and in what proportion, the amenability of the material to beneficiation techniques, and the losses in mass to be expected from the removal of contaminants and generally from the beneficiation and grinding methods to be employed.

Table 8. Pre- and post-grinding beneficiation techniques applied.

Mineral No.	Beneficiation Required		Hand-Cobbing (Pre-Grinding)	Chemical Dissolution (Pre-and Post-Grinding)	Density Separation (Pre-Grinding)	Other (Pre- and Post-Grinding)
	Pre-Grind	Post-Grind				
Q-1	No	Yes		Post: hydrochloric acid wash to remove grinding contaminants		
Q-107	No	No				
B-11	Yes	No	Hand-picked cleanest chunks after disaggregation		Density separation of quartz *	Pre: magnet separation of magnetite after disaggregation
F-17	No	No				
N-108	No	No				
CB-25	No	Yes		Post: hydrochloric acid wash to remove grinding contaminants		
TY-27	No	Yes		Post: hydrochloric acid reflux to remove grinding contaminants		Post: magnet separation of metal ball-milling contaminants in slurry
CH-29	No	No				

* Not successful.

Table 8 . (continued)

Mineral No.	Beneficiation Required: Pre-Grind	Beneficiation Required: Post-Grind	Hand-Cobbing (Pre-Grinding)	Chemical Dissolution (Pre- and Post-Grinding)	Density Separation (Pre-Grinding)	Other (Pre- and Post-Grinding)
CR-37	Yes	No	Hand-picked best fiber bundles from rock matrix after disaggregation			Pre: water flotation to remove contaminants introduced by sawing
GF-38	Yes	No	Magnetite, mica, carbonates chipped and hand-picked from disaggregated sample			Pre: water flotation to remove contaminants introduced by sawing
AF-45	Yes	No	Mica, carbonates chipped and scraped away; hand-picked best fiber bundles from disaggregated sample			Pre: water flotation to remove contaminants introduced by sawing
TF-48	Yes	No	Hand-picked best fiber bundles from loose rock contaminants			
AG-55	Yes	Yes	Remove magnetite, probable fibrous veins, other mineral phases by chipping and scraping during disaggregation			Pre and Post removal of magnetite by magnet

Table 8. (continued)

Mineral No.	Beneficiation Required: Pre-Grind	Beneficiation Required: Post-Grind	Hand-Cobbing (Pre-Grinding)	Chemical Dissolution (Pre- and Post-Grinding)	Density Separation (Pre-Grinding)	Other (Pre- and Post-Grinding)
R-60	Yes	No	Remove matrix minerals by hand-chipping and picking during disaggregation		Density separation of quartz	
G-68	Yes	No	Remove magnetite and other minerals by hand-chipping and picking during disaggregation		Density separation of quartz	
C-71	Yes	No	Remove magnetite, mica, and other minerals by hand-chipping and picking during disaggregation		Density separation of quartz, mica *	
A-102	Yes	No			Density separation of quartz	
T-77	Yes	No	Remove carbonates, mica by hand-chipping and picking during disaggregation	Pre: treat with acetic acid to remove carbonates	Bromoform separation of mica, quartz	

* Not successful.

Table 8. (concluded)

Mineral No.	Beneficiation Required		Hand-Cobbing (Pre-Grinding)	Chemical Dissolution (Pre- and Post-Grinding)	Density Separation (Pre-Grinding)	Other (Pre- and Post-Grinding)
	Pre-Grind	Post-Grind				
T-79	Yes	Yes		Post: acetic acid wash to remove carbonates		Sieved prior to jet-milling
TA-99	No	No				

Beneficiation Techniques

The general methods, procedures, material, and apparatus employed in the separation of desired minerals from unwanted contaminant materials are described in this section; specific procedures followed for each mineral are described in the individual sample reports. Relatively simple separatory techniques were chosen to conserve the selected materials--techniques that may be applied to material varying widely in size. To control contamination, especially cross-contamination among the selected materials, all apparatus was thoroughly cleaned immediately before each use and many separatory steps were performed in a vented hood.

Separatory methods performed by hand include cobbing and hand-picking of two types: removal of fine-grained contaminant phases, and "high grading." These techniques, laborious preliminaries to more sophisticated methods, have the advantage of conserving scarce materials. All methods require that the starting material be reduced to a size at which adequate liberation of the wanted and unwanted minerals can be obtained. The size reduction methods employed are discussed in the next section. "High grading" involves the selection of the larger fragments of relatively pure desired material from the broken rock mass. Cobbing is the breaking away of unwanted portions from the selected larger fragments, generally by using hammers and chisels. A special cobbing technique is applied to relatively soft materials in which the unwanted phases are concentrated as coatings on fracture surfaces or as veins. A sharp knife works well in scraping away such material and in picking out larger grains embedded in the desired material. Hand-picking of finely ground material is very time consuming. Because a large quantity of product was desired for this program, a minimum grain size of $\geq$0.5 mm was used, and fines were hand-picked only to remove relatively scarce and obvious contaminants from concentrates of desired material. This was done with forceps or a wetted fine brush or needle.

Removing wall rocks from cross-fiber vein specimens of asbestiform minerals presented a special problem. These minerals are too hard and tough and, generally, too firmly attached to the adjacent rock to be separated by the foregoing cobbing methods. Breakage occurs more often throughout the mass of parallel fibers rather than between the fibers and the wall rocks. This problem was overcome by cutting the wall rock from the fibrous mineral veins with a rock saw.

Several of the selected mineral samples contained carbonate minerals, predominantly calcite and dolomite, either as minor contaminants (as in the commercially processed samples), or as major mineral phases (as in the natural rock samples). The carbonates were generally fine-grained and intimately associated with the desired mineral phase. Acid dissolution is usually the most effective method of removing these contaminants. The fine-grained nature of the carbonates, however, made it necessary to reduce the grain size of the sample somewhat before proceeding to acid dissolution.

The carbonate digestions were performed in large beakers with dilute (2.91 N) acetic acid. Once the grain size of the mineral sample had been reduced to expose the carbonate phase adequately, the sample was suspended

in the dilute acid. Digestion of carbonates is essentially complete when no further effervescence (evolution of CO_2) is evident. Depending upon the amount of carbonate material present, this digestion step required from less than 1 hour (e.g., samples with less than 2% carbonates) to 3 weeks (e.g., samples with greater than 20% carbonates) to reach completion. While the carbonate digestion step could be speeded up in heavily contaminated samples by using a more concentrated acetic acid solution, the risk of chemically altering the desired mineral phase increases with increasing acid concentration. During digestion, the mineral sample was stirred periodically to ensure thorough mixing with the acid. Samples containing agglomerated fine material were continuously agitated in an ultrasonic bath to ensure that the carbonates were kept in contact with the acid. When necessary, the acid bath was renewed with fresh solution.

Once the evolution of CO_2 had ceased and the material had settled from suspension, the acid solution was decanted. The remaining mineral concentrate was agitated as before in a large volume of distilled water and allowed to settle from suspension. The wash water was decanted. The washing procedure was repeated at least four more times, a process more efficient than rinsing the concentrate on filter paper and with less risk of contamination. After the concentrate was thoroughly washed, the material was oven-dried at a low temperature setting.

Two techniques that exploit the magnetic properties of certain minerals were used for separative work. The first depends on the ferromagnetism of magnetite, which is a major contaminant dispersed throughout several of the selected materials. The desired mineral was ground to a fine grain size to release the magnetite adequately. (Air jet milling to the final product size was required to liberate minute magnetite particles from antigorite.) The magnetite was then removed with an ordinary handheld magnet wrapped in glassine weighing paper. If the mineral sample was also contaminated with carbonates, the magnetite was separated before the acid treatment to remove carbonates; this avoided oxidizing magnetite to hematite during the digestion and drying steps.

A second magnetic technique that exploits the differences in magnetic susceptibility of minerals was used for the separation of silicate minerals contaminated by other silicates. Chemically, silicates are members of solid solution series. Although the associated silicates may differ significantly in chemistry, in many instances their specific gravities are very similar. This precludes efficient isolation of the desired silicate from unwanted silicates by density separation with the use of heavy liquids (discussed below). Neither can the silicate contaminants be removed by dissolution with strong acids because the desired mineral also would be dissolved or severely affected by this acid. The second magnetic technique, however, effects separation by subjecting narrowly limited size fractions of mineral grains to a strong, uniform magnetic field, using a Frantz isodynamic magnetic separator.

A final beneficiation method involved density separation of minerals by use of heavy liquids. To efficiently treat large quantities of material by this method, the specific gravities of desired and unwanted materials must

differ by at least 0.2 g/cm^3. The simple sink-float version of this method was used for ground material with grain sizes consistent with adequate liberation of the associated phases.

The selected liquids were intermediate in density between those of the desired and unwanted phases. The high specific gravities of most of the desired minerals for which this method is appropriate make those minerals the "sinks" fraction, whereas the lighter contaminant phases are the "floats," which rise to the surface of the liquid where they may be skimmed off or decanted. For the sink-float pairs separated in this program, bromoform and acetylene tetrabromide (1,1,2,2-tetrabromoethane) were appropriate because their densities fall about halfway between those of the least dense desired mineral and the most dense major contaminant. The density of bromoform may be adjusted by dilution with acetone and that of acetylene tetrabromide with ethanol. If the material was fairly coarse-grained, stirring was sufficient to break up agglomerated masses in the liquids. If much fine-grained material was present, agitation in an ultrasonic bath while stirring broke up particle agglomerates. The beakers of heavy liquid were then left to stand undisturbed briefly until migration of grains to the bottom or to the surface was completed. The top portion of the liquid carrying the "floats" was decanted, and the liquid was retrieved by filtration. The desired "sinks" were filtered from the remaining liquid.

The appropriate diluent, acetone or ethanol, was used to wash the residue of heavy liquid from the desired mineral following exactly the same procedure that was described for washing acetic acid solution from mineral concentrates with distilled water. That procedure was then repeated with distilled water to wash away residual acetone or ethanol. Finally, the excess water was decanted and the mineral concentrate was oven-dried at a low temperature setting.

As noted previously, two drying methods were employed. Whether drying was performed slowly at ambient temperature in the laboratory or more rapidly using an oven, the material was covered with a cowl of aluminum foil to minimize contamination by airborne dust. The dry beneficiated materials were stored in clean, sealed, wide-mouth glass jars until final grinding.

SIZE REDUCTION TECHNIQUES

Several different grinding steps were used in the production of the final mineral standards. Some grinding steps produced materials amenable to beneficiation procedures. For those mineral specimens requiring little or no beneficiation, preliminary grinding steps produced an appropriately sized feed material for the final grinding apparatus to be employed.

Disaggregation of nonfibrous minerals obtained as rock specimens was usually accomplished with a large stainless steel mortar and pestle or, if it was necessary to separate desired phases from contaminant veins, with a mason's hammer and chisels. The mortar and pestle were specially fabricated for this program from strongly magnetic stainless steels so that abraded metal fragments could be removed from the ground sample with a magnet.

The disaggregation step produced 1 to 3 cm sample chunks which had to be further reduced in size for either the beneficiation procedures or final grinding. A large agate (natural chalcedony) mortar and pestle with an effective Moh hardness of nearly 7 was used for intermediate size reduction of nonfibrous materials having intermediate hardnesses, i.e., less than 7. Beryl (Moh hardness:7.5-8) and several other relatively hard nonfibrous minerals were ground with a large mortar and pestle composed of "Diamonite," a synthetic sintered alumina composite material having an effective Moh hardness of nearly 9.

Disaggregation of the fibrous minerals obtained as rock samples was a two-stage process. First, the rows of fiber bundles were removed from the adjacent massive rock plates by sawing. A water-cooled circular trim (rock) saw with a diamond dust coated metal blade was used to remove the nonfibrous wall rocks; the slabs of fiber bundles were cut to 1-cm thicknesses because of the feed size requirements of the mill to be employed. Disaggregation of the slabs of fiber bundles was accomplished with a mason's hammer and chisels. No further fiber size reductions were required before final grinding.

One of three types of apparatus were used to grind each selected mineral sample to a particle size range in accordance with the program specifications: ball mill, air jet mill, or centrifugal knife mill.

A large, polyurethane-lined mill jar was obtained to grind the silica polymorphs. This lining is resistant to abrasion and acts as a resilient cushion that minimizes loss of crystallinity. A 100-pound supply of relatively clean and coarse (percent retained: 40 on 30 mesh, 56 on 40 mesh, 3 on 50 mesh U.S. Standard sieves) quartz sand was used in break-in runs and clean-up runs between grinding runs of selected materials. Each mill jar and appropriate charge of stainless steel balls were subjected to five break-in runs to scour the surfaces of the jar interiors and the balls. Tridymite (TY-27) was milled with this equipment. It was found that cristobalite (CB-25) could safely be air jet milled.

Air jet milling was used to grind to the specified particle size all the nonfibrous minerals that required reduction and to disaggregate agglomerates in those synthetic minerals already meeting specifications for particle size. Cristobalite (CB-25) was ground by air jet milling only after preliminary tests demonstrated that milling energy is moderate enough not to degrade crystallinity or cause phase transformation.

The air jet-milling unit is a 10.16-cm Micron-Master Jet Pulverizer (distributed by the Jet Pulverizer Company, Palmyra, New Jersey). All its components are stainless steel except the top and bottom rubber liners of the grinding chamber. The sample feed had to be fairly uniform in size, from 2-mm maximum diameter to very finely powdered material. The milling is accomplished in a 10-cm-diameter, annular grinding chamber into which four nozzles, arranged clockwise, inject 50 scfm of dry filtered air compressed to 90 psig. Feed material is introduced by a Venturi nozzle. Size reduction is accomplished almost exclusively by the impact of particles of feed material against each other. The effluent air stream outlet to the cyclone collection system is at the center of the grinding chamber, and the

circulating, inward-directed air flow prevents much contact of the feed material with the periphery of the grinding chamber. Because these conditions minimize the mill components being abraded by much harder materials, contamination of the product by mill components is slight. The effluent air carries the ground material into a cyclone where the coarse particles are separated and fall to a collection container below. The finest powder is carried away through an effluent air outlet and is collected by filtering.

Reduction of each mineral sample to the required size range could not be accomplished in one pass through the air jet mill. Individual sample properties such as mineral hardness and starting particle size distribution determined the number of passes through the mill required to attain the specified particle size distribution. Individual sample properties, particularly the starting particle size distribution, determined the feed rate into the milling chamber, and thus the length of time required to complete one pass. In general, the first pass required 100 to 200% more time than subsequent passes.

The jet mill was thoroughly cleaned, and a grinding test was performed with 2.3 kg of the quartz sand, described above, to scour contaminants from previous runs of materials. Three passes reduced the test quartz to a uniformly fine powder and permitted a determination of optimum milling conditions. The resultant product demonstrated that air jet milling produces a uniform product, with minimal contamination.

A centrifugal knife mill, the Retsch Ultra-Centrifugal Mill (type ZM-1, manufactured in West Germany and distributed in the United States as the Microjet 10 by the Micro Materials Corporation, Westbury, New York) was used to comminute the group 2 fibrous minerals. Fibrous feed material is introduced into the mill at the center of a tungsten carbide-coated rotor that turns at selected speeds of 10,000 or 20,000 rpm. The material is thrown against a circle of 24 inward-facing knife-like pins that stand about 1 cm apart at the periphery of the rotor. A stainless steel sieve ring forms the inner wall of the intermediate collection chamber just outside the circle of rotor pins. The fibers are thrown against the rotating knives and are sheared between the pins and the sieve ring. A sieve ring with 1-mm perforations was used for the first milling pass, and a ring with 0.08-mm perforations was used for subsequent milling passes. Ground material is collected by the effluent air stream from the intermediate collection chamber passing to a cyclone where coarse particles separate and fall to a collection container underneath. The effluent air carries the finest material to a filter bag above the cyclone. This mill has relatively few parts coming in contact with the feed material and can be easily disassembled and cleaned.

Feed material had to be less than 1 cm in length to avoid bridging the gaps between pins. Also, the feed particles must be relatively small and nonabrasive to prevent damage to the sieve rings. Iterative milling of the fibrous materials reduced fiber length to the specified size limits.

The fibrous minerals ground in the Retsch (knife) mill each exhibited distinct milling properties. Feed rates through the same sieve ring were not at all similar from one mineral type to the next. For one sample

second and third passes through a sieve ring required successively shorter periods of time, while for another successive passes required longer periods of time. As feed rates slowed, the mill began to overheat, which necessitated shutting it down and cooling it for two hours. Manhours spent, as well as total elapsed time required to grind the fibrous minerals were thus considerably greater than those for the nonfibrous minerals. Because of the many difficulties encountered with the fibrous minerals, money and time constraints prevented complete size reduction of the full kilogram of some samples: approximately 150 g each of crocidolite and fibrous grunerite were completely ground to the specified particle size; these were labelled A grade whereas the remainder of the material, which contained oversized particles, was labelled B grade.

The individual characteristics of the minerals dictated the type of mill that was employed and the milling time required to produce the desired particle size in the final product. Table 9 summarizes the mill types employed for each sample; the number of passes through each mill type required to produce the specified particle distributions are also given. Table 10 summarizes the actual manhours required to complete the size reduction of each mineral standard.

EVALUATION OF GRINDING METHODS BY DIFFERENTIAL SCANNING CALORIMETRY (DSC)

Phase transformations for two silica polymorphs, cristobalite (263°C) and tridymite (110° and 160°C), occur in a temperature range amenable to examination by DSC. This is convenient because the area under the DSC peak associated with a phase inversion is directly proportional to the heat exchanged in the process. The energy released by the phase change before and after grinding was compared to indicate the sensitivity of the mineral to grinding.

The reproducibility of the Perkin Elmer DSC-1B was determined with indium. DSC sensitivity was determined to be 0.0600 in./mcal; the standard deviation was 0.0010 (12 measurements). A single sample of indium was used to check the day-to-day reproducibility of the instrument. The response reproducibility of the DSC to the indium fusion was expected to be somewhat better than it was for the silica polymorphs. In some cases, because of the constraints on the overall program, only a few samples were analyzed, whereas the nature of other experiments resulted in numerous runs. Nevertheless, evidence was found in the DSC analysis to help select the final comminution procedures.

Cristobalite

The cristobalite α to β inversion produces an endotherm that peaks in the region between 259° and 272°C. The variation in peak temperature reflects the differences in ordering within the crystal structure of the particles from the several different synthesis lots, as well as differences in individual sample histories.

The DSC data for cristobalite are shown in Table 11. Initial tests were conducted with samples from a single batch. The DSC curve in Figure 19 is

Table 9. Mills and milling steps employed

IITRI Sample No.	Milling Apparatus	Number of Passes
Q-1	Air Jet Mill	3
Q-107	None required	-
B-11	Air Jet Mill	7
F-17	None required	-
N-108	None required	-
CB-25	Air Jet Mill	3
TY-27	Ball Mill	(6 hours milling time)
CH-29	Centrifugal Knife Mill	2 @ 0.08 mm*
CR-37A	Centrifugal Knife Mill	5 @ 1.0 mm; 10 @ 0.5 mm; 3 @ 0.08 mm
CR-37B	Centrifugal Knife Mill	5 @ 1.0 mm; 10 @ 0.5 mm; 1 @ 0.08 mm
GF-38A	Centrifugal Knife Mill	2 @ 1.0 mm; 2 @ 0.08 mm
GF-38B	Centrifugal Knife Mill	4 @ 1.0 mm; 1 @ 0.08 mm
AF-45	Centrifugal Knife Mill	2 @ 1.0 mm; 2 @ 0.08 mm
TF-48	Centrifugal Knife Mill	2 @ 1.0 mm; 3 @ 0.08 mm
AG-55	Air Jet Mill	3
R-60	Air Jet Mill	3
G-68	Air Jet Mill	5
C-71	Air Jet Mill	4
A-102	Air Jet Mill	3
T-77	Air Jet Mill	2
T-79	Air Jet Mill	3
TA-99	Air Jet Mill	2

* Indicates pore opening on sieve rings in the knife mill.

Table 10. Manhours required to accomplish final milling.

IITRI Sample Number	Milling Apparatus	Time for 1st Pass, hours	Total Milling Time, hours	Starting Mass, grams	Mass% Lost in Milling
Q-1	Air Jet Mill	4	12 (3 passes)	1900	20
B-11	"	2	12 (7 passes)	1766	34
CB-25	"	3	14 (3 passes	1450	15
CH-29	Knife Mill	16	24 (2 passes)	2600	20
CR-37A*	"	32	130 (18 total passes for 220 g)	1350	30
CR-37B	"	32	80 (16 total passes)	1350	30
GF-38A*	"	4	100 (4 total passes for 185 g)	1125	40
GF-38B	"	4	70 (5 total passes)	1125	40
AF-45	"	5	30 (4 total passes)	~2000	~20
TF-48	"	8	44 (5 total passes)	~2000	~30
AG-55	Air Jet Mill	6	18 (3 passes)	1720	15
R-60	"	2	12 (3 passes)	2241	20
G-68	"	1	8 (5 passes)	1754	27
C-71	"	2	12 (4 passes)	2251	27
A-102	"	1	8 (3 passes)	716	19
T-77	"	2	6 (2 passes)	1280	13
T-79	"	6	16 (3 passes)	~2000	N.D.**
TA-99	"	5	12 (2 passes)	1970	23

* Meets size criteria

** Not determined

Table 11. DSC data for cristobalite.

Run No.	Sample No.	Sample History	ΔH/w, mcal/mg	Peak Temp., °C	Peak Shape
1	CB-25A-1	As received, single batch.*	4.46	260	triangle
2	CB-25A-1	Reheat above sample.	4.57	260	"
3	CB-25B-1	Single batch jet milled 3 times.	4.32	267	"
4	CB-25B-1	Reheat above sample.	4.37	265	"
5	CB-25B-1	Reheat above sample.	4.20	265	"
6	CB-25C-1	CB-25B (jet milled), washed in 20 percent HF for 5 min.	4.51	265	"
7	CB-25C-1	Reheat above sample.	4.44	265	"
2	CB-25D-1	Final product, mixed batches & jet milled 3 times	3.76	265-272	trapezium (straight top)
3	CB-25D-1	Rerun above sample.	3.58	263-270	"
5	CB-25D-0(A)	Final product, 2nd sample.	3.80	265-272	"
6	CB-25D-8(A)	Final product, washed in conc. HCl.	3.63	265-272	"
	CB-25D-8(B)	Final product, washed in conc. HCl.	4.01*	265-272	"
4	CB-25D-0(B)	Final product, 3rd sample, same as CB-25D-0(A)	4.02	265-272	trapezium (straight top with glitch)
5	CB-25D-0(B)	Rerun above sample.	4.06	264-272	"
1	CB-25D-0(C)	Final product, 4th sample, same as CB-25-0(A).		80-200**	
2	CB-25D-0(C)	Rerun above sample.	3.90		trapezium (angled top)

* For single batch ΔH/w = 4.43 ± 0.098.
For final mixed batch ΔH/w = 3.80 ± 0.076.
** Peaks appear suspiciously at 110 and 160°C.

Table 11. (continued)

Run No.	Sample No.	Sample History	ΔH/w mcal/mg	Peak Temp., °C	Peak Shape
3	CB-25D-0(C)	Rerun above sample.	3.95		trapezium (angled top)
4	CB-25D-9(A)	Final product.	-		"
5	CB-25D-9(A)	Final product.	3.79		"
6	CB-25D-9(A)	Final product.	3.80		"
7	CB-25D-9(B)	Final product, acid treated.	3.75		"
8	CB-25D-9(B)		3.70		"
9	CB-25D-9(B)		3.75		"
10	CB-25D-9(B)		3.74		"
2	CB-25D-9(B)	Final Product.	3.84	259-270	"
3	CB-25D-9(B)	Rerun above sample.	3.84	260-270	trapezium (angled top)
6	CB-25D-10	Final product washed in conc. HCl	3.87	260-270	"
7	CB-25D-10	Rerun above sample.	3.79	260-270	"
8	CB-25D-10	Rerun above sample.	3.77	260-270	"
1	CB-25D-11(A)	Final Product.	3.85	262-272	"
2	CB-25D-11(A)	Rerun above sample.	3.88	260-270	"
3	CB-25D-11(A)	Rerun above sample.	3.71***	260-270	"
4	CB-25D-0(C)	Final product, rerun from 2-22-97.	3.80	260-270	"
5	CB-25D-0(C)	Rerun above sample.	3.96	260-270	"
6	CB-25D-0(C)	Rerun above sample.	3.86	260-270	"
1	CB-25D-0(C)	Rerun above sample.	3.82	260-270	"
1	CB-25D-11(C)	Final product.	3.84	260-270	"

***Rerun too soon.

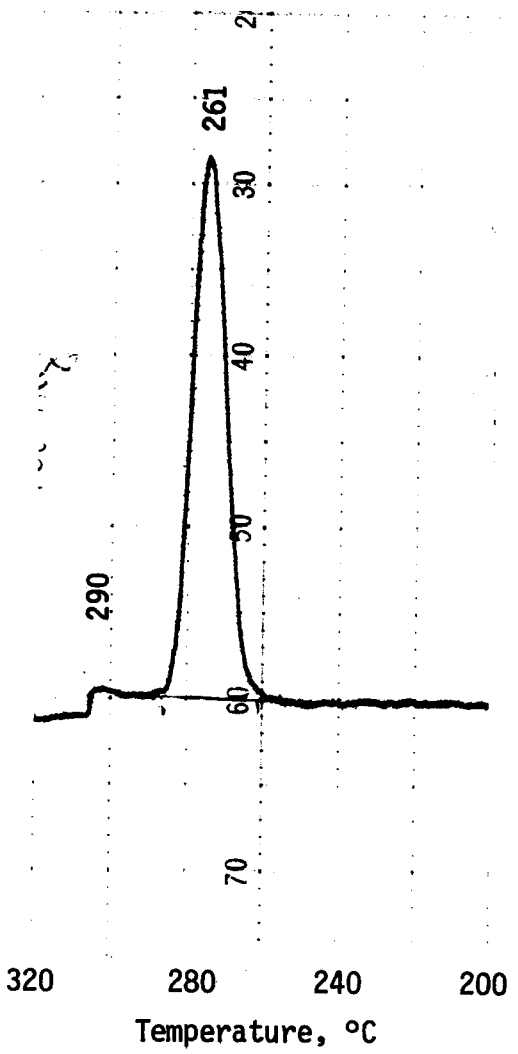

Figure 19. DSC curve for a 8.9-mg cristobalite sample taken from a single batch.

representative for these samples. A heat of transition of 4.43 cal/g with a standard deviation of 0.098 cal/g was measured for these samples. The apparent difference between the initial sample and the same sample after three passes through the air jet mill was found to be less than 4%. Subsequent hydrofluoric acid treatment of the air jet-milled sample brought it back up to within 1% of its value before air jet milling. Since the differences were too small to show significance, air jet milling was selected for the cristobalite comminution. All of the cristobalite batches were combined for the final grinding.

The DSC traces of the final ground mineral had a trapezium-shaped endotherm, the peak of which covered up to a 10°C temperature interval. The DSC curve for the final ground mineral is shown in Figure 20. The shape of the curve is attributed to an integration of the individual peaks of the particles in all the batches together. A broad triangular peak would result from a random scatter of peaks about a mean. The almost rectangular shape of the final mixture curve suggests that cristobalite tends to favor the extremes in inversion peak temperatures as shown by the dotted curves in Figure 20. The conditions of synthesis thus favor production of one or the other of two types of cristobalite, which vary only slightly from each other, rather than the production of a material with a random scatter of peak temperatures.

The final product gave a mean heat of reaction of 3.80 cal/g (with a standard deviation of 0.076 cal/g, or 2%), which was 14% lower than the value reported earlier in this section for a single batch (4.43 cal/g). This suggests that a batch-to-batch difference in heat of inversion of at least 14% may be present. Only one batch was selected for individual analysis, so the heat of inversion of the other batches can only be conjectured. No quartz or tridymite was detected by thermal analysis in the combined final material.

The air jet-milling action tends to discolor the ground powder with a small amount of fine metal dust from the mill walls. The added impurity level is much less than 1%, but its presence is unsightly. The final material was treated with several different concentrations of hydrochloric acid to select a valid procedure for removing the trace metal discoloration without also attacking the silica. A 10% hydrochloric acid solution for 30 min was sufficient to remove the metal discoloration. The DSC analysis shows that the treatment does not attack the cristobalite. Even treatment with a concentrated solution of hydrochloric acid or nitric acid did not appear to affect the DSC thermogram for cristobalite as shown in Table 12.

Table 12. Effect of clean-up treatment on cristobalite heat of inversion.

Clean-up Treatment	Heat of Inversion, cal/g
Before clean-up (6 samples)	3.80 ± 0.15
Clean-up with 10% hydrochloric acid (2 samples)	3.84
Clean-up with concentrated hydrochloric acid (2 samples)	3.82
Clean-up with concentrated nitric acid (2 samples)	3.81

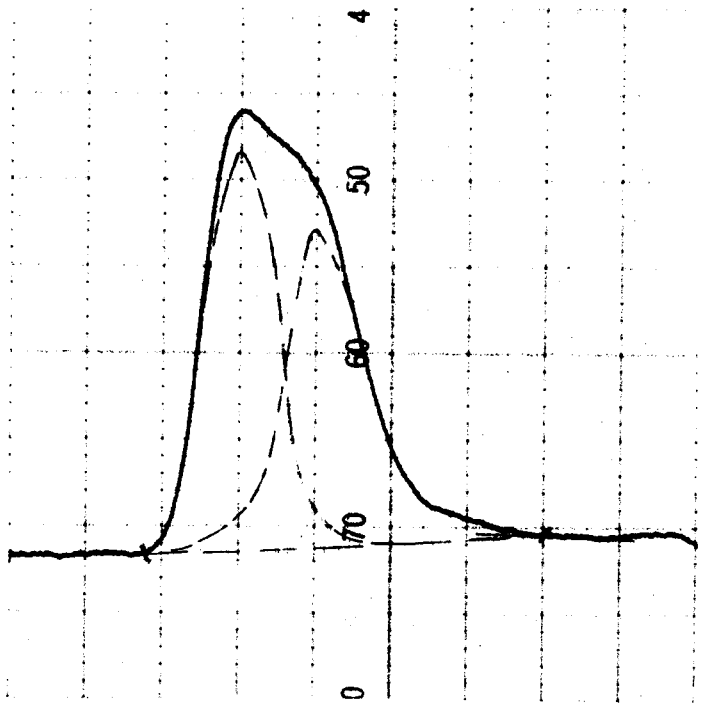

Figure 20. DSC curve for a 16.0-mg cristobalite sample taken from the final mixed batch.

Tridymite

Tridymite has two temperature inversions, which were examined by DSC: one in the region of 110°C and the other in the region of 160°C. This is shown in Figure 21 for a sample from a single synthesis batch. The first endotherm produces the larger of the two DSC peaks. The heat of inversion based on the peak area was calculated to be about 0.60 cal/g (110°C) and 0.42 cal/g (160°C) for a sample from the combined final batch, which was ball milled for 6 hours. An unusually large variability in the thermograms was found for tridymite. Part of this variability resulted from the uncertainty of the baseline position, but most of it was from the mineral itself. The mineral does not easily return to its most stable state at any given temperature. The curve in Figure 22 was generated by rerunning the sample in Figure 21 within an hour of the first run. A visible reduction in the first peak and change in position of the peak temperature is evident. This peculiarity of the tridymite was particularly easy to observe with the DSC due to the DSC's rapid recycle time. Rapid recycling of the sample can cause an inversion to become extremely reduced. Although usually reversible, the reduction was irreversible under certain conditions, which are not well understood. By spacing the heating cycles of the DSC at least 40 minutes apart, the reproducibility of the endotherm DSC areas was greatly improved for repeated runs on a given sample.

The first pass on the DSC invariably gave the largest endotherm. The endotherm sizes of the second and subsequent runs were smaller but, on the whole, reversible and, in time, were completely recovered. The DSC runs on the single batch as received TY-27-2 (batch 2 of the 19 individual batches received from Pennsylvania State University) are good examples of this effect (Table 13).

Table 13. Tridymite, single batch sample as received from supplier (TY-27-2). Results of reported heats of inversion measurements by DSC on a single sample.

			Heat of Inversion, cal/g	
Run No.	Time Between Runs, min	Total Time	110°C	160°C
1	1st run	0	0.757	0.439
2	50	50	0.680	0.504
3	40	90	0.625	0.450
4	7200	7290	0.682	0.479
5	15	7305	0.452	0.224
6	45	7350	0.677	0.511
7	25	7315	0.616	0.457
8	40	7415	0.645	0.477
9	15	7430	0.208	0.466
10	8400	15830	0.647	0.508
11	275	16105	0.697	0.546
		Average* -	0.659	0.492

*Runs 1, 5, and 9 were excluded from averages.

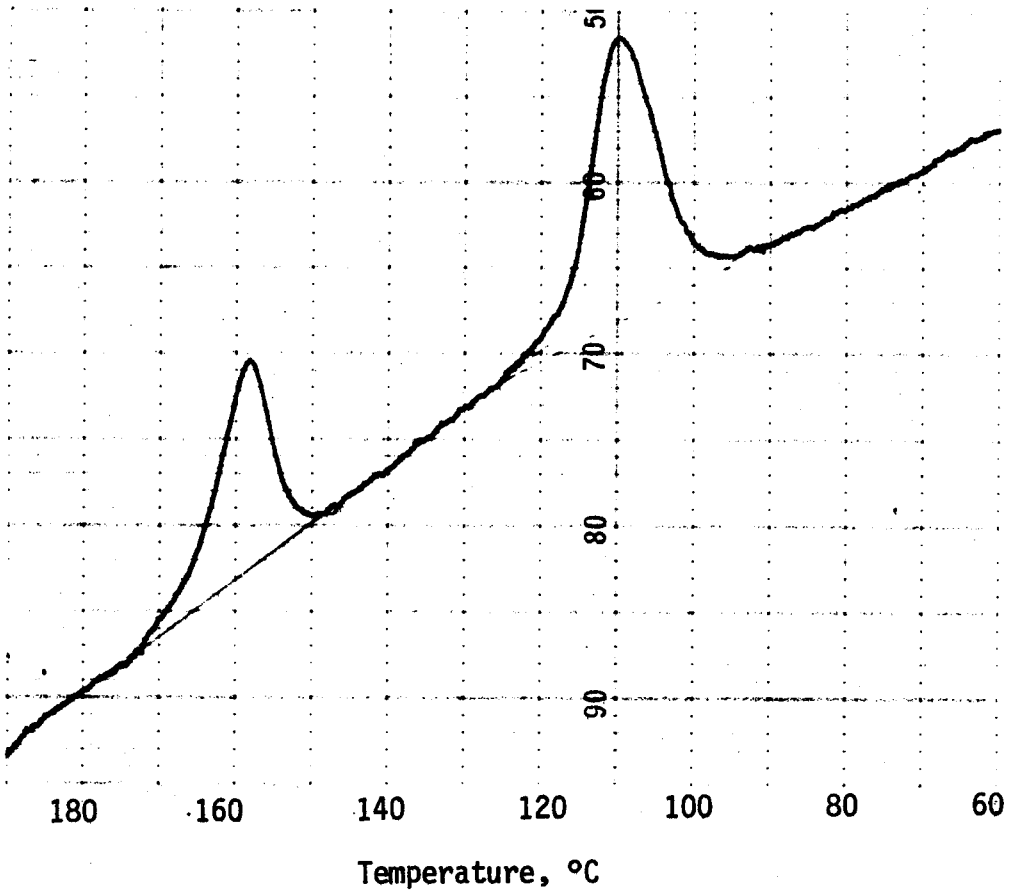

Figure 21. DSC curve for a 14.6-mg tridymite sample from a single batch; first DSC run through inversion endotherms.

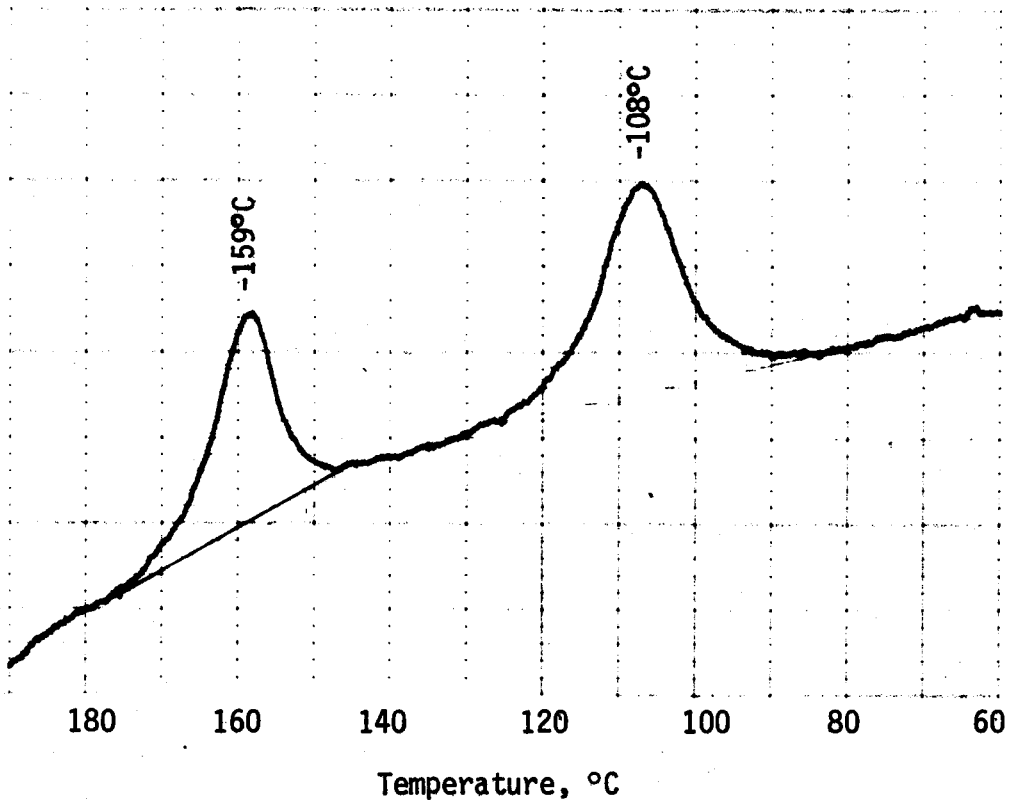

Figure 22. DSC curve for a 14.6-mg tridymite sample from a single batch; second DSC run through inversion endotherms.

The first peak in each of the first runs of air jet-milled and ball-milled samples showed a trapezium pattern. This pattern is evident in Figure 23 for a DSC run of a sample after three passes through an air jet mill. In the second and subsequent runs, the higher temperature portion of the first peak disappeared and was not reversible. The curve resulting from the second DSC run is shown in Figure 24. Heating the sample to just below the first inversion did not prevent the trapezium-shaped curve from making its one-time appearance, and it did not appear to be related to adsorbed water.

Both endotherms were reduced by grinding. The effects of grinding on the thermal pattern of tridymite are shown in Table 14.

Table 14. Comparison of grinding effects on tridymite inversions.

Sample Description	Heat of Inversion, cal/g	
	110°C	160°C
Single batch, as received	0.757 (4)*	0.439 (3)
Single batch, ball-milled 2 hr	0.724	0.476
Single batch, ball-milled 6 hr	0.690	0.327
Four batches, combined	0.845	0.576
Four batches, combined, air jet-milled three times	0.586	0.397
Final batch, ball-milled 6 hr	0.605	0.417
Final ground batch, treated with 10% HCl	0.695	0.375

*All the data are from single runs of each sample, except as noted in parentheses.

The changes in the 160°C endotherm were erratic and difficult to follow here, but the changes in the heat of inversion of the 110°C peak were sensitive to grinding. Ball milling was compared with air jet milling and was found to reduce the peak size much less (by 10%) than the latter (by 30%). The final ground material was prepared by ball milling for 6 hours. Clean-up of the final ground material with 10% hydrochloric acid did not appear to affect the 110°C peak.

REMOVING GRINDING CONTAMINANTS FROM SILICA POLYMORPHS

The grinding procedures used to prepare the silica polymorphs, quartz, cristobalite, and tridymite, occluded small traces of metal into the silica powders. The process gave the powders a light-gray color, which was removed by treatment with hydrochloric acid.

The concentrations of the acid and the length of contact with the powders needed to remove the metal was determined in a series of experiments with acids of different strengths. A 10% volume concentration of hydrochloric acid in distilled water was sufficient to remove the gray appearance from the quartz and cristobalite powders. These two powders were prepared by grinding in an air jet mill. Each was suspended with stirring in the acid solution for a period of 30 min under ambient temperature conditions. The dissolved metal salts were separated from the powder by repeated washings

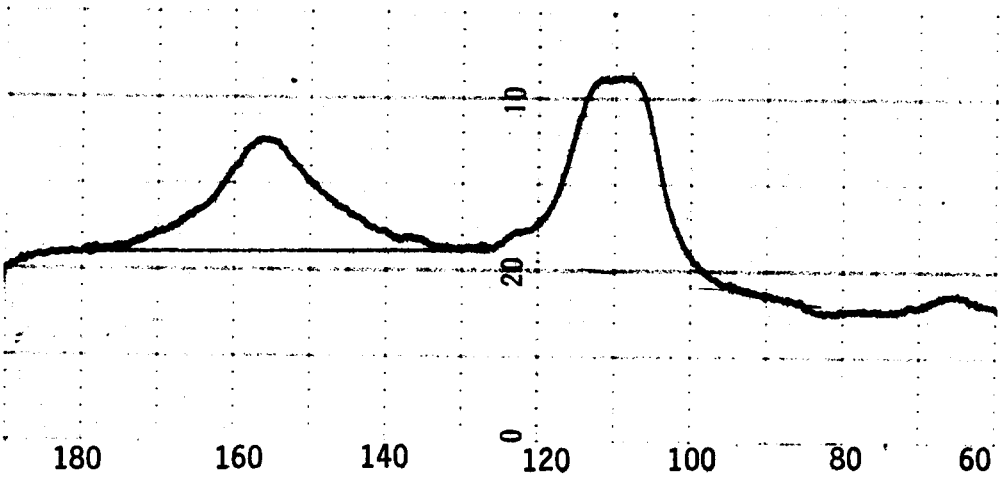

Figure 23. DSC curve for a 15.5-mg tridymite sample from four batches combined and jet milled three times; first run through inversion endotherms.

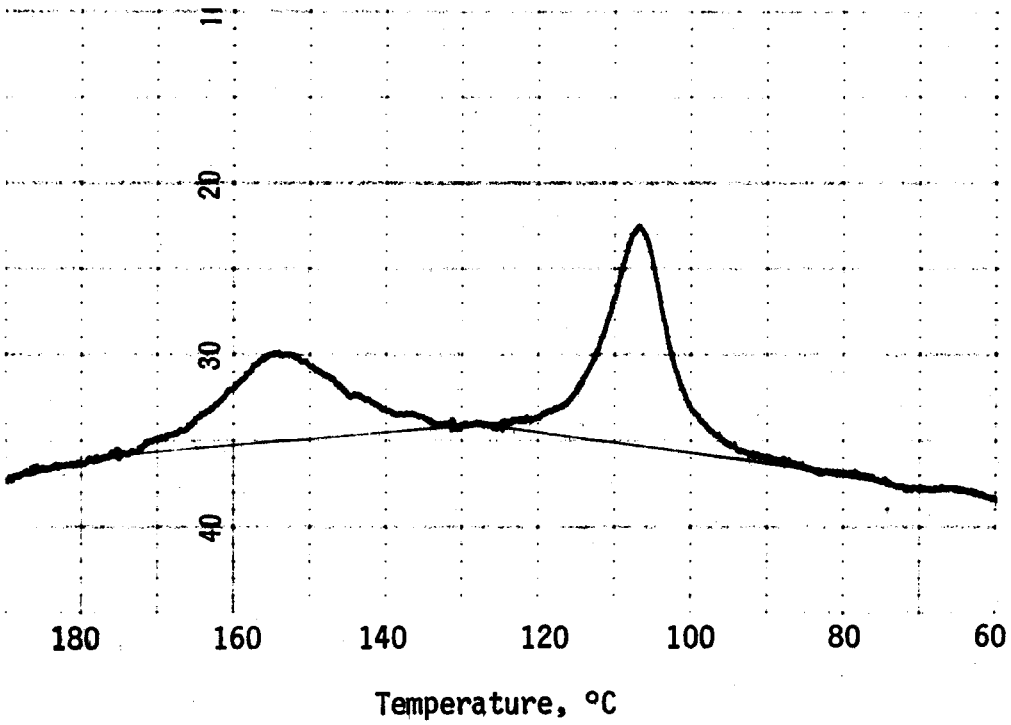

Figure 24. DSC curve for tridymite (TY-27) after air jet milling; second run through inversion temperature.

with distilled water and centrifugal separation of the suspended powder from the acid solution.

Because tridymite appeared to be more sensitive to modification by grinding, ball milling was selected for its comminution. Fine particles from wear of the metal balls added a light-gray color to the tridymite powder. This color could not be removed with the simple hydrochloric acid treatment used with the jet-milled quartz and cristobalite samples. It was necessary to reflux the ball-milled tridymite with a 20% hydrochloric acid solution for a period of 2 hr to remove the metal. The tridymite was separated from the dissolved metal by repeatedly washing the slurry with distilled water.

DSC (Perkin Elmer DSC-1B) was used to examine the effects of clean-up treatment on cristobalite and tridymite. The changes in the heats of inversion for cristobalite (~256°C) and tridymite (112° and 160°C) were monitored. The samples before and after acid clean-up treatment were compared (Table 15). No detectable changes were observed in the crystallinity of the silica polymorphs as a result of the clean-up treatment.

Table 15. Comparison of heats of inversion by DSC before and after clean-up treatment of silica polymorphs.

	Tridymite				Cristobalite	
	Before		After		Before	After
Inversion Temperature, C	112	160	112	160	260	260
Number of Samples	4	4	5	5	5	3
Average Heat of Inversion, mcal/mg	0.773	0.360	0.773	0.356	4.21	4.11
Standard Deviation, mcal/mg	0.041	0.030	0.027	0.024	0.21	0.04

PARTICLE SIZE SEPARATION AFTER GRINDING

Because of the substantial loss of materials during milling and to avoid altering the crystallinity of the samples, cristobalite and tridymite milling was halted before reducing all particles below 10 μm in diameter. Initial characterizations indicated these samples closely approximated all the size criteria for group 1 minerals except maximum particle size. Attempts to prepare stable suspensions of these samples resulted in rapid settling of the particles from the suspended state, caused by the combined effects of the oversized particles and agglomerates which had formed. Therefore, an attempt was made to use sedimentation to remove the greater-than-10 μm particles from small samples (100-g lots) of the acid-washed cristobalite and tridymite standards.

Cascade sedimentation was performed in an 11-liter jug filled with isopropanol to approximately the 10-cm height. For a known settling height

and particle size, the time required to settle a particle can be calculated from the rearranged Stokes equation[23]:

$$t = \frac{18\eta h \times 10^8}{(\rho_s - \rho_f)\, g d^2}$$

where:

t = time in seconds

η = viscosity of settling fluid in poise

h = settling height in cm

ρ_s = density of particles in g/cm^3

ρ_f = density of fluid in g/cm^3

g = acceleration due to gravity in cm/sec^2

d = particle diameter in μm

For cristobalite (density = 2.33 g/cm^3), the 10-μm-and-larger particles would settle to the bottom of the jug in 35 minutes; the oversized tridymite particles (density = 2.27 g/cm^3) would settle in 37 minutes. To eliminate particle collisions, which increase the settling behavior rate, particle concentrations in the settling fluid were kept at approximately 0.5% by volume.

The dry powders were first deagglomerated in a small volume of isopropanol with a Waring Blendor. The resulting suspensions were then poured into their respective settling vessels, and sufficient isopropanol was added (approximately 6 liters) to bring the suspension to a 10-cm height in the vessels. Manual shaking of the capped settling vessels completed the dispersion of the powders in the settling fluid.

After the appropriate settling time, the isopropanol containing the less-than-10-μm particles was drained from the settling vessel through a spigot located 10 cm below the height of the suspension. The particle-laden isopropanol was collected in another large settling vessel to allow sedimentation of the less-than-10-μm particles.

Although the suspensions to be settled were made to the theoretical dilution (0.5% by volume), some drag-down of the sub-10-μm particles occurred. Therefore, to achieve the maximum recoverable amount of the finer particles, the sedimentation was repeated several times. Successive drains from the sedimentation vessel were visually checked for clarity. After five additional sedimentation cycles, it was obvious from the clarity of the fluid being drained that successive sedimentation cycles would not yield sufficient quantities of sub-10-μm particles to require further sedimentation.

The isopropanol containing the less-than-10-μm particles was allowed to sit undisturbed until the fine particles had settled (approximately 1 week). The two size fractions (particles less than and greater than 10 μm)

produced for each mineral were recovered from the isopropanol by room temperature evaporation of the fluid. The less-than-10-μm and greater-than-10-μm size fractions produced weighed 69.9 g and 28.5 g, respectively, for cristobalite, and 87.1 g and 8.0 g, respectively, for tridymite.

The less-than-10-μm fractions of cristobalite and tridymite had mass median particle diameters of 5.3 μm and 4.9 μm, respectively. The greater-than-10-μm fractions were determined to have mass median particle diameters of 25.3 μm (cristobalite) and 14.5 μm (tridymite). Figures 25 and 26 illustrate the fractions produced.

PACKAGING

Comminuted minerals were packaged in isopropanol-washed, rectangular polyethylene containers. Table 16 summarizes the total sample masses supplied to NIOSH, and Table 17 lists the mass of material in individual containers for each mineral type. Ten bottles of each of samples Q-1, Q-107, CB-25, TY-27, N-108, AF-45, TF-48, and T-79 (not shown in Table 17) were supplied; each bottle contained precisely 100.5 g of mineral powder. To ensure sample homogeneity in the individual containers, the entire sample mass was mixed extensively in one large vessel prior to packaging.

Coarse (>10 μm) fraction

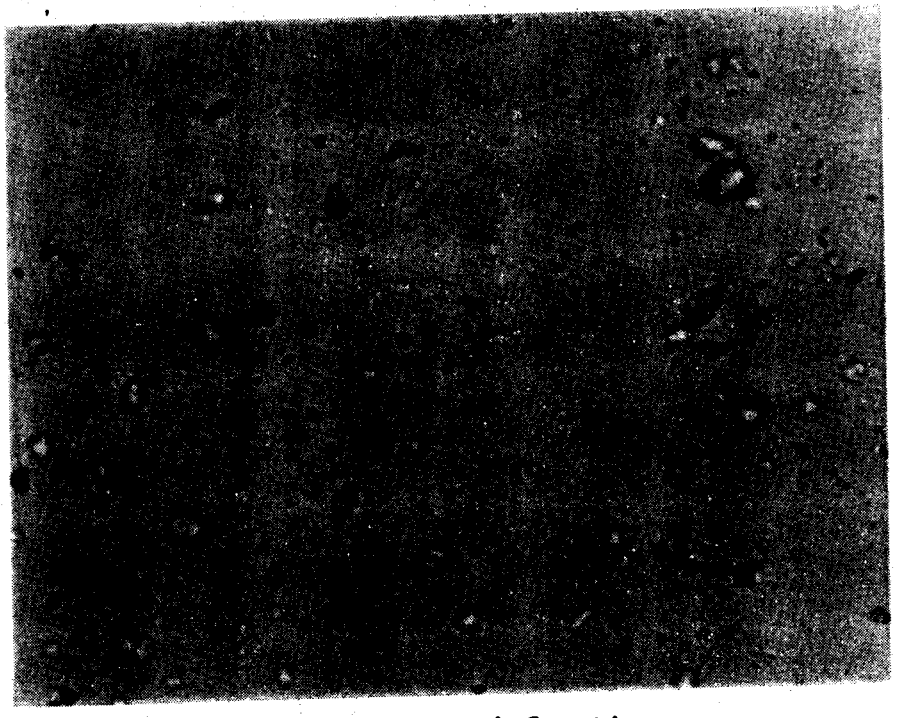

Fine (<10 μm) fraction

Figure 25. Size-separated cristobalite (CB-25). (Photographed in n_D = 1.66 at 520X with polars slightly uncrossed).

Coarse (>10 μm) fraction

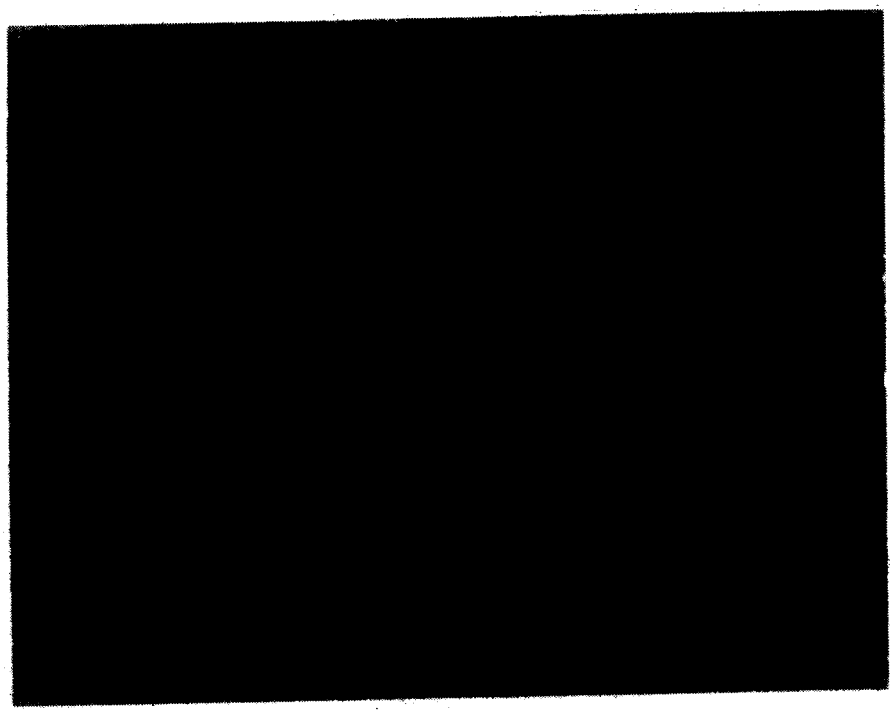

Fine (<10 μm) fraction

Figure 26. Size-separated tridymite (TY-27). (Photographed in n_D = 1.66 at 520X with polars slightly uncrossed).

Table 16. Quantities of samples supplied.

IITRI Sample No.	Mineral	Mass Supplied, g
Q-1	Quartz	1005.0
Q-107	Quartz	1005.0
B-11	Beryl	1007.8
F-17	Fluorite	1020.0
N-108	Nickel Oxide	1005.0
CB-25	Cristobalite	1005.0
TY-27	Tridymite	1005.0
CH-29	Chrysotile	1013.3
CR-37	Crocidolite	935.5
GF-38	Fibrous Grunerite	595.9
AF-45	Fibrous Anthophyllite	1005.0
TF-48	Fibrous Tremolite	1005.0
AG-55	Antigorite	658.6
R-60	Riebeckite	1019.1
G-68	Grunerite	1018.5
C-71	Cummingtonite	1014.3
A-102	Anthophyllite	502.7
T-77	Tremolite	1009.5
T-79	Tremolite	1005.0
TA-99	Talc	1019.3

Table 17. Container quantities of samples supplied.

Bottle No.	Beryl B-11 Mass, g	Fluorite F-17 Mass, g	Chrysotile CH-29 Mass, g	Crocidolite CR-37 Mass, g	Fibrous Grunerite GF-38 Mass, g	Antigorite AG-55 Mass, g
1	101.0	101.6	102.8	85.2A*	75.8A*	65.3
2	100.4	102.1	100.4	85.0A*	75.5A*	65.0
3	100.9	102.6	101.3	95.0	55.0	65.2
4	101.0	100.5	101.6	96.4	56.2	65.2
5	100.0	102.0	100.0	95.6	55.0	66.6
6	100.5	102.3	101.1	96.0	56.0	66.4
7	101.3	100.6	102.4	95.1	55.1	66.3
8	100.3	104.5	101.0	96.2	55.6	65.7
9	100.3	102.2	100.8	95.7	56.3	66.7
10	102.1	101.6	101.9	95.3	55.4	66.2
Total	1007.8	1020.0	1013.3	935.5	595.9	658.6

Bottle No.	Riebeckite R-60 Mass, g	Grunerite G-68 Mass, g	Cummingtonite C-71 Mass, g	Anthophyllite A-102 Mass, g	Tremolite T-77 Mass, g	Talc TA-99 Mass, g
1	101.5	107.3	101.6	100.3	100.6	101.9
2	100.2	100.8	100.6	101.8	101.4	100.4
3	100.8	101.7	101.3	100.1	100.5	102.1
4	103.9	102.3	101.2	100.5	100.9	102.4
5	101.2	101.0	100.5	100.0	102.1	102.5
6	101.3	100.4	101.4	-	100.3	100.9
7	102.0	101.0	100.6	-	101.6	100.5
8	103.6	100.2	101.9	-	100.8	102.4
9	101.9	100.8	101.6	-	100.1	102.0
10	102.7	103.0	103.6	-	101.2	104.2
Total	1019.1	1018.5	1014.3	502.7	1009.5	1019.3

*Fully size reduced powders; remainder of powder has over-sized particles (see Table 9).

SECTION 6

CHARACTERIZATION OF COMMINUTED MINERALS

PARTICLE SIZING

Every effort was made to meet the particle size criteria detailed in Section 2 for each mineral standard. In some instances, however, particle size criteria were sacrificed in order to meet the purity criteria, prevent damage to or alteration of mineral crystallinity, or provide as large a quantity as possible of the mineral standard (as in the cases of cristobalite and tridymite, see Section 5).

Two independent sizing methods, optical microscopy and MICROTRAC analysis, were used to monitor particle size distributions between grinding steps and after completion of grinding. The specific sizing procedures and results are presented below.

Interpretation of Particle Size Requirements

The mass median aerodynamic diameter (MMAD) of a specific particle type is the mass median diameter (MMD) of a unit density (ρ) particle that has the same terminal settling velocity as the particle type being measured. The MMD of a powder is that diameter for which the mass of larger particles and smaller particles are equal. Since all of the mineral standards have a density greater than unity, the MMAD for each standard can be calculated from:

$$MMAD = MMD \cdot \rho^{\frac{1}{2}}$$

The MMD cannot be determined directly by microscopy but can be calculated from the number median diameter (NMD) that divides the larger and smaller particles into equal numbers. The MMD is derived from the NMD by the following equation:[2,3]

$$\log MMD = \log NMD + 6.90 \log^2 \sigma_g$$

where σ_g is the geometric standard deviation. The σ_g is determined from a plot of the size data on log normal probability graph paper: the σ_g is the ratio of particle size at 84.13% to particle size at 50%. The same plot gives the NMD at the 50% size.

The size distribution specifications for MMAD (as detailed in Section 2) and σ_g can be used back to calculate the NMD as shown in Table 18:

Table 18. Calculation of NMD from size distribution criteria.

MMAD, μm	σ_g	NMD, μm
0.5	1.4	0.36
0.5	4.0	0.0016
5.0	1.4	3.6
5.0	4.0	0.16

The NMD in Table 18 were calculated from the MMAD without correcting for particle density. Therefore, the required NMD for minerals would actually be lower by a factor of one over the square root of the mineral density.

It is apparent from the calculation of NMD that only those size distributions that have a σ_g close to 1.4 will meet the desired size distributions, since there are no laboratory grinding or milling procedures that can practically reduce particle size much below 0.05 μm. In addition, the σ_g is a function of the comminution process and mineral properties. Therefore, the only possible means of obtaining the target size distributions for all the minerals would be to perform a size classification after comminution by settling or by centrifugal air separation. Size classifying techniques were not used in this study, except for small portions of cristobalite and tridymite, to conserve as much final product as possible.

Optical Microscopy Sizing

Particle size was measured microscopically using a calibrated eyepiece graticule. Particles in mineral groups 1, 3, and 4 were measured using Feret's diameter. Group 2 minerals were measured by fiber length. Particle size data for each of the groups are shown in Tables 19 through 21.

The MMADs (shown in Tables 19 and 20) are all greater than 5.0 μm and range from 5.5 μm to 56.1 μm. The data seem to indicate that none of the minerals meet the desired size distribution. The high values for the MMAD are, however, due to the shape factor for the minerals that cannot be easily measured microscopically.

Silverman et al., show that the volume shape factor for crushed quartz is 0.28.[23] This implies that the MMADs calculated from microscopical sizing are probably three times higher than the true MMADs. There is an additional error for the calculated MMADs that is caused by the graphical plotting of the size distribution data on log normal probability charts. To extract the median diameter and geometric standard deviation from the plot, the data must produce a straight line. None of the microscopy data, however, could be fit to a straight line. To evaluate these errors, the samples were subsequently sized with a laser light diffracting instrument, the MICROTRAC, which provides a direct MMD.

Table 19. Group 1 minerals size distribution determined by microscopy.

Size Range, μm	Quartz (Q-1)		Cristobalite (CB-25)		Tridymite (TY-27)		Beryl (B-11)		Fluorite (F-17)		Nickel Oxide (N-108)	
	No.	Cum. Pct.	No.	Cum. Pct.	No.	Cum. Pct.	No.	Cum. Pct.	No.	Cum. Pct.	No.	Cum. Pct.
<1	415	40.4	121	13.2	83	9.0	316	31.6	813	79.2	578	57.8
1-3	316	71.1	412	58.3	373	49.5	375	69.1	190	97.8	376	95.4
3-5	170	87.7	186	78.6	257	77.3	186	87.7	23	100.0	46	100.0
5-7	85	95.9	73	86.6	90	87.1	50	92.7				
7-10	33	99.1	75	94.8	69	94.6	52	97.9				
10-16	9	100.0	48	100.0	50	100.0	21	100.0				
Total	1028		915		922		1000		1026		1000	
NMD, μm		2.0		1.9		2.2		1.6		1.2		0.82
σ_g		2.05		2.21		2.02		2.75		1.33		2.20
MMD, μm		9.4		12.5		9.73		34.4		1.5		5.3
ρ, g/cm^3		2.65		2.33		2.27		2.66		3.18		6.90
MMAD, μm		15.3		19.1		14.7		56.1		2.7		13.9

Table 20. Groups 3 and 4 minerals: size distributions determined by microscopy.

Size Range, μm	Antigorite (AG-55)		Riebeckite (R-60)		Cummingtonite (C-71)		Grunerite (G-68)		Anthophyllite (A-102)		Tremolite (T-77)		Talc (TA-99)	
	No.	Cum. Pct.	No.	Cum. Pct.	No.	Cum. Pct.	No.	Cum. Pct.	No.	Cum. Pct.	No.	Cum. Pct.	No.	Cum. Pct.
<1	172	21.4	110	15.5	362	35.4	402	39.9	402	39.5	228	21.9	350	33.4
1-3	289	57.3	225	47.2	460	80.4	358	75.5	339	72.7	342	54.8	624	92.9
3-5	217	84.3	305	90.1	142	94.3	157	91.1	165	88.9	292	82.8	74	100.0
5-7	76	93.8	65	99.3	58	100.0	61	97.1	82	97.0	149	97.1		
7-10	45	99.4	5	100.0			29	100.0	31	100.0	30	100.0		
10-16	5	100.0												
Total	804		710		1022		1007		1019		1041		1048	
NMD, μm		2.7		2.1		3.8		2.6		2.6		3.4		1.3
σ_g		1.85		1.95		1.21		1.73		1.73		1.5		1.77
MMD, μm		8.4		8.0		4.2		6.4		6.4		5.6		3.45
ρ, g/cm^3		2.62		3.02		3.2		3.4		2.05		3.0		2.58
MMAD, μm		13.6		13.9		7.5		11.8		10.8		9.7		5.5

Table 21. Group 2 minerals: fiber lengths determined by microscopy.

Size Range, μm	Fibrous Grunerite (GF-38)		Fibrous Anthophyllite (AF-45)		Fibrous Tremolite (TF-48)		Crocidolite (CR-37)		Chrysotile (CH-29)	
	No.	Cumulative Percent	No.	Cumulative Percent	No.	Cumulative Percent	No.	Cumulative Percent	No.	Cumulative Percent
<1										
1-3										
3-5										
5-7										
7-10	113	21.5	76	12.0	136	21.2	147	25.2	40	18.0
10-16	269	72.6	348	66.9	337	73.8	286	74.1	110	68.0
16-22	108	93.2	130	87.4	115	91.7	105	92.1	34	83.5
22-28	24	97.7	16	89.9	27	95.9	23	96.1	9	87.7
28-34	6	98.9	36	95.6	20	99.1	15	98.6	8	91.3
>34-40	6	100.0	28	100.0	6	100.0	8	100.0	19	100.0
	526		634		641		584		220	
Median Fiber Length, μm		12		13		11		11.5		12

MICROTRAC Particle Sizing

The MICROTRAC Particle size analyzer[24] shown in Figure 27 provides direct mass or volume percentage size distribution data from light diffraction intensity measurements.[25] Approximately 0.5 to 2.0 g of sample is added to a chamber filled with filtered water to form a slurry. A portion of the sample slurry is then pumped to a cell that is irradiated by the laser light source. The laser light diffracted by the particles is collected by a patented spatial filter and detector that measure the radial light intensity to compute the size distribution.

There are several advantages to this method of particle sizing:

- a large sample size is used, which minimizes aliquot sampling bias
- particle shape errors are minimized by the turbulent particle motion in the slurry
- a large number of particles are counted (calculated to be more than 100,000) during a size determination.

Among these important instrument features, the most important may be the elimination of particle shape errors to provide a more accurate and precise measure of the size distribution. The results of these size distribution measurements are shown in Table 22.

The MMD, labeled PM in Figure 28, is computed by the instrument. The σ_g was obtained by plotting the 10% (PS), 50% (PM), and 90% (PH) cumulative values (Figure 28) and reading the value for 84.1%. As mentioned above, the σ_g is the ratio of the 84.1% to 50% values. The MMADs were then calculated as before.

The only drawback in using this instrument is that particles smaller than 1.4 μm are not detected or sized. Therefore, the true MMADs are somewhat smaller than those shown in Table 22.

Particle Size Data Evaluation

Minerals in groups 1, 3, and 4 just exceed the MMAD desired for the final ground products, as shown in Table 22. Each of the minerals in groups 3 and 4 were ground or milled through repeated passes until further reductions in particle size were negligible.

For most samples, it was impractical to isolate the coarser particles for separate comminution. There were several reasons that made this separation impractical:

- not enough coarse material was available to use as a single sample charge for further size reduction
- there was no reasonably rapid method for removing the larger particles

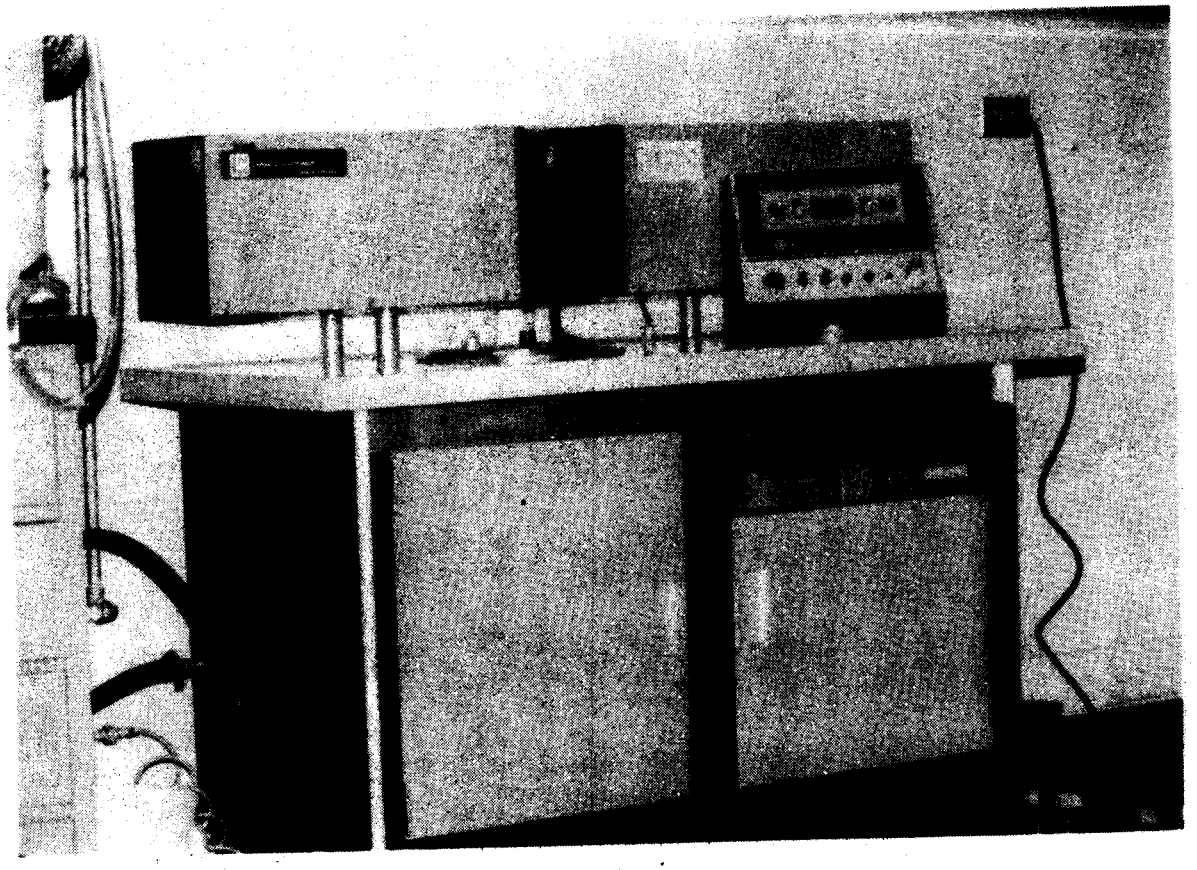

Figure 27. MICROTRAC particle size analyzer.

Table 22. Mass median aerodynamic diameters (MMAD) from MICROTRAC analysis.

Mineral	MMD, μm	84.1% Size, μm	σ_g	Density, g/cm^3	MMAD, μm
GROUP 1					
Quartz (Q-1)	3.8	6.0	1.6	2.65	6.2
Cristobalite (CB-25)	4.1	8.2	2.0	2.33	6.2
Tridymite (TY-27)	3.9	7.1	1.8	2.27	5.9
Beryl (B-11)	4.4	7.7	1.7	2.66	7.2
Fluorite (F-17)	7.3	12.7	1.7	3.18	13.1
Nickel Oxide (N-108)	2.4	5.6	2.4	6.90	6.2
GROUP 3					
Antigorite (AG-55)	3.7	7.0	1.9	2.62	6.1
Riebeckite (R-60)	3.2	5.1	1.6	3.02	5.6
Cummingtonite (C-71)	3.6	5.9	1.6	3.2	6.5
Grunerite (G-68)	3.7	5.9	1.6	3.40	6.8
Anthophyllite (A-102)	3.7	6.1	1.6	2.85	6.3
Tremolite (T-77)	4.1	6.8	1.6	3.0	7.1
GROUP 4					
Talc (TA-99)	3.8	19.0	5.0	2.58	6.1

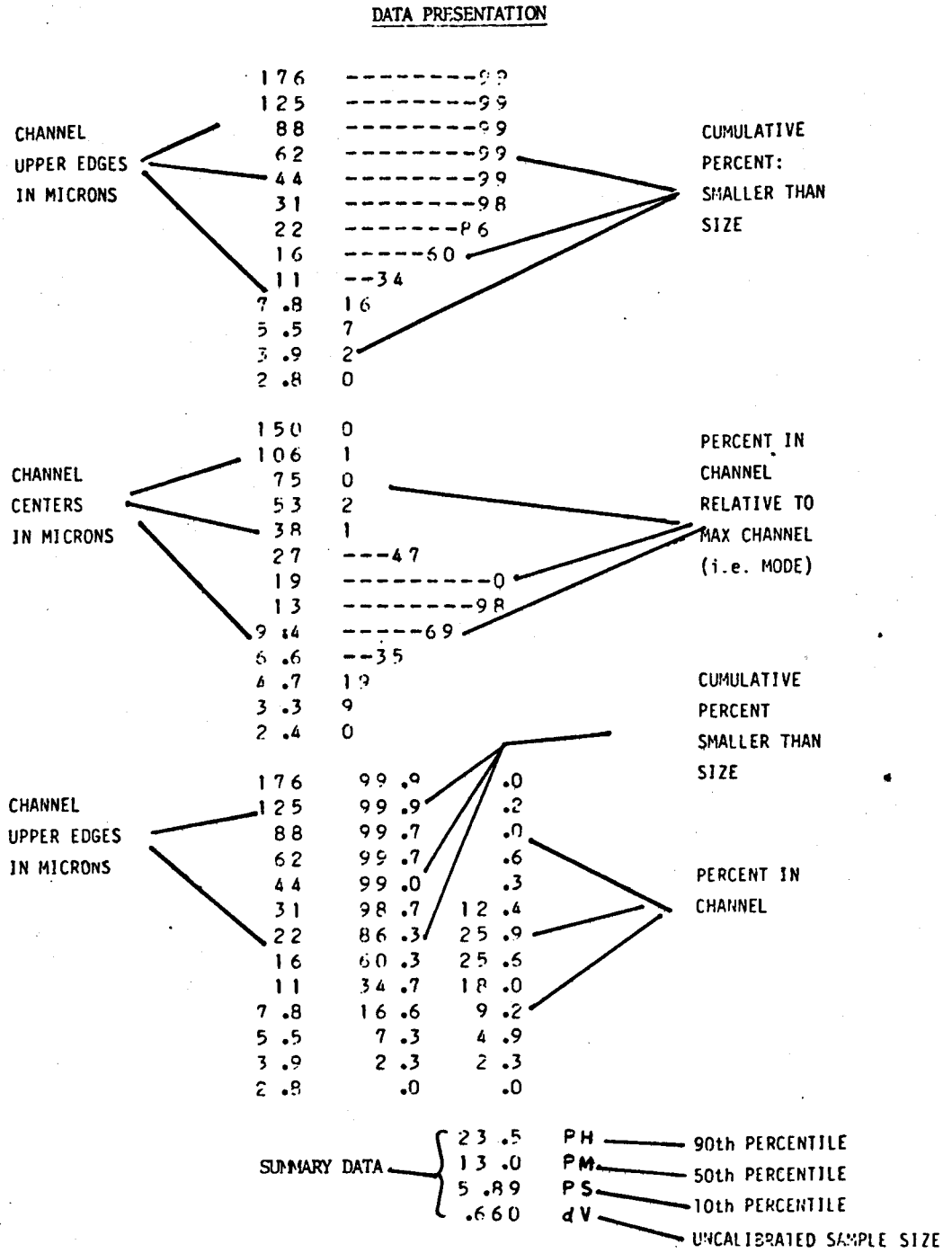

Figure 28. Data printout from MICROTRAC particle analyzer.

- excessive repeated grindings were undesirable since they might reduce sample crystallinity or add significant contaminants from the grinding mills.

Therefore, the final mineral size distributions represent the best balance between size, purity, and quantity that could be attained.

Two of the samples, fluorite (F-17), and talc (TA-99), showed some unusual size distribution results from the MICROTRAC data (Table 22). F-17 has a MMAD of 13.1 μm whereas the microscopical results show a MMAD of only 2.7. The higher MMAD by MICROTRAC analysis may be due to agglomerates in the slurry.

TA-99 has an unusually high σ_g of 5.0 by MICROTRAC, whereas the microscopical result is just 1.77. The MICROTRAC data show a possible presence of a bimodal distribution; however, it seems more likely that this apparent bimodal distribution is merely due to agglomerates. In the microscopical sizing, agglomerates were not sized, which explains the lower geometric standard deviations obtained by this sizing technique.

The median fiber lengths reported in Table 21 also just exceed the desired range of median fiber lengths. Since all of the fibers were ground in the Retsch mill, judged to be the best mill available for the task, the fiber length distributions were the minimum median sizes attainable for asbestos with this mill. The median fiber lengths shown for chrysotile and crocidolite are not true fiber lengths. These samples contain some tangled, egg-shaped masses of the mineral fibers along with the individual fibers. These fibers became tangled during milling and could not be deagglomerated by ultrasonic agitation of suspensions in acetone, water, or isopropanol, or by dispersion in isopropanol in a blender.

POLARIZED LIGHT MICROSCOPY (PLM)

Each sample was inspected a final time by PLM before packaging for shipment to identify and quantitate any phase impurities present in the sample (see Section 4). The PLM was also necessary because beneficiation techniques either reduced or completely removed the number and quantity of mineral phase impurities present in the sample. In addition, the microscopical survey yielded information on the amount and types of contaminants introduced by comminution techniques.

The folowing paragraphs describe particle morphologies, particle size ranges (Feret diameters measured), mineral phase impurities, and grinding contaminants noted in each mineral standard, as determined by PLM. Purity information also appears on the individual sample specification sheets.

Q-1, Quartz

The ground particles were more rounded and equant than the particles in the "unground" sample (Figure 29) and displayed good conchoidal fracture. Particle size ranged from 0.2 to 11 μm.

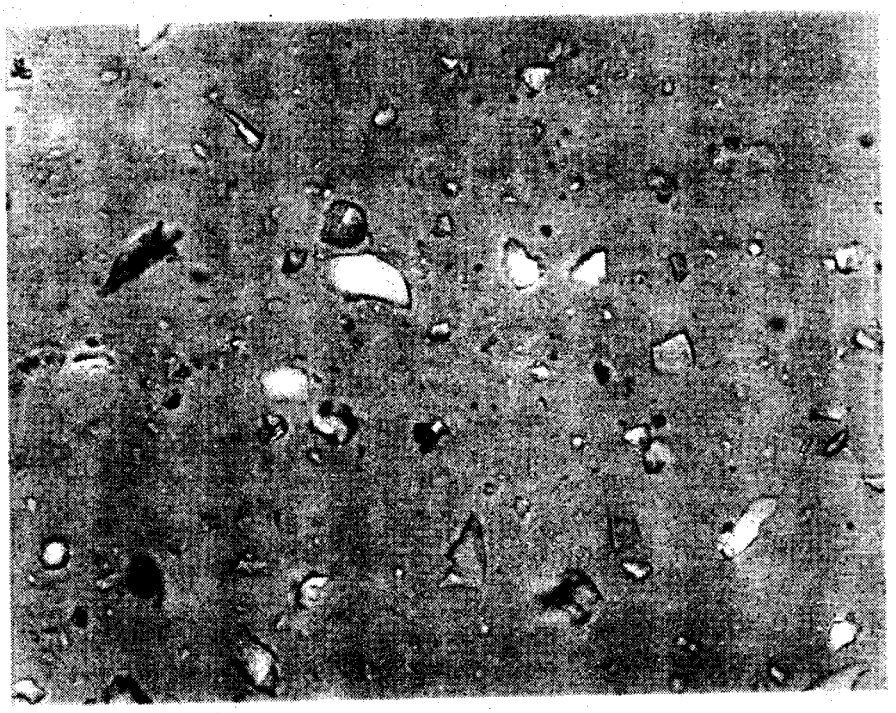

(a) Original sample (-325 mesh)

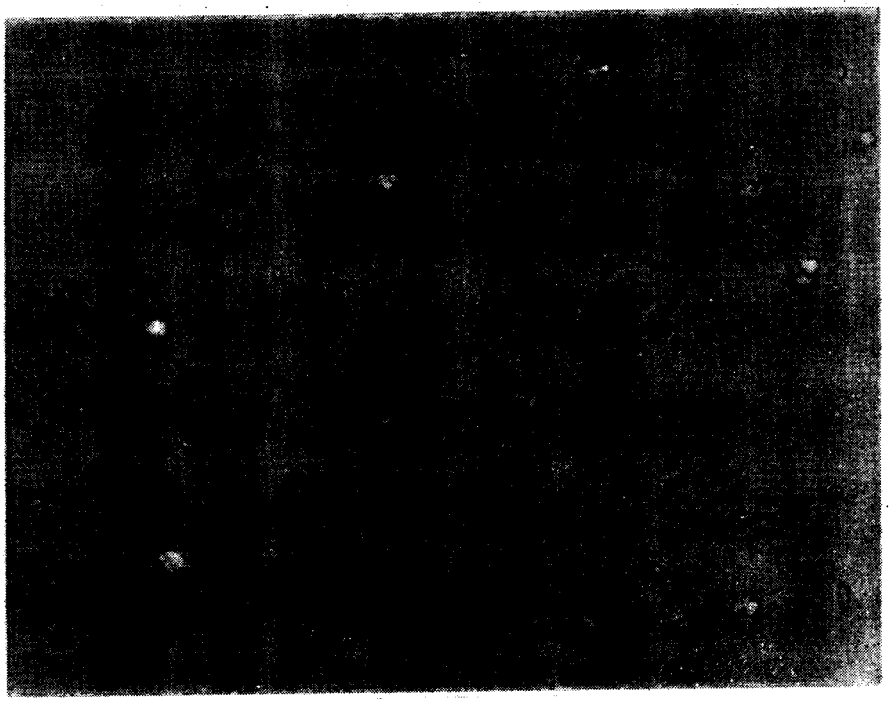

(b) NIOSH standard reference sample Q-1

Figure 29. Quartz (Q-1). (Photographed in n_D = 1.66, at 520X with polars slightly uncrossed.)

Contaminants introduced by grinding included flakes of gasket material of varying sizes and shapes, and rounded submicrometer metal and oxide particles. Together the contaminants represented less than 0.5% of the sample.

Q-107, Quartz

Particles in this sample tended to be flake-like rather than equant, and angular rather than rounded (Figure 30). The particle size range was quite wide, longest dimension being 18 μm.

B-11, Beryl

The finer (less than 3 μm) ground particles tended to be angular and irregular in shape, whereas the larger particles were quite rounded (Figure 31). All particles demonstrated good conchoidal fracture. Particle size ranged from 0.2 to 32 μm. Most of the particles were below the required 10-μm size.

Contaminants noted in the unground sample--mica, probable carbonate minerals, iron oxides--were reduced in concentration in the ground sample. Careful hand selection of rock fragments, as well as preferential loss in jet milling (much lower hardness of the contaminants allowed grinding to finer particle sizes and subsequent loss in the exhaust stream), were responsible for lower concentrations of contaminating mineral phases. Contaminants introduced by milling, however, were significant. They consisted primarily of 0.2 to 12 μm fragments of metal and constituted up to 1% of the sample.

F-14, Fluorite

Fluorite appeared as amorphous to rectangular and cubical particles, (Figure 32). Particles consisting of 20 or more intergrown fluorite crystals were not uncommon. Particle sizes ranged from 0.2 to 21 μm.

Contaminants present included calcium carbonate (1%), calcium sulfate (less than 1%), and iron oxides (less than 0.5%).

N-108, Nickel Oxide

Particles were rounded to spherical in shape (Figure 33) and tended to agglomerate into large, irregular clumps. Particle size was quite small, from 0.5 to 3 μm.

Few contaminants were noted in the sample, primarily iron oxides. These constituted less than 0.5% of the sample mass.

NIOSH standard reference sample Q-107

Figure 30. Quartz (Q-107). (Photographed in n_D = 1.39, at 520X with polars slightly uncrossed.)

(a) Original sample (-325 mesh)

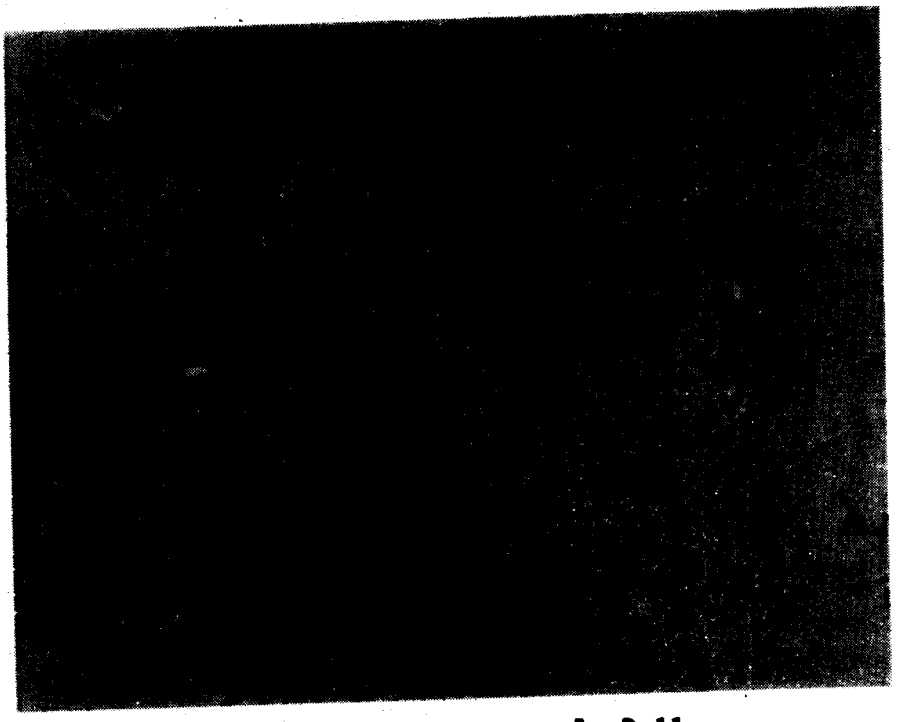

(b) NIOSH standard reference sample B-11

Figure 31. Beryl (B-11). (Photographed in n_D = 1.39, at 520X with polars slightly uncrossed.)

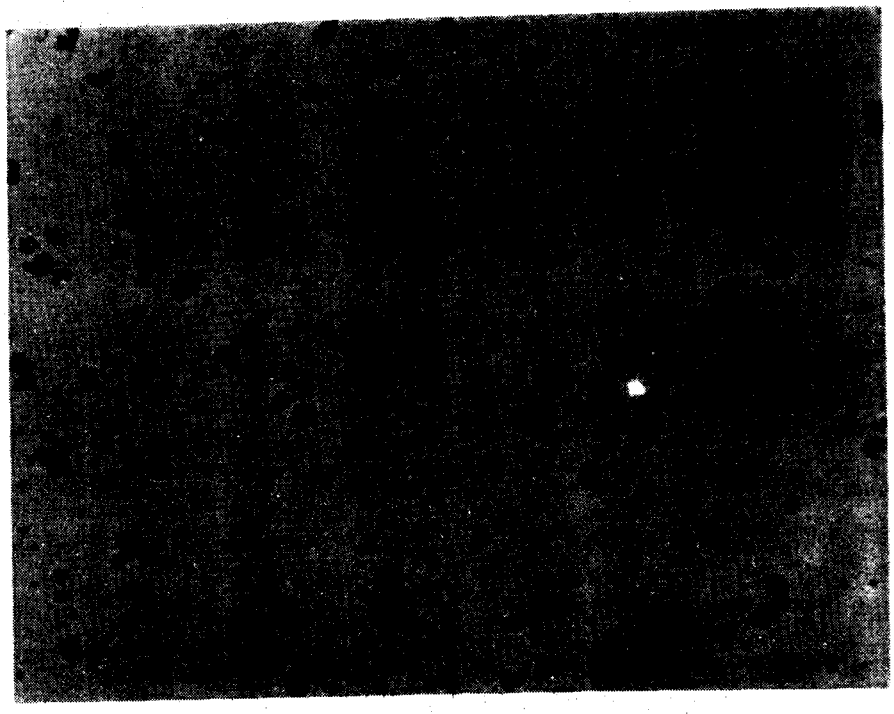

NIOSH standard reference sample F-17

Figure 32. Fluorite (F-17). (Photographed in n_D = 1.66, at 520X with polars slightly uncrossed.)

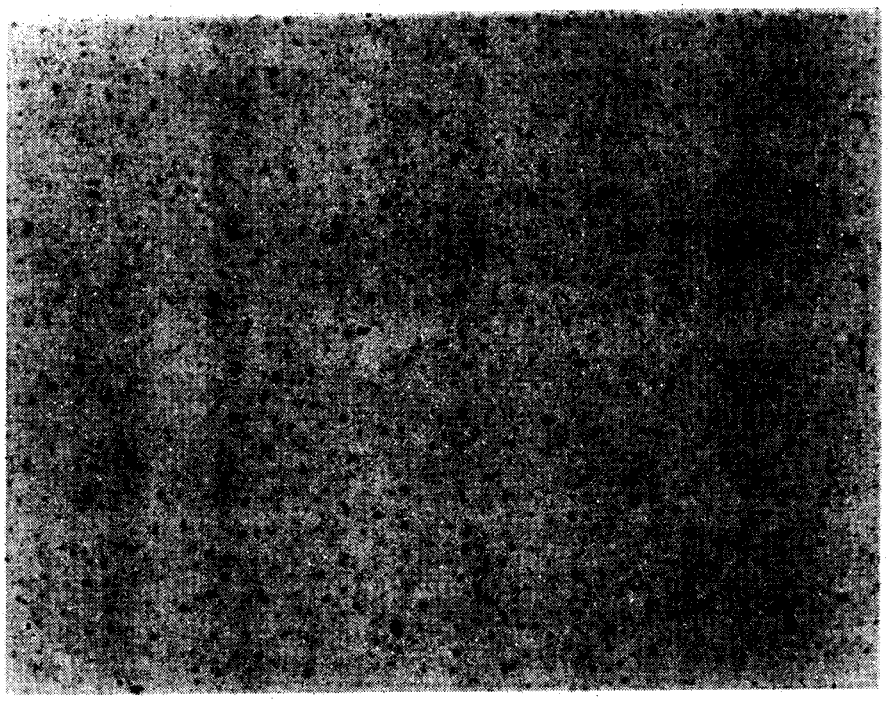

NIOSH standard reference sample N-108

Figure 33. Nickel oxide (N-108). (Photographed in n_D = 1.39, at 520X with polars slightly uncrossed).

CB-25, Cristobalite

Particles in the smaller sizes were more irregular and flake-like in shape compared to the "unground" sample (Figure 34). Large (greater than 3 μm) particles tended to be rounded and exhibited good conchoidal fracture. The particle size range was quite wide; whereas most of the particles were below 10 μm, particles as large as 40 μm were present. The 100 g sample of CB-25 subjected to cascade sedimentation contained no particles greater than 10 μm in diameter (see Section 5).

Some contaminants were introduced during grinding. These included large flakes of (jet-mill) gasket material, submicrometer metal particles, and 1 to 3 μm spherical metal oxide particles. Contaminants noted in the unground sample--hematite, high birefringence phase--were present in the same concentration levels in the ground sample; no preferential increase or decrease in concentration of the original contaminants was noted. Together, the various contaminants represented less than 1% of the sample mass.

TY-27, Tridymite

Particles tended to be irregular and angular in shape, as they were in the original unground sample (Figure 35). Conchoidal fracture was evident on most particles. Particle size ranged from 0.2 to 38 μm, with most below 10 μm in diameter.

Contaminants noted in the ground sample but not present in the unground sample included flakes of polyurethane and fine rounded steel particles introduced by the ball mill. Contaminants noted in the unground sample were present at approximately the same concentrations in the ground sample. All contaminants combined represented less than 1% of the sample mass.

CH-29, Chrysotile

Fiber length reduction was not the primary objective of grinding; rather, knife milling was meant to separate fiber bundles. Although some separation did occur, complete fiber bundle disaggregation was not possible to achieve. Approximately 50% of the sample remained as relatively short (0.5 to 150 μm), compact fiber bundles (Figure 36). Maximum individual fiber length noted was 98 μm.

Contaminants noted in the unground sample were present in the ground sample. Mineral contaminants included iron oxides (1%), carbonates (1 to 2%), quartz (1%), and mica (1%). Possible nonfibrous serpentine was present. Optically, it was not possible to determine whether these fragments were fibrous or not. The maximum concentration of the nonfibrous serpentine phase was less than 0.5%. Metal fragments introduced during mining and grading of the raw ore constituted approximately 1% of the sample. Metal fragments introduced during knife milling contributed another 1 to 2% the sample mass.

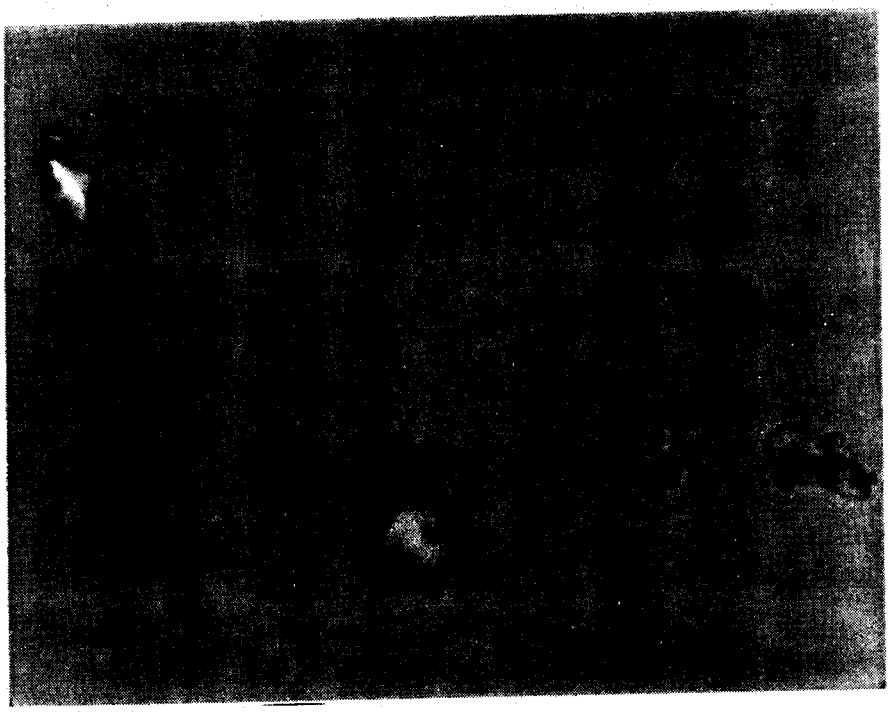

(a) Original sample (-325 mesh)

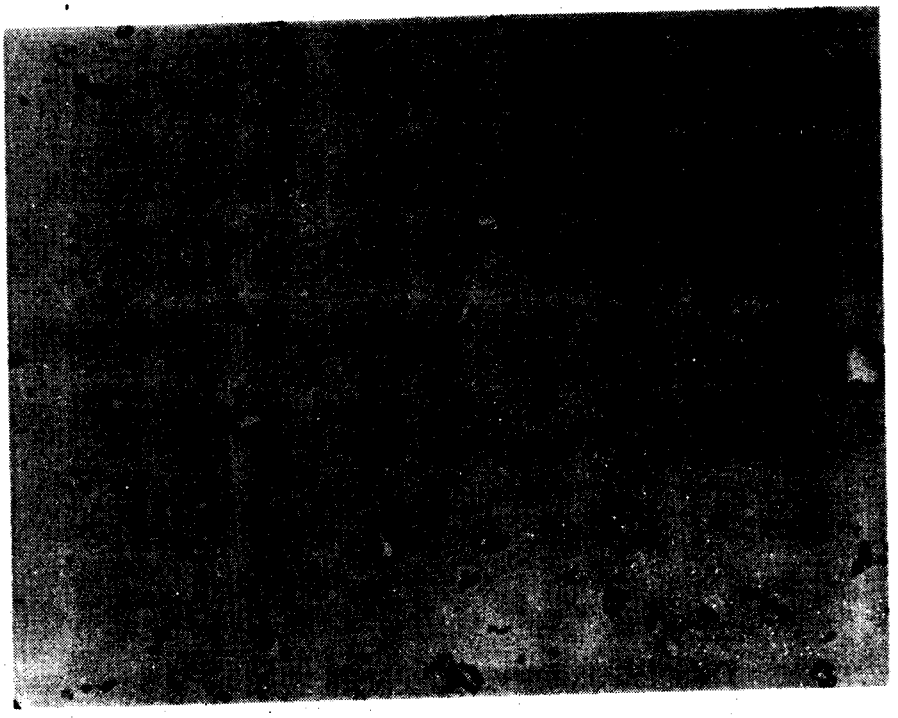

(b) NIOSH standard reference sample CB-25

Figure 34. Cristobalite (CB-25). (Photographed in n_D = 1.66, at 520X with polars slightly uncrossed).

(a) Original sample (-325 mesh)

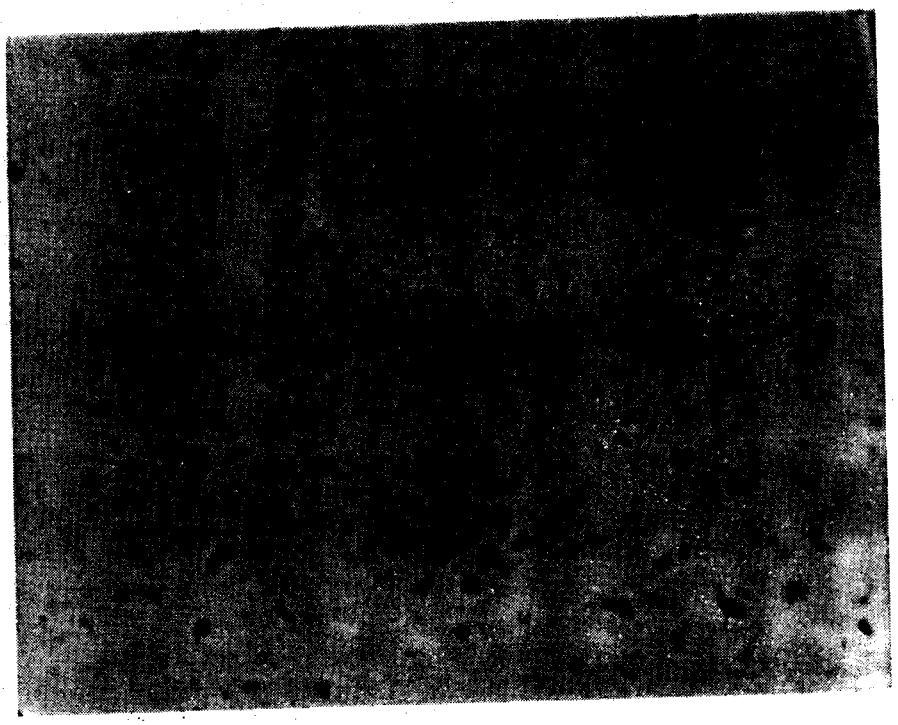

(b) NIOSH standard reference sample TY-27

Figure 35. Tridymite (TY-27). (Photographed in n_D = 1.66, at 520X with polars slightly uncrossed.)

(a) Original sample (-325 mesh)

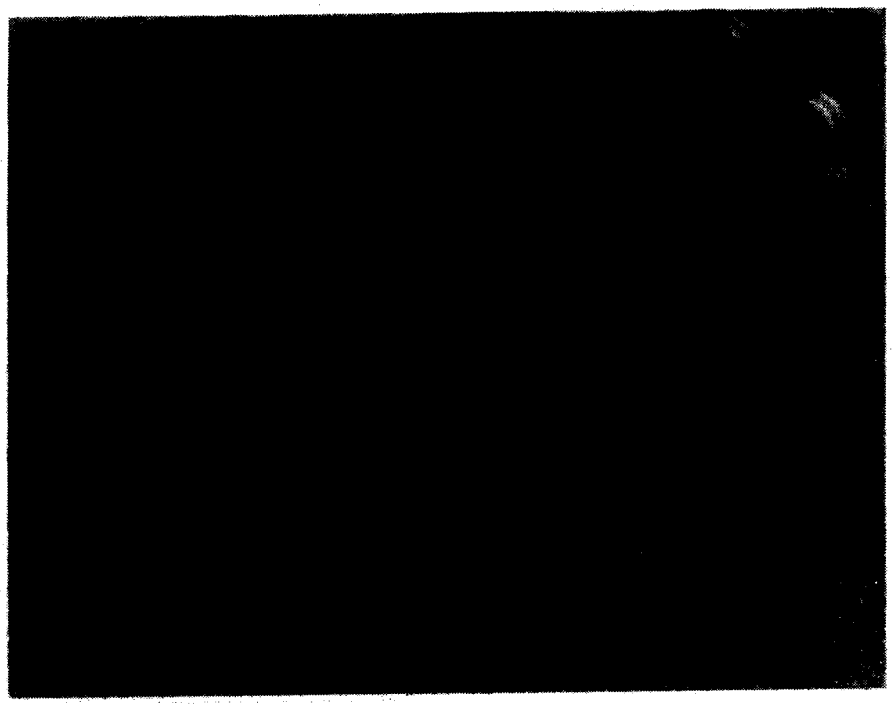

(b) NIOSH standard reference sample CH-29

Figure 36. Chrysotile (CH-29). (Photographed in n_D = 1.310, at 520X with polars slightly uncrossed.)

CR-37, Crocidolite

The sample exhibited quite an unusual morphology after grinding. The fibers, separated from bundles and reduced in length, tended to form rounded agglomerates that were spherical to elliptical in shape (Figure 37). These rounded particles were made up of short, fine individual fibers, demonstrated by the presence of incompletely rounded agglomerates (rounded-off on one end, open on the other end), with protruding individual fine fibers. The agglomerates were not easily separated into individual fibers. A small portion of the sample still existed as long fiber bundles that had resisted length reduction and separation along the fiber bundle lengths.

Individual fibers ranged in length from 0.5 to 36 μm. Large fiber bundles as long as 138 μm were noted.

Contaminants introduced during grinding included metal fragments and cellulose fibers (probably from the knife mill dust collection bag). These contaminants comprised less than 1% of the sample mass. Contaminants in the unground sample appearing in the ground sample constituted less than 2% of the sample. Most of these particles were too fine to identify; quartz, limestone, and hematite are the suspected primary contaminants.

GF-38, Fibrous Grunerite (Amosite)

This sample fractured quite well along both the horizontal and vertical fiber axes. Fiber length, as well as bundle widths, was considerably reduced by grinding. Individual fibers ranged in length from 0.5 to 90 μm. A few fiber bundles up to 150 μm in length remained. No significant matting or agglomeration of fibers was noted (Figure 38).

By carefully hand selecting fiber bundles for grinding, the fibrous sample was contaminated with less than 2% of nonfibrous minerals (quartz, mica, chlorite, trace of grunerite, and calcite). Grinding contaminants introduced were primarily metal fragments less than 3 μm in diameter and constituting less than 1% of the sample mass.

AF-45, Fibrous Anthophyllite

When the original sample was reduced in particle width and length the resultant particles were more lath-like than rod-like in structure (Figure 39). Many of the particles were quite blocky in shape due to minimal cleavage along the fiber bundle length. Reductions in bundle length and width by grinding were not as great on this sample as they were for the GF-38 sample.

Single fibers (defined by 3 to 1 aspect ratio and no apparent cleavage lines parallel to the fiber length) ranged in length from 0.5 to 96 μm. Fiber bundles as long as 210 μm were present; nearly equant fiber bundles up to 50 μm were also noted.

(a) Original sample (-325 mesh)

(b) NIOSH standard reference sample CR-38

Figure 37. Crocidolite (CR-37). (Photographed in n_D = 1.39, at 520X with polars slightly uncrossed.)

(a) Original sample (-325 mesh)

(b) NIOSH standard reference sample GF-38

Figure 38. Fibrous grunerite (amosite, GF-38). (Photographed in n_D = 1.39, at 520X with polars slightly uncrossed.)

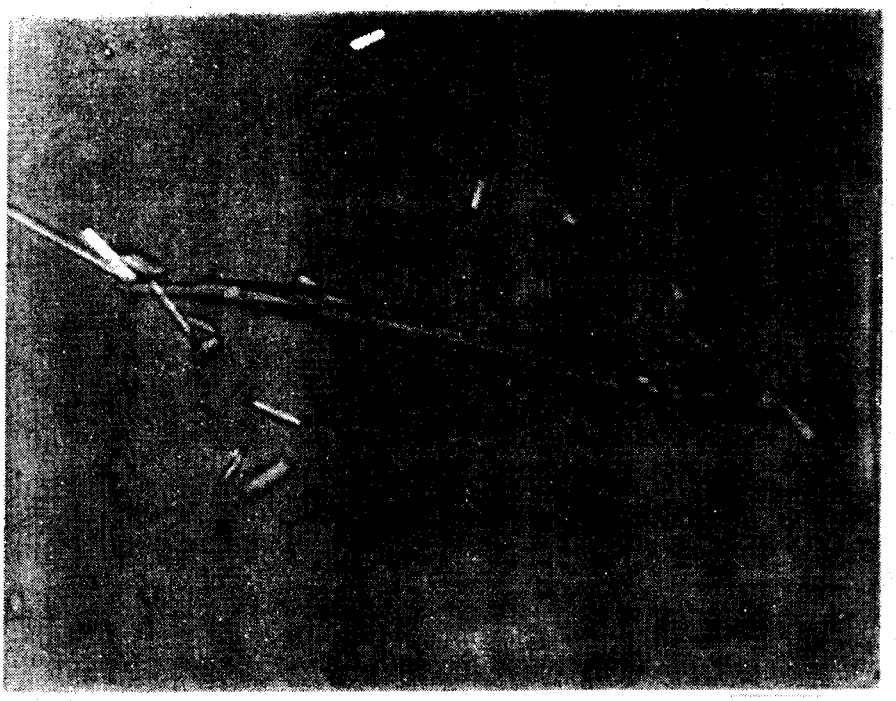

(a) Original sample (-325 mesh)

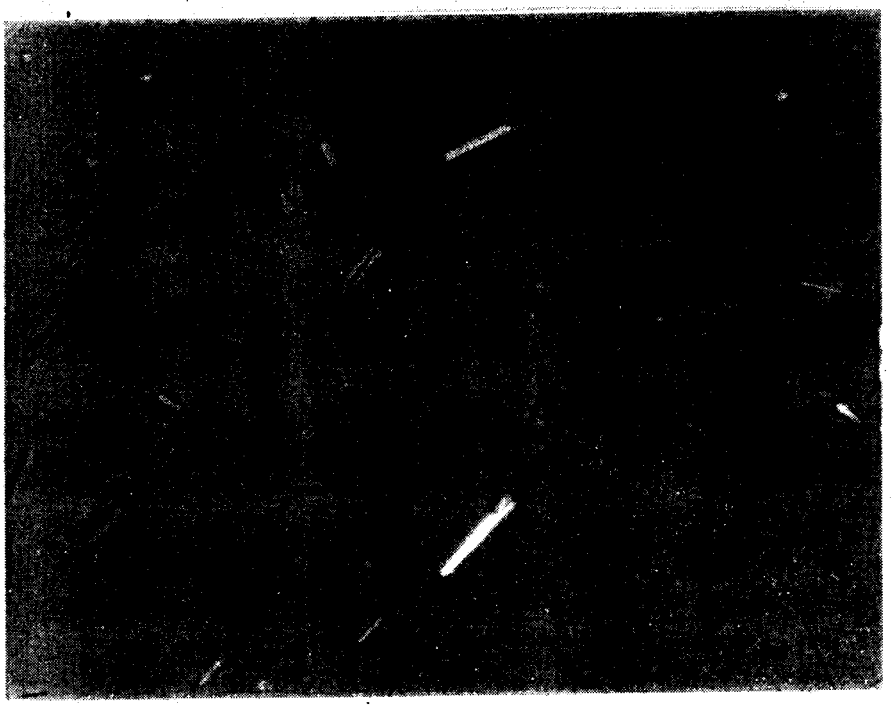

(b) NIOSH standard reference sample AF-45

Figure 39. Fibrous anthophyllite (AF-45). (Photographed in n_D = 1.39, at 520X with polars slightly uncrossed.)

Careful hand selection and cobbing of fiber bundles for grinding resulted in a sample containing less than 2% matrix material (primarily micaceous and carbonate minerals). Grinding contributed additional contaminants totaling less than 1% of the sample.

TF-48, Fibrous Tremolite

This sample was wuite similar to the AF-45 sample in that particles were more lath-like than rod-like (Figure 40). Fiber bundle width reduction was also difficult to accomplish in this sample.

Apparent single fibers ranged in length from 0.8 to 100 μm. Fiber bundles ranged in length from 3 to 186 μm. Few equant bundles were noted.

Contaminants noted in the unground sample (carbonates, mica) also appeared in the ground sample, and constituted approximately 3% of the sample mass. Grinding contaminants (metal fragments) contributed less than 1% of the sample mass.

AG-55, Antigorite

Grinding of the sample produced rounded, rough-textured particles of antigorite (Figure 41). Particles tended to be equant. The particle diameters ranged from 0.2 to 38 μm.

Contaminants noted in the original sample were reduced in the ground sample by careful hand selection and cobbing of fragments before grinding. Separation of magnetite from the ground sample with a handheld magnet also considerably reduced contaminant concentration. Mineral contaminants originally noted in the sample included hematite (1 to 2%), magnetite (3%), chrysotile (1 to 2%), quartz (less than 1%), limestone (less than 1%), and less than 0.5% each of talc, anthophyllite, sphene and chromite. Grinding introduced less than 1% metal contaminants.

R-60, Riebeckite

The ground particles tended to be thin prisms with (two-dimensional) aspect ratios ranging from 1:1 up to 5:1 (Figure 42). All particles were quite angular. Particle sizes (maximum lengths) ranged from 0.2 to 21 μm.

Contaminants noted in the original sample were lower in concentration in the ground sample because of careful selection of rock fragments for grinding. Mineral contaminants (quartz, tourmaline, mica, sphene, hematite) contributed 1 to 2% of the sample mass. Contaminants introduced during grinding were less than 0.5% of the sample.

(a) Original sample (-325 mesh)

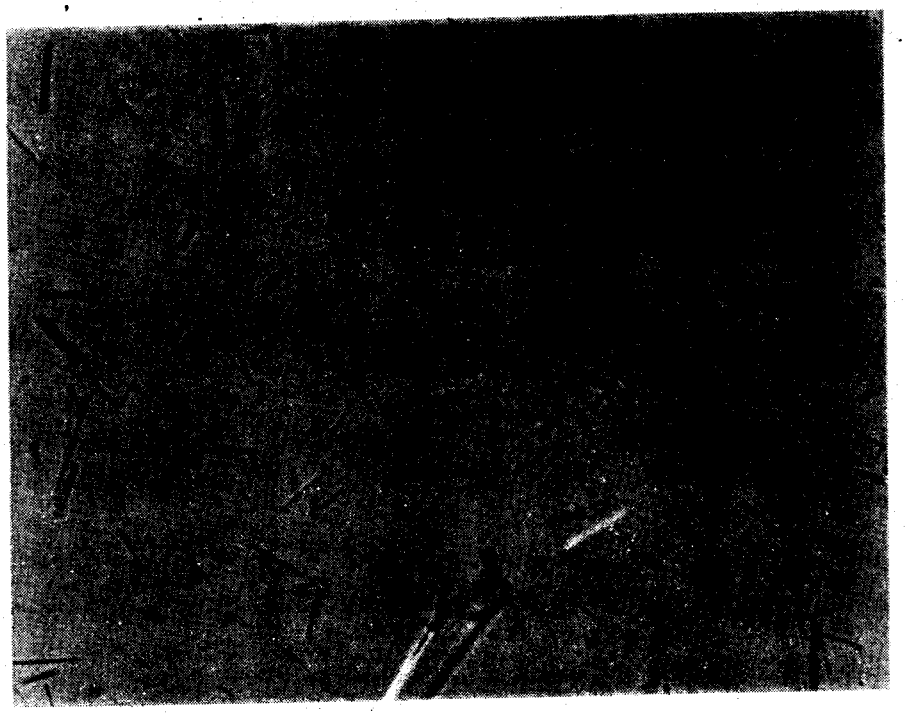

(b) NIOSH standard reference sample TF-48

Figure 40. Fibrous tremolite (TF-48). (Photographed in n_D = 1.39, at 520X with polars slightly uncrossed.)

(a) Original sample (-325 mesh)

(b) NIOSH standard reference sample AG-55

Figure 41. Antigorite (AG-55). (Photographed in n_D = 1.39, at 520X with polars slightly uncrossed.)

(a) Original sample (-325 mesh)

(b) NIOSH standard reference sample R-60

Figure 42. Riebeckite (R-60). (Photographed in n_D = 1.39, at 520X with polars slightly uncrossed.)

G-68, Grunerite

Particles in this sample were also quite prismatic. The prisms tended to be thick rather than thin (Figure 43). Some rounding of edges also occured. Elongated particle types predominated.

Particles were effectively reduced in size by the grinding method employed. Maximum particle size (length) noted was 14 μm.

Beneficiation techniques effectively reduced the quartz content of the sample. Mineral contaminants present represented 2 to 4% of the sample mass and included quartz, diopside, hematite, carbonate, and chlorite. Grinding contributed an additional 1% to the sample mass as metal fragments.

C-71, Cummingtonite

Particles tended to be elongated prisms with aspect ratios slightly greater than 2:1. Elongated particles were sharp and angular, although the more equant particles (approximately 20% of the cummingtonite) tended to have rounded edges (Figure 44).

Elongated prisms ranged in size (maximum dimension) from 0.5 to 14 μm. Equant prisms ranged in size from 0.2 to 10 μm.

Contaminants noted in the original sample were present at slightly lower concentrations in the ground sample. Mineral contaminants noted were mica (7%), quartz (4%), chlorite (1%), carbonate (less than 1%), iron oxides (less than 1%), and other minerals (less than 1%). Grinding introduced significant quantitites of metal contaminants. The metal fragments averaged 2 μm in size and constituted 3% of the sample.

A-102, Anthophyllite

Ground particles were generally prismatic in shape; elongation, however, was not extreme (Figure 45). Aspect ratios ranged from 1:1 to 4:1, with most particles exhibiting aspect ratios less than 2:1. Particles were not extremely angular but, rather, tended to have rounded edges.

Particle size (maximum length) ranged from 0.2 to 18 μm. Particles longer than 10 μm tended to have the higher aspect ratios.

Contaminants noted in the original sample were present in the ground sample. Concentrations of quartz and talc were reduced; these minerals represented approximately 8% and 1% of the sample, respectively. Rutile was still present at an approximate level of 3%. Grinding contaminants (metal fragments) represented 1% of the sample.

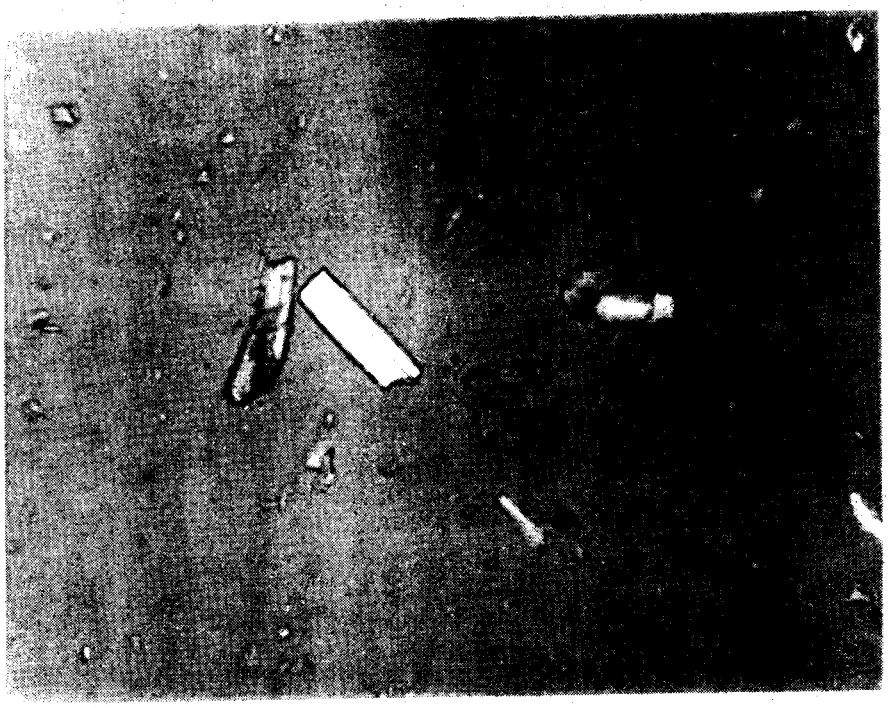

(a) Original sample (-325 mesh)

(b) NIOSH standard reference sample G-68

Figure 43. Grunerite (G-68). (Photographed in n_D = 1.39, at 520X with polars slightly uncrossed.)

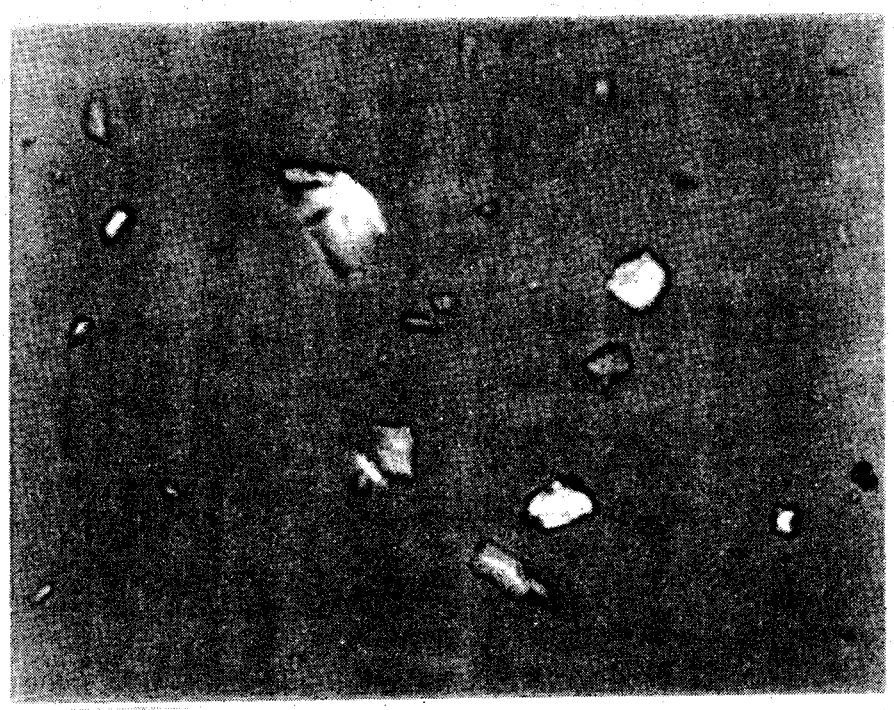

(a) Original sample (-325 mesh)

(b) NIOSH standard reference sample C-71

Figure 44. Cummingtonite (C-71). (Photographed in n_D = 1.39, at 520X with polars slightly uncrossed.)

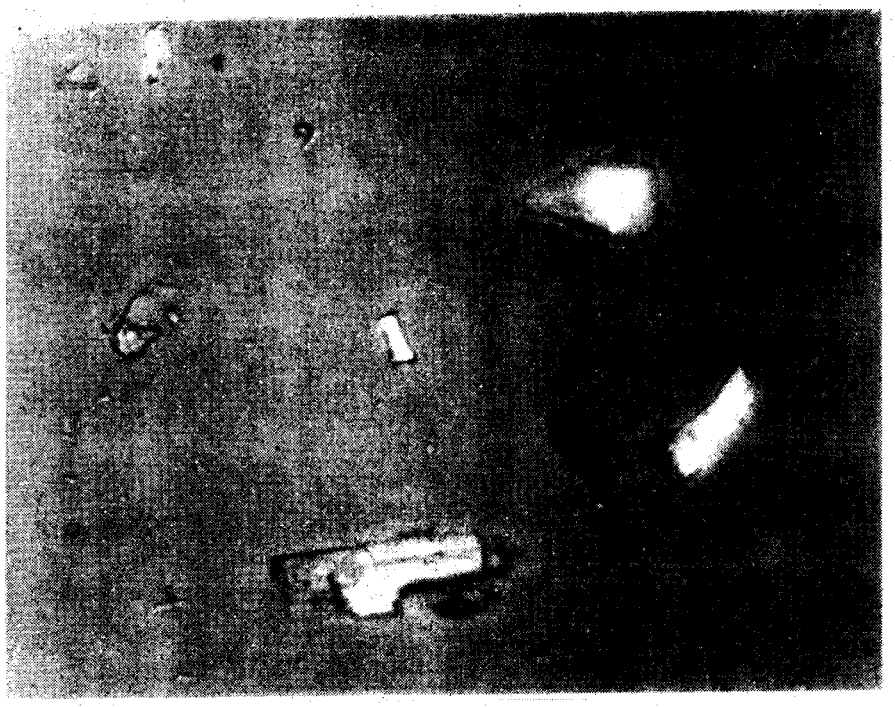

(a) Original sample (-325 mesh)

(b) NIOSH standard reference sample A-102

Figure 45. Anthophyllite (A-102). (Photographed in n_D = 1.39, at 520X with polars slightly uncrossed.)

T-77, Tremolite

Ground particles were primarily elongated prisms which tended to be quite thin in the third dimension (Figure 46). Few particles approached a 1:1 aspect ratio; most particles exhibited aspect ratios greater than 2.5:1. All particles were quite angular.

Because of the lath-like morphologies of the particles, geometric particle sizes were relatively large. Maximum particle length noted was 30 µm.

Beneficiation reduced carbonate mineral contamination to less than 1% of the sample. Other mineral contaminants noted (iron oxides, mica) together constituted less than 1% of the sample. Contaminants introduced during grinding (primarily metal flakes) comprised less than 1% of the sample.

T-79, Tremolite

Particle morphologies were quite similar to those noted in the T-77 sample. Flat, elongated prism-like particles with aspect ratios greater than 2.5:1 were the predominant morphologies in the sample (Figure 47). The maximum prism length noted was 24 µm.

Contaminants noted in the original sample were present to the same degree in the ground sample. Talc represented approximately 1% of the sample. Carbonate minerals were less than 1% of the sample, and serpentine minerals were present at a less than 0.5% level. Grinding contaminants did not increase significantly over what was originally in the sample with jet milling at IITRI. These contaminants included gasket material and metal fragments that, combined, represented less than 1% of the sample.

TA-99, Talc

Several different particle morphologies were noted in the ground sample. The dominant morphology was a thin, flat plate-like structure with rounded edges (Figure 48). Acicular and ragged, irregular fragments were also noted.

Particle sizes were quite small. Maximum particle size (maximum dimension) noted was 9 µm.

Contaminants present in the unground sample were present in approximately the same concentrations in the ground sample. Carbonate minerals represented approximately 1% of the sample mass. Mica, hematite, and quartz each contributed less than 1% of the sample mass. Contaminants introduced by grinding were negligible and comprised less than 0.5% of the sample.

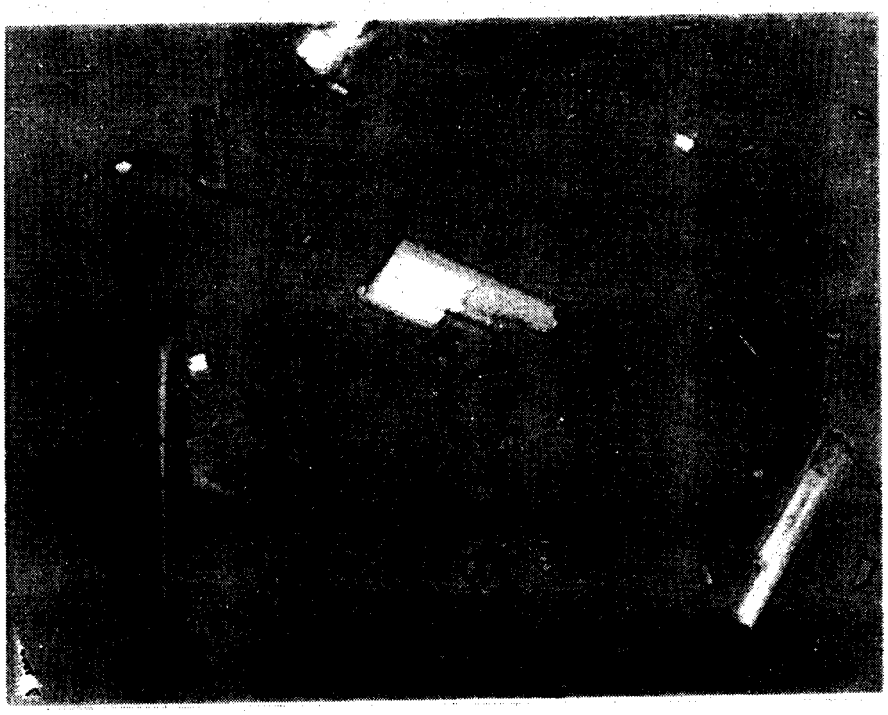

(a) Original sample (-325 mesh)

(b) NIOSH standard reference sample T-77

Figure 46. Tremolite (T-77). (Photographed in n_D = 1.39, at 520X with polars slightly uncrossed.)

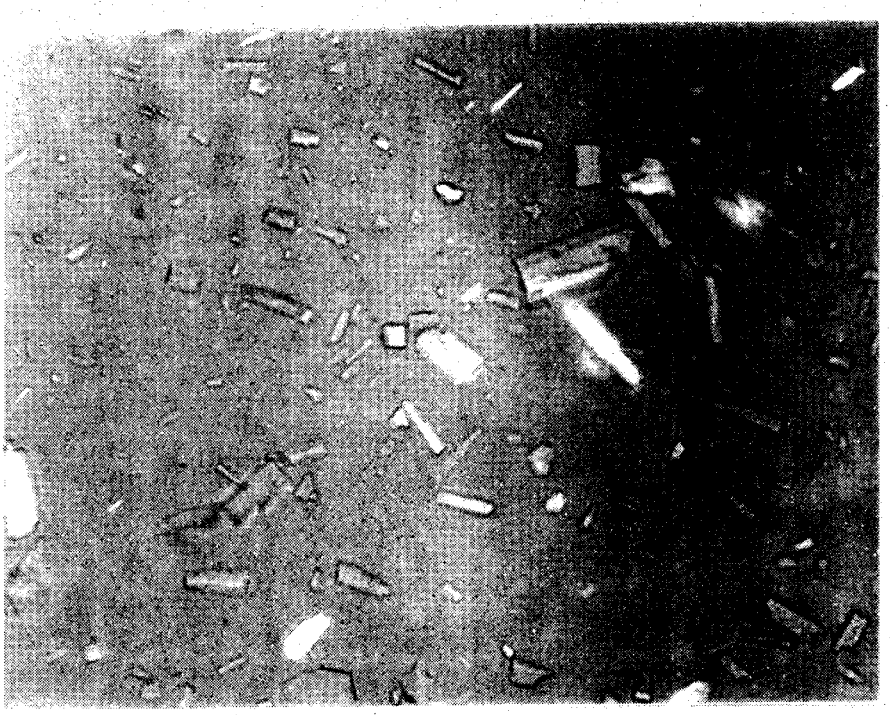

(a) Original sample (-325 mesh)

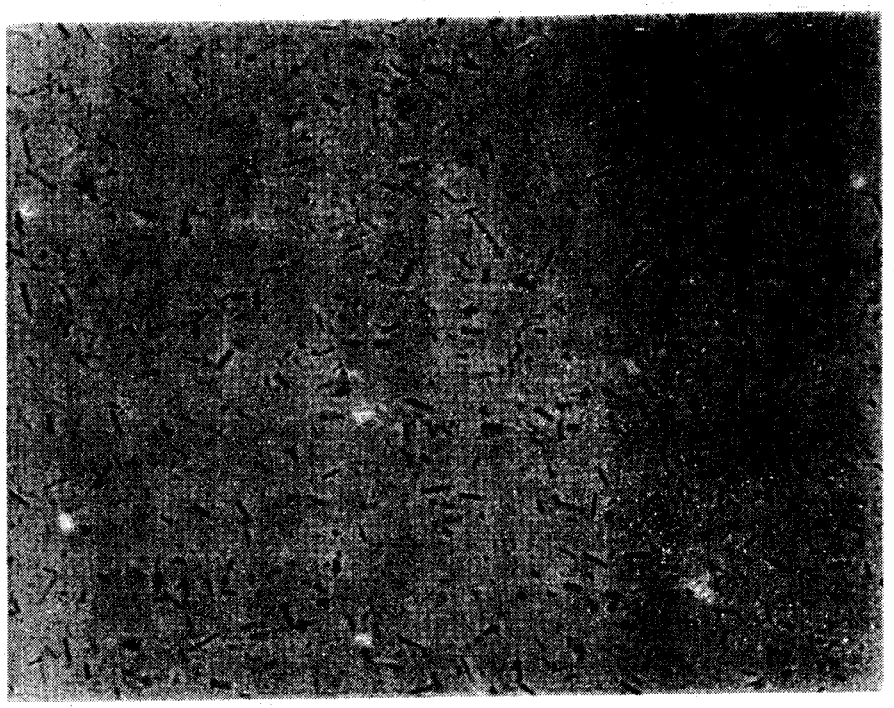

(b) NIOSH standard reference sample T-79

Figure 47. Tremolite (T-79). (Photographed in n_D = 1.39, at 520X with polars slightly uncrossed.)

(a) Original sample (-325 mesh)

(b) NIOSH standard reference sample TA-99

Figure 48. Talc (TA-99). (Photographed in n_D = 1.310, at 520X with polars slightly uncrossed.)

X-RAY DIFFRACTION (XRD) RESULTS

The specifications for characterization of prepared materials indicated that XRD would be performed as follows: "All of the minerals supplied shall be accompanied by an x-ray diffraction scan obtained using Cu K_α radiation. This should be a slow scan (<0.5°/min) from 7° to 90° 2θ on a logarithmic scale at high resolution." Any peaks found that did not correspond to those given for the desired material in the data file of the Joint Committee on Powder Diffraction Standards (JCPDS) were to be identified, and the contaminant(s) the peaks represented were also to be identified, if possible. Any peak of a desired mineral not found in its diffraction record was to be noted.

The sample of each prepared material was packed into a shallow bakelite tray. Special long trays were prepared so that samples would be 76.2 mm (3 in.) in length and, therefore, would intersect the whole x-ray beam at low 2θ angles. Sample packing was performed with a cleaned glass slide; care was taken to ensure that the surface of the sample mount was as even and flat as practicable. No attempt was made to eliminate probable preferred orientations of the fibrous and acicular minerals.

A General Electric XRD-5DF unit with SPG2 spectrogoniometer was used for the XRD. A primary nickel filter was used with a copper tube operated at 16 ma and 44.5 kv potential to give Cu K_α radiation. The specified scan was run at 0.4°/min from 7° to 90° 2θ with 1° beam slit, medium resolution Söller slit, and 0.02° detector slit. The scalar was set for full-range logarithmic scale, and the recorder was operated at 1° 2θ/in.

It was found that minor peaks of the desired material and trace contaminant phases could be determined better if a linear scale record over the same scanning range was prepared with somewhat different instrument set-up and compared with the specified scans. Linear scales of 2,000 to 10,000 counts/sec and appropriate time constants were combined with a recorder rate of 2° 2θ/in. The linear runs were made at a scan rate of 2°/mm. When a 3° beam slit and 0.2° detector slit with the medium resolution Söller slit were used, much greater peak intensities were obtained than under conditions used for the logarithmic scans. Higher intensity bombardment of the sample and a more compressed record of the scan on the chart permits the detection of minor peaks in the linear scan. The precise positions of such peaks were then identified in the higher resolution log scans. Samples of data sheets that accompany each diffraction scan are given in Figures 49 and 50.

In reading the chart, peak position in degrees 2θ was taken as the mean of the positions of the peak sides at one-half the peak height above background. The resulting 2θ value for each peak was found in the X-ray Diffraction Tables,[26] and the corresponding interplanar (d-) spacing was obtained when Cu K_α radiation had been used.

IIT RESEARCH INSTITUTE

X-ray Diffraction Conditions:	High resolution, slowscan, log-scale (Specified Characterization of Material)
Instrument:	General Electric XRD-5DF with SPG 2 Spectrogoniometer
X-ray Source:	Target: Copper Radiation: Nickel-filtered Kα KVP: 44.5 kv MA: 16 ma Port: Side
Set-up:	Target Take-off Angle: 4° Scanning Speed: Slowscan, 0.4°/min Beam Slit: 1° Soller Slit: Medium Resolution Detector Slit: 0.02° Filter: Nickel foil, 2 layers, each 0.00035 in. thick Scanning Range: 7° - 90° 2θ
Detector:	Counter: SPG 3 Scintillation counter
Recorder:	Chart Speed: 24 in./hr (1° 2θ/in.) Time Constant: 1 - 1.4 sec Scale: Logarithmic, full range setting Zero Response Setting:
Sample:	Length: 3 in. Sample Holder: Bakelite tray

Specimen:

Principal Known Contaminants:

Date:

Technician:

Figure 49. Sample data sheet.

IIT RESEARCH INSTITUTE

X-ray Diffraction Conditions: Fastscan, linear scale. (Qualitative Characterization of Material).

Instrument: General Electric XRD-5DF with SPG 2 Spectrogoniometer

X-ray Source:
Target: Copper
Radiation: Nickel-filtered Kα
DVP: 44.5 kv
MA: 16 ma
Port: Side

Set-up:
Target Take-off Angle: 4°
Scanning Speed: Fastscan, 2°/min
Beam Slit: 3°
Soller Slit: Medium Resolution
Detector Slit: 0.2°
Filter: Nickel foil, 2 layers, each 0.00035 in. thick
Scanning Range: 7° - 90° 2θ

Detector: Counter: SPG 3 Scintillation counter

Recorder: Chart Speed: 60 in./hr (2° 2θ/in.)

Time Constant:	sec	sec
Scale: Linear, range:	cps	cps
Scanning Range:	2θ	2θ

Sample:
Length: 3 in.
Sample Holder: Bakelite tray

Specimen:

Principal Known Contaminants:

Date:

Technician:

Figure 50. Sample data sheet.

The JCPDS data file contains d-spacing information for one or more specimen materials corresponding to each desired material in this program. The JCPDS file for anthophyllite was produced from a synthetic product; while no crystal habit is stated, it can be presumed to be nonfibrous. The prepared NIOSH standards of both fibrous (AF-45) and nonfibrous (A-102) anthophyllite were compared to this JCPDS material.

The JCPDS file for tremolite was produced from a fibrous, naturally occurring specimen. No high reliability (starred) JCPDS file exists for a naturally occurring nonfibrous tremolite of identical composition. Therefore the JCPDS file for the fibrous mineral was compared to both the fibrous (TF-48) and nonfibrous (T-77) prepared standards. It should also be noted that no JCPDS files exist for the fibrous minerals, crocidolite, and (fibrous) grunerite (amosite). JCPDS file data for the nonfibrous counterparts of these minerals had to be used for the fibrous standards as well as the nonfibrous standards prepared. In Appendix 2, the d-spacings of the prepared material are compared with those of corresponding materials from the JCPDS file, noting extraneous peaks and expected peaks not found for the desired material.

Table 23 summarizes the XRD results. The only samples in which impurities could be detected were fibrous anthophyllite (AF-45), cummingtonite (C-71), and anthophyllite (A-102). Microscopical analyses discussed in the preceding section showed that most of the natural mineral samples had trace level impurities in concentrations too low to be detected by XRD.

All of the samples conformed well to their JCPDS standard patterns.

THERMAL ANALYSES

Thermal Analysis Interpretations

Serpentines--

Differential thermal analysis (DTA) curves for some serpentines from the literature are shown in Figures 51[27] and 52 through 54.[28] Chrysotile does not show a thermal analysis pattern distinguishing it from other serpentines of similar composition. The serpentines are characterized by a large endotherm in the 450° to 800°C range and an exotherm between 800° to 850°C. A low-temperature endothermic peak, which is often present, is relatively small for pure samples. Alteration of the mineral by grinding or contamination with colloidal material can produce a relatively large low-temperature endotherm due to hygroscopic moisture. The high-temperature endotherm corresponds to the loss of constitutional water, whereas the exotherm is associated with the oxidation of ferrous to ferric iron. The exotherm is variable in size and is very sensitive to treatment history.

Differences in DTA patterns of the same material performed by different analysts are a common occurrence. Part of the differences may be due to differences in sample preparation. A sample initially showing only a small exotherm could easily be altered by grinding to give an exotherm many times

Table 23. Summary of x-ray diffraction results.

IITRI Number	Mineral Name	JCPDS File Number	Extraneous Peaks Present	Number of Contaminant Phases Detected
Q-1	Quartz	5-0490	0	
B-11	Beryl	9-430	0	
F-17	Fluorite	4-864	0	
N-108	Nickel Oxide	4-835	0	
CB-25	Cristobalite	11-695	0	
TY-27	Tridymite	18-1170	0	
CH-29	Chrysotile	21-543	0	
CR-37	Crocidolite	19-1061	0	
GF-38	Fibrous Grunerite	17-745	0	
AF-45	Fibrous Anthophyllite	16-401	11	2 (Quartz & Talc)
TF-48	Fibrous Tremolite	13-437	0	
AG-55	Antigorite	9-444	0	
R-60	Riebeckite	19-1061	0	
G-68	Grunerite	17-745	0	
C-71	Cummingtonite	17-726	4	2 (Quartz & Biotite)
A-102	Anthophyllite	16-401	24	2 (Quartz & Talc)
T-77	Tremolite	13-437	0	
TA-99	Talc	19-770	0	

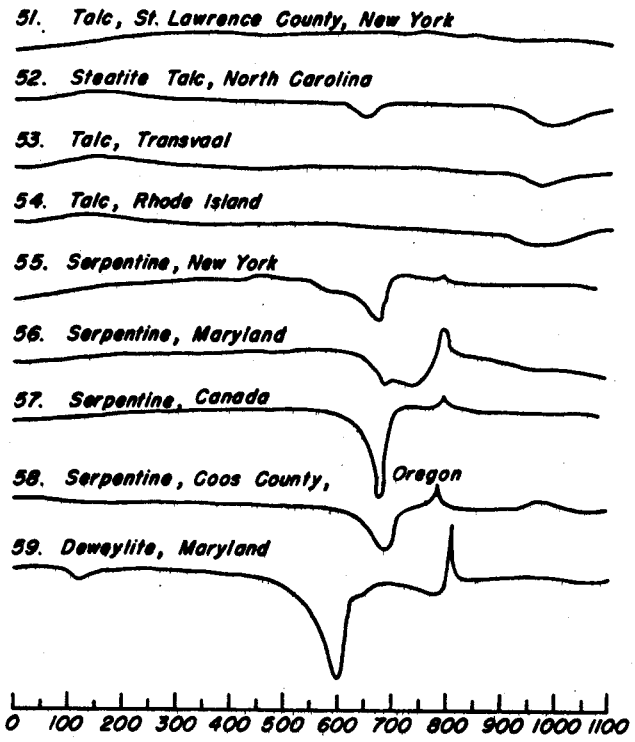

Figure 51. DTA curves of talc and serpentines.[27]

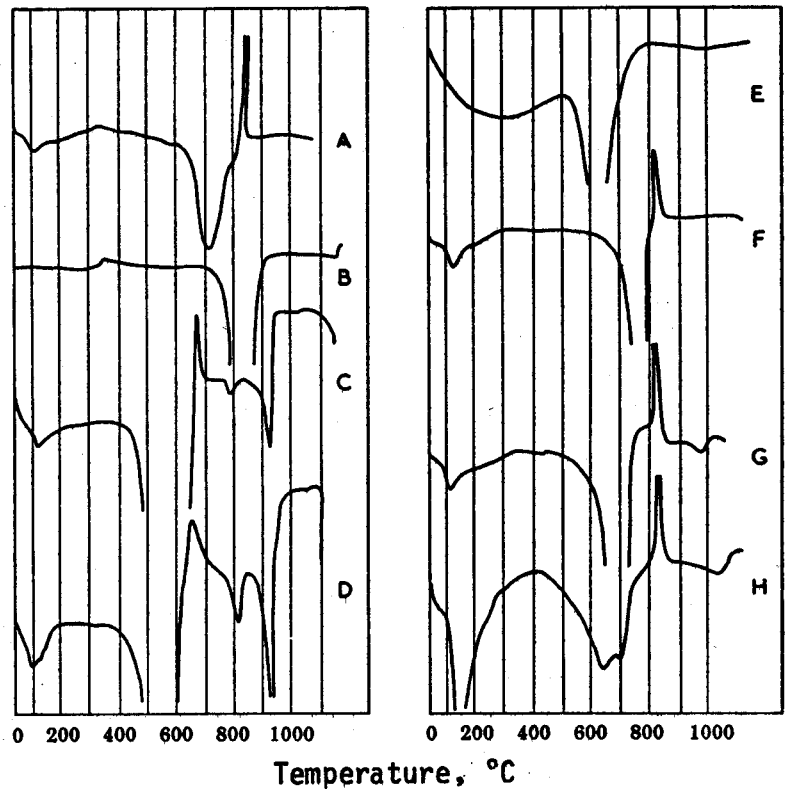

Figure 52. DTA curves for:

A. Antigorite, Antigorio, Piedmont, Italy
B. Bowenite, Khotan, Sin-kiang, China
C. Greenalite, Port Arthur, Ontario, Canada
D. Berthierine, Jayange, Lorraine, France
E. Cronstedite, Pribram, Czechoslovakia
F. Nickeliferous Antigorite, Thio, New Caledonia
G. Nickeliferous Antigorite, Nepoui, New Caledonia
H. Nickeliferous Antigorite, Les Deux Tonneaus, New Caledonia

(On curves C and D, peaks above 700°C are due to impurities.)[28]

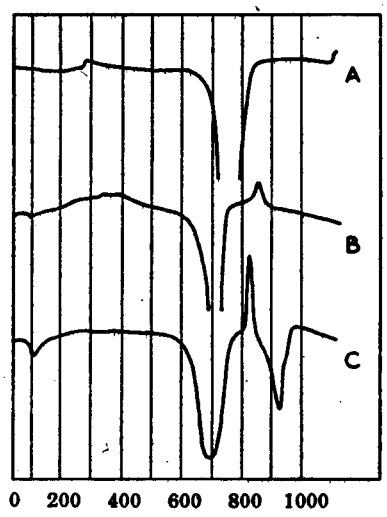

Figure 53. DTA curves for magnesian antigorites showing variable size of exothermic peak:

A. Bowenite, Khotan
B. Chrysotile, Montville, New Jersey
C. Pseudo-cubic Antigorite, Irhtem, Bou-Azza, Morocco (containing a small amount of calcite as shown by peak at 830 C)[28]

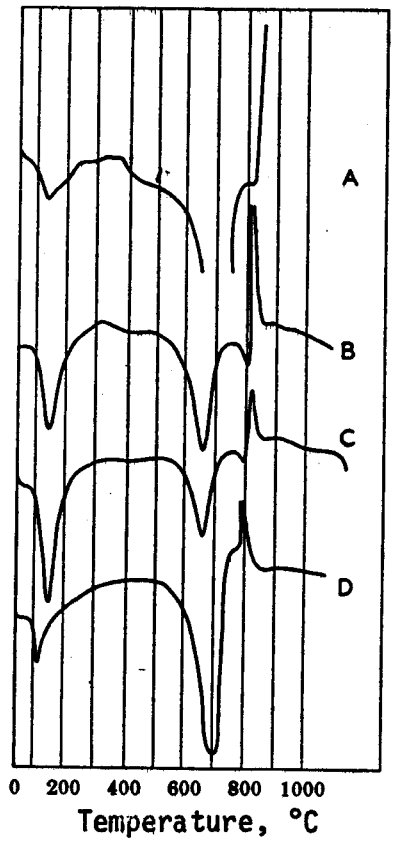

Figure 54. DTA curves for serpentines from Ambindavato, Madagascar, showing the effect of grinding and weathering:

A. Weathered rock, ground to give particles <2 μm equivalent spherical diameter
B. Fresh rock, ground to give particles <2 μm equivalent spherical diameter
C. Fresh rock, -60 mesh
D. Weathered rock, -60 mesh [28]

larger, although the position of the exotherm is not affected (see Figure 55). The position and shape, as well as the area of the endothermic peak, are affected by grinding. Martinez[29] has shown that these differences can be removed by sufficient grinding (Figure 56). The grinding seems to destroy the more stable bonds and particles with lower decomposition temperatures. The endothermic peak temperature is reduced by as much as 40°C by grinding.

The thermal analysis of serpentines is discussed in some detail by Caillere and Henin.[28] The DTA peak size and thermogravimetric (TG) weight loss are not always in good agreement because of apparent alterations in structure that accompany dehydration. The TG weight loss corresponds to only a part of the water that is known to be present, and is attributed to the loss of only hydrogen during dehydration rather than water since, in a stream of pure oxygen, a normal weight loss is obtained.

The peak temperature for dehydration is attributed to composition. Serpentines free of iron have been found to decompose between 760° and 800°C, whereas those rich in iron decompose at a lower temperature, between 600° and 650°C.[30] For a series of antigorite samples containing nickel oxide, the decomposition temperatures are as follows: 30% NiO - 450°C; 15% NiO - 570°C; 6% NiO - 650°C; 0% NiO - 800°C. Small amounts of impurities can affect the size of the endothermic peak, as well as its temperature. Thus, direct quantitative determination is difficult. The size of the peak does, however, help detect impurities in mixtures when a limited amount is present.

The exothermic peak has been related to the temperature at which forsterite is formed. Also, the size and shape have been shown to depend on the amount of Fe^{+2} or Ni^{+2} present. Some serpentines such as bowenite give no exothermic peak. In bowenite, the exotherm occurs before the end of the endothermic peak.

A more marked exotherm is found with weathered samples than with fresh serpentines. Similar exothermic peak enhancement has been observed, after grinding to less than 2 μm, by treating a lightly ground mineral in saline solution, or by alternate wetting and drying over a period of time.[28]

As a further detraction, the DTA patterns for serpentine can be confused with those of other minerals, including chalybite, chlorite, and magnesite.[28]

Amphiboles--

The DTA patterns for four common types of amphiboles--crocidolite, fibrous grunerite (amosite), anthophyllite, and tremolite-actinolite--were well documented by Vermaas.[31] His DTA curves are reproduced in Figures 57 through 61. Others have continued the study of crocidolite and amosite in more detail.[32-37] Using a technique of multiple analysis, Hodgson et al.[34-37] were able to unravel many of the processes responsible for the thermal effects observed. Their thermal analysis curves are shown in Figures 62 through 66. Anthophyllite and tremolite were examined by Wittles,[38] Figures 67 and 68. He found that magnesian anthophyllite

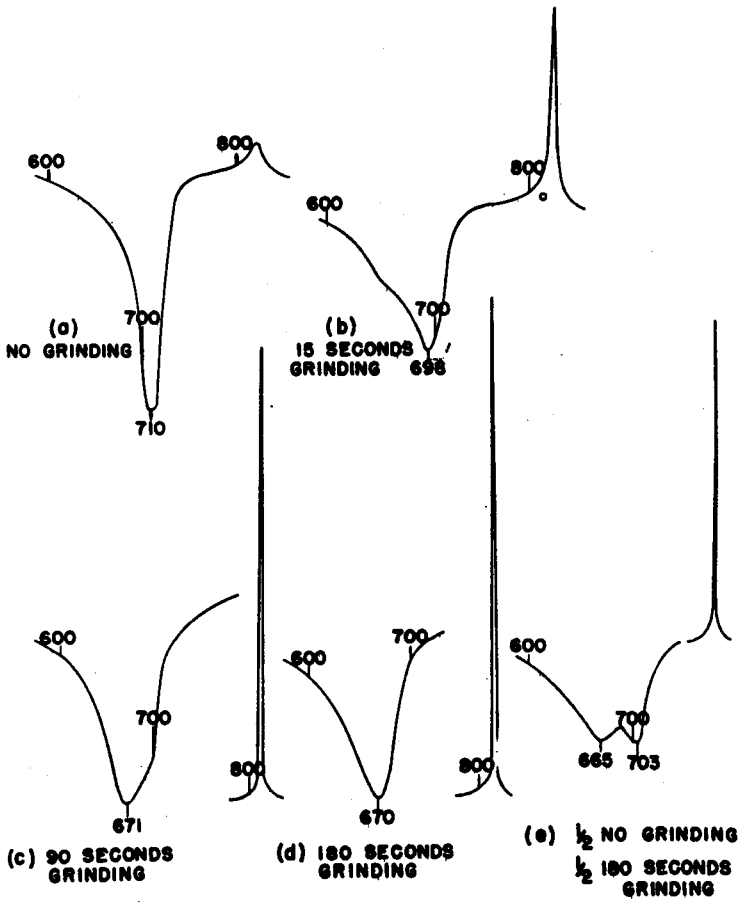

Figure 55. DTA peaks of chrysotile asbestos samples ground in Wig-L-Bug for varying lengths of time.[29]

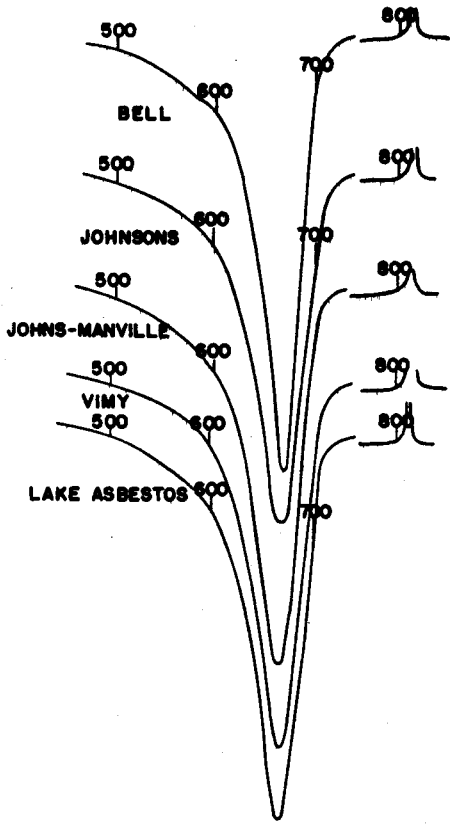

Figure 56. DTA peaks of chrysotile samples from various sources. Samples were prepared following a standard procedure of grinding for 180 sec in Wig-L-Bug.[29]

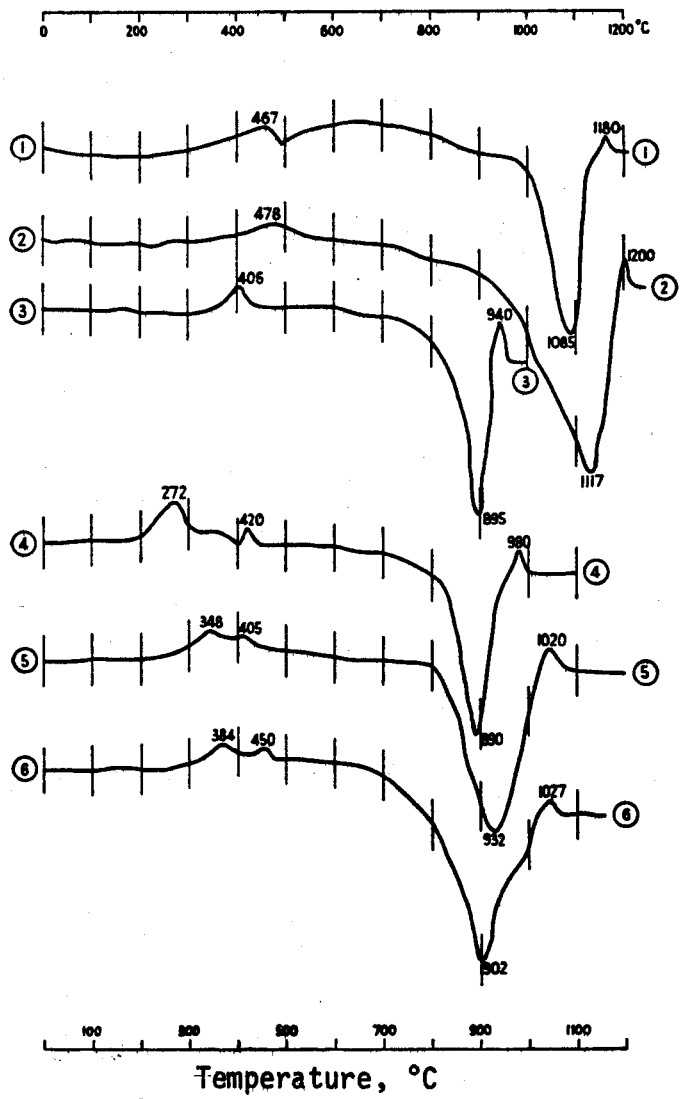

Figure 57. DTA curves of:

1. Riebeckite, Melmoth, Zululand, Natal
2. Riebeckite, "Potential Crocidolite," Stofbakkies Mine, Prieska
3. Crocidolite, Stofbakkies Mine, Prieska
4. Crocidolite, Bewaarkloof 2385, Malips, N. Transvaal
5. Crocidolite, Horngate 2575, dist. Pietersburg
6. Crocidolite, Western Australia (Transvaal Museum Sample) [31]

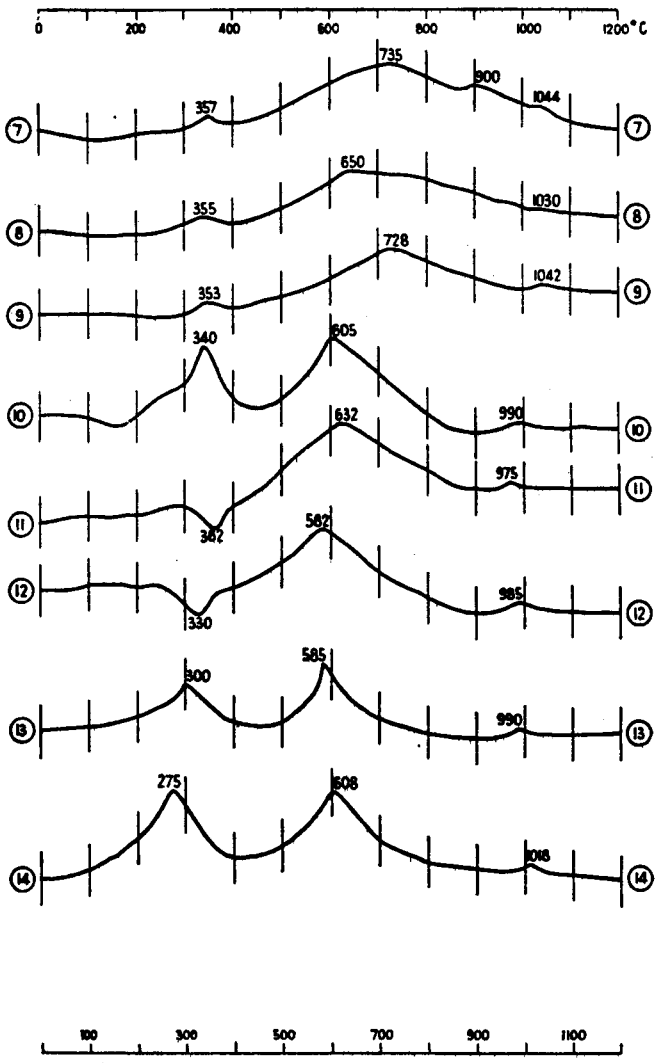

Figure 58. DTA curves of:

7. Amosite, 18 inch fibre, Penge Mine
8. Amosite, Hoogenhoog 173, dist. Pietersburg
9. Amosite, No. 5 Workings, Chuniespoort
10. Montasite, Uitkyk 122, dist. Pietersburg
11. Montasite, coated with iron oxides, Montana Mine
12. Montasite, coated with iron oxides, Montana Mine

→ Different samples

13. Montasite, Klaarstroom 67, dist. Zeerust
14. Montasite, Egnep, Ltd., Kranskloof 511, Pietersburg

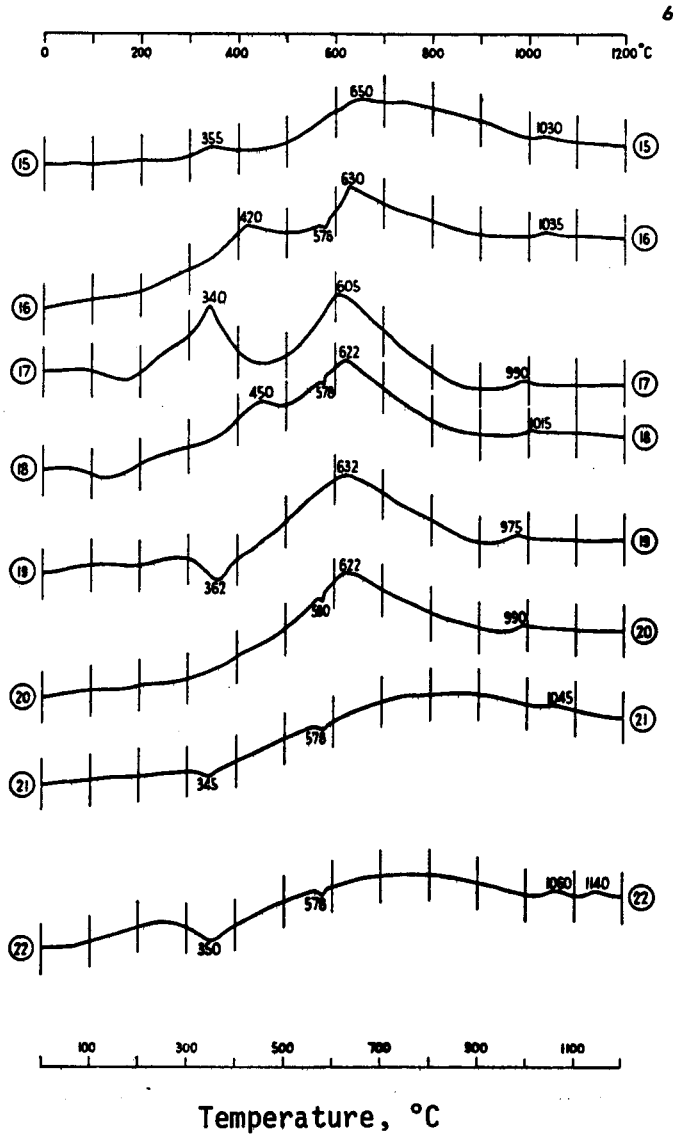

Figure 59. DTA curves of:

15. Amosite, Hoogenhoog 173, dist. Pietersburg
16. Amosite, acid treatment, Hoogenhoog 173, dist. Pietersburg
17. Montasite, Uitkyk 122, dist. Pietersburg
18. Montasite, acid treated, Uitkyk 122, dist. Pietersburg
19. Montasite, Montana Mine
20. Montasite, acid treated, Montana Mine
21. Amosite (altered) from near dolerite contact, Penge Mine
22. Amosite (altered), acid treated, from near dolerite contact, Penge Mine [31]

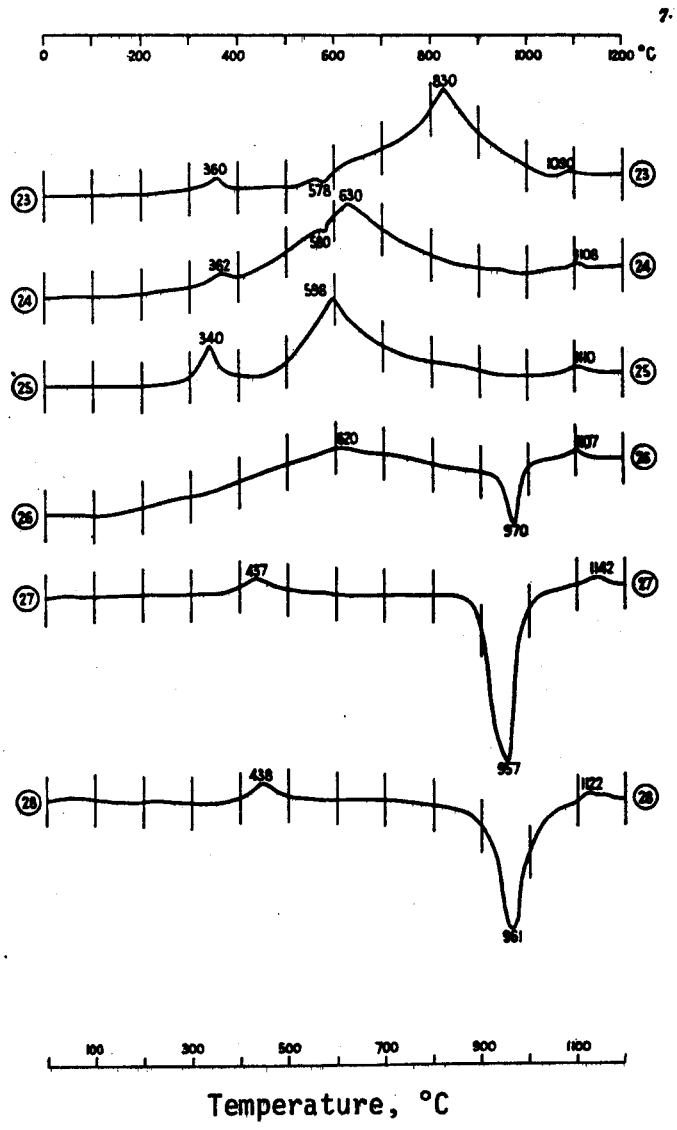

Figure 60. DTA curves of:

23. Grunerite, Penge Mine
24. Amosite, Horngate 2575, dist. Pietersburg
25. Montasite, Kranskloof 511, dist. Pietersburg
26. Blue member of Horngate 2575, doublet, dist. Pietersburg
27. Crocidolite, Horngate 2575, dist. Pietersburg
28. Crocidolite, acid treated, Horngate 2575, dist. Pietersburg [31]

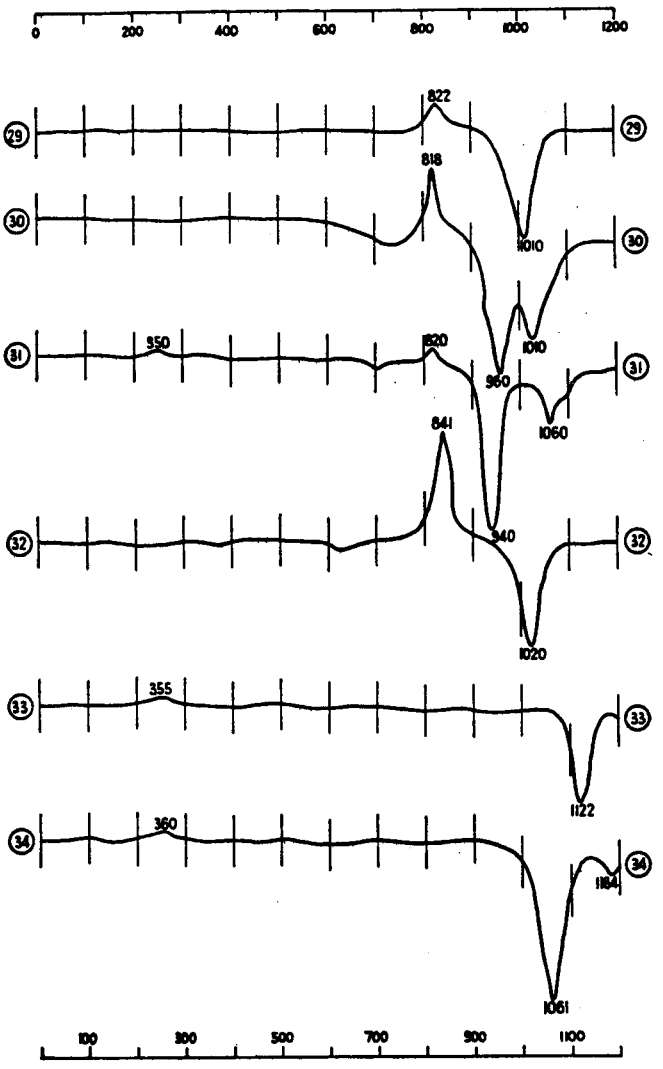

Figure 61. DTA curves of:

29. Anthophyllite, Beesthock 490, Transvaal
30. Tremolite, Ai-Ais, South West Africa
31. Tremolite, Heidelberg, Cape Province
32. Anthophyllite, Korea 663, Northern Transvaal
33. Actinolite, Waterpoort 125, Zoutpansberg
34. Actinolite, Binnenthal, Valais, Switzerland [31]

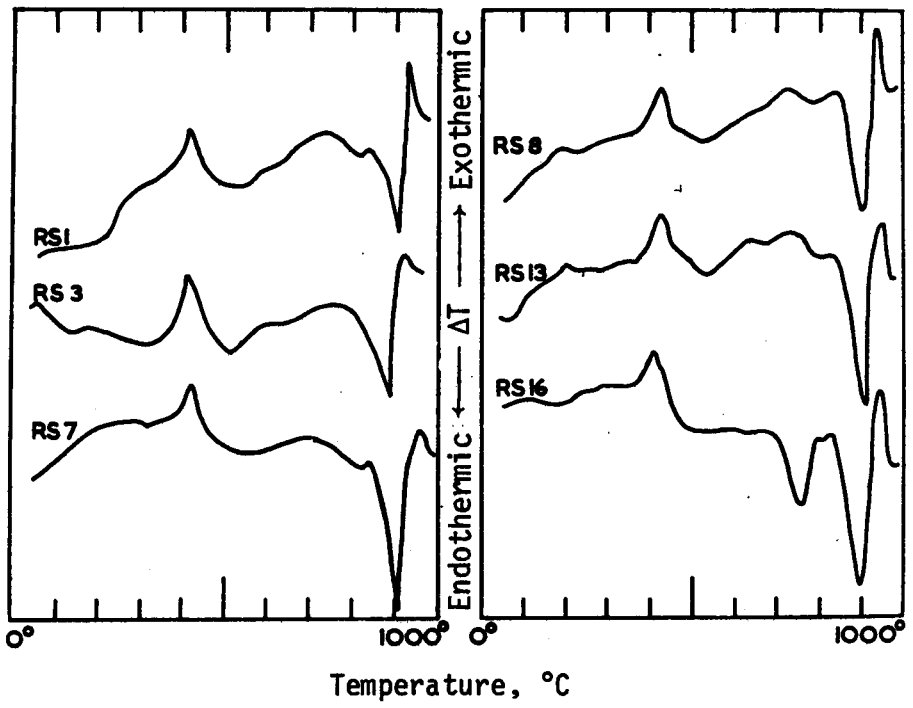

Figure 62. DTA curves for specimens of fiber from Westerberg (left) and Koegas (right), obtained in air at 10 deg/min.[37] All fresh except RSI, which is oxidized crocidolite.

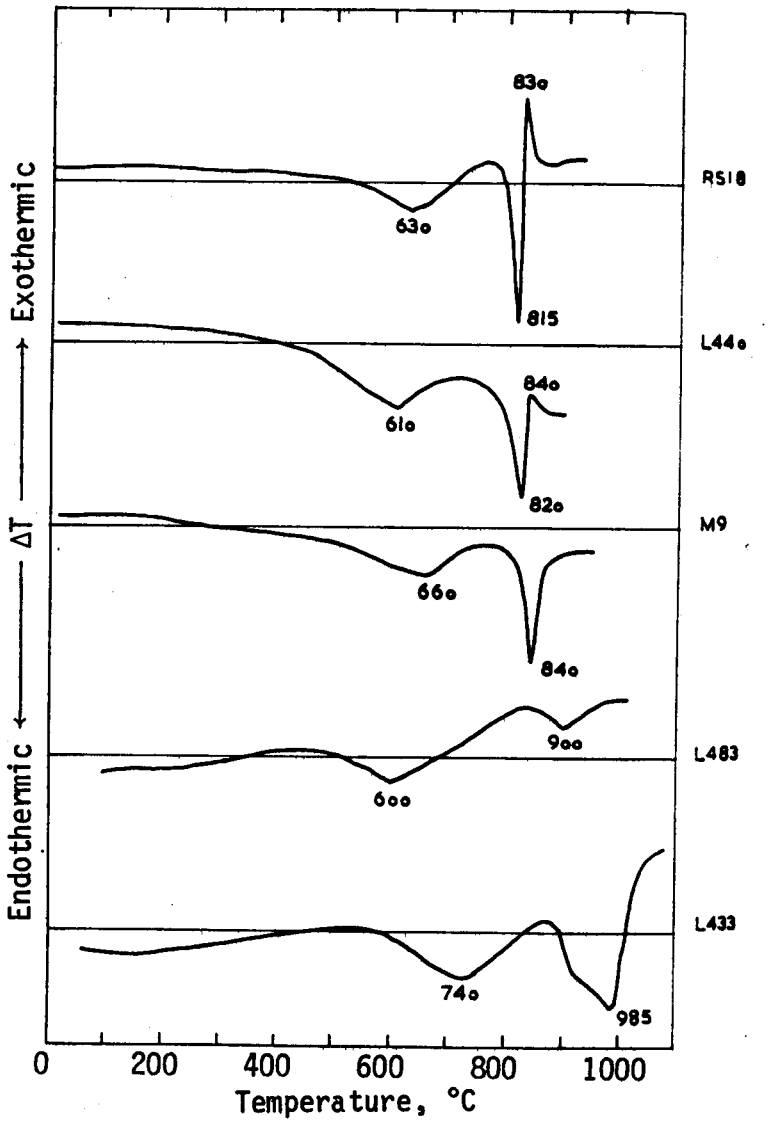

Figure 63. DTA curves of crocidolite:

RS18	Hounslow
L440	Kuruman Hills
M9	Malipsdrift
L483	Western Australia
L433	Bolivia[35]

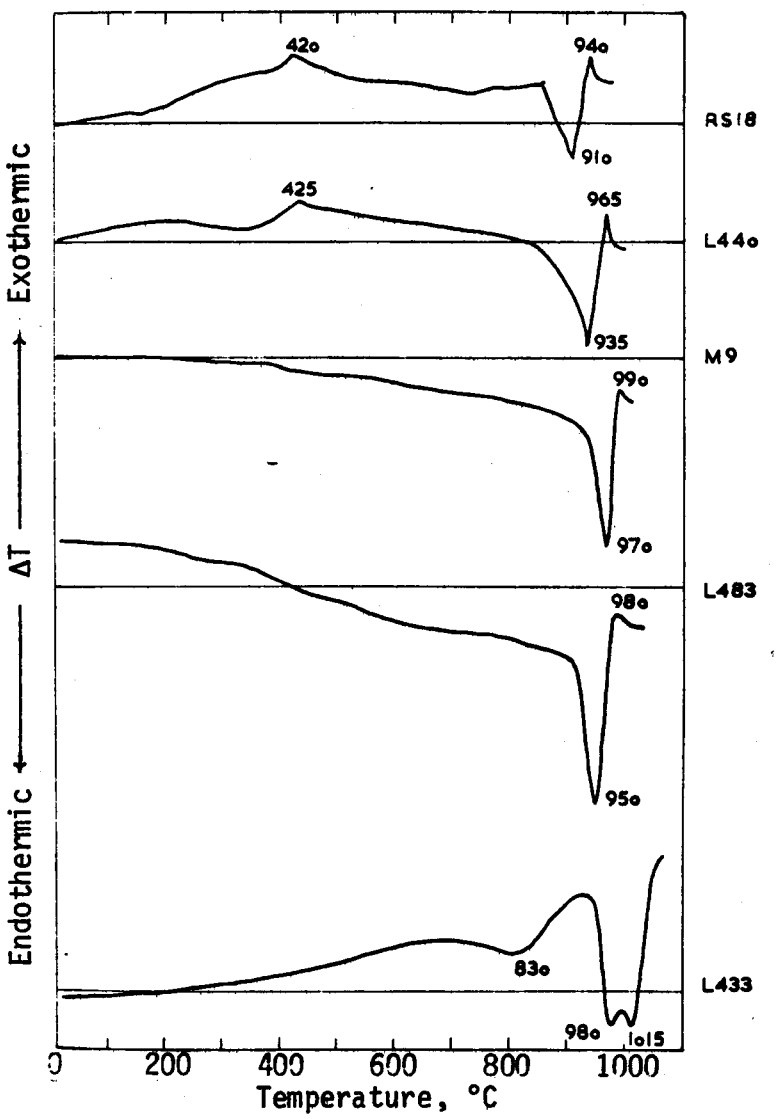

Figure 64. DTA curves of crocidolite in oxygen:

RS18	Hounslow
L440	Kurman Hills
M9	Malipsdrift
L483	Western Australia
L433	Bolivia[31]

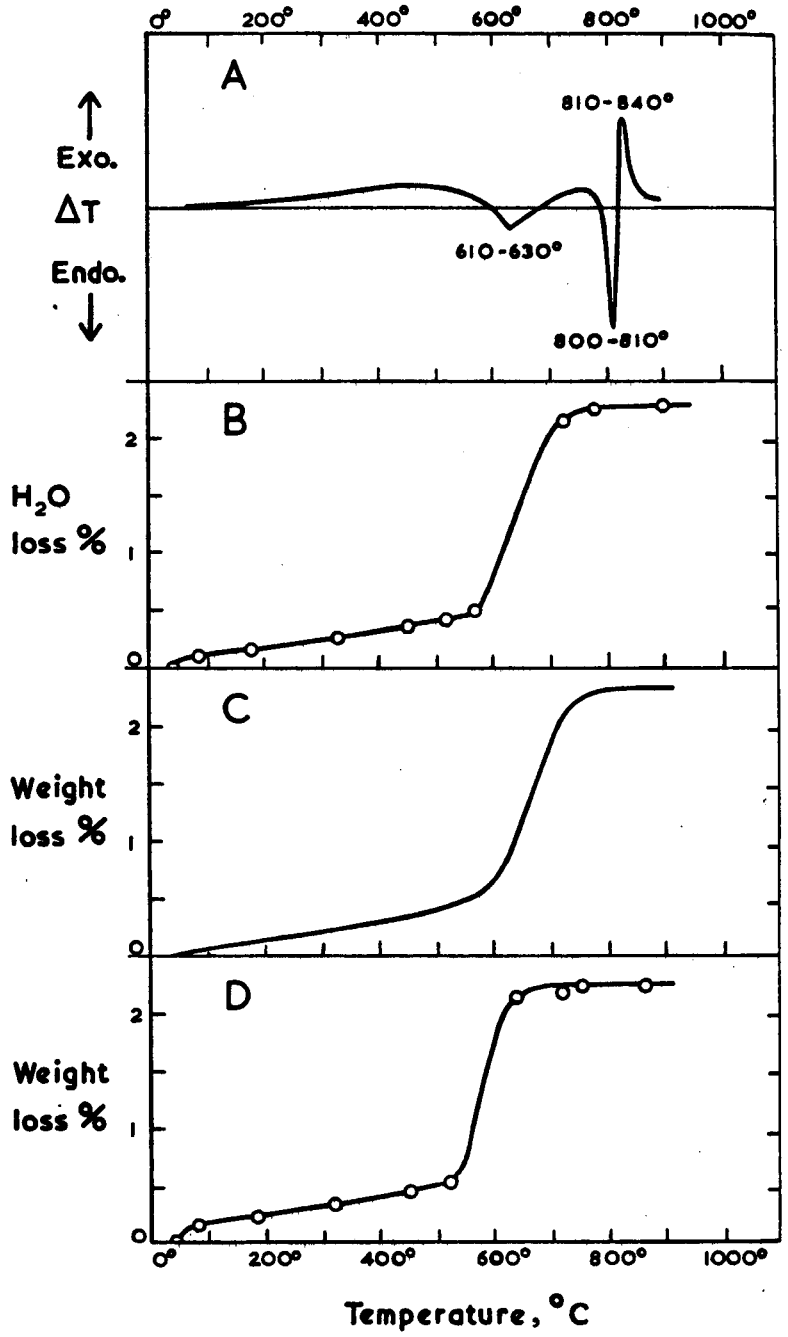

Figure 65. Thermal behavior of crocidolite in neutral atmosphere:

A. DTA curve
B. Dynamic dehydration, specimen RS7
C. TG curve specimen RS7
D. Static weight loss, specimen RS23 [34]

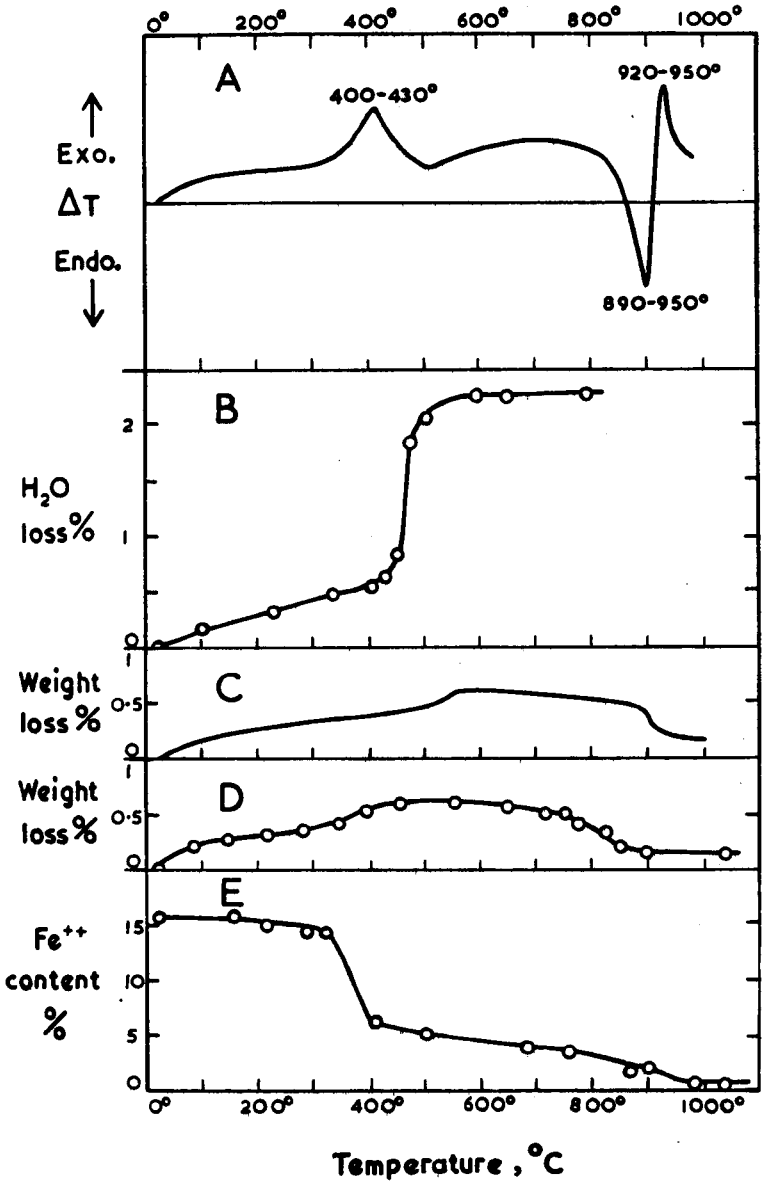

Figure 66. Thermal behavior of crocidolite in oxidizing atmospheres:

A. DTA curve
B. Dynamic dehydration, specimen RS7
C. TG curve, specimen RS7
D. Static weight loss, specimen RS7
E. Fe^{2+} contents of heated samples, specimen RS21 [34]

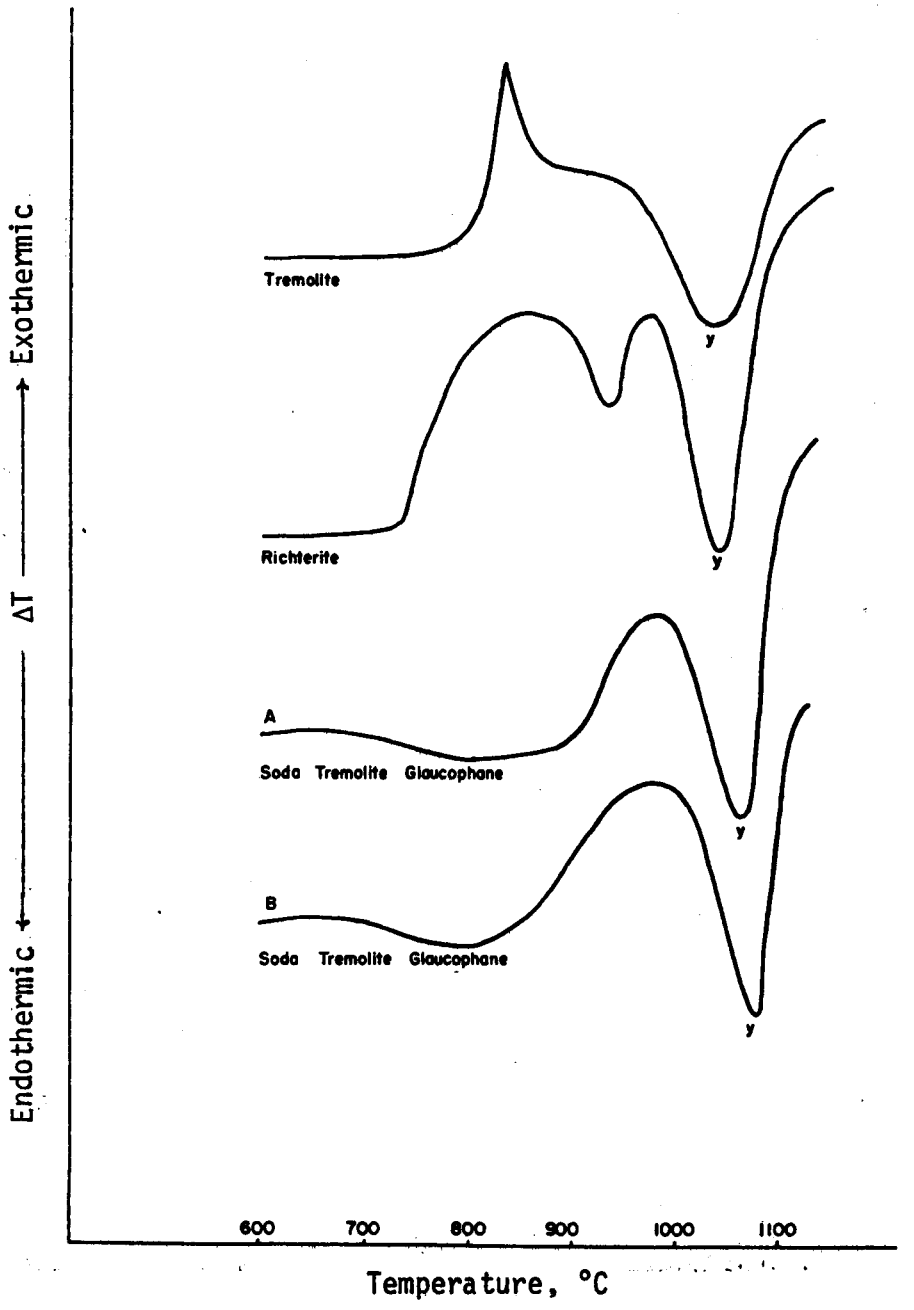

Figure 67. Thermographic curves of amphiboles.[38]

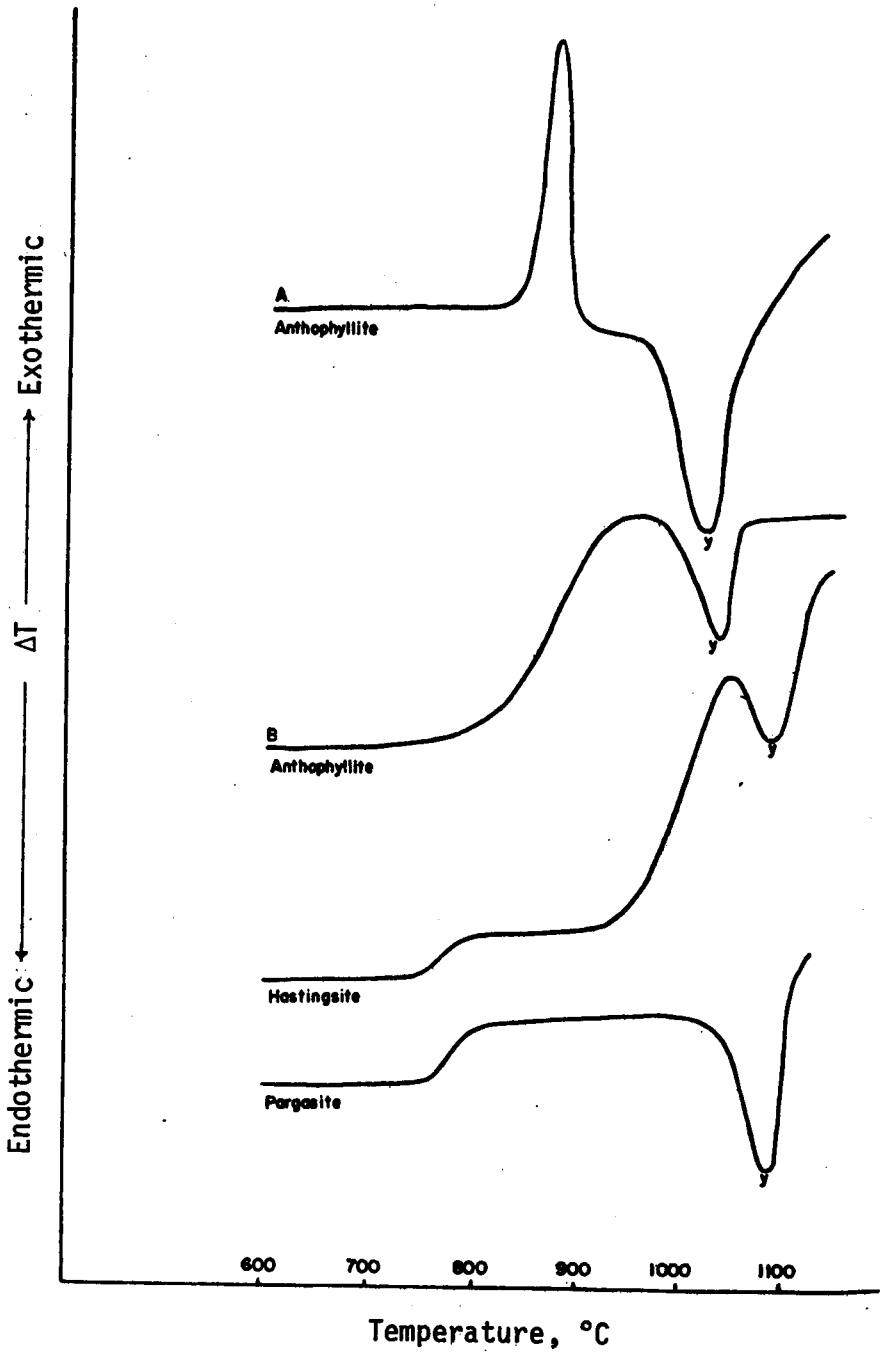

Figure 68. Thermographic curves of amphiboles.[38]

went through a reversible crystallographic contraction at 830°C, whereas tremolite, at 825°C, went through a similar contraction, but was not reversible. This could serve as a basis for distinguishing between the two.

The thermal decomposition of crocidolite is characterized by the removal of uncombined water, the decomposition of the constitutional hydroxly groups, and the concurrent oxidation of the ferrous iron.[31,32,34] (See Figures 57, and 62 through 66). Under a neutral atmosphere of argon or nitrogen, the uncombined water is lost at 50° to 400°C. An anhydride is formed by endothermic dehydroxylation at 570° to 700°C. At about 800°C, the anhydride undergoes endothermic decomposition giving acmite, cristobalite, a spinel, and liquid.[34] Melting is complete by 1050°C.

Under an oxidizing atmosphere of oxygen or air, uncombined water is lost below 400°C. At 400° to 600°C, hydrogen is given up (dehydrogenation) and an oxyamphibole is formed. The process is exothermic. At 600° to 900°C, the oxyamphibole decomposes endothermically and the ferrous iron, most of which is still present, is oxidized, giving acmite, hematite, cristobalite, and a spinel. The oxidation process is based on incorporation of oxygen into the sample (oxygenation) or on dehydrogenation. The hydrogen goes to the surface of the sample, and it reacts with oxygen to form water or, in an inert atmosphere, it evolves as molecular hydrogen.[35]

Crocidolite from weathered zones is characterized by decrease in OH groups, as well as decrease in the Fe^{+2}/Fe^{+3} ratio.[35] The DTA patterns, however, are not affected by the weathering. The DTA patterns are more affected by the concentration of magnesium in the mineral structure. The high temperature endotherm is shifted towards high temperatures as the magnesium content is increased. Magnesium blocking of the oxidation of ferrous iron is considered responsible for this shift.

Fibrous Grunerite (Amosite)--

A comparison of DTA, TG, dynamic dehydration, and x-ray diffraction studies for amosite under argon and under oxygen are shown in Figures 69 and 70.[36] The main DTA feature for amosite in an inert atmosphere include two endotherms at about 780°C and 1100°C. The endotherm at 780°C is due to dehydroxylation of the amphibole to form a pyroxene. The endotherm at 1100°C is probably associated with fusion. In oxygen or air, physically combined water is lost below 500° to 700°C. The mineral undergoes progressive oxidation in the range 300° to 1200°C in the oxidizing atmosphere in a sequence of reactions involving dehydrogenation, oxygen absorption, and dehydroxylation, which results in a broad exotherm in the range of 350° to 800°C.

The DTA curve in Figure 70 appears to be very much like those shown by Vermaas[31] (Figures 58-60). Vermaas also showed that nonfibrous grunerite (Figure 60) behaved like amosite when heated in air, but decomposition and oxidation seemed to occur at higher temperatures.

The DTA pattern for amosite in air or oxygen does not have enough distinguishing features to give reliable identification. A DTA run in an inert atmosphere would show a much more identifiable pattern.

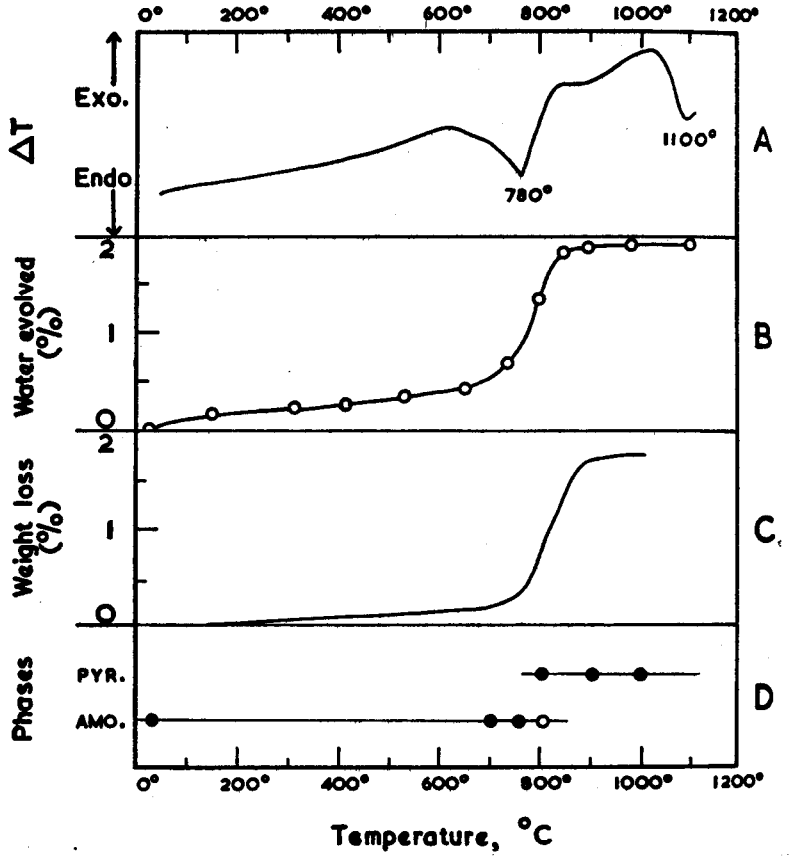

Figure 69. Dynamic heating in argon (amosite specimen PRS 5):

A. DTA curve
B. Dynamic dehydration curve
C. TG curve
D. Phases detected by x-rays, pyr = Pyroxene, amo = amosite [36]

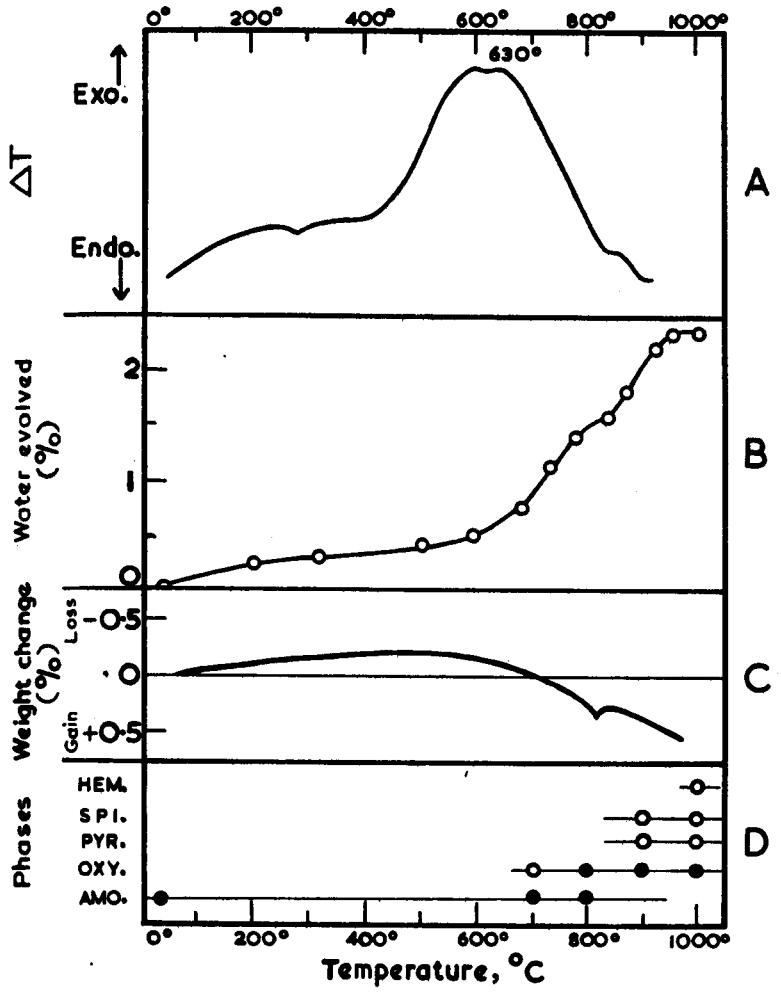

Figure 70. Dynamic heating in oxygen (amosite specimen PRS 5):

A. DTA curve
B. Dynamic dehydration curve
C. TG curve
D. Phases detected by x-rays, hem = hematite, spi = spinel, pyr = pyroxene, oxy = oxyamosite, amo = amosite [36]

Tremolite and Anthophyllite--

For tremolite and anthophyllite, an exotherm at 800° to 850°C is followed by a higher temperature exotherm at 950° to 1030°C (Figures 61, 67, and 68). The exotherm is associated with a crystal contraction which is apparently reversible for anthophyllite but not for tremolite.[38] The exotherm is believed to be due to oxidation of FeO, and thus, the size of the peak is expected to reflect, in general, the concentration of ferrous iron in the mineral. The endotherm corresponds to a dehydration and formation of pyroxene. For low-iron anthophyllites, there is a gap between the exotherm and the endotherm, which is completely washed out in the high ferroanthophyllite.

The DTA pattern for tremolite is very similar to that of anthophyllite. The second higher temperature endotherm for the tremolites shown in Figure 71 is believed due to talc impurities. In the case of actinolite, although it has a high iron concentration, the exotherm is curiously absent and only the endotherm is observed. It is not known if grinding should have a similar effect on the amphiboles as it does on the serpentines discussed earlier.

Talc--

The DTA pattern for talc is undistinguished except for a single, moderately sized endotherm that peaks at 870° to 1050°C.[28-32] The endotherm corresponds to the dehydroxylation of the mineral and results in formation of enstatite and amorphous silica. Some talc patterns are shown in Figures 51 and 71. The DTA pattern for talc is identical to that of pyrophyllite except that pyrophyllite decomposes at a temperature about 200°C lower.

Talc is found paragenically associated with carbonates (such as calcite, dolomite, and ankerite), amphiboles (especially anthophyllite, tremolite, and actinolite), serpentines, and chlorites. Of these, the DTA peaks of the carbonates and the amphiboles are likely to interfere.

Carbonate removal from talc can be done by a treatment with 3 N HCL for 4 hr, but the talc peak itself is also slightly affected by the treatment.[28]

Particle Size Effects--

That the particle size can affect the size and position of peaks in DTA of some minerals is well recognized. These effects have been documented and discussed in considerable detail by Mackenzie[28] and Smothers and Chiang.[39] Particle size effects are highly dependent on the minerals themselves. Some minerals are very sensitive to particle size effects, whereas others are not.

Thermal analysis response is affected by particle size in three ways: (1) the thermal diffusion through the sample may be changed, (2) the crystallinity of the mineral may be changed, and (3) the reaction rate may be changed for heterogeneous reactions as a result of a larger surface area accompanying decreased particle size.

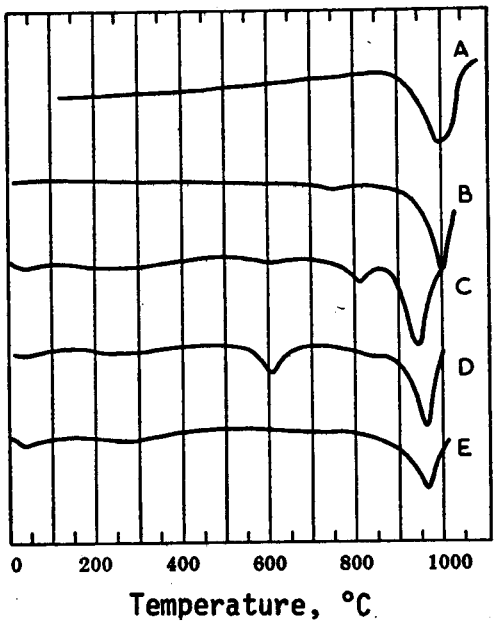

Figure 71. Differential thermal curves for talc samples from:

A. Vermont, United States
B. Tijola, Spain
C. Darnius, Spain (contaminated with dolomite)
D. Masanet, Spain (contaminated with chlorite and/or magnesite)
E. Same locality, after treatment with 3 N HCl for 4 hr [28]

Kinetic effects are not involved in solid state phase transitions, and only the first two effects are possible. As a result of thermal diffusion, a decrease in the particle size will tend to increase the thermal resistance of the packed powder in the DTA cell. The apparent furnace temperature at which a reaction takes place will shift to higher temperatures; in addition, a peak will be spread out over a larger-than-normal temperature interval. As a result of crystallinity changes, a material undergoing phase change may have a reduced peak area although neither the apparent temperature nor the size of the base will be affected.

Keith and Tuttle[40] found that the quartz α to β transition temperature can be quite variable for natural quartz because of purities; however, the particle size itself, from 0.5 mm equivalent spherical diameter (e.s.d.) to <0.02 mm e.s.d., had no effect on the inversion temperature. Nagelschmidt, Gordon, and Griffin[41] examined quartz in carefully sized powders using x-ray diffraction, before and after hydrofluoric acid treatment. They found that quartz samples less than 2 µm in diameter gave lower intensities than larger size fractions. Fractions less than 1 µm in diameter contained about 68% quartz, whereas etching to remove the amorphous surface layer brought the quartz content back up to 95%.

Dempster and Ritchie[42] used DTA to compare the particle size and quartz content of quartz powders after various periods of grinding. They confirmed the x-ray results of Nagelschmidt et al. (that crystallinity had a particle size dependence) and showed that this was related to grinding. They were able to restore the crystallinity to 100% by etching the powders with hydrofluoric acid.

For the quartz powders run on our DTA equipment, the phase transition peak clearly shows a reduced peak area after grinding without shifting the peak position or broadening the peak base. This is an indication that the crystallinity of the quartz is being changed by the grinding process.

Thermal Analysis of the Comminuted Minerals

The thermal analyses of the final mineral samples were performed at Pennsylvania State University under the direction of Dr. Leslie E. Cross. The thermal data are summarized in Table 24.

There are insufficient data in the open literature on TG curves for these minerals to make many useful comparisons. The TG curves generated are easily reproducible and are believed to be very accurate representations of these samples. Some weight gain is experienced for samples TY-27 (tridymite), CR-37 (crocidolite), GF-38 (fibrous grunerite), R-60 (riebeckite), and G-68 (grunerite). The cause of the weight gain is unknown. In the case of the amphibole samples, the weight gain may be associated with oxidation of iron in the mineral structure.

Table 24. Thermal characterization of comminuted samples.

Mineral	Sample Designation	Thermal Effect	Weight Loss (Gain) Wt.%
Quartz	Q-1	(DTA) endotherm at 570°; peak ~¼ of NBS standard material.	
		(TG) flat trace, 0-1200°	<0.2
Beryl	B-11	(TG) 0-450°	0.51
		850-1030°	1.21
		1120-1200°	0.37
		0-1200°	2.19
		(DTA) no detectable peaks	
Fluorite	F-17	(TG) 0-400°	2.23
		400-530°	0.30
		590-670°	1.14
		0-1200°	3.87
		(DTA) no moderate or large peaks.	
Cristobalite	CB-25	(TG) 0-500°	0.28
		0-1200°	0.44
		(DTA) small transition peak at 260°; no quartz evident at 570°.	
Tridymite	TY-27	(TG) 0-1200°	0.44
		(DTA) 110° and 160° transitions hardly discernable; no cristobalite evident at 260° or quartz at 570°.	
Chrysotile	CH-29	(TG) 0-130°, loss of surface water	1.8
		330-430°	0.5
		540-580°	2.4
		628-674°	8.9

Table 24. (continued)

Mineral	Sample Designation	Thermal Effect	Weight Loss (Gain) Wt.%
Chrysotile (contd.)	CH-29	674-820°	0.8
		0-1200°	15.36
		(DTA) 600-700°, large dehydration endotherm peak at 665°.	
		820°, very large, sharp exotherm oxidation of iron.	
Antigorite	AG-55	(TG) 0-600°	2.5
		600-690°	12.1
		690-870°	1.0
		0-1200°	15.6
		(DTA) 570-700°, very large endotherm followed by sharp, large exotherm.	
		815°, peak temperature same as initial sample before grinding.	
Riebeckite	R-60	(TG) 0-255°	0.50
		500-830°	0.65
		870-915°	0.72
		0-1200°	0.10
		(DTA) 810°, small peak.	
		950°, small peak.	
		Both peaks very much reduced from that of initial sample.	
Grunerite	G-68	(TG) 0-280°	0.42
		500-940°	4.4
		0-1200°	2.04
		(DTA) no noticeable peaks.	

Table 24. (continued)

Mineral	Sample Designation	Thermal Effect	Weight Loss (Gain) Wt.%
Cummingtonite	C-71	(TG) 0-1200°, gradual weight losses; losses and gains give wavy pattern.	0.67
		(DTA) 440-500°, small exotherm.	
Tremolite	T-77	(TG) 0-390°	0.70
		1035-1090°	1.92
		0-12000°	2.63
Talc	TA-99	(TG) 0-860°	0.90
		860-935°	4.45
		0-1200°	5.92
		(DTA) 900°, small endotherm.	
Anthophyllite	A-102	(TG) 0-260°	0.50
		870-1030°	0.72
		1030-1105°	1.04
		0-1200°	2.66
		(DTA) no noticeable peaks.	
Nickel Oxide	N-108	(TG) 0-280°	0.35
		0-1200°	0.29
		(DTA) no noticeably formed peaks.	
Crocidolite	CR-37	(TG) 0-500°, loss of surface water.	1.3
		>500°, continuous weight gain.	0.3
		0-1200°	0.99
		(DTA) 880-940°, small endotherm, much reduced in size from before size reduction.	

Table 24. (continued)

Mineral	Sample Designation	Thermal Effect	Weight Loss (Gain) Wt.%
Amosite	GF-38	(TG) 0-400°, steady weight loss.	0.8
		500-900°, weight regained.	1.6
		0-1200°, net weight gain very similar in pattern to that of R-60, riebeckite.	
		(DTA) no detectable peaks in curve.	
Fibrous Anthophyllite	AF-45	(TG) 0-120°	0.65
		380-470°	0.35
		560-640°	0.27
		855-915°	0.15
		990-1070°	0.90
		0-1200°	3.03
		610°, very small endotherm barely evident.	
		(DTA) 800°, small exotherm.	
		1000°, small endotherm.	
		All peaks are reduced compared with initial material peaks before grinding.	
Fibrous Tremolite	TF-48	(TG) 0-210°	0.45
		210-435°	0.35
		630-700°	0.74
		1015-1070°	1.70
		0-1200°	3.46
		(DTA) 1010°, moderate endotherm, reduced compared with initial material peak.	

Thermal analysis provides information to explain structural changes within a given mineral sample, but it is not as useful when unambiguous data with which to identify or quantify the presence of impurities is required.

The thermal analysis patterns of fibrous serpentines are not distinguishable from other serpentines, nor are the thermal analysis patterns of fibrous amphiboles distinguishable from those of nonfibrous amphiboles. Thus, thermal analysis cannot be used to distinguish clearly between the two types without other supporting information.

INFRARED SPECTRA OF SAMPLES

Infrared (IR) spectra were run for the 7 minerals comprising groups 1 and 4 as an additional search technique for the presence of impurities. The IR spectra were recorded on a Perkin Elmer 621 Spectrophotometer over the wavelength region of 2.5 to 50 μm. Frequency accuracy is good to ±1 cm^{-1}. All the mineral samples were pelletized for their spectral determination. Cesium iodide (CsI, Harshaw Chemical Company) was used as the salt-matrix. This material had no absorption bonds in the wavelength region examined. In all cases, about 0.2 g of CsI was mixed with ≈0.001 g of the mineral, the two ground together (agate mortar and pestle) and then pelletized (20,000 psi) with the use of standard techniques. During the spectral determinations, the spectrophotometer was flushed with dry nitrogen (the boil-off from LN_2) to minimize water vapor absorption with concomitant energy diminution and poor instrument response.

A typical IR spectrum is presented in Figure 72. In Tables 25 and 26 are listed the frequencies of the more well-defined bands of all samples analyzed. In cases where confusion could exist, artifacts due to the operation of the spectrometer (grating and filter changes) have been indicated. In general, the derived spectra agree with those reported in the literature,[43] but there are some small differences. The significance of these differences is somewhat questionable. The frequencies reported in the literature appear to be consensus values based on many determinations on different samples of unreported purity, with spectrometers of varying resolving power. For these reasons, we do not believe that the small differences between our spectra and those reported in the literature are significant. In this respect, it is perhaps worth noting that the IR spectra of a commercially processed quartz (Q-107, Min-U-Sil-10) run in this laboratory was identical to that of the natural α-quartz specimen Q-1.

Within the precision with which the spectra of these compounds are known, it is difficult to make any determination of purity based on the IR spectra, with perhaps the exception of F-17 and TY-27. The spectrum of F-17 shows some weak absorptions at 1490 and 1400 cm^{-1} that could possibly be assigned to calcium carbonate, but, in all probability, equally well to many other compounds. In the TY-27 sample, three weak absorptions occur at ≈690, 390, and 365 cm^{-1}, which could be due to a quartz. Without performing careful quantitative studies, however, this possibility cannot be confirmed.

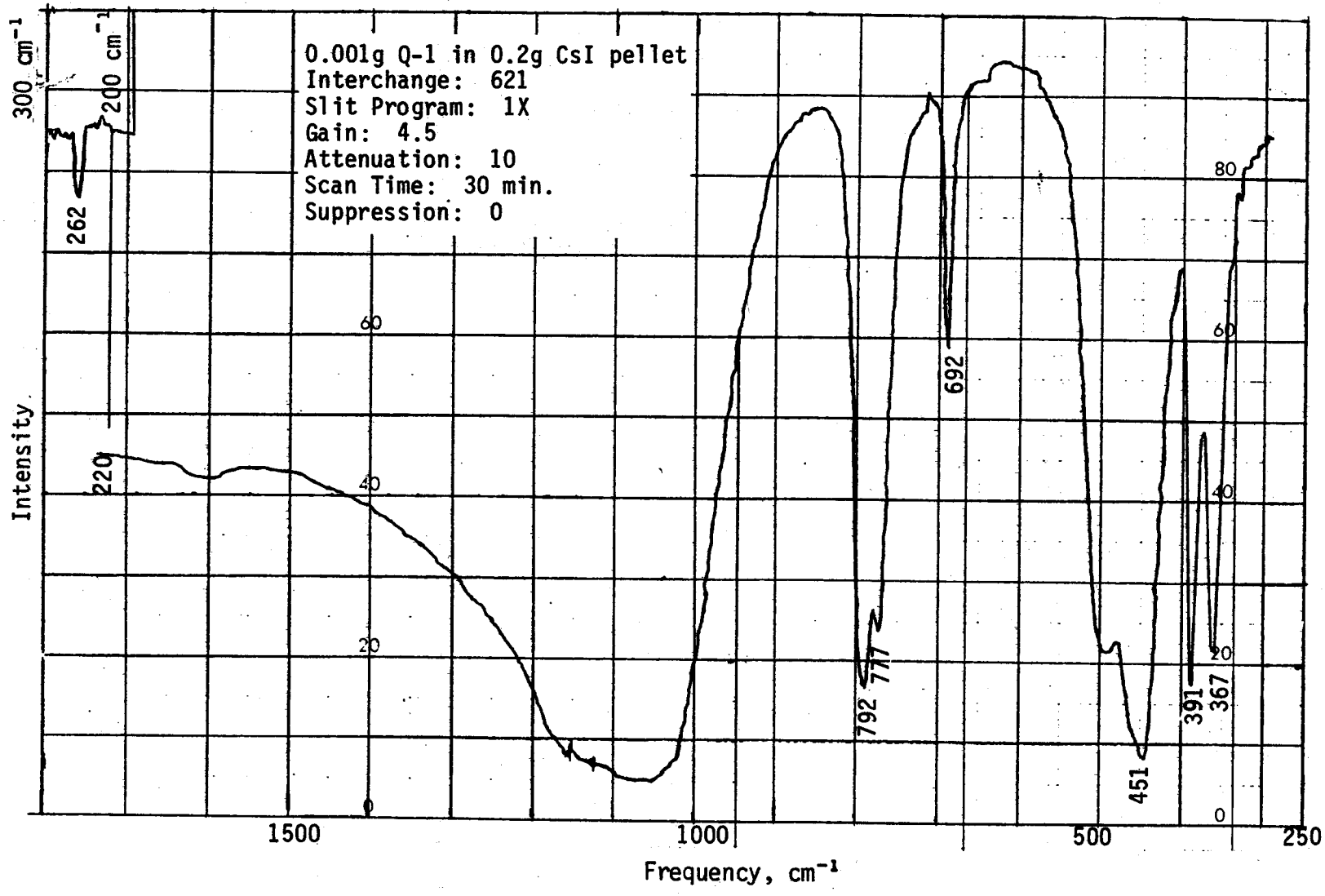

Figure 72. Typical infrared spectrum ((Q-1, quartz).

Table 25. Infrared spectral frequencies (cm^{-1}) for the SiO_2-type minerals.

Quartz (Q-1)	Tridymite (TY-27)	Cristobalite (CB-25)
1075 bm*	1090 bm	1080 bm
792 vs	787 s	791 s
777 vs	556 w	612 s
692 m	525 m	471 vs
497 vs	494 vs	380 m
451 vs	390 w†	294 m
391 vs		
367 vs		
262 w		

* bm indicates a strong, broad band with an ill-defined maximum.

† Could be due to a quartz

Table 26. Infrared spectral frequencies for talc, beryl, fluorite, and nickel oxide

Talc (TA-99)	Beryl (B-11)	Fluorite (F-17)	Nickel oxide (N-108)
3685 m	3600 w	1490 w	420 bm
1010 vs	1628 w	1400 w	
680 m.sh.	1170 bm	1250 w	
664 vs	1020 bm	863 w	
525 vs	940 bm	790 w	
450 bm*	810 s	590-200†	
416 vs	735 s		
385 vs	669 s		
380 vs.sh.	583 s		
340 w.	508 vs		
	481 vs		
	426 vs		
	355 m		

* bm indicates a strong, broad band with an ill-defined maximum.

† Absorption onset at 590 extending to short wavelength range of instrument.

REFERENCES

1. Gravatt, C. C., P. D. La Fleur, and K. F. J. Heinrich, eds. 1978. Proceedings of a Workshop on Asbestos: Definitions and Measurement Methods. National Bureau of Standards Special Publication 506.

2. Haartz, J. C., B. A. Lange, R. G. Draftz, and R. F. Scholl. Selection and Characterization of Fibrous and Nonfibrous Amphiboles for Analytical Methods Development. In: NBS-SP-506. pp. 295-312.

3. Bates, R. A. 1960. Geology of the Industrial Rocks & Minerals. Harper & Brothers, New York.

4. Deer, W. A., R. A. Howie, and J. Zussman. 1966. An Introduction to the Rock-Forming Minerals. Wiley & Sons, Inc., New York.

5. Deer, W. A., R. A. Howie, and J. Zussman. 1963. Rock-Forming Minerals--Vol. 4 Framework Silicates. Wiley & Sons, Inc., New York.

6. Deer, W. A., R. A. Howie, and J. Zussman. 1963. Rock-Forming Minerals--Vol. 3 Sheet Silicates. Wiley & Sons, Inc., New York.

7. Deer, W. A., R. A. Howie, and J. Zussman. 1963. Rock-Forming Minerals--Vol. 2 Framework Silicates. Wiley & Sons, Inc., New York.

8. Lamey, C. A. 1966. Metallic & Industrial Mineral Deposits. McGraw-Hill, New York.

9. Lefond, S. J., ed. 1975. Industrial Minerals & Rocks. American Institute of Mining, Metallurgical & Petroleum Engineers, Inc., New York.

10. Minerals Yearbook 1973, Vol. I Metals, Minerals & Fuels. 1975. U.S. Department of Interior, Bureau of Mines, U.S. Government Printing Office, Washington, D.C.

11. Minerals Yearbook 1972, Vol. II Area Reports: Domestic. 1975. U.S. Department of Interior, Bureau of Mines, U.S. Government Printing Office, Washington, D.C.

12. Minerals Yearbook 1972, Vol. III Area Reports: International. 1975. U.S. Department of Interior, Bureau of Mines, U.S. Government Printing Office, Washington, D.C.

13. Minerals Yearbook 1973, Vol. II Area Reports: Domestic. 1976. U.S. Department of Interior, Bureau of Mines, U.S. Government Printing Office, Washington, D.C.

14. Minerals Yearbook 1973, Vol. III Area Reports: International. 1976. U.S. Department of Interior, Bureau of Mines, U.S. Government Printing Office, Washington, D.C.

15. E/MJ International Directory of Mining & Mineral Processing Operations--1975. 1975. Engineering & Mining Journal Mining Informational Services, McGraw-Hill, New York.

16. 1973 Reference Manual and Buyers Guide. 1973. Canadian Mining Journal, National Business Publications, Ltd., Quebec.

17. Mining International Yearbook. 1975. Walter R. Skinner, Financial Times, Ltd., London.

18. Mining Annual Review--1975. 1975. Mining Journal, London.

19. Bates, R. L. 1960. Geology of the Industrial Rocks and Minerals. Harper Brothers, New York.

20. Ramdahr, P. 1969. The Ore Minerals and Their Intergrowths. Pergamon Press, Oxford, England.

21. Powder Diffraction File. Joint Committee on Powder Diffraction Standards, 1601 Park Lane, Swarthmore, Pennsylvania 19081.

22. Standard X-ray Diffraction Powder Patterns. 1953. NBS Circular 539, Vol. 1 pp. 69-70.

23. Silverman, L., C. E. Billings, and M. W. First. 1971. Particle Size Analysis in Industrial Hygiene. Academic Press, New York.

24. The MICROTRAC Particle Analyzer. Leeds and Northrup Co. North Wales, Pennsylvania.

25. Wertheimer, A. L. and W. L. Wilcock. 1976. Light Scattering Measurements of Particle Distributions. Applied Optics. 15:1616-1620.

26. Fang, J. H. and F. Donald Bloss. 1966. X-Ray Diffraction Tables. Southern Illinois University Press. Carbondale and Edwardsville, Illinois.

27. Kauffman, A. J., Jr., and E. Don Dilling. 1950. Differential Thermal Curves of Certain Hydrous and Anhydrous Minerals with a Description of the Apparatus Used. Economic Geology. 45:222-244.

28. Mackenzie, R. C. 1957. The Differential Thermal Investigations of Clays. Mineralogical Society. London.

29. Martinez, E. 1961. The Effect of Particle Size on the Thermal Properties of Serpentine Minerals. The American Mineralogist. 46:901-912.

30. Symkatz-Kloss, W. 1974. Differential Thermal Analysis: Application and Results in Mineralogy. Springer-Verlag. New York.

31. Vermaas, F. H. S. 1952. The Amphibole Asbestos of South Africa. Transactions and Proceedings of the Geological Society of South Africa. 55:199-229.

32. Rouxhet, P. G., J. L. Gillard, and J. J. Fripiat. 1972. Thermal Decomposition of Amosite, Crocidolite and Biotite. Mineralogical Magazine. 38:583-592.

33. Addison, W. C., and A. D. White. 1968. The Oxidation of Bolivian Crocidolite. Mineralogical Magazine. 36:791-796.

34. Hodgson, A. A., A. G. Freeman, and H. F. W. Taylor. 1965. The Thermal Decomposition of Crocidolite from Koegas, South Africa. Mineralogical Magazine. 35:5-30.

35. Hodgson, A. A. 1965. The Thermal Decomposition of Miscellaneous Crocidolites. Mineralogical Magazine. 35:291-305.

36. Hodgson, A. A., A. G. Freeman, and H. F. W. Taylor. 1965. The Thermal Decomposition of Amosite. Mineralogical Magazine. 35:445-463.

37. Cilliers, J. J. LeR., A. G. Freeman, A. Hodgson, and H. F. W. Taylor. 1961. Crocidolite from the Koegas-Westerberg Area, South Africa. Economic Geology. 56:1421-1437.

38. Wittels, M. 1951. The structural disintegration of Some Amphiboles American Mineralogist. 37:28-36.

39. Smothers, W. J., and Y. Chiang. 1958. Differential Thermal Analysis: Theory and Practice. Chemical Publishing Co., Inc. New York.

40. Keith, M. L., and O. F. Tuttle. 1952. Significance of Variation in the High-Low Inversion of Quartz. American Journal of Science. Bowen Volume. Part 1. 203-280.

41. Nagelschmidt, G., R. L. Gordon, and O. G. Griffen. 1952. Nature. Surface of Finely Ground Silica. 169:539-540

42. Dempster, P. B., and P. D. Ritchie. 1952. Surface of Finely Ground Silica. Nature. 169:538-539.

43. Gadsen, J. A. 1975. Infrared Spectra of Minerals and Related Inorganic Compounds. Butterworth. London.

APPENDIX 1

MINERAL SOURCES CONTACTED WHICH DID NOT SUPPLY SAMPLES

Quartz

Western Electric Merrimac Valley Works
Mr. Joseph M. Lyons
1600 Osgood Street
North Ardover, Massachusetts 91845

Beryl

Beryl Ores
Arvada, Colorado

Gariep Minerals
P.O. Box 176
Springbok, Cape Province
Republic of South Aftica

Great Salt Lake Mineral & Chemical Co.
765 North 10500, W.
Ogden, Utah 84402

L. W. Judson
c/o Post Office
Hermosa, South Dakota 57744

Kawecki Berylco Industries, Inc.
Tuckertown Rd.
Reading, Pennsylvania 19603

Northwest Beryllium Corp.
218-219 American National Bank Bldg.
Rapid City, South Dakota 57701

Peerles Mine
Keystone, South Dakota 57751

Rio Tinto (Rhodesia) Ltd.
61 Jameson Ave., Central
Salisbury Cl. Rhodesia

U.S. Beryllium Corp
306 Bon Durant Bldg.
Pueblo, Colorado 81003

Fluorspar

Cerro-Spar Corp.
Babb-Barnes Mine & Mill
P.O. Box 235
Salem, Kentucky 42078

Cia Minera Rio Colorado
San Luis Potsi, Mexico

J. Irving Crowell, Jr.
P.O. Box 96
Beatty, Nevada 89003

D&F Minerals Co. (Mr. F. Dougherty)
900 12th Street
Canyon, Texas 79015

Fluorita de Rio Verde, SA
San Luis Potosi, Mexico

General Mining & Finance Corp.
General Mining Bldg.
6 Hollard St.
Johannesburg, South Africa

Harshaw Chemical Co.
6801 Cochran Road
Solon, Ohio

Minera Frisco SA
San Francisco Del Oro
Chiahuahua, Mexico

Minera Las Cuevas SA
San Luis Potosi, Mexico

Minerva Mining Division
P.O. Box 531
Eldorado, Illinois 62930

Fluorspar (continued)

Newfoundland Fluorspar Div.
Aluminum Co. of Canada Ltd.
St. Lawrence, Newfoundland
Canada

Reynolds Fluorspar SA
Coahuila, Mexico

U.S. Energy Corp.
Fluorine Queen Mine
625 East Madison, Suite 1
Riverton, Wyoming 82501

Willden Fluorspar Co.
P.O. Box 536
Delta, Utah 84624

Asbestos (and Talc)

Advocate Mines Ltd.
1104 Royal Trust Tower
Toronto Dominion Centre
Toronto, Ontario, Canada

Amosa (Pty) ltd.
c/o Cape Industries Ltd.
Burlington House, 22 Rissick St.
Johannesburg, South Africa

Director
Artex-Hungarian Trading Co.
P.O. Box Budapest 62 N. 167
Budapset, Hungary

Asbestos Corp. Ltd.
Thetford Mines
Quebec, Canada

Atlas Asbestos Co.
P.O. Box 805
Coalingua, California 93210

Bell Asbestos Mines Ltd.
P.O. Box 99
Thetford Mines
Quebec, Canada

W. H. Harper
The Boots Company, Ltd.
Nottingham NG 23AA
England

Director
Calgoorlie School of Mines
Calgoorlie, Wester Australia

State of California Dept. of
conservation
Division of Mines and Geology
Division Headquarters
Resources Building, Rm. 1341
1461 Ninth Street
Sacramento, California 95814

Dr. H. R. Steacy
Geological Survey of Canada
Dept. of Energy, Mines, and Resources
601 Booth Street
Ottawa, Ontario, Canada K1A OE8

Canadian Johns-Manville
P.O. Box 1500
Asbestos, Quebec, Ontario
Canada

Cape Asbestos SA Pty. Ltd.
P.O. Box 8544
Johannesburg, South Africa

Cape Blue Mines (Pty) Ltd.
c/o Cape Industries Ltd.
Burlington House, 22 Rissick St.
Johannesburg, South Africa

Charter Consolidated Ltd.
26th Floor, 500 Collins St.
Melblourne, Victoria, Australia 30

Charter Consolidated Ltd.
P.O. Box 28
Toronto Dominion Centre
Toronto, Ontario, Canada M5K 1B8

Asbestos (and Talc) (continued)

Charter Consolidated Ltd.
70 Jameson Ave. Central
Salisbury C-4, Rhodesia

Charter Consolidated Ltd.
44 Main Street
Johannesburg, South Africa

Chrysotile Corp. of Australia
Pty. Ltd.
Royal Exchange Bldg.
56 Pitt Street
Sydney, New South Wales,
Australia 2000

Cleveland Cliffs Iron Co.
Ishpemming, Michigan

Prof. E. Vigliani
Clinica del Lavoro "Luigi Devoto"
20122 Milano
Via S. Barnabas 8
Italy

Coalingua Asbestos Co.
P.O. Box 1045
Coalingua, California 93210

Coegas Asbestos Mine
Cape Blue Mines Pty. Ltd.
Coegas Brug
Cape province, South Africa

Egnep (Pty) Ltd.
c/o Cape Industries Ltd.
Burlington House, 22 Rissick St.
Johannesburg, South Africa

Fibre Research Laboratory
Iver Lane, Cowley Uxbridge
Middlesex UB8 2JQ
England

GAF Corp.
Industrial & Floor Products Div.
140 West 51st Street
New York, New York 10020

General Mining & Finance Corp.
General Mining Bldg.
6 Hollard St.
Johannesburg, South Africa

Messrs. Hancock and Wright
193 Stirling Hwy.
Clarement, Western Australia 6010

Harris Mining Co.
Newland Highway
Spruce Pine, North Carolina 28777

Proprietor
Hawthorneden
El Dorado, Ontario, Canada

Homestead Mining
Lead, South Dakota

Johns-Manville Corp.
5680 South Syracuse Circle
Denver, Colorado 80217

Kuruman Cape Blue Asbestos
P.O. Box 10505
Johannesburg, South Africa

Robert C. Reed
Michigan Dept. of Natural Resources
Steven T. Mason Building
Lansing, Michigan 48926

Mineral Information Service
Division of Mines
Ferry Building
San Francisco, California 91411

Dr. Gilson
MRC Pneumoconiosis Unit
Llandough Hospital
Penarth, Glam. CF6 1XW
Cardiff, South Wales

Director
National Institute for Metallurgy
1 Yale Road
Milner Park
Johannesburg, South Africa 2001

Asbestos (and Talc) (continued)

New York State Geological Survey
Albany, New York

E. B. Freeman
Ontario Bureau of Mines
W-2411 Whitney Block
Parliament Buildings
Toronto, Ontario, Canada M71 1W3

Dr. R. I. Gait
Royal Ontario Museum
100 Queens Park
Toronto, Ontario, Canada M5S 2C6
416/978-2011

Pacific Asbestos Corp.
P.O. Box 127
Copperoppolis, California 95228

R.F.D. Parkinson & Company, Ltd.
Doulting, Shepton Market
Somerset BA4 4RF
England

Powhatan Mining Co.
6721 Windsor Mill Road
Baltimore, Maryland 21207

Chamber of Mines Rhodesia Inc.
Chamber of Mines Bldg.
Gordon Ave., P.O. Box 712
Salisbury, Rhodesia

Rhodesian & General Asbestos Corp.
Asbestos House
P.O. Box 1100
Bulawayo, Phodesia

Office of the Mayor
City Hall
Rockport, Massachusetts

Chamber of Mines of South Africa
5 Hollard St.
Box 809
Johannesburg, South Africa

Director
Geological Survey
Private Bag X112
Pretoria, South Africa 0001

Dr. Jack Redden
South Dakota School of Mines
Rapid City, South Dakota

Turner & Newall Ltd.
Bernard Licoln
c/o TAC Construction Mat. Ltd.
Trafford Park, Manchester M17 1RU
England

United Asbestos Inc.
Matachewan, Ontario, Canada

Dr. Jack Zussman
Dept. of Geology
University of Manchester
Manchester, England

Dr. James R. Kramer
Dept. of Geology
McMaster University
Hamilton, Ontario, Canada L8S 4MI

Dr. Tibor Zoltai
Dept. of Geology
University of Minnesota
Bloomington, Minnesota

Dr. R. L. Stanton
Dept. of Geology
University of New England
Armidale, New South Wales, Australia

Dr. D. Hogarth
Geology Dept.
University of Ottawa
Ottawa, Ontario, Canada

Dr. John Prucha
Syracuse University
Syracuse, New York

Asbestos (and Talc) (continued)

Roselle Girard
Bureau of Economic Geology
University of Texas at Austin
Austin, Texas 78712

Prof. E. Occella & Dr. Visetti
Engineering Faculty
University of Turin
Turin, Italy

Prof. T. N. Clifford
Geology Department
University of the Witwatersrand
1 Jan Smuts Ave.
Johannesburg, South Africa 2001

Usauli Asbestos Ltd.
6 Hollard St.
Johannesburg 2001, Transvaal
South Africa

Chief Geologist/Mineralogist
Vermont Marble Co.
61 Main Street
Proctor, Vermont 05765

Chamber of Mines of Western
Australia, Inc.
Westus House, 4-6 Bennett St.
East Perth, Western Australia 6000

Dr. J. H. Lord
Geological Survey of Western
Australia
Mineral House
66 Adelaide Terrace
Perth, Western Australia 6000

Talc (and Asbestos)

Amalgamated Metal Corp., Ltd.
2 Metal Exchange Building
Leader Hall Avenue
London #C3V 1LD, England

American Talc Co.
Alpine, Alabama 35014

Aurial Mine
Sampleyre, Italy

Barton Mines Corp.
5 Mines Up Gore Mountain
North Creek, New York 12853

Mr. R. M. Kirkwood, Manager
Canada Talc Industries, Ltd.
Madoc, Ontario, Canada

Cima Franscia Mine
Sondria, Italy

Dr. Tryggve Baak
Cyprus Research
2435 Military Ave.
Los Angeles, California 90064

Eastern Magnesia Talc Co.
Johnson, Vermont 05656

Ente Minerario Sarda
Cagliari, Italy

Grantham Mines
1915 South Coast Highway
Laguna Beach, California 92651

International Talc Co., Inc.
420 Lexington Avenue
New York, New York 10006

Ministry of Commerce & Industry
Republic of Korea

Nittetsu Mining Co., Ltd.
Yusen Bldg.
3-2 Marunouchi 2-Chome
Chi Yoda-Ku
Tokyo, Japan

Pioneer Talc Co., Inc.
Box 121
Van Horn, Texas 79855

Talc (and Asbestos)

S.A. Des Talc De Luzenac
Mt. Soularac
French Pyrenees

San Vittore Mine
Belangero, Italy

Standard Industrial Minerals, Inc.
Route 4, Box 1
Bishop, California 93514

Texas Talc Co.
Box 17130
Ballas, Texas 75217

Tullio Quattrociocchi
L'Industria Mineraria
Rome, Italy

United Sierra Division
Cyprus Mines Corp.
Cameron, Montana

Dr. C. S. Thompson
R.T. Vanderbilt Co.
30 Winfield Street
East Norwork, Connecticut 06855

Vermont Talc Co.
Chester, Vermont 05143

Western Talc Co., Inc.
Box 368
Yermo, California 92398

Westex Talc Co., Box 15038
Houston, Texa 77020

Windsor Minerals, Inc., P.O. Box 680
Windsor, Vermont 05089

APPENDIX 2

X-RAY DIFFRACTION (XRD) DATA OF THE COMMINUTED MINERALS

Table 2-1. XRD data of quartz.

JCPDS 5-0490		Q-1	
dÅ	I/I_o	dÅ	I/I_o (Estimated)
4.26	35	4.27	40
3.343	100	2.35	100
2.458	12	2.46	20
2.282	12	2.28	25
2.237	6	2.24	10
2.128	9	2.13	15
1.980	6	1.98	10
1.817	17	1.82	30
1.801	<1		
1.672	7	1.67	10
1.659	3	1.66	5
1.608	<1		
1.541	15	1.54	25
1.453	3	1.45	5
1.418	<1		
1.382	7	1.38	15
1.375	11	1.37	20
1.372	9		
1.288	3	1.29	5
1.256	4	1.26	10
1.228	2	1.23	2
1.1997	5	1.20	7
1.1973	2		
1.1838	4	1.18	8
1.1802	4	1.18	8
1.1530	2	1.15	5
1.1408	<1		
1.1144	<1		
1.0816	4	1.08	5
Plus 11 lines to 0.9285			

Table 2-2. XRD data of beryl.

JCPDS 9-430		B-11	
dÅ	I/I_o	dÅ	I/I_o (Estimated)
7.98	90	8.11	90
4.60	50	4.66	60
3.99	45	4.02	50
3.254	95	3.28	95
3.015	35	3.03	70
2.867	100	2.88	100
2.660	4	2.68	5
2.523	30	2.53	30
2.293	12	2.32	20
2.213	8	2.22	15
2.208	4		
2.152	16	2.16	20
2.060	4		
2.056	6		
1.9926	20	2.00	20
1.8308	8	1.84	5
1.7954	18	1.80	15
1.7397	20	1.75	35
1.7110	14	1.72	15
1.7007	4		
1.6265	18	1.64	30
1.5953	8	1.60	6
1.5710	10	1.58	8
1.5690	8		
1.5349	6	1.54	6
1.5320	8		
1.5138	16	1.52	25
1.4882	2	1.49	3
1.4566	10	1.46	15
1.4535	12		
1.4324	14	1.44	25
1.4148	2		
1.3682	8	1.37	12
1.3656	6		
1.3306	<1	1.34	2
1.3117	<1		
1.2977	<1		
1.2774	12	1.28	25
1.2654	14	1.27	20
Plus 18 lines to 1.0157		Plus 4 lines to 1.09	

Table 2-3. XRD data of fluorite.

JCPDS 4-864		F-17	
dÅ	I/I_o	dÅ	I/I_o (Estimated)
3.153	94	3.18	95
1.931	100	1.94	100
1.647	55	1.65	50
1.366	12	1.37	10
1.253	10	1.23	8b
1.1150	16	1.12	8b
1.0512	7		
0.9657	1		
0.9233	7		
0.9105	1		
0.8637	9		
0.8330	3		

b = broad peak

Table 2-4. XRD data of nickel oxide (bunsenite).

JCPDS 4-835		N-108	
dÅ	I/I_o	dÅ	I/I_o (Estimated)
2.410	91	2.42	90
2.088	100	2.10	100
1.476	57	1.48	60
1.259	16	1.26	20
1.206	13	1.21	15
1.0441	8		
0.9582	7		
0.9838	21		
0.8527	17		
0.8040	7		

Table 2-5. XRD data of cristobalite.

JCPDS 11-695		CB-25	
dÅ	I/I_o	dÅ	I/I_o (Estimated)
4.05	100	4.06	100
3.53	4		
3.14	12	3.14	25
2.841	14	2.85	30
2.485	20	2.49	50
2.465	6		
2.340	2		
2.118	6	2.12	7
2.019	4	2.02	10
1.929	6	1.94	20
1.870	8	1.88	20
1.757	<2		
1.730	2		
1.690	4	1.69	7
1.634	2		
1.612	6	1.61	20
1.600	4		
1.571	<2		
1.567	<2		
1.533	4	1.53	7
1.494	6	1.50	10
1.431	4	1.43	7
1.419	4	1.42	2
1.398	4	1.40	2
1.379	<2		
1.365	4	1.37	5
1.352	4		
1.346	<2	1.34	5
1.333	4		
1.299	4	1.30	5
1.281	4	1.28	5
1.242	<2		
1.233	2		
1.223	4	1.22	2
1.210	4		
1.206	4		
1.188	2	1.18	2
Plus 45 lines to 0.7809			

Table 2-6. XRD data of tridymite.

JCPDS 18-1170		TY-27	
dÅ	I/I_o	dÅ	I/I_o (Estimated)
4.328	90	4.34	90
4.236	2	4.24	2
4.107	100	4.12	100
3.867	20		
3.818	50	3.83	70
3.672	2	3.66	2
3.642	4		
3.461	2		
3.396	4	3.41	2
3.297	<1		
3.250	4	3.27	10
3.215	2		
3.171	<1	3.18	2
3.126	<1		
3.087	<1		
3.049	<1		
3.017	4	3.03	4
2.975	25	2.98	25
2.776	8	2.79	4
2.609	2		
2.540	<1		
2.500	16	2.51	15
2.490	14	2.49	25
2.385	2	2.40	2
2.342	2		
2.308	16	2.31	15
2.294	2		
2.238	2		
2.205	2		
2.137	2		
2.117	4		
2.086	8	2.09	4
2.049	8	2.05	2
2.031	<1		
1.976	<1	1.97	1
1.943	<1	1.94	1
1.905	<1		
1.874	2	1.88	1
1,855	2		
1.829	2		
1.783	4		
1.715	2		
1.695	12	1.70	1
1.654	2		
1.635	8		

Table 2-6. (concluded)

JCPDS 18-1170		TY-27	
dÅ	I/I_o	dÅ	I/I_o (Estimated)
1.600	10		
1.546	2		
1.534	10	1.53	4
Plus 10 lines to 1.402			

Table 2-7. XRD data of chrysotile.

JCPDS 21-543		CH-29	
dÅ	I/I_o	dÅ	I/I_o (Estimated)
7.37	100	7.35	100
4.57	50	4.78	20
4.05	10		
3.65	70	3.66	70
2.45	10*		
2.270	30		
2.205	30		
2.092	30	2.10	10
1.827	30		
1.744	30		
1.535	50	1.54	20
1.506	30		
1.463	30	1.46	3
1.313	30		
1.222	1*		
1.219	1		

*Possibly due to lizardite

Table 2-8. XRD data of crocidolite.

JCPDS 19-1061		CR-37	
dÅ	I/I_o	dÅ	I/I_o (Estimated)
9.02	4		
8.40	100	8.55	100
4.89	10		
4.51	16	4.55	30
3.88	10		
3.66	10		
3.42	12	3.44	20
3.27	14	3.28	10
3.12	55	3.12	70
2.976	10		
2.801	18		
2.726	40	2.73	60
2.602	14	2.61	20
2.541	12	2.55	25
2.324	12	2.33	10
2.301	4		
2.268	10	2.27	10
2.191	4		
2.176	16	2.18	5
2.079	6		
2.031	8		
2.000	4		
1.888	4		
1.866	6		
1.805	6		
1.659	10		
1.635	6		
1.617	8		
1.593	10		
Plus 9 lines to 1.301			

Table 2-9. XRD data of fibrous grunerite (amosite).

JCPDS 17-745		GF-38	
dÅ	I/I_o	dÅ	I/I_o (Estimated)
9.15	20	9.39	20
8.33	100	8.45	100
5.17	5		
4.84	5		
4.62	10	4.71	8
4.55	10	4.62	8
4.13	40	4.19	10
3.86	30		
3.46	30		
3.26	40	3.29	50
3.06	70	3.08	70
2.99	10		
2.756	70	2.78	20
2.628	40	2.64	10
Plus 41 lines to 1.300			

Table 2-10. XRD data of fibrous anthophyllite.

JCPDS 16-401		AF-45		
dÅ	I/I_o	dÅ	I/I_o (Estimated)	
		9.56	100	Talc*
9.21	5			
		9.13	10	
8.33	70	8.35	70	
5.03	5			
4.67	20			
4.49	35	4.52	15	+ Talc*
		4.29	10	Quartz†
4.14	5	4.14	15	
3.97	5			
3.66	15	3.66	30	
		3.36	10	Quartz†
3.23	50	3.25	50	
		3.13	60	Talc*
3.06	100	3.06	100	
2.872	15	2.89	10	
2.831	20	2.84	10	
2.822	15			
2.750	15	2.76	10	
		2.69	8	Talc*
2.552	5	2.55	12	
2.536	5			
		2.32	5	Talc*
2.266	10			
		2.14	7	Talc*
2.023	5	2.07	5	
1.855	15	1.85	5	
1.841	10			
		1.83	3	Quartz†
1.822	15			
1.615	15	1.62	15	
1.608	5			
1.500	25	1.51	15	
		1.42	30	Talc* + Quartz†
		1.33	15	
1.289	5			

* Talc JCPDS 19-770
† Quartz JCPDS 5-0490

Table 2-11. XRD data of fibrous tremolite.

JCPDS 13-437		TF-48	
dÅ	I/I_o	dÅ	I/I_o (Estimated)
		9.44	30
8.98	16	9.14	25
8.38	100	8.50	90
5.07	16	5.12	10
4.87	10	4.86	10
4.76	20	4.78	35
4.51	20	4.54	25
4.20	35	4.23	40
3.87	16		
3.38	40	3.40	30
3.27	75	3.29	50
3.12	100	3.14	100
3.03	10	3.04	5
2.938	40	2.95	40
2.805	45	2.82	40
2.730	16	2.74	30
2.705	90	2.72	40
2.592	30	2.60	20
2.527	40	2.54	20
2.407	8		
2.380	30	2.39	20
2.335	30	2.34	30
2.321	40	2.33	20
2.298	12	2.31	10
2.273	16	2.28	10
2.206	6	2.22	2
2.181	6		
2.163	35	2.17	25
2.042	18		
2.015	45	2.02	15
2.002	16	2.00	10
1.963	6	1.97	5
1.929	6		
1.892	50	1.90	45
1.864	16		
1.814	16	1.82	25
1.745	6		
1.686	10		
1.649	40		
1.639	10		
Plus 9 lines to 1.439		Plus 14 lines to 1.19	

Table 2-12. XRD data of antigorite.

JCPDS 9-444		AG-55	
dÅ	I/I_o	dÅ	I/I_o (Estimated)
7.33	100	7.42	100
4.60	60b	4.64	40
4.40	10		
4.25	10		
4.09	10		
3.90	5		
3.66	100	3.69	70
3.53	5		
3.35	5	3.34	5
3.17	5		
3.02	5		
2.865	5		
2.720	5		
2.623	30		
2.502	100	2.51	60
2.450	10	2.45	20
2.425	10		
2.335	70		
2.149	60	2.16	30
1.963	70		
1.815	5	1.80	5
1.791	10		
1.739	10b		
1.636	40		
1.535	80	1.54	50
1.501	70	1.51	35
1.452	2		
1.415	20		
1.379	20		
1.327	10		
1.309	50	1.31	20
1.296	2		
Plus 11 lines to 0.9511			

b = broad peak

Table 2-13. XRD data of riebeckite.

JCPDS 19-1061		R-60	
dÅ	I/I_o	dÅ	I/I_o (Estimated)
9.02	4		
8.40	100	8.57	100
4.89	10		
4.51	16	4.53	25
3.88	10		
3.66	10		
3.42	12	3.43	25
3.27	14	3.29	10
3.12	55	3.15	75
2.976	10		
2.801	18	2.82	30
2.726	40	2.73	50
2.602	14	2.60	5
2.541	12	2.55	10
2.324	12	2.34	10
2.301	4		
2.268	10		
2.191	4		
2.176	16	2.18	5
2.079	6		
2.031	8	2.04	10
2.000	4		
1.888	4		
1.866	6		
1.805	6		
1.659	10	1.66	10
1.635	6		
1.617	8		
1.593	10		
1.583	8		
1.576	6		
1.520	4		
1.509	4		
1.504	4		
1.429	6	1.44	10
1.352	4		
1.333	6		
1.301	6		

Table 2-14. XRD data of grunerite.

JCPDS 17-745		G-68	
dA°	I/I_o	dA°	I/I_o (Estimated)
9.15	20	9.30	15
8.33	100	8.43	100
5.17	5		
4.84	5		
4.62	10	4.60	5
4.55	10	4.48	5
4.13	40	4.19	10
3.86	30		
3.46	30		
3.26	40	3.28	30
3.06	70	3.08	65
2.99	10		
2.756	70	2.77	25
2.628	40		
2.503	40	2.51	8
Plus 40 lines to 1.300			

Table 2-15. XRD data of cummingtonite.

JCPDS 17-726		C-71		
dÅ	I/I_o	dÅ	I/I_o (Estimated)	
		10.30	100	Biotite*
9.12	50	9.30	20	
8.30	100b	8.44	100	
5.09	20			
4.83	20			
4.55	40			
		4.28	40	Quartz†
4.14	40			
3.87	30			
3.45	30			
		3.36	100	Quartz† + Biotite*
3.26	80	3.28	50	
3.06	90	3.08	90	
2.987	20			
2.754	70	2.77	30	
2.623	50	2.65	30	Biotite*
2.544	10			
2.504	30			
2.364	10			
2.293	30	2.29	20	
2.241	15			
2.213	15			
2.190	50	2.20	20	
2.095	15			
2.038	20b	2.02	5	
Plus 41 lines to 0.983				

b = broad peak
* Biotite JCPDS 2-75
† Quartz JCPDS 5-0490 (more lines are seen on a linear plot)

Table 2-16. XRD data of tremolite.

JCPDS 13-437 (unspecified habit)		T-77	
dÅ	I/I_o	dÅ	I/I_o (Estimated)
8.98	16	9.14	20
8.38	100	8.48	90
5.07	16	5.12	15
4.87	10	4.90	15
4.76	20	4.77	20
4.51	20	4.53	18
4.20	35	4.22	25
3.87	16	3.89	15
3.38	40	3.40	40
3.27	75	3.28	50
3.12	100	3.13	100
3.03	10		
2.938	40	2.95	45
2.805	45	2.81	30
2.730	16	2.74	30
2.705	90	2.71	60
2.592	30	2.60	20
2.529	40	2.54	30
2.407	8	2.45	5
2.380	30	2.39	10
2.335	30	2.34	30
2.321	40	2.32	25
2.298	12	2.30	15
2.273	16	2.28	15
2.206	6		
2.181	6		
2.163	35	2.17	40
2.042	18	2.04	15
2.015	45	2.01	20
2.002	16	2.00	10
1.963	6	1.97	5
1.929	6		
1.892	50	1.90	30
1.864	16	1.88	5
1.814	16	1.82	10
1.746	6		
1.686	10	1.69	5
1.649	40	1.65	35
1.639	10	1.62	5
Plus 9 lines to 1.439		Plus 9 lines to 1.30	

Table 2-17. XRD data of anthophyllite.

JCPDS 16-401 (unspecified habit)		A-102	
dÅ	I/I_o	dÅ	I/I_o (Estimated)
		9.66	100 Talc*
9.21	5	9.26	20
8.33	70	8.46	80
5.03	5		
		4.97	5
4.67	20		
4.49	35	4.54	25 + Talc*
		4.30	20 Quartz†
4.14	5	4.16	20
3.97	5		
		3.92	7
3.66	15		
		3.64	25
		3.37	100 Quartz†
3.23	50	3.25	60
		3.15	70 Talc*
3.06	100	3.07	100
2.872	15	2.89	15
2.831	20	2.84	22
2.822	15		
2.750	15	2.76	20
		2.69	50 Talc*
		2.59	30 Talc*
2.552	5	2.56	15
		2.51	30 Talc*
2.536	5		
		2.44	10 Quartz†
		2.32	20 Talc*
2.266	10	2.29	12 + Quartz†
		2.25	10
		2.16	25 Talc*
		2.14	30 Quartz†
2.023	5	2.07	5
		1.99	15 Quartz† + Talc*
1.855	15		
		1.85	15 Talc*
1.841	10		
1.822	15	1.84	12
		1.74	25 Talc*
		1.69	5 Quartz†
1.615	15	1.62	20
1.608	5		
		1.58	7
		1.55	7 Quartz†

Table 2-17. (concluded)

JCPDS 16-401 (unspecified habit)		A-102	
dÅ	I/I_o	dÅ	I/I_o (Estimated)
		1.51	25 Talc*
1.500	25	1.50	20
		1.42	40 Quartz† + Talc*
		1.33	15 Talc*
1.289	5	1.29	5

* Talc JCPDS 19-770
† Quartz JCPDS 5-0490

Table 2-18. XRD data of talc.

JCPDS 19-770		TA-99	
dÅ	I/I_o	dÅ	I/I_o (Estimated)
9.35	100	9.55	100
4.67	8	4.72	20
4.59	45	4.61	25
4.53	12	4.51	5
4.33	6		
4.12	6		
3.87	2		
3.69	2		
3.52	<2		
3.12	40	3.14	70
2.643	6	2.65	5
2.635	18		
2.627	8		
2.610	14	2.62	15
2.597	20	2.61	15
2.589	14		
2.496	20	2.50	40
2.479	30		
2.464	14		
2.457	10		
2.360	2		
2.337	2		
2.289	2		
2.278	2		
2.265	2		
2.234	4	2.23	5
2.227	6		
2.208	6		
2.188	2		
2.164	<2		
2.130	4b		
2.104	4b		
2.086	2		
2.071	2		
1.967	2		
1.921	2		
1.870	4	1.88	4
1.731	10b	1.74	2
1.726	4b		
1.714	4b		
1.708	4b		
1.692	4		
1.684	6b	1.69	2
1.668	6b	1.68	2

Table 2-18. (concluded)

JCPDS 19-770		TA-99	
dÅ	I/I_o	dÅ	I/I_o (Estimated)
1.654	2b		
1.558	2		
1.540	<2		
1.529	55	1.53	35
1.524	12b		
1.511	12		
1.503	2b		
1.411	4b		
1.386	4b	1.40	2
1.376	2b		
1.336	2		
1.321	8	1.32	4
Plus 17 lines to 1.169			

b = broad peak